Development of Novel and Suitably Tailored Adsorbents for Chromium and Mercury Detoxification

THESIS

Submitted in partial fulfilment

of the requirements for the degree of

DOCTOR OF PHILOSOPHY

by

A. SANTHANA KRISHNA KUMAR

Under the supervision of

Prof. N. Rajesh

BIRLA INSTITUTE OF TECHNOLOGY AND SCIENCE, PILANI

HYDERABAD CAMPUS, INDIA

2013

BIRLA INSTITUTE OF TECHNOLOGY & SCIENCE, PILANI
HYDERABAD CAMPUS

CERTIFICATE

This is to certify that the thesis entitled "**Development of Novel and Suitably Tailored Adsorbents for Chromium and Mercury Detoxification***"* submitted by **A. SANTHANA KRISHNA KUMAR, ID. No. 2010PHXF035H** for the award of Ph. D. degree of the Institute embodies the original work done by him under my supervision.

Signature in full of the supervisor : _____

Name in capital block letters : **N. RAJESH**

Designation : **Professor, Dept. of Chemistry**

Date: :

DEDICATED
TO
MY FAMILY

CHAPTER I

INTRODUCTION

CHAPTER II

MATERIALS AND METHODS

CHAPTER III

Long Chain Amine Impregnated Polystyrene Divinylbenzene Polymeric Sorbents for the Removal of Chromium

CHAPTER IV

Long Chain Amine and Biopolymer Modified Sodium Montmorillonite for the Removal of Chromium and Mercury

CHAPTER V

Customized Biopolymer Sorbents and Graphene Oxide for the Adsorption of Chromium and Mercury

CHAPTER VI

Conclusions and Suggestions for Future Work

ACKNOWLEDGEMENT

At the outset, I would like to thank the Almighty for giving me the strength to do the research work with good health.

My deep sense of gratitude to **Prof. B. N. Jain,** Vice Chancellor (BITS, Pilani), for permitting me to carry out my doctoral work in the institute.

My heart-felt gratitude to **Prof. V. S Rao,** Director (BITS-Pilani, Hyderabad Campus), for permitting me to carry out my research work in the campus.

I wish to express my sincere gratitude and heartfelt thanks to my guide **Prof. N. Rajesh**, Department of Chemistry, for his excellent guidance, constant encouragement, enormous patience and good advice with a smiling face throughout my research work. I would like to acknowledge him for his moral support at every instance, without which, this work would not have been completed. I owe it to you sir

I am indebted to **Dr. Vidya Rajesh, FIC,** Academic Research Division, (ARD) BITS-Pilani, Hyderabad campus, for her co-operation, involvement and encouragement at every stage of this research work.

I am grateful to **Prof. Suman Kapur,** *Former* Dean R&C Division, **Prof. M. Moorthy MuthuKrishnan** (*Former* FIC, R&C Division), **Prof. P. Yogeeswari** (FIC,SRCD) BITS-Pilani, Hyderabad campus for the valuable support.

I acknowledge **Dr. K.V.G Chandrasekhar,** DRC Convener, **Dr. Krishnan Rangan** and **Dr. Anupam Bhattacharya,** Doctoral Advisory committee members for their constant encouragement and valuable suggestions.

My sincere thanks and respectful regards to **Prof. K. Sumithra**, Head, Department of Chemistry, BITS-Pilani Hyderabad campus, for providing me with all the necessary laboratory facilities and encouragement at various stages of my research work.

I wish to express my thanks to all the faculty of Department of Chemistry, for their support and encouragement to carry out this research work.

I deeply acknowledge **Department of Science and Technology (DST)**, New Delhi, India and **Birla Institute of Technology and Science (BITS-Pilani, Hyderabad Campus)** for providing me the fellowship. I would like to acknowledge Indian Institute of Science (IISc) Bangalore, India, Central Electrochemical Research Institute (CECRI) Karaikudi, India, Alagappa University, Karaikkudi, India, Indian Institute of Technology (IIT), Madras, India, Karunya University, Coimbatore, India, Thiyagarajar College, Madurai, India for their valuable assistance in characterization of the adsorbents. I want to thank my research group, my lab mates, (Dr. S. Kalidhasan, Mr. M. Barathi, Ms. Manasi and Shivani) and all my friends in and out of the department for their support and making the last few years an exciting and memorable experience.

I humbly dedicate this doctoral thesis to my PARENTS.

Date: **A. Santhana Krishna kumar**

ABSTRACT

The detoxification of chromium and mercury from industrial effluents at various levels (ppb to μg) assumes considerable importance. A variety of methods such as precipitation, extraction, reverse osmosis, membrane separation/filtration, *etc*. have been utilized for this purpose. Each of these methods possesses their own merits and demerits. In order to overcome some of the inadequacies in some of the existing techniques, it is imperative to develop newer and eco-friendly methods. The first work presented in the thesis deals with an efficient approach for the removal of chromium based on the impregnation of trioctylamine (TOA) on a macroporous Amberlite XAD-1180 polymeric matrix. Chromium(VI) could be quantitatively adsorbed in an acidic medium (pH 2-3), while chromium(III) could be retained on the resin matrix at alkaline pH. The comprehensively characterized adsorbent showed a high adsorption capacity of 171.82 mg g^{-1} in accordance with the Langmuir isotherm model. The adsorption follows second order kinetics and a study of the various thermodynamic parameters such as Gibbs energy, entropy and the enthalpy changes showed that the adsorption decreases with an increase in temperature. Column studies and regeneration data validated the performance efficiency of the adsorbent with large sample volume tolerance (1 Litre) and high preconcentration factor (100). The resin column could be regenerated using NaOH after the removal of total chromium without any loss in the performance efficiency for nearly 15 cycles. Chromium could be effectively separated from a synthetic mixture of various ions, thus making it a viable proposition for the detoxification of chromium from industrial effluents.

Another green methodology is developed for the effective adsorption for chromium(VI) using aliphatic primary amine as a guest in Amberlite XAD-4 polymeric sorbent host. The adsorption of chromium was quantitative at pH 2.5. The adsorption process was in accordance with pseudo second order kinetics and the maximum adsorption capacity was found to be 75.93 mg g^{-1} with good adherence to Langmuir isotherm model. The free energy change ΔG^0 increased with temperature and the negative ΔH^0 and ΔS^0 values indicate the exothermic nature of adsorption and decreased randomness at the adsorbent-solution interface. In aqueous medium, the water molecules surround the hydrophobic host polymeric

matrix and this cage effect is responsible for the reduction in entropy of the system. The regeneration of the adsorbent was effective in alkaline medium and the efficacy of the adsorbent was tested for the removal of chromium from tannery wastewater.

The fourth chapter deals with an effective solid phase extraction method is proposed for mercury based on the adsorption of tetrachloromercurate(II) anion with trioctylamine intercalated onto sodium montmorillonite. Various isotherm models were employed to correlate the experimental adsorption data. The electrostatic interaction between $HgCl_4^{2-}$ and the protonated amine is well supported by Langmuir isotherm model with a maximum adsorption capacity of 140.84 mg g^{-1}. The ordered transition state that arises due to the proximity of the $HgCl_4^{2-}$ and the positively charged amine is accompanied by a decrease in the translational entropy of the system. The N_2 adsorption-desorption isotherm study revealed the mesoporous nature of the adsorbent and the thermodynamically favorable adsorption process resonates well with the ensuing negative free energy and enthalpy changes in accordance with the sorption mechanism. Packed bed column study demonstrated the scale up to 800 mL sample volume at 10 mg L^{-1} Hg(II) and the adsorbent could be regenerated and re-used for 10 cycles with thiourea as the eluent. The removal of mercury from a coal fly ash sample validated the method.

Clay materials are well suited for heavy metal adsorption in view of their excellent surface area and cation exchange capacity. The adsorption of hexavalent chromium is achieved using dodecylamine intercalated sodium montmorillonite as a potential adsorbent. The adsorption involves primarily the electrostatic interaction of hydrogentetraoxochromate(VI) anion with the protonated dodecylamine and the surface hydroxyl groups of the clay material. The pseudo second order kinetic model fits the experimental data and an adsorption capacity of 23.69 mg g^{-1} was obtained from the Langmuir isotherm model. The exothermically favorable spontaneous adsorption process and the decrease in entropy explain the thermodynamics of the adsorption. The adsorbent could be regenerated using NaOH and column adsorption studies provide a sample break through volume of 300 mL on a laboratory scale. The adsorbent could be utilized for the successful removal of chromium from tannery wastewater.

Biopolymer composites are known for their utility in diverse applications. Another effective methodology for the detoxification of chromium is proposed using cellulose-montmorillonite composite material as the adsorbent. The interaction of surfactant modified sodium montmorillonite (NaMMT) with cellulose biopolymer is followed by the subsequent adsorption of Cr(VI) from aqueous solution as hydrochromate anion onto the surface of the biocomposite material. The material exhibited a maximum adsorption capacity of 22.2 mg g^{-1} in accordance with the Langmuir isotherm model. The mesoporous nature of the material was ascertained from the nitrogen adsorption isotherm study and the adsorption process was in accordance with second order kinetics. The spontaneity of the adsorption process could be confirmed from the study of the adsorption thermodynamics. The composite material could be regenerated using sodium hydroxide as the eluent. The adsorbent could be reused with quantitative recovery for 10 adsorption-desorption cycles. An aqueous phase feed volume of 400 mL could be quantitatively treated by column method at 100 mg L^{-1} concentration of Cr(VI) with a preconcentration factor of 50. The applicability of the method is demonstrated in the quantitative removal of total chromium from a chrome tannery effluent sample.

In the final method of fourth chapter deals with microwave-assisted preparation and characterization of chitosan-surfactant modified NaMMT clay composite material followed by its interesting application to detoxify chromium. Cr(VI) could be effectively adsorbed in a weakly acidic medium (pH 5) from a large sample volume. The surface hydroxyl groups in clay can be protonated and this could also serve as a source of electrostatic interaction with the hydrochromate oxyanion. The material exhibited a superior adsorption capacity of 133 mg g^{-1} and the adsorption data fitted well with Langmuir and Freundlich isotherm models. The experimental data also showed a good correspondence to the pseudo second order kinetics and the sorption thermodynamics correlated to the endothermic nature of the adsorption. The adsorbent could be regenerated using ascorbic acid or sodium sulfite which is indicative of the greener aspect in the methodology.

The fifth chapter deals with the utility of chitosan as an excellent platform for impregnating the ionic liquid, tetraoctylammonium bromide by ultrasonication and its subsequent adsorption for chromium(VI). The effective mass transfer due to sonication coupled with the

hydrogen bonding interaction between chitosan-ionic liquid and the electrostatic interaction involving the amino groups in chitosan and hexavalent chromium governs this three centre (3c) co-operative mechanism. The adsorption followed a pseudo second order kinetics with a Langmuir adsorption capacity of 63.69 mg g^{-1}. Various isotherm models were used to correlate the experimental data and the adsorption process is exothermic with a decreased randomness at the solid-solution interface. The thermodynamics of the spontaneous adsorption process could be explained through a positive co-operative effect between the host (chitosan) and the guest (ionic liquid). The adsorbed chromium(VI) could be converted to ammonium chromate using ammonium hydroxide, thereby regenerating the adsorbent. The method could be translated into action in the form of practical application to a real sample containing chromium.

Another interesting interaction is proposed involving exfoliated graphene oxide (EGO), ionic liquid (IL) Aliquat 336 and hexavalent chromium. Graphene oxide was impregnated with the ionic liquid and the interaction primarily involves electrostatic affinity between the quaternary ammonium cation and surface hydroxyl groups in EGO. The IL-EGO combination functions as an effective adsorbent for hexavalent chromium. The IL-EGO adsorbent acts as a good host in welcoming the incoming guest, hydrochromate anion and several interesting interactions such as cation-π, electrostatic as well as anion-π could be conceptualized in this process. The adsorbent features are ably supported by various physico-chemical characterization techniques and the effect of various analytical parameters affecting the adsorption is examined in detail. A high Langmuir adsorption capacity of 285.71 mg g^{-1} is augmented by the thermodynamically favourable adsorption process. Kinetic studies confirm the pseudo second order model and furthermore, the process could be upgraded by column study to a sample volume of 1200 mL. Effective regeneration of the adsorbent could be accomplished with ammonium hydroxide and the potential of this novel adsorbent material has been examined in removal of total chromium from a tannery effluent sample.

Last work of the thesis focuses on an interesting method for the adsorption of mercury involving its interaction with cellulose and mercaptobenzothiazole (MBT). Cellulose acts as a host and MBT as guest in the first instance followed by the subsequent complexation of mercury with MBT. The soft-soft interaction between mercury and sulfur enhances the effective complexation with MBT. The most favorable experimental conditions, isotherm models, mechanism of interaction and thermodynamics are discussed. The negative values of free energy obtained at various temperatures together with an endothermic adsorption process affirm the spontaneity of adsorption. FT-IR, SEM, EDS and XRD techniques were utilized to characterize the MBT impregnated cellulose as well as the mercury-loaded adsorbent. With a high adsorption capacity of 204.08 mg g^{-1} and a sample, volume of 500 mL could be quantitatively treated by column method. Potassium thiocyanate functions as a valuable reagent for the desorption of mercury. The practical application was tested for the adsorption of mercury vapor emanating from a used Compact Fluorescent Lamp (CFL).

Keywords: Amberlite XAD-1180, Amberlite XAD-4, exfoliated graphene oxide (EGO), chromium(VI), mercury, Aliquat 336, tetraoctylammonium bromide, 2-mercaptobenzothiazole, cellulose, chitosan, montmorillonite, trioctylamine, dodecylamine, n-octylamine, ultrasonication, microwave irradiation, preconcentration factor, sodium hydroxide, ammonium hydroxide, solid phase extraction, tannery effluent, coal fly ash sample.

TABLE OF CONTENTS

CONTENTS

List of Abbreviations and Symbols

%	Percentage
b	Langmuir constant
Cr	Chromium
k_{int}	Intra-particle diffusion constant
q_o	Maximum adsorption capacity
q_e	Equilibrium concentration
R	Universal gas constant
R_L	Dimensionless constant in Langmuir isotherm model
t	Time
T	Temperature
ΔG^0	standard Gibb's free energy
ΔH^0	standard enthalpy
ΔS^0	standard entropy
AA	Ascorbic acid
BET	Brunauer-Emmett-Teller
BJH	Barrett-Joyner-Halenda
DPC	Diphenylcarbazide
DTZ	Diphenylthiocarbazide
MBT	2-mercaptobenzothiazole,
EDX	Energy dispersive X-ray
MMT	Montmorillonite
FI	Freundlich isotherm

FT-IR	Fourier transform infrared spectroscopy
ICP-AES	Inductively coupled atomic emission spectrometry
ICP-MS	Inductively coupled mass spectrometry
TOA	Trioctylamine
IL	Ionic liquid
EGO	Exfoliated graphene oxide
LI	Langmuir isotherm
IL	Ionic Liquid
MQW	Milli-Q water
MW	Microwave
PFO	Pseudo first order kinetics
ppb	Parts per billion
ppm	Parts per million
PS-DVB	Polystyrene-Divinyl benzene
PSO	Pseudo second order Kinetics
PXRD	Powder X-ray diffraction
rpm	Revolutions per minute
RTIL	Room temperature ionic liquid
SEM	Scanning Electron Microscopy
SPE	Solid Phase Extraction
TBABr	Tetrabutylammoniumbromide

List of Figures

List of Tables

INTRODUCTION

The presence of heavy metals in the environment is an important concern in view of their toxicity and tendency to bioaccumulate in the food chain at relatively low concentrations. Most of the heavy metals have been recognized as priority pollutants and are reported to accumulate in the environment causing potential short-term and long-term adverse effects. The tremendous increase in the use of heavy metals in diverse industrial applications has resulted in an increased amount of "metal pollution" of water bodies. [1, 2] *'Heavy metals'* is a collective term applied to the group of metals and metalloids with an atomic density greater than 6 g cm^{-3}. It is widely recognised and usually applied to the elements such as Cd, Cr, Cu, Hg, Ni, Pb, and Zn which are commonly associated with pollution and toxicity problems. The global awareness of their underlying detrimental effects, has received great attention in recent decades as a major pollutant in surface and groundwater.[3] Among the above metals, chromium and mercury deserve importance in view of their varied applications and the toxicity to the environment at low concentrations.

Separation techniques for heavy metals involve solvent extraction,[4] ion exchange,[5] membrane techniques[6] and solid phase extraction (SPE)[7]and these techniques ought to be coupled to a good analytical method to detect the metal ions at trace levels. A careful introspection reveals SPE as the popular choice for heavy metal adsorption. Solid phase extraction (SPE) is the most popular technique currently available for rapid and selective separation. It plays a pivotal role in metal ion removal at various concentration levels. The separation techniques would enhance the sensitivity by bringing the concentration of analyte to the required detection limits by using a suitable analytical method. An overview of the chemistry of chromium and mercury and a review of literature involving SPE methods for their detoxification is presented in the following pages.

1.1 Chemistry of Chromium

1.1.1 History, Occurrence and Physicochemical Characteristics

The French chemist Nicholas-Louis Vauquelin hypothesized as early as 1797 chromium as a separate and distinct element. He isolated the oxide of this element from a Siberian

mineral crocoite ($PbCrO_4$), and in 1798, Vauquelin isolated metallic Cr by heating chromic oxide (Cr_2O_3) with charcoal and coined the new element as "chromium" since it produced distinct and unique colored chemical compounds.[8] Chromium (atomic number 24) is a transition element present in group 6B in the periodic table. Chromium metal is shiny, silvery and hard as well as brittle. It has a high melting point (1857.0°C) and boiling point (2672.0°C). The oxidation states vary from –2 to +6, and the most stable oxidation states are +3 and +6.[8] Chromium is the earth's 21st most abundant element and the sixth most abundant transition metal.[9] The principal chromium ore is ferric chromite ($FeCr_2O_4$), Cr(III) and Cr(VI) are well known in their stable oxidation states. The hydrolysis[10] of Cr(III) produces mononuclear species $Cr(OH)^{2+}$, $Cr(OH)_2^{+}$, $Cr(OH)_4^{-}$, neutral species $Cr(OH)_3$, poly nuclear species $Cr_2(OH)_2^{n+}$ and $Cr_3(OH)_4^{5+}$. The hydrolysis of Cr^{6+} produces anionic species[9] such as CrO_4^{2-}, $HCrO_4^{-}$, $Cr_2O_7^{2-}$. At low pH, $Cr_2O_7^{2-}$ and $HCrO_4^{-}$ predominates, while at a pH greater than 6.5, Cr(VI) exists in the form of CrO_4^{2-}. [9] Chromium is a hard acid and forms relatively strong complexes with oxygen and nitrogen donor ligands.[11] Chromium(VI) compounds are of more concern than Cr(III) due to their high water solubility and mobility. The most soluble, mobile and toxic forms of Cr(VI) in soils are chromate and dichromate. Hexavalent chromium is rapidly reduced to trivalent chromium under aerobic conditions. [12]

1.1.2 Toxicity of Chromium

Acute exposure to Cr(VI) causes nausea, diarrhoea, liver and kidney damage, dermatitis, internal haemorrhage, and respiratory problems.[13] Inhalation may cause acute toxicity, irritation and ulceration of the nasal septum and respiratory sensitization (asthma).[14] Chromium is both beneficial and detrimental. Chromium(III) is an essential trace element in mammalian metabolism. In addition to insulin, it is responsible for reducing blood glucose levels, and is used to control of diabetes.[15] It has also been found to reduce blood cholesterol levels by diminishing the concentration of low density lipoproteins "LDLs" in the blood.[15] Cr(III) is supplied in a variety of foods such as Brewer's yeast, liver, cheese, whole grain breads and cereals, and broccoli.[13] Chromium compounds are widely used in electroplating, metal finishing, pigments, leather tanning, wood protection, catalysis, electrical and electronic equipments.[13] The volume and characteristics of different

wastewater streams from a tannery depend on the processes adopted for water consumption, which vary from tannery to tannery. Hexavalent chromium compounds are known to be genotoxic and chronic inhalation of hexavalent chromium compounds increases the risk of lung cancer. The mechanism of genotoxicity relies on pentavalent or trivalent chromium.[8] The damage is presumed to be caused by hydroxyl radicals produced during reoxidation of pentavalent chromium by hydrogen peroxide molecules present in the cell. The understanding of chromium chemistry, geochemistry and toxicity assumes considerable importance in developing efficient remediation methods that can reduce the hazards associated with this heavy metal.

1.2 Chemistry of Mercury

Mercury atomic number 80, is known as quicksilver or hydrargyrum.[16] It is a heavy, silvery transition metal that exists as a liquid at or near room temperature and pressure. Cinnabar is an important ore of mercury.[16] The ancient Greeks used mercury in ointments and the Romans used it in cosmetics.[17]It alloys easily with many metals, such as gold, silver, and tin. These alloys are called amalgams. Its ease in amalgamating with gold is used in the recovery of gold from its ores.[18]

1.2.1 Forms of Mercury and their Toxicity

Mercury is a naturally occurring element that is found in air, water and soil. It exists in several forms elemental or metallic mercury, inorganic mercury compounds, and organic mercury compounds. It is used in thermometers, fluorescent light bulbs and electrical switches. At room temperature, exposed elemental mercury can evaporate to become a toxic vapour. Inorganic mercury compounds in the form of mercury salts are generally present as white powder or crystals. Inorganic mercury compounds have been included in products such as fungicides, antiseptics or disinfectants. Some skin lightening creams, as well as some traditional medicines, contain mercury compounds.[18] Mercury exists in three oxidation states: Hg^0, Hg^+ (+1) and Hg^{2+} (+2) respectively. The latter forms a variety of inorganic as well as organometallic compounds. Although, all the species of mercury are toxic, the effects are related to its chemical form. The environmentally significant forms are elemental mercury (Hg^0), inorganic mercury (Hg^{2+}), monomethylmercury (CH_3Hg^+), monoethylmercury ($CH_3CH_2Hg^+$) and dimethylmercury

(CH_3HgCH_3). In the biogeochemical cycle of Hg, these species could be transformed into each other and dynamically transported through the aquatic and atmospheric paths. The transformation of inorganic mercury into methyl mercury by sulphate-reducting bacteria and the subsequent accumulation through the aquatic food chain is an important concern.[19] Mercury has a unique volatility among the various elements this makes it quite mobile in the environment. Methylated Hg has special chemical characteristics (due to the methyl group) that make it prone to bioaccumulate in animals and plants. In contrast, inorganic Hg does not bioaccumulate. Methylmercury is considerably more toxic than elemental mercury, because it is efficiently adsorbed from the gastrointestinal tract and rapidly transported through biological membranes causing neuronal damage.[20] Mercury(II) being a soft acid, binds to sulfhydryl groups in proteins resulting in structural alteration.[21]

1.2.2 Application of Mercury

Mercury is used in medical and scientific products like thermometers, barometers, manometers and dental fillings. A major use of mercury is in electrical equipment such as fluorescent lamps, and batteries. The used Compact Fluorescent Lamps (CFL)[22] and coal fly ash[23] are other important sources of mercury pollution.

1.2.3 Overview of Remediation Methods of Chromium and Mercury

The permitted levels for Cr(III) & Cr(VI) in waste water are 2 mg L^{-1} and 0.05 mg L^{-1} respectively [8, 24, 25] and industrial processes that produce aqueous effluents rich in chromium ought to be treated effectively. Several treatment technologies have been developed to remove chromium from wastewater. Common methods include ion exchange,[26] membrane separation,[27] solvent extraction,[28] sedimentation,[29] reduction, [30] reverse osmosis,[31] dialysis/electrodialysis,[32] adsorption[33] and chelation.[34] Chemical precipitation has traditionally, been most commonly used in the form of hydroxide precipitation. However, the disadvantage of precipitation is the production of sludge and this leads to disposal problems. The toxicity of mercury also warrants effective remediation methods.[35] The EPA recommends a limit of 2.0 µg L^{-1} mercury in water.[36] Due to the very low concentration levels of mercury(II) in water samples, an enrichment step should be included prior to the analysis in order to achieve a final concentration level

matching the detection limits along with the analytical technique selected.[37] The interference effect of matrix components of the sample is an important factor to be considered in the remediation of mercury. In order to solve these problems, preconcentration and separation techniques such as solid phase extraction, cloud point extraction, solvent extraction, ion-exchange, co-precipitation, etc., have been utilized for the detoxification of mercury.[38-42] The most commonly used analytical methods for mercury include inductively coupled plasma optical emission spectrometry (ICP-OES)[43] and inductively coupled plasma mass spectrometry (ICP-MS).[44] However, owing to its simplicity, high sensitivity, relative freedom from interferences, and low cost cold vapour atomic absorption spectrometry (CV-AAS) is the widely used analytical technique for mercury speciation in environmental samples.[45] Solid phase extraction involving a variety of solid supports coupled with a suitable extractant is the desired choice for the remediation of chromium and mercury at low concentrations.

1.2.4 Solid Phase Extraction

Solid Phase Extraction (SPE) is an efficient separation method in environmental application[46] for the preconcentration of trace elements and their separation from various sample constituents. Solid-phase extraction (SPE) with the use of alkyl-bonded and other surface modified silica gels have been used in the last 15 years as an alternative to liquid–liquid extraction in the analysis of various samples. The method enables rapid and complete isolation of the analyte of interest from a complex matrix with a preconcentration factor of several orders of magnitude to be achieved. The fast adsorption kinetics and treatment of a large sample volume is another advantage of SPE. Polymeric resins, biopolymers and clay materials as supports can be customized to extract metal ions effectively from a complex matrix.

1.2.5 Polymeric Resins

Interest in the development of polymeric resin and their applications for the separation of metal ions in the form of a hybrid polymeric adsorbent material has intensified over the past few years.The ionic polymeric resins are essentially based on polystyrene-divinyl benzene (PS-DVB) copolymers. The porous resins have become effective sorbents for industrial wastewater treatment. These resins are physically and chemically stable, and

have vast surface area comparable to activated carbon. During the manufacturing process the pore structure and surface polarity of the resin may be controlled so that certain heavy metals could be preferentially adsorbed.[47]

The nonionic resins may be classified into three categories:

(i) Gel-type

(ii)Macroporous

(iii)Hypercrosslinked

(i) Gel-type Resin

The gel-type resins have a homogeneous, nonporous structure.[48] The polymeric network of the resin may swell in appropriate solvents.[49,50] However, these resins are poor sorbents to be used in wastewater treatment.

(ii) Macroporous Resin

Macroporous resins were first developed in the 1960's. These are capable of effectively adsorbing organic pollutants, due to their porous polymeric matrix.[51]

(iii) Hypercrosslinked Resin

These sorbents are produced by crosslinking polymers of macroporous resin in a suitable solvent.[52] The crosslinking strengthens the structure and modifies the surface properties of the porous polymeric network. As a result, hyper crosslinked resins have sorption characteristics superior to the macroporous sorbents.[53] Hyper crosslinked sorbents have been successfully applied for the removal and recovery of organic pollutants such as benzene derivatives and heterocyclic compounds. The advantages of macroporous and hypercrosslinked resin sorbents lies in the possibility of controlling their resin structure, internal surface area, and pore size distribution. This can be achieved by varying the polymerization conditions, such as the amounts of monomers added and pore-forming agents used in the polymerization reaction .[54,55]

1.2.6 Characteristics of Porous Resin Sorbents

The physical description of macroporous resins ranges from 'hard, sturdy insoluble spheres' for Amberlite XAD[54] to 'round plastic balls' and 'tough beads with high crush strengths' for Dowex based resins.[56] Macroporous resin sorbents have surface areas comparable to those of activated carbon. The surface areas of polystyrene-divinylbenzene

resin are reported to be as high as 750 m^2 g^{-1} for Amberlite XAD-4.[54] The pore diameter of polystyrene-divinylbenzene resins is about as 6 nm, and the pore volume varies from 10 to 90%. Commercial macroporous resin sorbents have an average pore diameter less than 100 nm. [54] Among the two most common macroporous resins, polystyrene-divinylbenzene resins are nonpolar and these are hydrophobic, whereas polyacrylate-divinylbenzene resins are relatively polar and hydrophilic. Figures 1.1 &1.2 illustrate the respective chemical structures of these two resins.[54] The polystyrene-divinylbenzene resins are mechanically less stable than the polyacrylate-divinylbenzene resins, attributed to the lesser reactivity between divinylbenzene and styrene in the copolymerization process.[57] The surface area of hypercrosslinked resin sorbents is greater than 800 m^2 g^{-1}. In general most of the Amberlite and Dowex based resins have surface areas close to 1000 m^2g^{-1}. The hyper crosslinked network exhibits a low packing density with more free volume and a highly coherent inner surface.[58]

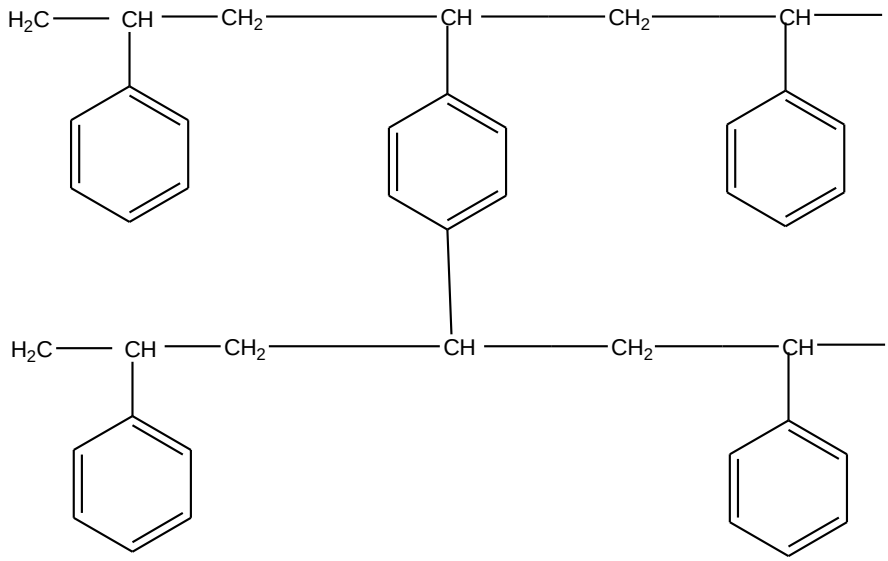

Figure 1.1 Structure of polystyrene-divinylbenzene resins, such as Amberlite XAD-2 and XAD-4

The hypercrosslinked resins consist of oxygen- and chlorine-containing functional groups, which are by- product residues of the crosslinking reaction. The presence of polar

functional groups on the surface of polystyrene-divinylbenzene copolymers results in an increase of surface polarity and hydrophilicity, and may enhance the sorption of polar sorbates.[59] Warshawsky[60] and Grinstead[61] were the first to describe the synthesis and applications of solvent impregnated resins (SIPR's) in 1971. Amberlite XAD resins (XAD-2, XAD-4, XAD-7, XAD-16, XAD-1180 and XAD-2000) are very useful for the removal and preconcentration of metals and its complexes. These resins possess surface area in the range 300-800 m^2g^{-1} with pore volume and average pore diameter in the range 0.9-1.5 cm^2g^{-1} and 4-9 nm respectively. This structure imparts excellent physical, chemical and thermal stability and is a good choice for the removal of variety of metal ions.[62] Chwastowska and Mozer[63] used an Amberlite XAD-4 loaded pyridylazo napthol for the preconcentration of Cu, Zn, Cd, Ni, Pb and Fe from river water. Cynex 302 loaded Amberlite XAD-8 resin matrix has been used for the quantitative sorption of Cu and Cd from 2.5 M HCl.[64] Amberlite XAD-7 and Amberlite XAD-4 resins loaded with oxine and 2-[2-(5-chloropyridylazo)-5-dimethylaminophenol] as extractants were used for the preconcentration of Ce^{3+}, La^{3+} and Pr^{3+} from aqueous solutions.[65] Maleic acid impregnated Amberlite XAD-4 was studied for the uptake of Cr(III, VI) from aqueous solution.[66]

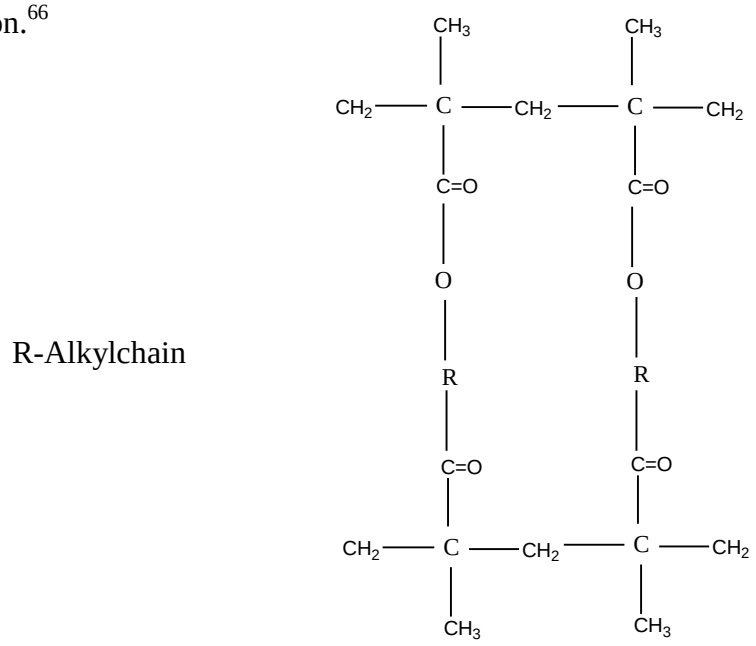

Figure 1.2. Structure of polyacrylate-divinylbenzene, such as Amberlite XAD-7

1.2.7 Amine-Impregnated Resins

The impregnated amines (usually long chain) are homogeneously dispersed on the PS-DVB backbone and are loaded by non-covalent interaction such as van der Waals or dipole-dipole interaction. The impregnation achieved either by dry method, wet method, modifier addition methods or by column method. After the amine impregnation, the solvent can be removed by gentle evaporation. A macromolecular resin containing tri-n-octylamine (TOA) yields highly selective separation of Zn(II), Cu(II) from a HCl solution.[67] The extraction of Au(III) from HCl solution with the extractant tri-n-dodecylammonium chloride impregnated in Amberlite XAD-2 resin was investigated and it was found that the system can be used to selectively extract gold from solutions containing zinc and copper.[68] The kinetics and equilibrium extraction of Pd(II), Pt(IV) and Rh(III) from HCl media using impregnated resins containing trioctyl and decyl amine (Alamine 336) impregnated onto Amberlite XAD-2 resin were studied and compared. The coextraction of Pd(II) and Pt(IV) from Rh(III) at low HCl concentrations was achieved, as well as partial separation of Pd(II) and Pt(IV) at high acid concentrations.[69] Solvent impregnated polymeric resins (SIPR's) can be prepared by a wet-impregnation technique using different polymer matrices, A quaternary ammonium salt (Aliquat 336) was employed as the extractant with acetone as the solvent for impregnation. Batch sorption studies showed that solvent-impregnated resins containing Aliquat 336 can be effectively used for the removal of hexavalent chromium from aqueous solutions.[70] Removal of Cr(VI) from aqueous solution was studied using SIPR's prepared by wet impregnation of Amberlite XAD-7 with Aliquat 336 as the extractant.[71]

1.3 Clays

Clays are hydrous aluminosilicate minerals that dominantly make up the colloid fraction of soils, sediments, rocks and water. Clay minerals can be classified into three groups as summarized. They are 2:1 type of clay, 1:1 type and layered silicic acids.[72]

(i) 2:1 Type Clay

These clays belong to the smectite family with the crystal structure consisting of nanometer thick layers of aluminium octahedron sheet sandwiched between two silica tetrahedron sheets (Figure 1.3). Stacking of the layers leads to van der Waals gap

between the layers. Isomorphic substitution of Al with Mg, Fe, Li in the octahedron sheets and/or Si with Al in tetrahedron sheets gives each three-sheet layer an overall negative charge, which is counterbalanced by exchangeable metal cations in the interlayer space, such as sodium.

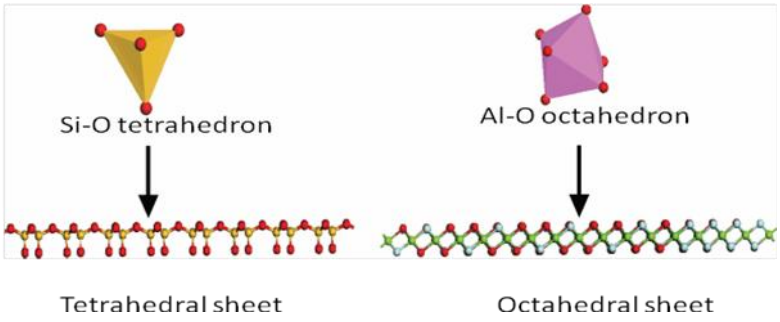

Figure 1.3 Silica and alumina tetrahedra and octahedra[72]

(ii) 1:1 Type Clay

The clays consist of layers made up of one aluminium octahedron sheet and one silica tetrahedron sheet. Each layer bears no charge due to the absence of isomorphic substitution in either octahedron or tetrahedron sheet (Figure 1.4).

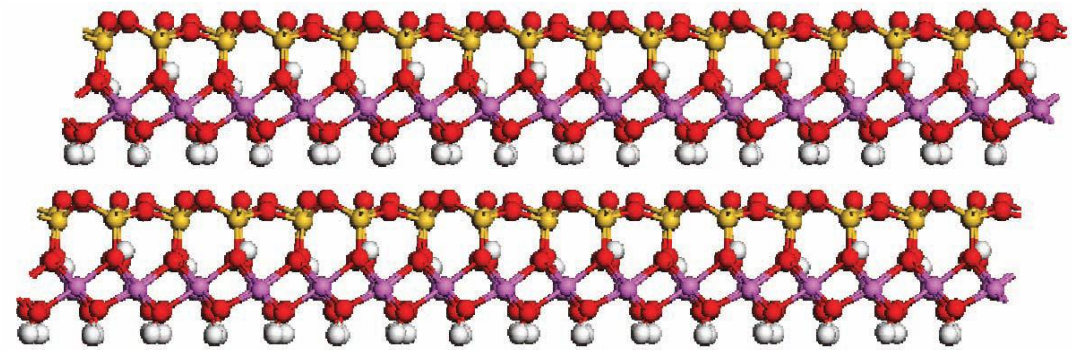

Figure 1:4 1:1 type clay[72]

Hence, except for water molecules neither cations nor anions occupy the space between the layers, and the layers are held together by hydrogen bonding between hydroxyl groups in the octahedral sheets and oxygen in the tetrahedral sheets of the adjacent layers.

(iii) Layered Silicic Acids

The clays consist mainly of silica tetrahedron sheets with different layer thickness. Their basic structures are composed of layered silicate networks and interlayer hydrated alkali metal cations. The silanol groups in the interlayer regions favour the organic modification by grafting organic functional groups in the interlayer regions (Figure 1.5). The different types of clay and specific examples are summarized in

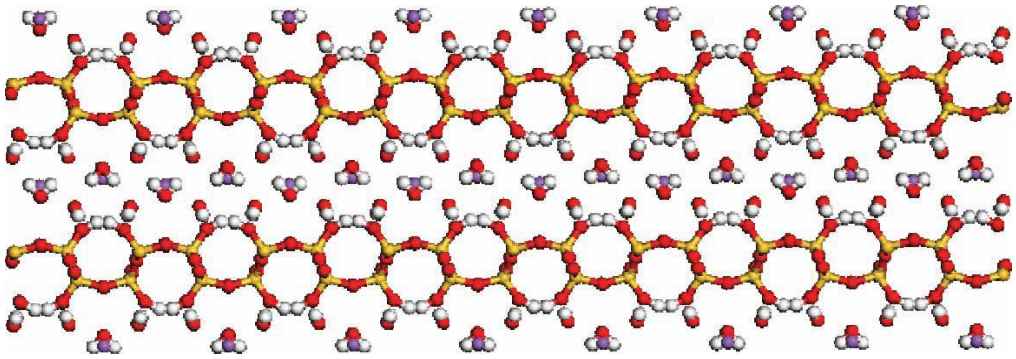

Figure 1.5 Layered silicic acids[72]

Table 1.1 Classification of clays[72]

Sl.No	Type of clay	Example	Formula	Substitution	Layered charge
1	2:1 type	Montmorillonite	$M_x(Al_{2-x}Mg_x)Si_4O_{10}(OH)_2 \cdot nH_2O$	Octahedral	Negative
2	1:1 type	Kaolinite	$Al_2Si_2O_5(OH)_4$	---------	Neutral
3	Layered Silicic Acids	Kanemite	$Na_2Si_4O_9 \cdot 5H_2O$	Tetrahedral	Negative

1.4 Montmorillonite (MMT)

Montmorillonite is a natural 2:1 type layered clay mineral with high cation exchange capacity, swelling ability and high surface area. Montmorillonite has been widely used in a number of industrial applications due to small particle size, bearing constant negative charge on surface and sheet-like structure.[73] Montmorillonite (MMT) clay, a type of layered silicate, naturally forms stacks of plate-like structures, or platelets (Figure 1.6). Stacking of layers leads to a regular van der Waals gap between them called as interlayer or gallery. The cations are attracted to the net negative charge within the clay platelets. The cations can be shared by two neighboring platelets, resulting in stacks of platelets that are closely held together.

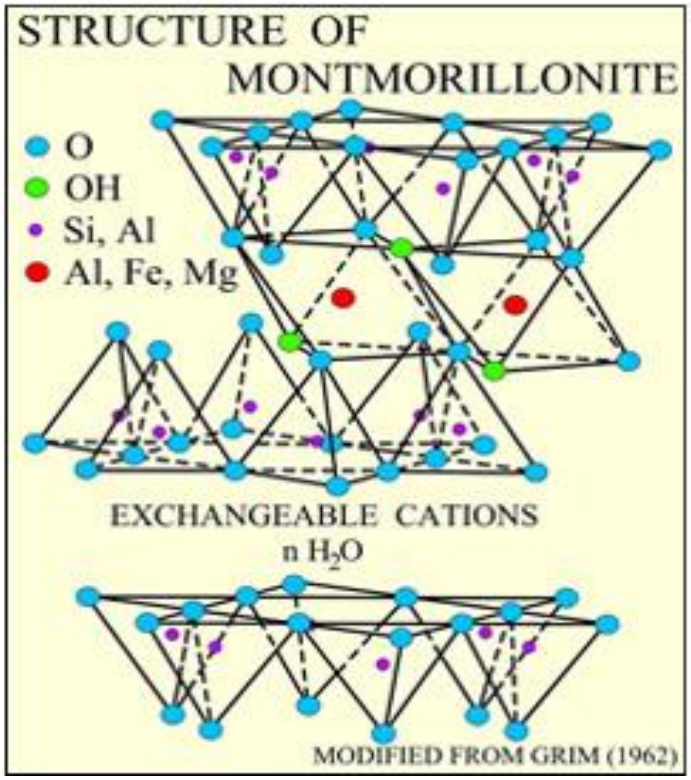

Figure 1.6 Structure of montmorillonite[74]

1.4.1 Surface Modifications

Surface modification of clay minerals has received attention since it fosters creation of new materials and applications. The organoclays produced by montmorillonite modified with quaternary alkylammonium cations have been used in a wide range of applications.[75] The potential of organoclays as an effective adsorbent for remediation of water contaminated by pollutants from industrial effluents is well known.[76] Organoclays are relatively low cost adsorbents and have been studied for the removal of hexavalent chromium present in water. [77-81] However, some aspects related to the adsorption of Cr(VI) onto the organoclay have not yet been fully elucidated. The research on heavy metal–clay surface interactions is of great interest and the clay minerals and their modified forms are widely used for the removal of these metals from aqueous solutions and remediation of contaminated soils.[82-85]

1.5 Organo Clays

The Na^+ form of montmorillonite is a 2:1 layered silicate that swells when contact with water.[86] The inner layer is composed of an octahedral sheet of the general form $M_{2-3}(OH)_6$ (where M is typically Al^{3+}), which is situated between two SiO_4 tetrahedral sheets.[87] The replacement of Al^{3+} for Si^{4+} in the tetrahedral layer and Mg^{2+} or Zn^{2+} for Al^{3+} in the octahedral layer results in a net negative charge on the clay surface. The charge imbalance is balanced by exchangeable cations such as H^+, Na^+ or Ca^{2+} on the layer surfaces. In aqueous solutions, water is intercalated into the interlamellar space of montmorillonite, leading to an expansion of the minerals. Clays, although possess negative surface charge, have little or weak affinity for heavy metal ions such as Co^{2+}, Zn^{2+}, and Cu^{2+}. Surfactants have been widely used to alter the surface properties of the swelling clays in order to improve the sorption ability.[88,89] Most of the previous studies focused on using cationic surfactants to adsorb organic matter and metallic anions including chromium.

1.6 Clay Composite

Polymer-clay hybrids have attracted considerable attention over the last decade. Many studies have been carried out on the preparation and characterization of nano composites with synthetic polymers and have been reviewed recently. [90,91]

1.6.1 Clay–Biopolymer Composites

Montmorillonite is naturally hydrophilic and this makes them poorly suited to mixing and interacting with most polymer matrices.[92] Hence, these clays must be suitably treated before they can be used to make a composite. Clay platelets are much larger than one nanometer in every dimension and preparing a composite out of untreated clay would not be a very effective use of material, because most of the clay would be stuck inside, unable to interact with the matrix leading to particle agglomeration. In contrast, favorable interactions between the polymer and clays lead to dispersed nanocomposite with enhanced properties. MMT clays have large active surface area of 700-800 m^2 g^{-1} and moderate negative surface charge. On treatment with surfactants, the silicate layers attain hydrophobic/organophilic character and results increase in the interlayer spacing. As the negative charge originates in the silicate layer, the cationic head group of surfactant resides at the layer interface and the aliphatic tail projects away from the surface. Hence, the spacing between the layers depends on the cation exchange capacity and the chain length of the quaternary ammonium cation. The preparation of layered silicate nanocomposites requires effective delamination of the layered clay structure and total dispersal of resulting platelets in the polymer matrix. Strong interfacial interaction between the polymer matrix and the clay is required and common methods to synthesize polymer nanocomposites are:

a) In-situ polymerization, in which the monomer migrates into the galleries of the layered silicate so that the polymerization can occur within the intercalated sheets.

b) Solution processing, in which the organoclays are added to the polymer solutions and mixed in a suitable solvent which is later removed using vacuum.

c) Melt intercalation, in which the layered silicate is mixed with the polymer matrix in the molten state.

All the methods yield the optimum dispersion of nanoclays. In principle, three different types of composites are evolved depending on processing conditions.[72]

(i) Conventional Composite

When the polymer does not intercalate between the silicate sheets and phase separated composite is obtained.

(ii) Intercalated Nano Composites

Herein, a single extended polymer chain is intercalated between the silicate layers resulting in a well ordered multilayer morphology with alternating polymeric and inorganic layers.

(iii) Exfoliated or Delaminated Nano Composite

When the silicate layers are completely and uniformly dispersed in a continuous polymer matrix it results in an exfoliated nanocomposite. These structures are shown in Figure 1.7.

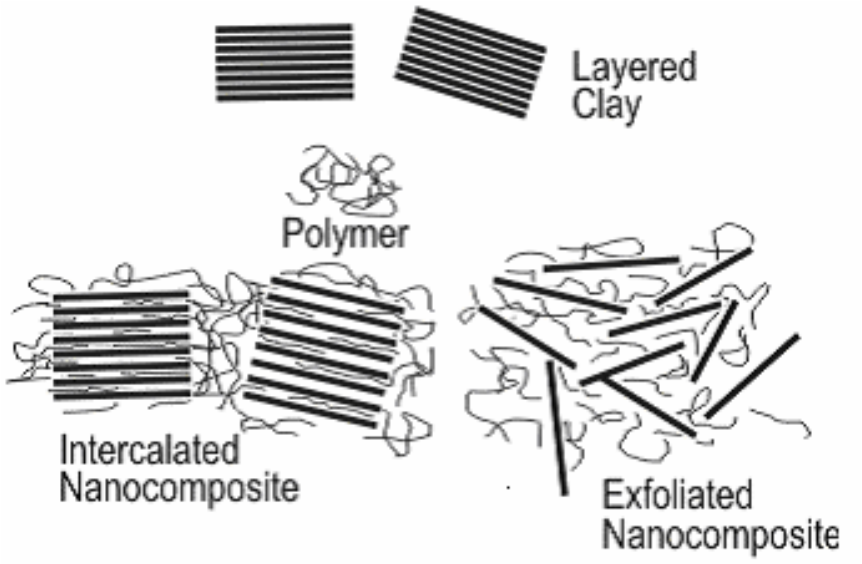

Figure 1.7 various types of clay–biopolymer composites

Nano composites based on the intercalation of chitosan, a cationic natural biopolymer, in Na^+ montmorillonite are known to be bidimensional nanostructured materials. This is due to the specific arrangement of the biopolymer as a bilayer when the amount of intercalated chitosan is higher than the cationic exchange capacity (CEC) of the clay.[93] The cationic biopolymer chitosan (poly-β (1,4)-2- amino-2-deoxy-D-glucose) can be intercalated in Na^+ montmorillonite through cationic exchange and hydrogen bonding interaction and the resulting nanocomposites show interesting structural and functional

properties.[94] The high mechanical strength, hydrophilic character and biodegradability makes chitosan an excellent chelating polymer for heavy metal removal.[95,96]

1.7 Chelating Adsorbents

Chelation originates from the Greek word "claw" or "grab" wherein the ligands in sorbents bind to the metal ions by complexation. A chelating adsorbent comprises of a chelating ligand moiety introduced into the polymeric frame work for the selective and specific complexation with the metal ion. The selectivity of the sorbents is governed primarily by the Pearson's hard-soft acid-base concept (HSAB)[11] and the ability of chelation highly depends on the favorable conditions created by donor and acceptor atoms (such as N, O, S, P, etc) of the functional group. These sorbents are well distinguished from conventional ion exchange resins by their high selectivity and fast sorption kinetics. The most important features of the chelating sorbents and their analytical properties depends on the nature of chemically active group, which is characterized as mono, di, or multidentate ligands and the appropriate solid supports that are being used for the chemical modification of different polymeric sorbents. [97]

1.7.1 Chelating Biopolymer Support

Biopolymers are known for heavy metal ion removal as well as solid support.[98] Biopolymers such as chitosan, lignocellulose, chitin, cellulose and lignin are known to adsorb heavy metal ions from aqueous solutions.[99] Among the various natural biopolymers, cellulose has attracted considerable attention for the removal of metal ions.[8,100] Cellulose is a polysaccharide with the formula $(C_6H_{10}O_5)_n$, consisting of a linear chain of several $\beta(1\rightarrow4)$ linked D-glucose units. Native cellulose is known to exist in two different crystalline forms I_α and I_β. Cellulose produced by algae and bacteria is rich in I_α while cellulose of higher plants consists largely the I_β form.[101] The property of cellulose depends on the degree of polymerization and this long chain macromolecule is held together by hydrogen bonding between the chains,[102,103] which results in high chemical and mechanical stability. The hydrophobic nature is attributed to the strong glycosidic bonds. These connect the cellobiose units and are responsible for the hydrophilic nature of the biopolymer. Unmodified cellulose has a low heavy metal adsorption, due to the non-availability of effective adsorption sites. Different kinds of

cellulose and its derivatives obtained from various sources have been utilized for the removal of metal ions. In view of the poor ion intake and selectivity, cellulose is seldom being used as such for conventional ion exchange. Hence, functionalization of cellulose in its hydroxyl group is used for the removal of heavy metals and these yield desirable properties such as higher adsorption capacity, distribution coefficient, fast sorption kinetics, etc. Different sorbents based on the cellulose are synthesized by functionalization, immobilization, etc. Specifically, two main approaches are utilized in the conversion of cellulose to its useful form for adsorbing heavy metal ions from aqueous solution i) direct modification, involving the cellulose backbone by way of introduction of chelating or metal binding functionalities, ii) grafting of selected monomers to the cellulose backbone and subsequent functionalization of these grafted polymer chains with certain chelating moieties. Ligands such as dithizone impregnated cellulose has been utilized for the recovery of Cu(II), Zn(II) and Ag(I) from sea water by column method.[104] Chelating agents bonded to cellulose support was used for the recovery of heavy metal ions from environmental samples.[105] The application of cellulose with suitable modifications for selective metal ions is given in Table 1.2. Although modified cellulose materials have several positive features, the ligand functionalization to the polymeric support results in limited sample breakthrough volume.

Table 1.2 Various functional groups modified cellulose for removal of heavy metals

S. No	Type of adsorbents	Metal ion removed	Reference
1	Polyacrylamide grafted coconut coir pith	Hg(II)	106
2	o-benzenedithiol-modified cellulose	Hg(II)	107
3	Polyacrylamide grafted on cotton cellulose	Hg(II)	108
4	Polyethyleneimine modified cellulose	Hg(II)	109
5	Cellulose powder modified with 2-aminoethanethiol	Hg(II)	110
6	Cotton cellulose grafted Acrylamide	Hg(II)	111
7	Cellulose grafted Glycidylmethacrylate	Cu(II), Pb(II), Ni(II)	112

1.7.2 Chitosan

Chitosan, a nitrogenous polysaccharide composed mainly of poly(β-1-4)-2-amino-2-deoxy-D-glucopyranose, is obtained through the deacetylation of chitin. Presently, chitosan attracts more interest as an effective adsorbent for heavy metals.[113] Chitosan is produced by alkaline N-deacetylation of chitin, which is widely found in the exoskeleton of crustaceans. The growing need for new sources of low-cost adsorbent, the rising problems of waste disposal and the increasing cost of synthetic resins undoubtedly make chitosan one of the best suited materials for wastewater treatment. Chitosan is biodegradable and non-toxic biopolymer with good adsorption capacity. However, chemical and physical modifications are to be carried out on chitosan to enhance the adsorption capacity and is well established as an excellent natural adsorbent for metal ions due to the presence of the amino ($–NH_2$) and hydroxyl (–OH) groups. These groups serve as effective coordination and reaction sites. [114-117] Apart from increasing the sorption properties these modifications allow the expansion of the porous network due to

the gel formation, which eventually decreases the crystallinity of the adsorbent. Chemical modifications also enhance the sorption properties while preventing the dissolution of chitosan in strong acids and improving the mechanical strength of chitosan. The chemical modifications may include cross-linking using a cross-linking agent, grafting of a new functional group and acetylation.[118,119] Chemical cross-linking can alter the crystalline nature of chitosan and enhance the resistance of chitosan against acid and alkali. Some of the most commonly used cross-linking agents include glutaraldehyde (GLA), epichlorohydrin (ECH) and ethylene glycol diglycidyl ether (EGDE). [120,121] Various researches on chitosan have been done in recent years and in 1988, the utilization of chitosan for cadmium removal was investigated. It was demonstrated that an adsorption capacity[122] 5.93 mg g^{-1} of Cd^{2+} chitosan could be achieved in the pH range 4.0–8.3. The interaction between chitosan and Cr(VI) was intensively investigated and it was observed that an adsorption capacity[123] 273 mg g^{-1} chitosan was achieved at pH 4.0. A comparative study on the adsorption capacity of chitosan for various metal ions such Cu^{2+}, Cd^{2+}, Ni^{2+} , Pb^{2+}, and Hg^{2+} reveals[124] that chitosan exhibits good binding capacity for Hg^{2+} (Table 1.3). Another similar research evaluated the sorption of some more metal ions onto chitosan. It was found that the maximum adsorption capacities[125] of chitosan for Hg^{2+}, Cu^{2+}, Ni^{2+} and Zn^{2+} were 815, 222,164 and 75 mg g^{-1}, respectively. However, the result of mercury removal was different from that obtained in the latter study which indicated that an adsorption capacity[126] 430 mg g^{-1} of Hg^{2+} was achieved by chitosan. In another study, adsorption of copper on chitosan revealed that 1 g chitosan could adsorb 4.7 mg Cu^{2+} at pH 6.2.[127] It was later reported that pH 5.5 was found to be optimum for copper removal and about 13 mg of Cu^{2+} could be absorbed by 1 g chitosan at equilibrium condition. The difference in chitosan adsorption capacity between the two studies is attributed to the fact that a bigger particle size of chitosan (200 mesh) was used in the former study.[128] The crosslinking effects of chitosan were also further investigated[129] and it was found that non crosslinked chitosan has a potential to adsorb 30 mg g^{-1} of Cr^{6+} chitosan.

Table 1.3 Chitosan based sorbents for some heavy metals

Sl. No	Material	Heavy metals (sorption capacity mg g^{-1})							Ref
		Cr^{6+}	Ni^{2+}	Pb^{2+}	Hg^{2+}	Zn^{2+}	Cu^{2+}	Cd^{2+}	
1	Chitosan	273							123
2			2.40	16.36	51.55		16.8	8.54	124
3			164		815	75	222		125
4					430				126
5								4.7	127
6								13.0	128
7	Crosslinked chitosan	50					86		129
8	Chitosan croos linked with ethylene glycol diglycidyl ether						46		130
9	Chitosan beads							250	131
10	Ethylenediamine-modified cross-linked magnetic chitosan resin	48.7							132
11	Aminated chitosan	28.7							133
12	Chitosan-Fecarbide nanoparticles	32.0							134

This is consistent with the fact that cross-linking reduces the adsorption capacity of chitosan, but this loss is necessary to ensure the stability of chitosan. Similar experimental work demonstrated the adsorption of Cu^{2+} onto chitosan crosslinked with ethylene glycol diglycidyl ether (EGDE).[130] Such an increase in particle size of chitosan, decreases the surface area available for adsorption, resulting in lower adsorption. The crosslinking effect of glutaric aldehyde(GDA) on the removal of Cd^{2+} using chitosan beads was demonstrated[131] and it was reported that the adsorption capacity of the crosslinked gel beads exponentially decreased by 60% from 250 mg g^{-1} of Cd^{2+}. A pH of 6.0 was found to be optimum for Cu^{2+} removal and that the uptake of Cu^{2+} on chitosan crosslinked with GLA, ECH and EGDE beads were 59.67, 62.47 and 45.94 mg g^{-1}, respectively. The adsorption capacity of the biopolymer based adsorbent[132-134] was listed in Table 1.3. Overall, the results mentioned previously indicate that chitosan is a good adsorbent for heavy metals. It is widely acknowledged that the excellent adsorption behaviour of chitosan for heavy metal removal is attributed to: (1) hydrophilicity of chitosan due to large number of hydroxyl groups, (2) Primary amino groups for effective coordination and (3) flexible structure of polymer chain of chitosan giving suitable conformation for adsorption of metal ions.

1.8 Exfoliated Graphene Oxide (EGO)

In the carbon family, graphene is a newly emerging carbon material with hexagonally, sp^2-hybridized and one-atom-thick layer structure.[135] It has attracted enormous attention due to its peculiar properties such as excellent electronic and mechanical properties and high thermal conductivity. Graphene is a giant aromatic macromolecule with several remarkable properties comparable to carbon nanotubes (CNT). Among the graphene derivatives, graphene oxide (GO) is of prime importance and has been extensively studied for various applications.[136] Graphene is regarded as a rising luminary in the carbon family in recent years owing its high specific surface area. Graphite is inexpensive and available in large quantities nevertheless it , does not readily exfoliate to yield individual graphene sheets. Graphene oxide considered as the oxidized graphene, contains oxygen-containing functional groups on the surfaces.[137] Considering the oxygen-containing functional groups and high surface area (theoretical value of 2620 m^2 g^{-1}), graphene oxide has high

sorption capacity. Graphene oxide is bestowed with multiple functional groups such as hydroxyl, carboxylic, carbonyl and epoxy for effective complexation with metal ions.

However, reports on the application of graphene oxide as sorbent for the removal of heavy metal ions from aqueous solution are limited. Graphene oxide has been utilized for the removal of heavy metal ions such as copper,[138] cadmium and cobalt,[139] mercury[140]and arsenic[141]from aqueous solution. Photocatalytic reduction of Cr(VI) has been reported using TiO_2 reduced graphene oxide composites.[142] The utility of graphene oxide has also been illustrated in the removal of humic acid[143] and organic dyes[144] from aqueous medium. The chemical reduction of Cr(VI) using EDTA reduced graphene oxide has been reported. [145] Graphene oxide also finds its application in a wide range of chemical transformations.[146]

1.9 Scope and Objective of the Work

The above account of a brief review for the detoxification of chromium and mercury shows that diverse materials and methods are employed in varying matrices. The innovations in the methodology have evolved with a view to overcome the drawbacks of the existing methods when applied to a specific problem. Since, each methodology differs with respect to selectivity and sensitivity, their field application depends on the nature of the samples to be treated. A cautious introspection reveals that there is an undeniable need to look for more effective remediation strategies. Taking into cognizance these aspects and other factors such as availability, biodegradability, greener solvents, etc efforts were focused towards the development of novel materials for the detoxification of chromium and mercury. Conventional, ultrasound and microwave assisted methods were employed in the preparation of adsorbent materials. The work presented in the following chapters deals with the development of the following:-

1. Solid phase extraction of Cr(VI) using amine impregnated resins, clays and surfactant modified clays intercalated onto the biopolymers (cellulose, chitosan).
2. Solid phase extraction of mercury using amine impregnated clays and 2-mercaptobenzothiazole impregnated onto cellulose biopolymer.

3. Solid phase extraction of Cr(VI) using ionic liquid impregnated onto exfoliated graphene oxide and chitosan.

Physicochemical and spectroscopic techniques were utilized for the characterization of the prepared adsorbent before and after adsorption of the metal ions. The effect of various analytical parameters such as pH, concentration of heavy metals, adsorbent dosage, contact time etc. was studied in detail. Adsorption isotherms, thermodynamics and kinetics of adsorption were also studied and column studies were performed to scale up the process. The developed methods were applied for the removal of chromium and mercury from electroplating, tannery and coal fly ash samples. The greener aspect in the developed methods is emphasized through the facile regeneration of the adsorbents.

Chapter 3 This chapter deals with the development of SPE methods for chromium using long chain amine impregnated synthetic polymeric sorbents such as Amberlite XAD-1180 and Amberlite XAD-4. The preparation, characterization, mechanistic aspects and application to the removal of carcinogenic chromium(VI) are discussed in detail.

Chapter 4 This chapter explains in detail the preparation, characterization, mechanistic aspects of various long chain amines intercalated onto the clays and its application to the removal of carcinogenic chromium(VI) and mercury. Biopolymers intercalated onto the surfactant modified clays and its application towards to the removal of chromium(VI) is also discussed in this chapter.

Chapter 5 This chapter explores in detail the preparation, characterization, mechanistic aspects of (a) Aliquat-336 (Room temperature ionic liquid) impregnated onto exfoliated graphene oxide and (b) Tetraoctylammonium bromide(TOABr) impregnated onto chitosan and their application towards the removal of Cr(VI). The last part of this chapter describes the interaction of 2-mercaptobenzothiazole impregnated onto cellulose and its application for demercuration from a used CFL lamp.

Chapter 6 This chapter presents the overall summary and important conclusions.

References

1. Malakul, P.; Srinivasan, K. R.; Wang, H. Y. *Ind. Eng. Chem. Res.* **1998,** *37,* 4296.
2. Mohan, D.; Singh, K. P. *Water Res.* **2002,** *36,* 2304.
3. Zizek, S.; Horvat, M.; Gibiar, D.; Fajon, V.; Toman, M. *Sci. Total Environ.* **2007,** *377,* 407.
4. Kalidhasan, S.; Sricharan, S.; Ganesh, M.; Rajesh, N. *J. Chem. Eng. Data* **2010,** *55,* 5627.
5. Galán, B.; Castañeda, D.; Ortiz, I. *Water Res.* **2005,** *39,* 4317.
6. Pugazhenthi, G.; Kumar, A. *AIChE J.* **2005,** *51,* 2001.
7. Rajesh, N.; Deepthi, B.; Subramaniam, A. *J. Hazard. Mater.* **2007,** *144,* 64.
8. Kalidhasan, S. PhD Thesis, **2012,** BITS-Pilani.
9. Mohan, D.; Pittman Jr., C. U. *J. Hazard. Mater.* **2006,** *137,* 762.
10. N. Rajesh, A.S. Krishna Kumar, S. Kalidhasan, V. Rajesh, *J. Chem. Eng. Data* **2011,** 56, 2295.
11. R. G. Pearson, *J. Am. Chem. Soc.* **1963,** *85,* 3533.
12. Irwin, R. J.; Mouwerik, M. V. N.; Stevens, L.; Seese, M. D.; Basham, W. Environmental Contaminants Encyclopedia Chromium(VI) (Hexavalent Chromium) Entry, National Park Service Water Resources Divisions, Fort Collins, CO, **1971.**
13. Saha, R.; Nandi, R.; Saha, B. *J. Coord. Chem.* **2011,** *64,* 1782.
14. Kimbrough, D. E.; Cohen, Y.; Winer, A. M.; Creelman, L.; Mabuni, C. A. *Crit. Rev. Environ. Sci. Technol.* **1999,** *29,* 1.
15. Clarkson, T.W. *Environ. Health. Perspect.* **1992,** *100,* 31.
16. Wilder Leonardo Gamboa Ruiz, PhD Thesis, **2010,** University of Barcelona, Spain.
17. http://en.wikipedia.org/wiki/Mercury_(element)
18. Fitzgerald, W. F.; D. R. Engstrom, R. P. Mason, D. A. Nater. *Crit. Rev. Environ. Sci. Technol.* **1998,** *32,* 1.

19. Clarkson, T.W.; Marsh, D.O. Mercury toxicity in man: A.S. Prasad (Ed.), Clinical, Biochemical, and Nutritional Aspects of Trace Elements, vol. 6, Alan R. Liss, Inc., New York, **1982,** pp. 549–568.
20. Sweet, L.; Zelikoff, T. *J. Toxicol. Environ. Health B,* **2001,** *4,* 161.
21. Chumchal, M. M.; Rainwater, T. R.; Osborn, S. C.; Roberts, A. P.; Abel, M. T; Cobb, G. P.; Smith, P. N; Bailey, F. C. *Environ. Toxicol. Chem.* **2011,** *30,* 1153.
22. Bussi, J.; Noel Cabrera, M.; Chiazzaro, J.; Canel, C.; Veiga, S.; Florencio, C.; Enrique, A.; Marcelo Belluzzi, D. *J. Chem Technol Biotechnol.* **2010,** *85,* 478.
23. Liu, Y.; Kelly, D. J.; Yang, H.; Lin, C. C. H.; Kuznicki, S. M.; Xu, Z. *Environ. Sci. Technol.* **2008,** *42,* 6205.
24. Baral, A.; Engelken, R. D. *Environ. Sci. Policy,* **2002,** *5,* 121.
25. Xu, Y.; Zhao, D. *Water Res.* **2007,** *41,* 2101.
26. Rengaraj, S.; Joo, C. K.; Kim, Y.; Yi, J. *J. Hazard. Mater.* **2003,** *102,* 257.
27. Shaalan, H.; Sorour, M.; Tewfik, S. *Desalination* **2001,** *14,* 315.
28. Salazar, E.; Ortiz, M. I.; Urtiaga, A. M. *Ind. Eng. Chem. Res.* **1992,** *31,* 1516.
29. Song, Z.; Williams, C. J.; Edyvean, R. G. J. *Water Res.* **2000,** *34,* 2171.
30. Chen, J. M. N.; Hao, O. J. N. *Crit. Rev. Environ. Sci.Technol.* **1998,** *28,* 219.
31. Ozaki, H.; Sharma, K.; Saktaywin, W. *Desalination* **2002,** *144,* 287.
32. Mohammadi, T.; Moheb, A.; Sadrzadeh, M.; Razmi, A. *Sep. Purif. Technol.* **2005,** *41,* 73.
33. Babel, S.; Kurniawan, T. A. *J. Hazard. Mater.* **2003,** *97,* 219.
34. Tels, M. *Resour. Conserv. Recycling.* **1987,** *14,* 71.
35. Wuilloud, J. C. A.; Wuilloud, R. G.; Olsina, R. A.; Martinez, L. D. *J. Anal. Atom. Spectrom.* **2002,** *17,* 389.
36. E.P.A. National Primary Drinking Water Regulations, 40 CFR Ch.I (7- 1-02 ed.), US Environmental Protection Agency (EPA), Washington, DC, **2002.** http://www.access.gpo.gov/nara/cfr/waisidx 02/40cfr141 02.html.
37. Balarama Krishna, M. V.; Karunasagar, D.; Rao, S. V.; Arunachalam, J. *Talanta* **2005,** *68,* 329.

38. Duan, T.; Song, X.; Xu, J.; Guo, P.; Chen, H.; Li, H. *Spectrochim. Acta.* **2009,** *61,* 1069.
39. Segade, S. R.; Tyson, J. F. *Talanta* **2007,** *71,* 1696.
40. Soliman, E. M.; Saleh, M. B.; Ahmed, S. A. *Anal. Chim. Acta* **2004,** *523,* 133.
41. Jiang, H.; Hu, B.; Jiang, Z.; Qin, Y. *Talanta* **2006,** *70,* 7.
42. Li, Y.; Hu, B. *Spectrochim. Acta* **2007,** *62,* 1153.
43. Wuilloud, J. C. A.; Wuilloud, R. G.; Silva, M. F.; Olsina, R. A.; Martinez, L. D. *Spectrochim. Acta* **2002,** *57,* 365.
44. Chen, J.; Chen, H.; Jin, X. Chen, H. *Talanta* **2009,** *77,* 1381.
45. S. Rio-Segade, C. Bendicho, *Talanta* **1999,** *48,* 477.
46. Camel, V.; *Spectrochim. Acta. Part B.* **2003**, *58*, 1177.
47. Tsyurupa M. P.; Maslova L. A.; Andreeva A. I.; Mrachkovskaya T. A.; Davankov V. A. *React. Funct. Polym.* **1995,** *25,* 69.
48. Okay O. *Prog. Polym.* **2000,** *25,* 711.
49. Davankov V. A.; Tsyurupa M. P. *Pure Appl. Chem.* **1989,** *61,* 1881.
50. Kunin R. Porous Polymers as Adsorbents-a Review of Current Practice. Rohm and Haas Company. Philadelphia, **1980.**
51. Weber W. J. Jr.; van Vliet B. M. *J. Am. Wat. Works Assoc.* **1981,** *73,* 420.
52. Davankov V. A.; Rogoshin S. V.; Tsyurupa, M. P. Macronet Polystyrene Structures for Ionites and Method of Producing Same. Patent USA 3729457, **1969.**
53. Streat M.; Sweetland L. A. *Trans I Chem E* **1998,** *76,* 115.
54. Kunin R. *Pure Appl. Chem.* **1976,** *46,* 205.
55. Weber W. J. Jr.; van Vliet B. M. *J. Am. Wat. Works Assoc.* **1981,** *73,* 426.
56. The Dow Chemical Company, Dowex Optipore Adsorbents: Fluidized bed properties of Dow Polymeric Adsorbents. **2001.**
57. Davankov V. A.; Rogoshin S. V.; Tsyurupa, M. P. *J. Polym. Sci.: Symposium* **1974,** *47,* 95.
58. Tsyurupa M. P.; Davankov V. A.; Rogoshin, S. V. *J. Polym. Sci: Symposium* **1974,** 47, 189.

59. Trochimczuk A. W.; Streat M.; Kolarz B. N. *React. Funct. Polym.* **2001,** *46,* 259.
60. Warshawsky, A. *Talanta* **1974,** *21*, 624.
61. Grinstead, R. R. Report by the Dow Chemical Co., On Contract No. 14-12-808 to the Water Quality Office of US Environmental Protection Administration, **1971.**
62. SivaKesavaRaju, CH. PhD Thesis, **2006,** IIT Madras, India.
63. Chwastowska, J.; Mozer, E. *Talanta*, **1985**, *32*, 574.
64. Kabay, N.; Demiraoglu, M.; Ekinci, H.; Yuksel, M.; Saglam, M.; Streat, M. *React. Funct. Polym*, **1998,** *38,* 219.
65. Masi, A. N.; Olsina, R. A. *Fresenius J. Anal. Chem.* **1997,** *357*, 65.
66. Yalcin, S.; Apak, R. *Anal. Chim. Acta*, **2004,** *505,* 25.
67. Akita, S.; Takeuchi, H. *J. Chem. Eng. Jpn.* **1990,** *23,* 439.
68. Villaescusa, I.; Salvado, V.; J. De Pablo, *React. Func. Polym.* **1997,** *32,* 125.
69. Rovira, M.; Cortina, J. L.; Arnaldos, J.; Sastre, A. M. *Solv. Extr. Ion Exch.* **1998,** *16,* 1279.
70. Kabay, N.; Arda, M.; Saha, B.; Streat, M. *React. Func. Polym.* **2003,** *54,* 103.
71. Saha, B.; Gill, R. J.; Bailey, D. G.; Kabay, N.; Arda, M. *React. Func. Polym.* **2004,** 60, 223.
72. Zeng, Q. H.; Yu, A. B.; Lu, G. Q.; Paul., D. R. *J. Nanosci. Nanotechnol.* **2005,** *5,* 1574.
73. Yuan, P.; Fan, M.; Yang, D.; M.; Hongping He, Liu, D.; Yuan, A.; Zhu, J. X.; Chen. T. H. *J. Hazard. Mater.* **2009,** *166,* 821.
74. Montmorillonite (http://pubs.usgs.gov/of/2001/of01-041/htmldocs/clays/smc.htm)
75. Paiva, L. B.; Morales, A.R.; Diaz, F. R.V. *Appl.Clay Sci.* **2008,** *42,* 8.
76. Beall, G. W. *Appl. Clay Sci.* **2003,** *24*, 11.
77. Krishna, B. S.; Murty, D. S. R, Jai Prakash, B. S. *Appl. Clay Sci.* **2001,** 20, 65.
78. Li, Z.; Bowman, R. S. *Environ. Eng. Sci.* **1998,** 15, 237.
79. Majdan, M.; Maryuk, O.; Pikus, S.; Olszewska, E.; Kwiatkowski, R.; Skrzypek, H. *J. Mol. Struct.* **2005,** *740*, 203.
80. Atia, A. A. *Appl. Clay Sci.* **2008,** *41,* 73.
81. Huang, Y.; Ma, X.; Liang, G.; Yan, Y.; Wang, S. *Chem. Eng. J.* **2008,** *138*, 187.

82. Abollino, O.; Aceto, M.; Malandrino, M.; Sarzanini, C.; Mentasti, E. *Water. Res.* **2003,** *37,* 1619.
83. Kaya, A.; Oren, A. H. *J. Hazard. Mater.* **2005,** *125,* 183.
84. Krikorian, N.; Martin, D. F. *J. Environ. Sci. Health, Part A* **2005,** *40,* 601.
85. Ozdemir, G.; Yapar, S. *J. Hazard. Mater.* **2009,** *166,* 1307.
86. Su-Hsia Lin, Ruey-Shin Juang, *J .Hazard. Mater.* **2002,** *92,* 315.
87. Zhu, L.; Ren, X.; Yu, S. *Environ. Sci. Technol.* **1998,** *32,* 3374.
88. Krishna, B. S.; Murty, D. S. R.; Jai Prakash, B. S. *J. Colloid Interface Sci.* **2000,** *229,* 230.
89. Huh, J. I.; Song, D. I.; Jeon, Y.W. *Sep. Sci. Technol.* **2000,** *35,* 243.
90. Ray, S. S.; Okamoto, M. *Prog. Polym. Sci.* **2003,** *28,* 1539.
91. Hussain, F.; Hojjati, M.; Okamoto, M.; Gorga, R. E. *J. Comp. Mat.* **2006,** *40,* 1511.
92. Alexandre M.; Dubois P. *Mater. Sci. Eng.* **2000,** *28,* 1.
93. Darder, M.; Colilla, M.; Ruiz-Hitzky, E. *Appl. Clay Sci.* **2005,** *28,* 199.
94. Darder, M.; Colilla, M.; Ruiz-Hitzky, E. *Chem. Mater.* **2003,** *15,* 3774.
95. Park, J. W.; Park, M.O.; Park, K. K. *Bull. Korean Chem. Soc.* **1984,** *5,* 108.
96. Tianwei, T.; Xiaojing, H.; Weixia, D. *J. Chem. Technol. Biotechnol.* **2001,** *76,* 191.
97. Nalwa, H. Advanced Functional Molecules and Polymers, vol.4, Gordon and Breach Science publishers, Singapore, **2001.**
98. Nevarez, N. M.; Casarrubias, L. B.; Canto, O. S.; Celzard, A.; Fierro, V.; Gomez, R. L. Sánchez, G. G. *Carbohydr. Polym.* **2011,** *86,*732.
99. Qian, L.; Zhang, H. *Green Chem.* **2010**, *12*, 1207.
100. Crini, G. *Prog. Polym. Sci.* **2005,** *30,* 38.
101. John, A.; Mahadeva, S. K.; Kim, *J. Smart Mater. Struct.* **2010**, *19,* 045011.
102. Pinkert, A.; Marsh, K. N.; Pang, S.; Staiger, M. P. *Chem. Rev.* **2009**, *109*, 6712.
103. 103. Klemm, D.; Heublein, B.; Fink, H. P.; Bohn, A. *Angew. Chem. Int. Ed.* **2005**, *44*, 3358.

104. Weliky, N.; Weetall, H.H.; Gilden, R.V.; Campbell, D. H. *Immunocemistry,* **1964,** *1,* 219.
105. O'Connell, D. W.; Birkinshaw, C.; O'Dwyer, T. F. *Bioresour. Technol.* **2008,** *99,* 6709.
106. Anirudhan, T. S.; Unnithan, M. R.; Divya, L.; Senan, P. *J. Appl. Polym. Sci*. **2007,** 104, 3670.
107. Takagai, Y.; Shibata, A.; Kiyokawa, S.; Takase. T. *J. Colloid Interface Sci.* **2011,** *353,* 593.
108. Bicak, N.; David, C.; Sherrington, D. C.; Senkala, B. F. *React. Funct. Polym.* **1999,** *41,* 69.
109. Navarro, R.; Sumi, K.; Fujii, N.; Matsumura, M. *Water Res.* **1996,** 30, 2488.
110. Aoki, N.; Fukushima, K.; Kurakata, H.; Sakamoto, M.; Furuhata, K. *React. Funct. Polym.* **1999**, *42*, 223.
111. Bicak, N.; Sherrington, D. C.; Senkal, B. F. *React. Funct. Polym.* **1999,** *41,* 76.
112. O'Connell, D. W.; Birkinshaw, C.; O'Dwyer, T. F. *J. Appl. Polym. Sci.* **2006,** *99,* 2888.
113. Wan Ngah, W. S.; Fatinathan, S. *Chem. Eng. J.* **2008,** *143,* 62.
114. Chang, M. Y.; Juang, R. S. *J. Colloid Interface Sci.* ***2004,*** *278,* 18.
115. Juang, R. S.; Shao, H. J. *Adsorption* **2002,** *8,* 71.
116. Wan Ngah, W. S.; Fatinathan, S. *Colloids Surf. A* **2006,** *277,* 241.
117. Wan Ngah, W.S.; Ghani, S. A.; Kamari, A. *Bioresour. Technol.* **2005,** *96,* 443.
118. Sun, S.; Wang, A. *Sep. Purif. Technol.* **2006,** 51, 409.
119. Sun, S.; Wang, A. *Sep. Purif. Technol.* **2006,** *49,* 197.
120. Lee, S. T.; Mi, F. L.; Shen, Y. J.; Shyu, S. S. *Polymer* **2001,** *42,* 1879.
121. Wan Ngah, W. S.; Endud, C. S.; Mayanar, R. *React. Funct. Polym.* **2002,** *50,* 625.
122. Jha, I. N.; Iyengar, L.; Rao, A. V. S. P. *J. Environ. Eng.* **1988,** *114,* 962.
123. Udaybhaskar, P.; Iyengar, L.; A.V. S. P. Rao, *J. Appl. Polym. Sci.* **1990,** 39, 739.
124. Huang, C. P.; Chung, Y.C.; Liou, M. R. *J. Hazard. Mater.* **1996,** *45,* 265.
125. McKay, G.; Blair, H. S.; Findon, A. *Ind. J. Chem.* **1989,** *28,* 356.

126. Peniche-Covas, C.; Alvarez, L. W.; Arguella-Monal, W. *J. Appl. Polym. Sci.* **1991,** *46,* 1147.
127. Wan Ngah, W.S.; Isa, I. M. *J. Appl. Polym. Sci.* **1998,** 67, 1067.
128. Annachhatre, A.P.; Win, N. N.; Chandrkrachang, S.; Stevens, W. J.; Rao, M. S.; Chandrkrachang, S. (Eds.), Proceedings of the Second Asia-Pacific Symposium, Asian Institute of Technology, Bangkok, Thailand, **1996,** pp. 169–173.
129. Schmuhl, R.; Krieg, H. M.; Keizer, K. *Water S.A.* **2001,** 27, 1.
130. Wan Ngah, W. S.; Endud, C.S.; Mayanar, R. *React. Funct. Polym.* **2002,** *50,* 181.
131. Hsien, T.Y.; Rorrer, G. L.; Chen, R. H.; Chen, H. S. (Eds.), Proceedings of the Third Asia-Pacific Symposium on Chitin and Chitosan, National Taiwan Ocean University, Keelung, Taiwan, **1998,** pp. 111–120.
132. Hu, X.J.; Wang, J. S.; Liu, Y.G.; Li, X.; Zeng, G. M.; Bao, Z. L.; Zeng, X. X.; Chen, A.W.; Long, F. *J. Hazard. Mater.* **2011,** *185,* 306.
133. Yan, Z.; Haijia, S.; Tianwei, T.; *Korean J. Chem. Eng.* **2007,** *24,* 1047.
134. Wu, Y.; Jiang, Y.; Han, D.; Wang, F.; Zhu, J. *Microchim. Acta* **2007,** *159,* 333.
135. Rao, C. N. R.; Sood, A. K.; Subrahmanyam, K. S.; Govindaraj, A. *Angew. Chem. Int. Ed.* **2009,** *48*, 7752.
136. Ramesh, P.; Bhagyalakshmi, S.; Sampath, S. *J. Colloid Interface Sci.* **2004,** *274,* 95.
137. Huang, X.; Yin, Z.; Wu, S.; Qi, X.; He, Q.; Zhang, Q.; Yan, Q.; Boey, F.; Zhang, H. *Small* **2011**, *7*, 1876.
138. Yang, S. T.; Chang, Y.; Wang, H.; Liu, G.; Chen, S.; Wang, Y.; Liu, Y.; Cao, A. *J. Colloid Interface Sci.* **2010,** *351*, 122.
139. Zhao, G.; Li, J.; Ren, X.; Chen, C.; Wang, X. *Environ. Sci. Technol.* **2011,** *45*, 10454.
140. Gao, W.; Majumder, M.; Alemany, L. B.; Narayanan, T. N.; Ibarra, M. A.; Pradhan, B. K.; Ajayan, P. M. *ACS Appl. Mater. Interfaces* **2011,** *3,* 1821.
141. Mishra, A. K.; S. Ramaprabhu, *J. Hazard. Mater.* **2011,** *185,* 322.
142. Liu, X.; Pan, L.; Lv, T.; Zhu, G.; Lu, T.; Sun, Z.; Sun, C. *RSC Adv.* **2011,** *1,* 1245.

143. Hartono, T.; Wang, S.; Ma, Q.; Zhu, Z. *J. Colloid Interface Sci.* **2009,** *333*, 114.
144. Ramesha, G. K.; Kumara, A. V.; Muralidhara, H. B.; Sampath, S. *J. Colloid Interface Sci.* **2011,** *361,* 270.
145. Hui-Ling Ma, Zhang,Y.; Qi-Hui Hu, Yan, D;. Zhong-Zhen Yu; Zhai, M. *J. Mater. Chem.* **2012,** *22,* 5914.
146. Dreyer, D. R.; Park, S.; Bielawski, C.W.; Ruoff, R. S. *Chem.Soc. Rev.* **2010,** *39,* 228.

MATERIALS AND METHODS

This chapter gives an outline of the materials used and the general experimental procedures for the detoxification of chromium and mercury.

2.1 Chemicals and Reagents

Analytical grade reagents were used throughout. The aqueous solutions were prepared in Milli Q water (Elix 3, conductivity 0.12 µS cm^{-1}). Amberlite XAD-1180 (Fluka, 20-50 mesh), Montmorillonite (Sigma Aldrich), Montmorillonite (Fluka), graphite (Sigma Aldrich), 2-mercaptobenzothiazole (Sigma Aldrich), Cetyltrimethylammoniumbromide (CTABr) (Sisco Research Laboratories, India), Amberlite XAD-4, chitosan, cellulose, are obtained from Himedia, India. Trioctylamine (Spectrochem, India), n-octylamine (Spectrochem, India), do-decylamine (Himedia, India), Mercury chloride ($HgCl_2$), Potassium dichromate ($K_2Cr_2O_7$), diphenylcarbazide, ascorbic acid (AA), nitric acid (HNO_3), sulfuric acid (H_2SO_4), hydrochloric acid (HCl), Hydrogen peroxide (H_2O_2) sodium hydroxide (NaOH), thiourea ($(NH_2)_2C=S$), sodium nitrite ($NaNO_2$), sodium sulphite (Na_2SO_3), sodium metabi-sulphite, tricaprylmethylammoniumchloride, (Aliquat 336), tetraoctylammoniumbromide (TOABr), methanol and acetone, are procured from S.D. Fine Chemicals, Mumbai (India) and Merck (India) respectively. Industrial waste water samples were collected from Chennai and Bangalore (India).

2.2 Physico-chemical Characterization Instruments

The pH of the reaction medium was adjusted using an Elico LI-127, model pH meter. Domestic microwave oven (LG India) with a power range of 700W and an Ultrasonic bath (Biotechnics, India) with frequency 18 kHz was used in the preparation of the adsorbent. Batch adsorption studies were performed using an orbital incubator shaker (Biotechnic, India). A peristaltic pump (DBK, India) was utilized to permeate the working solution for packed bed column studies. The FT-IR Spectra of the samples were recorded using Jasco-V-650 FT-IR, as well as Jasco-4200 FT-IR spectrometer in the range of 4000-400cm^{-1}using KBr (spectroscopy grade) with high resolution. The solid state ^{13}C NMR spectra (CP-MAS) were recorded with Bruker DSX-300 NMR spectrometer with 75.4 MHz at ambient temperature. The change in morphology of the

polymeric sorbent was acquired using Hitachi S-3000H Scanning electron microscope (SEM) and JEOL JSM-6390. Brunauer Emmett Teller(BET) surface area measurements were performed with a Micromeritics Porosimeter model ASAP 2020 analyzer in nitrogen atmosphere and this was out gassed at room temperature for 12 hr. The XRD pattern was recorded in a XPERT-PRO X-ray diffractometer using CuKα radiation in the 2θ range of 1-60º. The Energy Dispersive X-ray spectrum (EDS) was recorded with a Hitachi S-3000H spectrometer and JEOL JSM-6390, in the range 0-10 keV and the concentration of chromium in the aqueous phase was analyzed quantitatively with the help of Jasco V-650 UV- visible spectrophotometer respectively. 1 cm matched quartz cells were used for the absorbance measurements. An Olympus CH20i model optical microscope was used to obtain the images of the adsorbent before and after the adsorption of chromium and mercury. Mercury was analyzed by CV-AAS technique using a mercury analyzer (Model MA 5840, Electronics Corporation of India Ltd. Hyderabad, India).

2.3 Analysis of Hexavalent Chromium

The concentration of chromium in the aqueous phase was analyzed by the standard spectrophotometric method.[1] This involves the formation of red-violet complex of Cr(VI) with diphenylcarbazide method at λ_{max}540 nm. In the estimation of total chromium, the samples were oxidized using alkaline peroxide (H_2O_2/NaOH) to the hexavalent state and analyzed spectrophotometrically**.**

2.4 Analysis of Mercury

The concentration of Hg(II) in the solution phase was estimated by the standard Cold Vapour-Atomic Absorption Spectrophotometric (CV-AAS) technique.[2] The generation of mercury vapor was analyzed by CV-AAS technique using a mercury analyzer (Model MA 5840, Electronics Corporation of India Ltd. Hyderabad, India), which provides lower detection limit for mercury and has found widespread application for this determination. The sample solution containing mercury is subjected to chemical reduction using $SnCl_2$ and the elemental mercury formed is carried to a spectrophotometric cell by a stream of air for adsorption measurement at 253.7 nm. The technique has been found useful for the determination of as low as 10 ng of mercury.

2.5 Adsorption Studies

2.828 g of potassium dichromate was diluted to 1000 mL with Milli Q water to give 1000 μg mL^{-1} Cr(VI). Adsorption experiments were performed by a known weight of the adsorbent with Cr(VI) of a known concentration at various time intervals in an orbital incubator shaker. The pH of the medium was adjusted to the required range using sulfuric acid, hydrochloric acid and sodium hydroxide respectively. After the attainment of equilibrium, the reaction mixture was filtered and the percentage of chromium removed from the reaction mixture was estimated by measuring the concentration in the liquid phase by standard spectrophotometric method at λ_{max} 540 nm. Mercury vapor was analyzed by CV-AAS technique using a mercury analyzer at 253.7 nm. The metal ion uptake by adsorbent was calculated from the difference between the initial and equilibrium concentration in the aqueous phase as follows, [3]

$$q_e = \frac{(C_o - C_e)\ V}{W} \qquad (1)$$

Where q_e is the amount of chromium /mercury adsorbed at equilibrium (mg g^{-1}), C_o and C_e refer to the initial and equilibrium Cr(VI)/Hg(II) concentration (mg L^{-1}), W is adsorbent dosage (g) and V is the solution volume (L).

2.5.1 Langmuir Adsorption Isotherm

The Langmuir adsorption isotherm[4] is based on the fact that adsorption is homogeneous and monolayer coverage. The isotherm also assumes that all the sites are equivalent with uniform surface coverage. The ability of a molecule to adsorb at a particular site is independent of the occupation of neighboring sites. The Langmuir equation can be used for describing equilibrium conditions for the adsorption behavior in various adsorbate-adsorbent systems. The Langmuir equation is given by

$$q_e = \frac{q_o b\, C_e}{1+bC_e} \qquad (2)$$

The linear form of the Langmuir isotherm model is described as

$$\frac{C_e}{q_e} = \frac{1}{q_o b} + \frac{C_e}{q_o} \qquad (3)$$

Where 'C_e' is the equilibrium metal ion concentration and 'q_e' is the amount of adsorbate adsorbed per gram of adsorbent at equilibrium (mg g^{-1}); 'q_o' and 'b' are Langmuir constants related to the sorption capacity and intensity respectively. A plot of C_e/q_e vs C_e gives the q_o and b. The feasibility of the adsorption process is also determined by R_L, known as the separation factor, which is given as

$$R_L = \frac{1}{1 + bC_o} \qquad (4)$$

The R_L value has considerable importance when it is between 0-1, [5] where it implies an effective interaction between the adsorbent and the adsorbate. The values greater than 1 are an indication of an unfavorable isotherm and R_L equal to zero is accounted for a totally irreversible isotherm. These features are summarized in Table 2.1

Table 2.1. R_L Values with the type of equilibrium isotherms

R_L value	Nature of equilibrium isotherm
$R_L > 1$	Unfavorable
$R_L = 1$	Linear
$0 < R_L < 1$	Favorable
$R_L > 0$	Irreversible

2.5.2 Freundlich Isotherm

The Freundlich isotherm[6] pertains to monolayer (chemisorption) and multilayer adsorption (physisorption) and is based on the assumption that the adsorbate adsorbs onto the heterogeneous surface of an adsorbent. The Freundlich adsorption equation can be expressed

$$q_e = K_F C_e^{1/n} \quad (5)$$

The linear form of this isotherm model is given as

$$\log q_e = \log K_F + \frac{1}{n} \log C_e \quad (6)$$

K_F and n are the Freundlich constants that indicate the adsorption capacity and the adsorption intensity respectively. A favorable adsorption would to have Freundlich constant n between 1 and 10. A higher value of n (smaller value of 1/n) implies effective interaction between the adsorbent and adsorbate. When $1/n < 1$, it corresponds to a normal L-type Freundlich isotherm[7] while $1/n > 1$ reflects a co-operative sorption.[8] The logarithmic plot of q_e against C_e gives the constants K_F and n.

2.5.3 Redlich–Peterson (R-P) Isotherm

The Redlich–Peterson model relates the amount of chromium(VI) adsorbed at equilibrium q_e and the respective isotherm constants A, B and an exponent g given by the equation.[9]

$$q_e = \frac{AC_e}{(1 + BC_e^{g})} \quad (7)$$

In an efficient adsorption process the value of g lies between 0-1. Furthermore, when the exponent g equals unity, the above expression reduces to the simple Langmuir isotherm equation. The relevant isotherm parameters were obtained from the linearized expression

$$\ln(AC_e / q_e - 1) = g \ln C_e + \ln B \quad (8)$$

The parameters g and B are obtained from the slope and intercept of the plot ln (AC_e / q_e-1) against ln C_e.

2.5.4 Dubinin–Radushkevich (D-R) Isotherm

The adsorption mechanism and the interaction between adsorbate and adsorbent can be modeled through D-R isotherm[10] where q_m is the maximium adsorption capacity and β is

a constant related to adsorption energy (mol^2KJ^2). The values of q_m and β were computed from the slope and intercept of the plot lnq_e vs ε^2

$$\ln q_e = \ln q_m - \beta \varepsilon^2 \qquad (9)$$

Another parameter called the Polanyi potential (ε) is related through the expression

$$\varepsilon = RT \ln\left(1 + \frac{1}{C_e}\right) \qquad (10)$$

In addition, the adsorption energy is related to the mean free energy E_{DR} (KJ mol^{-1}) of adsorption and the constant β can be related through the expression

$$E_{DR} = 1/(2\beta)^{-0.5} \qquad (11)$$

The nature of the adsorption mechanism is ascertained from the E_{DR} values. The mean free energy value lying between 1-8 kJ mol^{-1} indicates physisorption and 8-16 kJ mol^{-1} reflects ion exchange adsorption.[11]

2.5.5 Temkin Isotherm

The Temkin isotherm model is based on the assumption that the adsorption energy decreases linearly with the surface coverage. The Temkin isotherm is best expressed as [12]

$$q_e = \frac{RT}{b} \ln A + \frac{RT}{b} \ln Ce \qquad (12)$$

where RT/b = B. The linear plot of q_e versus lnC_e gives the constants A and B. The variation of adsorption energy and the Temkin equilibrium constant can be calculated from the slope and the intercept of the plot q_e versus lnC_e.

2.5.6 Elovich Isotherm

Elovich model[13] is based on the fact that the adsorption sites increase exponentially with adsorption, thereby leading to a multilayer adsorption. The Elovich equation is expressed in linearized form as

$$\ln\left(\frac{q_e}{C_e}\right) = \ln\left(K_E q_m\right) - \frac{q_e}{q_m} \qquad (13)$$

where K_E is the Elovich equilibrium constant (L mg^{-1}) and q_m is the Elovich maximum adsorption capacity (mg g^{-1}) The respective isotherm parameters can be obtained from the slope and the intercept of the plot ln (q_e/C_e) against q_e

2.6 Adsorption Kinetics

The study of the kinetics of adsorption is an important parameter to find the rate of adsorption process and this indicates the efficiency of the method. The kinetics of adsorption process depends on the time dependence and the concentration distribution of the metal ion in both bulk solution and solid sorbent. The pseudo first and second order kinetic models were applied to the experimental data obtained in order to investigate the adsorption mechanism of metal ion on a specific adsorbent.

The study of adsorption kinetics in wastewater provides valuable insight into the reaction pathway and the mechanism. Generally, the adsorption is assumed to take place by utilizing the following mechanisms: [14]

(i) external mass transfer

(ii) Intra-particle diffusion

(iii) physical / chemical adsorption

2.6.1 Pseudo First Order Kinetics

The first-order rate expression of Lagergren[15] can be expressed mathematically as

$$\log (q_e - q_t) = \log q_e - \frac{k_1 t}{2.303} \qquad (14)$$

where q_e and q_t (mg g^{-1}) are the amounts of chromium or mercury adsorbed per unit mass of adsorbent at equilibrium and time, t(min), respectively, and k_1 is the rate constant. The value of adsorption rate constant (k_1) for the sorbents at different initial chromium/mercury concentrations were obtained from slopes of the plots of log (q_e-q_t) vs time

2.6.2 Pseudo-Second Order Kinetics

A pseudo second order reaction model [16] utilized in the study of adsorption can be expressed mathematically as:

$$\frac{t}{q_t} = \frac{1}{k_2 q_e^2} + \frac{t}{q_e} \qquad (15)$$

Where k_2 (g $mg^{-1}min^{-1}$) is the equilibrium rate constant of pseudo second order adsorption. The slope and intercept of the plot of t/q_t against t gives the parameters q_e and k_2 respectively.

2.6.3 Intraparticle Diffusion

In order to interpret the adsorption mechanism, it is necessary to identify the steps that overall govern the adsorption of Cr(VI)/ Hg(II) on the sorbent. The mathematical models proposed by Boyd et al.[17] and Reichenberg[18] is used to differentiate between the intra-particle and mass transfer controlled mechanisms. The three main steps involved in the uptake of Cr(VI)/ Hg(II) by the sorbent are

(i) Transport of Cr(VI)/Hg(II) from bulk solution to the external surface of the sorbent.

(ii) Transport of sorbate into the pores of the sorbent.

(iii) Adsorption of metal ion on the surface of the sorbent.

It is generally accepted that the third process is quite rapid and does not represent the rate determining step in the uptake of Cr(VI)/Hg(II).

In the first case, the transport of ions to the boundary occurs, thereby leading to the formation of liquid film with a concentration gradient surrounding the sorbent. Besides, adsorption on the outer surface of adsorbent, there is also a possibility of transport of adsorbate ions from the solution into the pores of the sorbent (pore diffusion) due to the rapid stirring in a batch process. However, when pore diffusion limits the adsorption process, the relationship between initial solute concentration and the rate of adsorption would not be linear. The Weber-Morris model is adopted to study the intra-particle

diffusion and this relates the amount of chromium and mercury adsorbed against square root of time.[19]

$$q_t = k_{int}\sqrt{t} + C \qquad (16)$$

where k_{int} is the intra-particle diffusion constant and q_t is the amount of chromium (VI)/ mercury adsorbed at time t. A linear plot of q_t vs $\sqrt{t}$ with non-zero intercept signifies that the intraparticle diffusion is not the only rate limiting step.

2.7 Adsorption Thermodynamics

The study of thermodynamics is an important factor in SPE in order to ascertain the feasibility and nature of the adsorption process. The thermodynamic parameters namely, standard free energy (ΔG^o), standard enthalpy (ΔH^o) and standard entropy (ΔS^o) changes were determined at various temperature ranges. These parameters were obtained from the following equations. [20, 21]

$$\Delta G^o = -RT \ln K \qquad (17)$$

$$\ln K = \frac{-\Delta H^o}{RT} + \frac{\Delta S^o}{R} \qquad (18)$$

Where is R is gas constant (J K^{-1} mol^{-1}), T is the temperature (Kelvin) and K is obtained from the ratio of the concentration of Cr(VI)/Hg(II) in the solid and liquid phase respectively. The Van't slope and intercept in the plot of ln K vs 1/ T gives the parameters ΔH^o and ΔS^o respectively.

2.8 Application to Industrial Effluents for Chromium Removal

The application and validation of the method was tested in a tannery effluent. The total chromium present in the tannery effluents were determined after removing the organic matter by digestion with HNO_3-H_2SO_4 mixture followed by alkaline peroxide oxidation.[22] The concentration of chromium was estimated by the standard spectrophotometric method using diphenylcarbazide at λ_{max}540 nm. The Cr(III)

concentration is calculated from the difference between the total Cr(III) and Cr(VI) concentrations.

2.9 Application to Study the Removal of Mercury from a Coal Fly Ash Sample

Fly ash is an important source of mercury pollution generated in thermal power plants and comprises of fine particles that rise with the flue gases.[23] In addition to mercury, some of the major metallic constituents present in fly ash include aluminum, iron, manganese, chromium, arsenic and lead. [24] The fly ash sample was collected from a thermal power plant. A known weight of the sample was pretreated using HF-HNO_3-H_2SO_4 mixture [24], filtered and diluted to a known volume prior to the adsorption and analysis of mercury.

References

1. Mendham, V. J.; Denny, R. C.; Barnes, J. D.; Thomas, M. J. K. Vogel's Textbook of Quantitative Chemical Analysis, 6th Ed., *Pearson education, Singapore:* **2002**, *1*, 668.
2. Karunasagar, D.; Balarama Krishna, M. V.; Anjaneyulu, Y.; Arunachalam. *J. Environ. Pollut.* **2006,** *143*, 153.
3. Rajesh, N.; Krishna Kumar, A. S.; Kalidhasan, S.; Rajesh. V. *J. Chem. Eng. Data* **2011,** *56*, 2295.
4. Langmuir, I. *J. Am. Chem. Soc.***1918**, *40*, 1361.
5. Hall, K. R.; Eagleton, L. C.; Acrivos, A.; Ver Meulen, T. *Ind. Eng. Chem. Fundam.* **1966,** *5*, 212.
6. Freundlich, H. M. F. *Z. Phys. Chem.* **1906,** *57*, 385.
7. K. Selvi, S. Pattabhi and K. Kadirvelu, *Bioresour. Technol.* **2001,** *80*, 87.
8. V. K. Garg, R. Gupta, R. Kumar and R. K. Gupta, *Bioresour. Technol.,* **2004,** *92*, 79.
9. Redlich, O.; Peterson, D. L. *J. Phys. Chem.* **1959,** *63*, 1024.
10. Dubinin, M. M.; Radushkevich, L.V. *Proc. Acad. Sci. USSR. Phys. Chem. Sect.* **1947,** *55*, 331.
11. Srivastava, V.; Weng, C. H.; Singh, V. K.; Sharma, Y. C. *J. Chem. Eng. Data* **2011**, *56*, 1414.

12. Temkin, M. I. *Zh. Fiz. Chim*. **1941,** *15*, 296.
13. Elovich, S. Y.; Larinov, O. G. *Izv. Akad. Nauk. SSSR, Otd. Khim. Nauk* **1962,** *2*, 209.
14. Wang, S. S.; Zhou, Y.; Jiang, Y.; Sun, C. *J. Hazard. Mater.* **2008**, *157*, 374.
15. Lagergren, S. *Sven. Vetenskapsakad. Handl.* **1898,** *24*, 1.
16. Ho, Y. S. *J. Hazard. Mater.* **2006,** *B136*, 681.
17. Boyd, G. E.; Adamson, A. W.; Mayers, L. S. *J. Am. Chem. Soc.* **1947**, *69*, 2836.
18. Reichenberg, D. *J. Am. Chem. Soc.***1953**, *75*, 589.
19. Weber, W. J.; Morris, J. C. *J. Sanit. Eng. Div. Am. Soc. Civ. Eng*. **1963,** *89*, 31.
20. Sun, X.; Wu, D.; Chen, J.; Li, D. *J. Chem. Technol. Biotechnol.* **2007**, *82*, 267.
21. Ozcan, A. S.; Ozcan, A. *J. Colloid Interface Sci.* **2004**, *276*, 39.
22. Balasubramanian, S.; Pugalenthi, V. *Talanta* **1999,** *50*, 45.
23. Liu, Y.; Kelly, D. J.; Yang, H.; Lin, C. C. H.; Kuznicki, S. M.; Xu, Z. *Environ. Sci. Technol.* **2008**, *42*, 6205.
24. Sushil, S.; Batra, V. S. *Fuel* **2006,** *85*, 2676.

Long Chain Amine Impregnated Polystyrene-Divinylbenzene Polymeric Sorbents for the Removal of Chromium

3.1 Introduction

This chapter deals with the adsorption of chromium using amine impregnated polymeric resin matrix. Over the past few decades,[1] porous polymeric resin has emerged as a potential alternative to activated carbon due to its controllable pore structure and stable physical and chemical properties, as well as regenerability of adsorbent. They are widely used as an adsorbent in purification and separation processes.[2,3] Porous polymeric resins can be classified into two categories namely, macroporous and hypercrosslinked. These resins are produced by suspension copolymerization of a monomer and a cross-linking agent.[4,5] Conventional polymer-based chelating ion-exchange resins[6] have great selectivity for the separation of various metal ions. Solvent-impregnated Polymeric resins (SIPR's) can be considered as alternative adsorbent materials since they are also capable of selective sorption. Lederer and co-workers[7] first reported the use of solvent impregnated ion-exchange resins (containing Dowex-50), with HCl as a developing solvent, for the following separations: Cu–Cd, Th–Fe–UO_2^{++}, Th–Ce–Fe, Al–Zr and Ti–Fe–Al. Warshawsky [8] and Grinstead[9] were the pioneers responsible for introducing the concept, synthesis and applications of ''solvent-impregnated resins" for metal removal. Warshawsky[10]tested diphenylglyoximes impregnated onto macroreticular XAD-2 resin beads and found that the β-isomeric form sorbed palladium and nickel with a selectivity factor of 20 and 100. respectively. Warshawsky and Berkovitz[11] have also reported the use of hydroxyoxime based solvent impregnated resins for selective copper extraction. Warshawsky et al. [12] also synthesized SIPRs incorporating phosphoric acid and phosphoric ester compounds compounds for the selective removal of zinc from cobalt and the extraction of uranium from nitric acid solution. In 1981, an exhaustive review of the preparation and potential applications of SIPRs has been reported.[13] Literature survey reveals that the various ligand loaded Amberlite XAD resins have been used as sorbents for the detoxification of heavy metals.[14-16]

Herein, we present a novel and environmentally benign approach for the removal of chromium based on the impregnation of trioctylamine (TOA) and n-octylamine on macroporous Amberlite XAD-1180 and XAD-4 polymeric matrix.

The first part of this chapter deals with an enhanced method for the adsorption of chromium by impregnation of trioctylamine in a Amberlite XAD-1180 resin matrix.

The second part of this chapter deals with the impregnation of n-Octylamine in Amberlte XAD-4 polymeric matrix and its application towards the adsorption of chromium.

Trialkylamine impregnated macroporous polymeric sorbent for the effective adsorption of chromium

3.2.1 Introduction

This chapter discusses the trialkylamine impregnated macroporous polymeric sorbent for the effective removal of chromium. Amberlite XAD-1180 belongs to one such class of resins known to have high surface area, excellent physical, thermal and chemical stability. Even though the literature reveals an upswing in the number of methods for the detoxification of chromium, [17,18] there is a need to seek more efficient and improved methods for its removal from various sources. Low cost adsorbents such as activated carbon,[19] wheat residue derived black carbon, [20] agricultural biowaste [21]and so forth are known for the solid phase extraction and speciation of chromium. Dowex M4195 chelating resin,[22] functionalized pyridine copolymer with amine groups, [23] and hybrid inorganic and organic adsorbents have proved their excellent utility in the removal of chromium. In this context, chemically modified polystyrenedivinylbenzene resins have been utilized for the preconcentration of many metal ions including chromium.[24-27] Amberlite XAD-1180 belongs to one such class of resins known to have high surface area and excellent physical, thermal, and chemical stability. The chelation of Cr(VI) with diphenyl carbazide and the subsequent adsorption on Amberlite XAD-1180 has been reported.[28] Amine impregnated Amberlite XAD-4 has been utilized for the collection of precious metals such as platinium and palladium from water. [29] However, a literature survey reveals that XAD-1180 resins impregnated with long-chain amines have not been explored for the removal of chromium. The chapter deals with an improved approach for the adsorption of chromium using a long-chain amine (trioctylamine) impregnated in an Amberlite XAD-1180 resin matrix. The polymeric sorbent before and after the adsorption was thoroughly characterized using various analytical techniques followed by a detailed study of the kinetics, thermodynamics, regeneration of sorbent, and other factors that affect the adsorption. The feasibility of the method has been successfully demonstrated for the removal of chromium in synthetic effluents and in real industrial wastewater samples.

3.2.2 Experimental Section

(i) Adsorbent Preparation

The Amberlite based macroporous polymeric resins are known to have a specific surface area in the range (150 to 900) m^2g^{-1} and an average pore diameter of (4 to 9) nm.[30] 4 g of Amberlite XAD -1180 resin was dispersed in acetone medium and stirred magnetically with 0.05 mol L^{-1} TOA in acetone for two hours. The dispersion of the resin was uniform with acetone as the medium. The homogenous dispersion of the amine in the polymeric matrix was attained in two hours. The preparation of the adsorbent is given as a flow chart in Figure 3.1. The adsorbent was separated by filtration, dried and characterized through various analytical techniques.

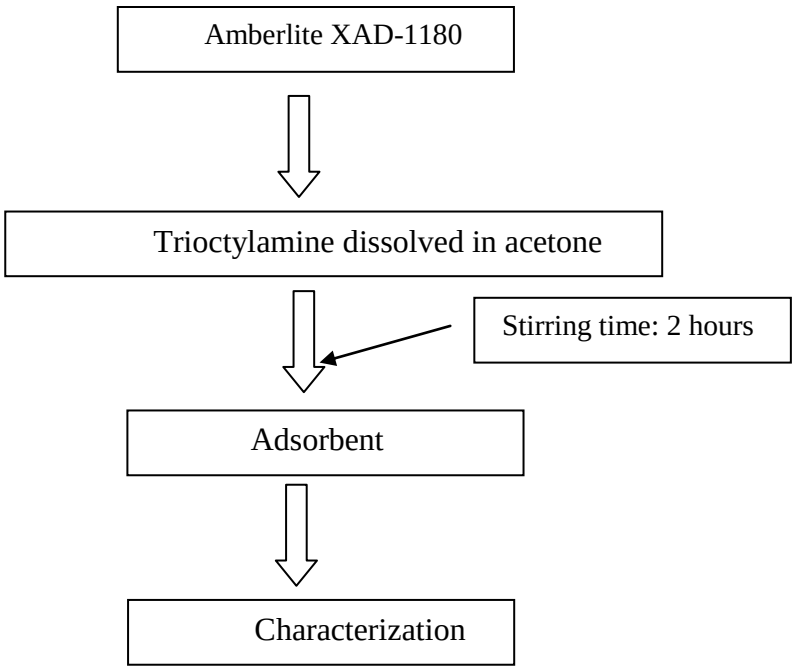

Figure 3.1. Adsorbent preparation

(ii) Adsorption Studies

The batch study was performed by equilibrating 0.2 g of the adsorbent containing 25 mL of chromium(VI) solution (100 μg mL^{-1}) at pH 3 in a conical flask at room temperature for the desired time interval in an orbital incubator shaker (Biotechnic, India). The concentration of chromium after adsorption was analyzed spectrophotometrically using the standard diphenyl carbazide method.[31]

(iii) Column Study

A glass column 1.5 cm in diameter and 25 cm in length was used for the dynamic studies. 3.0 g of the adsorbent was dispersed with 25 mL Milli-Q water to form slurry and then poured into the column. Cotton was placed at the bottom of the column for the resin to settle properly and packed up to a height of 2 cm. A 1 L volume of an aqueous solution containing 100 μg mL^{-1} chromium(VI) solution was adjusted to pH 3 and loaded on the column filled with the resin. The flow rate was maintained at 5 mL min^{-1} and the concentration of chromium(VI) in the aqueous phase was measured spectrophotometrically. The adsorbed chromium could be quantitatively recovered using 10 mL of 3 mol L^{-1} NaOH and the column could be re-used for the adsorption study.

3.2.3 Results and Discussion

(i) Characterization of Adsorbent

The FT-IR study (Figure 3.2) showed characteristic bands at 3046 cm^{-1} (aromatic C-H stretching), 2924 cm^{-1} (aliphatic C-H stretching), 2368 cm^{-1} (protonated nitrogen) [32] 1605 cm^{-1} (aromatic C=C stretching), and 1267 cm^{-1} (C-N stretching). There is a considerable change in the spectrum after the adsorption of chromium(VI) and a prominent new peak appeared at 889 cm^{-1} corresponding to the stretching vibration of Cr=O in $HCrO_4^-$. [33] This indicates that the nitrogen of the amine is protonated and forms an ion-pair with $HCrO_4^-$ in the acidic medium. The adsorbent was also characterized by X-ray diffraction and the pattern is depicted in Figure 3.3. characteristic new peak which shows the presence of the hexavalent chromium was observed at 2θ value corresponding to 31.7^0 and 45^0 which is in near accordance with the reported value in the literature.[34]

The Energy Dispersive X ray (EDX) spectrum (Figure 3.4) clearly indicates the presence of chromium observed in the range (5 to 6) keV[35] after the adsorption on the amine impregnated resin along with the other elemental constituents such as carbon, oxygen, sulfur and nitrogen. The sulfur peak arises from the sulfuric acid medium used for chromium adsorption.[36]

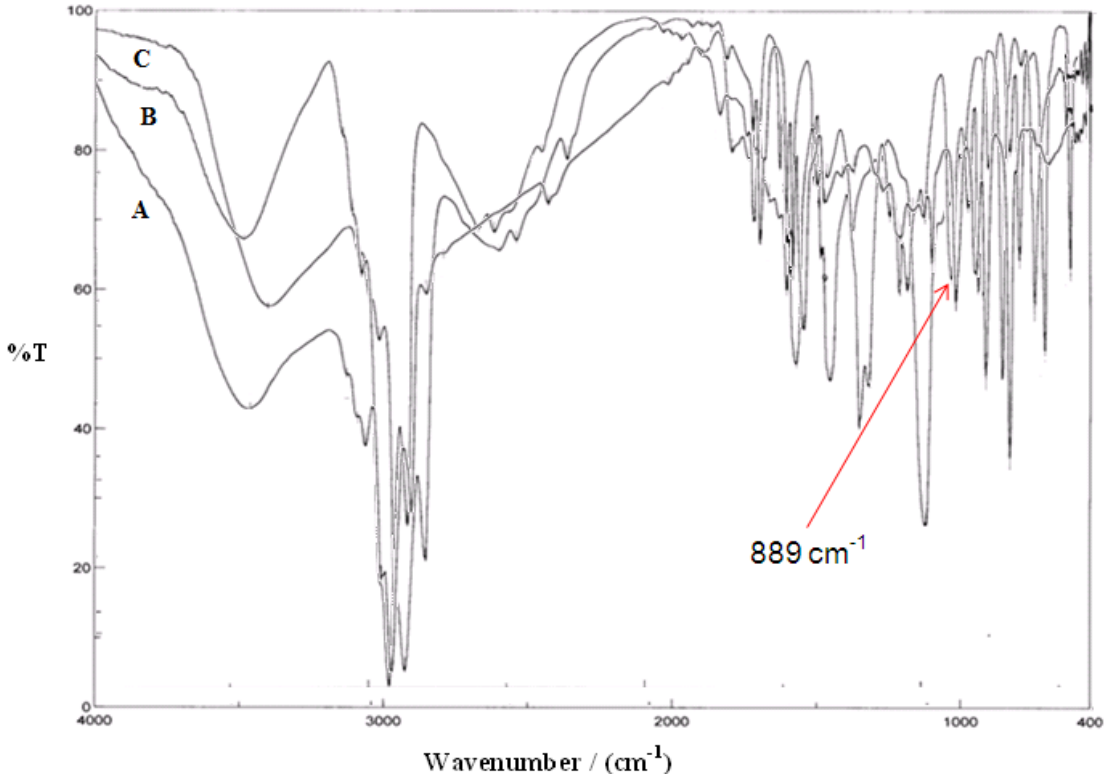

Figure 3.2 FT-IR spectrum of the polymeric adsorbent in various forms (A) adsorbent (B) after adsorption of chromium(VI) (C) after desorption of chromium(VI)

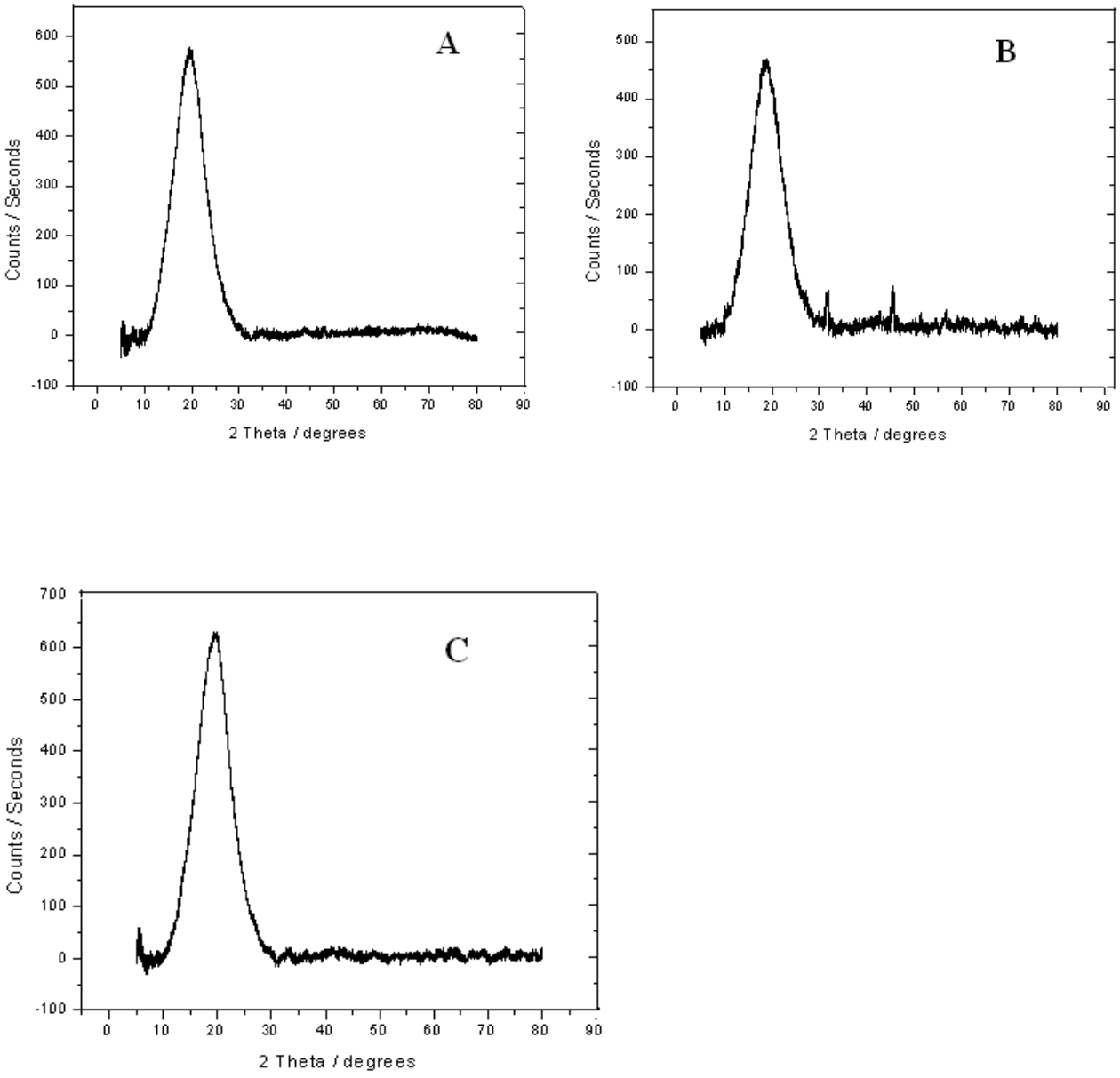

Figure 3.3 Powder XRD pattern of the polymeric adsorbent in various forms (A) adsorbent (B) after adsorption of chromium(VI) (C) after desorption of chromium(VI)

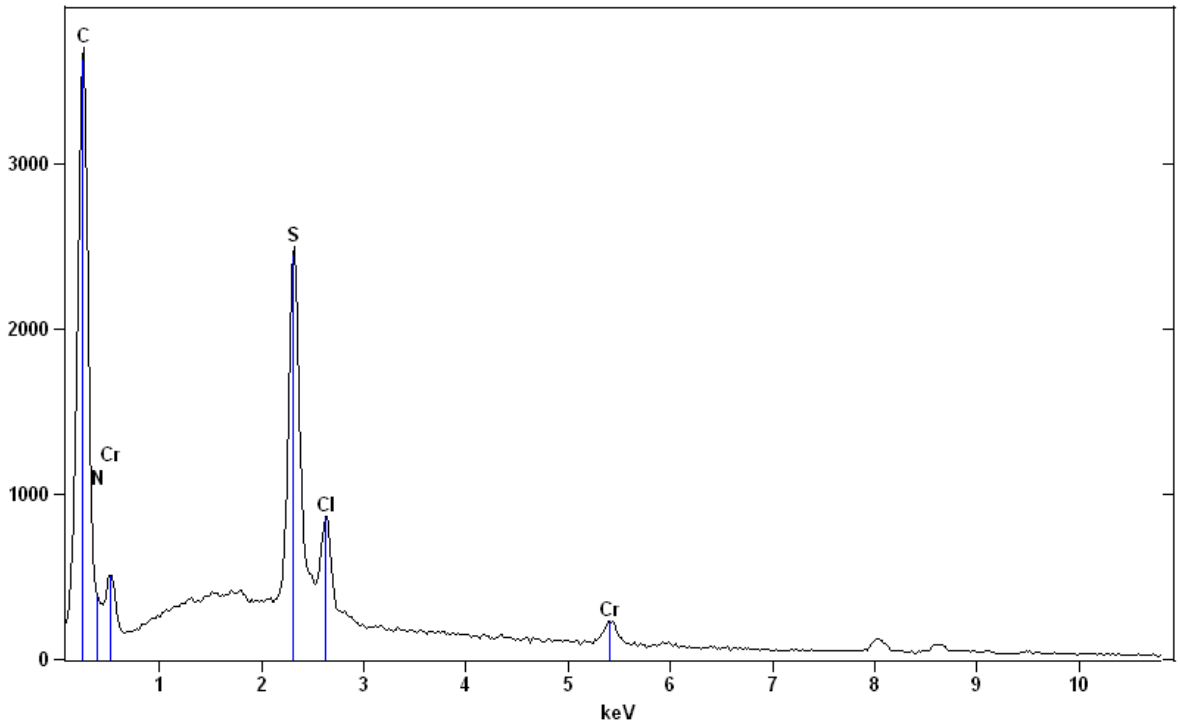

Figure 3.4 EDX spectrum of the adsorbed Cr(VI) on the resin matrix

(ii) Amount of Adsorbent

The amount of adsorbent used in batch study was varied in the range (0.05 to 0.5) g. The results are presented in Figure 3.5A. The adsorption capacity was found to be a maximium when the amount of adsorbent was in the range (0.2 to 0.5) g in 25 mL of sample volume used for the batch experiments.

(iii) Optimization of pH and Mechanism of Adsorption.

It is well known that the predominant species of chromium(VI) in acidic media are $HCrO_4^-$ and $Cr_2O_7^{2-}$.[37] The optimum pH for maximum recovery of chromium was observed in the pH range 2-3, and the species $HCrO_4^-$ is associated as an ion pair with the protonated amine. This was also substantiated from the FT-IR study as mentioned before. The variation of pH against the adsorption of chromium is shown in Figure 3.5B. It is evident that above pH 3, there is a considerable decrease in the adsorption of chromium. The proposed mechanism of adsorption represented in Figure 3.6, shows the impregnated resin and the subsequent ion-pair formation associated with the polymeric adsorbent.

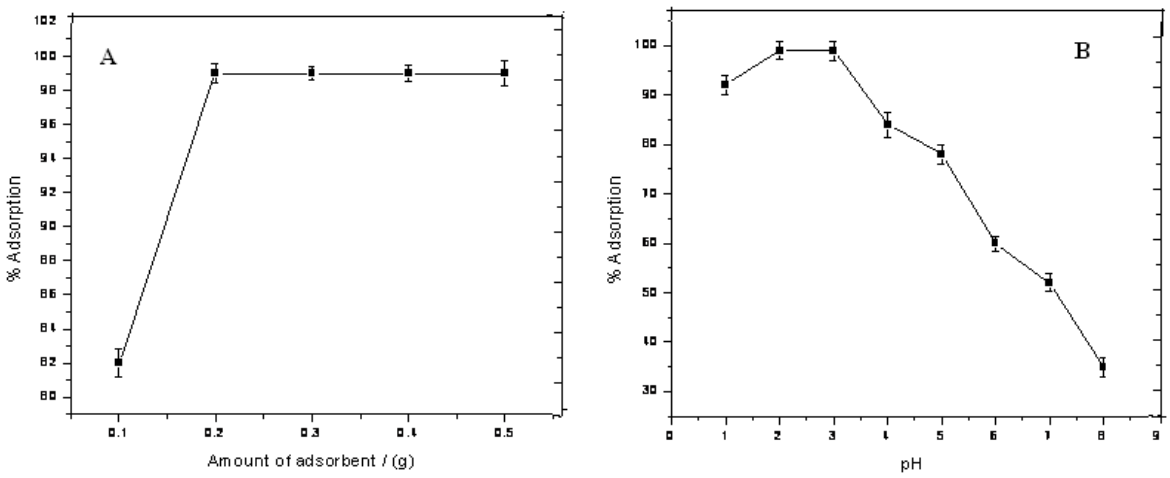

Figure 3.5 Effect of (A) Amount of adsorbent (B) pH

(iv) Adsorption Isotherms

The Langmuir [38] (Figure 3.7A) and Freundlich [39] (Figure 3.7B) isotherm models were used to study the adsorption behavior of chromium(VI) on amine impregnated Amberlite XAD-1180. A higher regression coefficient was obtained using the Langmuir isotherm, and the results (Table 3.1) were consistent with the experimental data. The Freundlich constants indicate the adsorption capacity and the adsorption intensity, respectively. The value of the constants K_F and n in the Freundlich equation were found to be 22.2 mg $^{1-1/n}$ g $^{-1}$ L $^{1/n}$ and 1.8045, respectively. These parameters indicate good uptake and affinity of the metal ion toward the adsorbent. The values of q_o and b in the Langmuir equation were found to be 171.82 mg g^{-1} and 0.1278 L mg^{-1} respectively. The dimensionless constant (R_L) in the Langmuir model was found to be 0.072 which is indicative of favorable adsorption.[40] The applicability of the monolayer coverage of chromium on the surface of the resin is evident from the Langmuir data.

(v) Kinetics of Adsorption

The rate of adsorption increased with time and reached its maximum at 30 min. The first-order [41] and pseudo second-order models[42] were used to fit the experimental data. The results of the plots of t/q_t versus t (Figure 3.8A) and log (q_e-q_t) versus t (Figure 3.8B) give the kinetic parameters. It can be seen from Table 3.2 that the adsorption data is consistent with the pseudo second-order model in view of the higher regression coefficients. The intra particle diffusion[43] k_{int} and the relevant plot are given in Table 3.2 and Figure 3.8C.

The plot is indicative of boundary layer control as well as a diffusion-controlled process. [44]

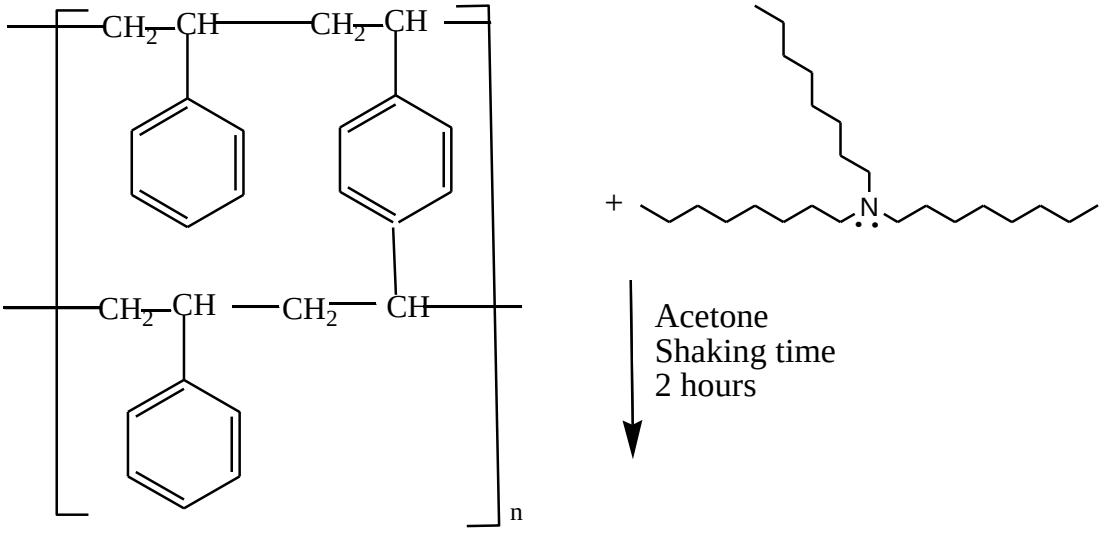

Polystyrene-divinyl benzene
Amberlite- XAD 1180

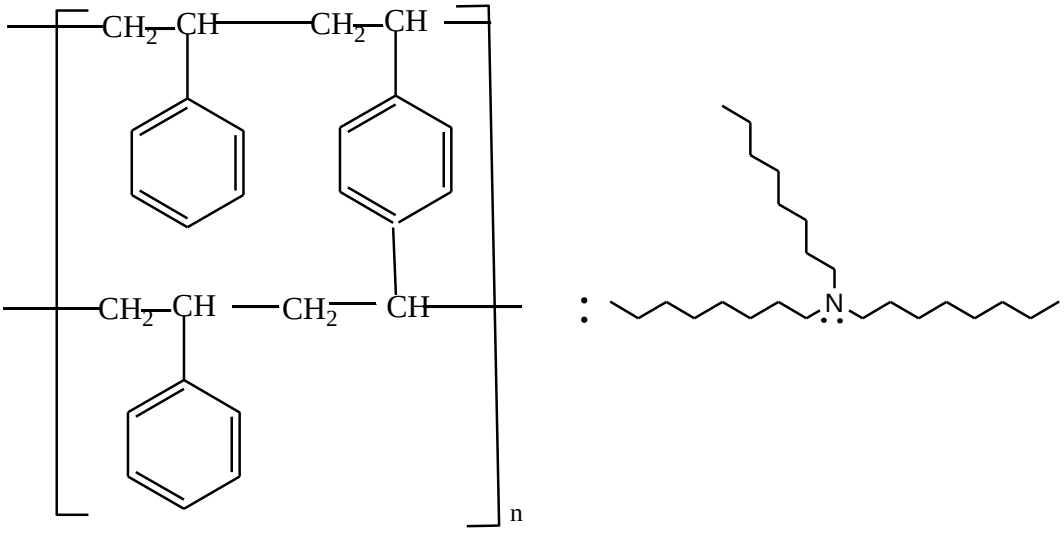

Polystyrene-divinyl benzene
Amberlite- XAD 1180

polymeric adsorbent impregnated with tri- octylamine

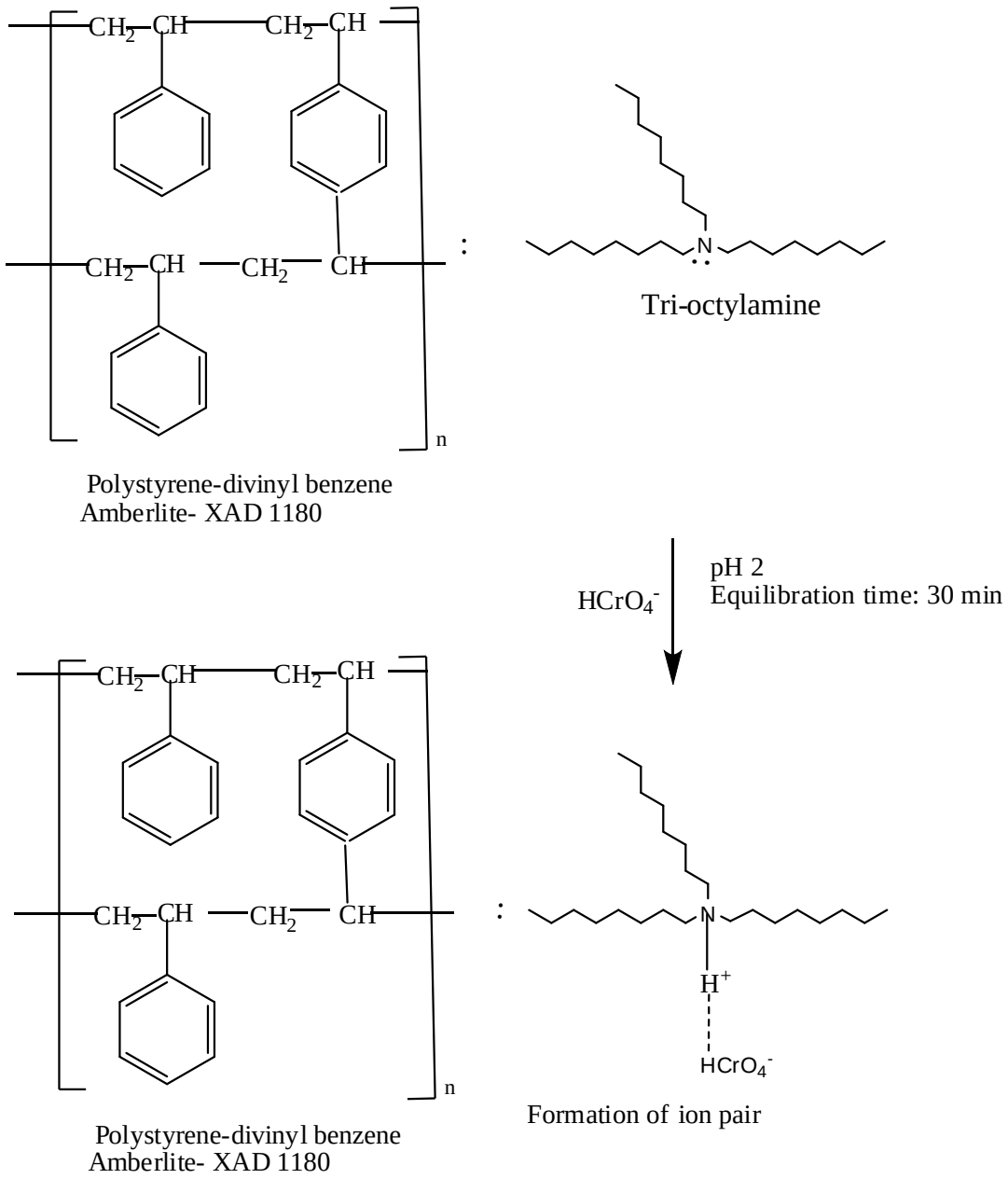

Figure 3.6. Impregnation of the resin with amine and formation of ion pair

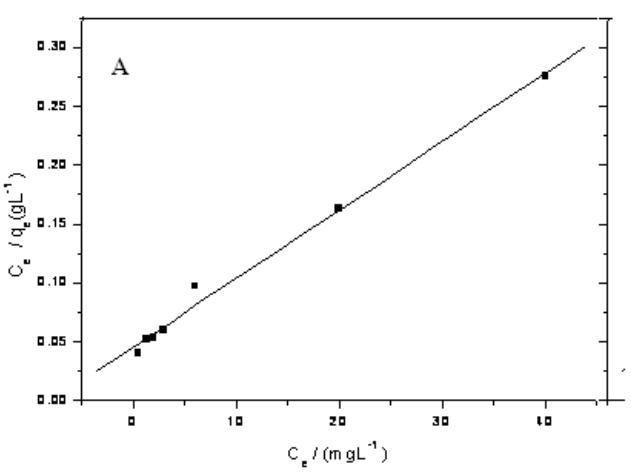

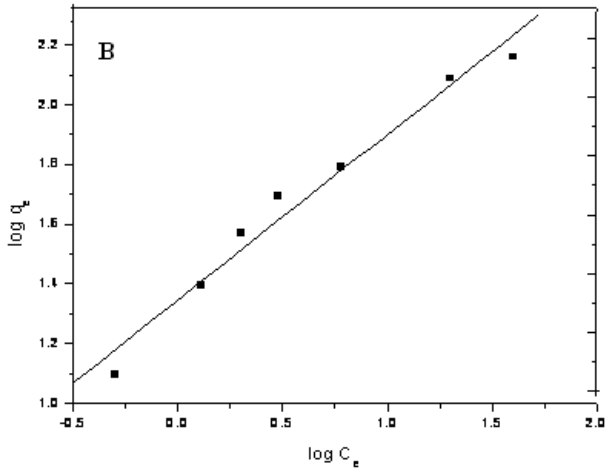

Figure 3.7 Isotherms (A) Langmuir (B) Freundlich

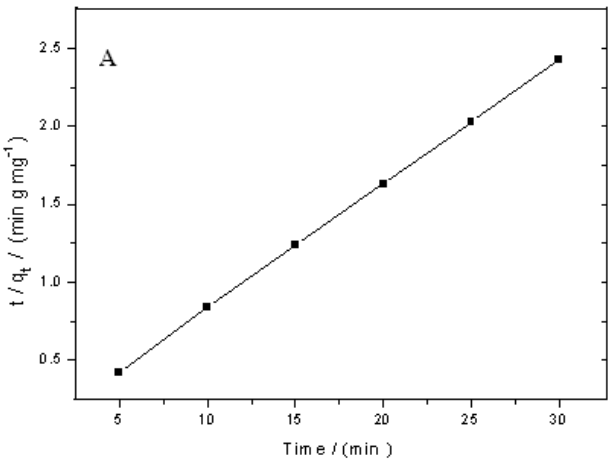

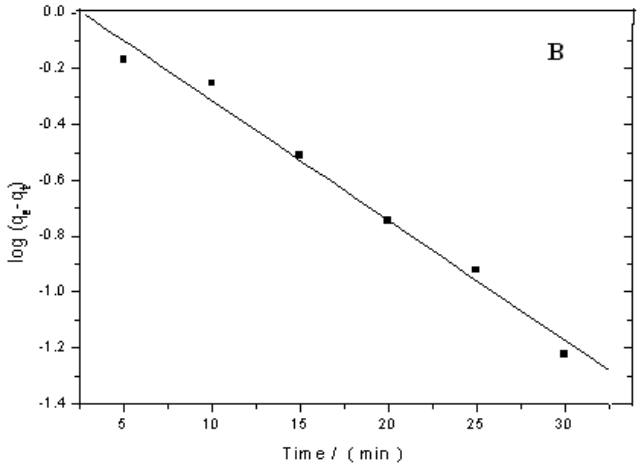

Figure 3.8 (A) Second order kinetics (B) First order kinetics

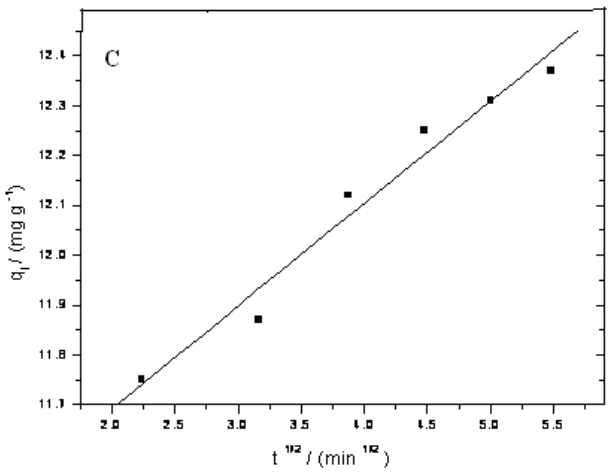

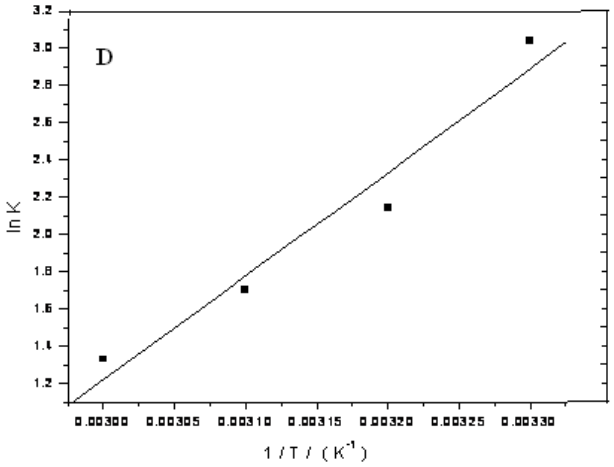

Figure 3.8 (C) Intraparticle diffusion (D) van't Hoff plot

Table 3.1. Langmuir and Freundlich isotherm parameters for the adsorption of chromium(VI)

Langmuir				Freundlich		
q_o / (mg g^{-1})	R_L	b / (L mg^{-1})	r^2	K_f / (mg $^{1-1/n}$ g^{-1} L $^{1/n}$)	n	r^2
171.82	0.072	0.1278	0.99	22.2	1.8045	0.97

Table 3.2. Kinetic studies and Intra-particle diffusion rate constant for the adsorption of chromium(VI)

q_e / (mg g^{-1})	k_2 / (g mg^{-1} min^{-1})	R_2^2	k_1 / (min^{-1})	R_1^2	k_{int}
12.43	0.1746	0.9999	0.0988	0.9845	0.2054

(vi) Adsorption Thermodynamics

The thermodynamic parameters such as Gibbs energy, enthalpy and entropy change were calculated at different temperatures.[45,46] The spontaneity of adsorption is ascertained from the equilibrium constant (K) and the Gibbs energy values. Broadly speaking, K>1 implies that the adsorption is effective and spontaneous at a given temperature. The K value is obtained by taking the ratio of the concentration of the metal ion in the adsorbent to that in the solution. The K values were found to decrease with temperature and this is reflected in the Gibbs energy values obtained at higher temperature. A plot of ln K against 1/T is shown in Figure 3.8D and the corresponding thermodynamic parameters are presented in Table 3.3. The amount of chromium(VI) adsorbed decreased with an increase in temperature from 30 ^{0}C to 55 ^{0}C. Lower temperatures are favorable for the adsorption process, which is evident from the ΔG^0 values obtained at different temperatures. In the adsorption process which follows an ion pair mechanism, more energy is released (exothermic) and this is evident from the negative ΔH^0 value. The negative ΔS^0 value indicates less randomness at the adsorbent-solution interface.

Table 3.3. Thermodynamic parameters for the adsorption of chromium(VI)

Temperature / (K)	K	ΔG^0/ (kJ mol^{-1})	ΔS^0/ (J mol^{-1} K^{-1})	ΔH^0/ (kJ mol^{-1})
303	20.97	-7.66	-128.90	-46.34
313	8.51	-5.57		
318	5.49	-4.50		
328	3.78	-3.62		

(vii) Effect of Sample Volume

The effect of sample volume for the adsorption of chromium(VI) on the resin was investigated in the range (100 to 1600) mL maintaining an overall concentration of 100 µg mL^{-1}. As can be seen from the Figure 3.9, it is evident that the adsorption of chromium is quantitative up to a 1000 mL sample volume with a preconcentration factor of 100. There are various factors such as bed height, quantity of adsorbent and diameter of the column which affect the performance efficiency. On loading, the column with a known sample volume, the polymeric resin swells and the adsorbent bed undergoes expansion. In a small diameter column, the effective expanded bed operation is achieved when the expanded bed volume is about twice the volume of the packed bed.[47] At higher sample volume (beyond 1000 mL), the degree of expansion is more and the distance between the particles in the polymeric sorbent increases. Hence, less amount of Cr(VI) is adsorbed on the column, due to the non-availability of effective adsorption sites.

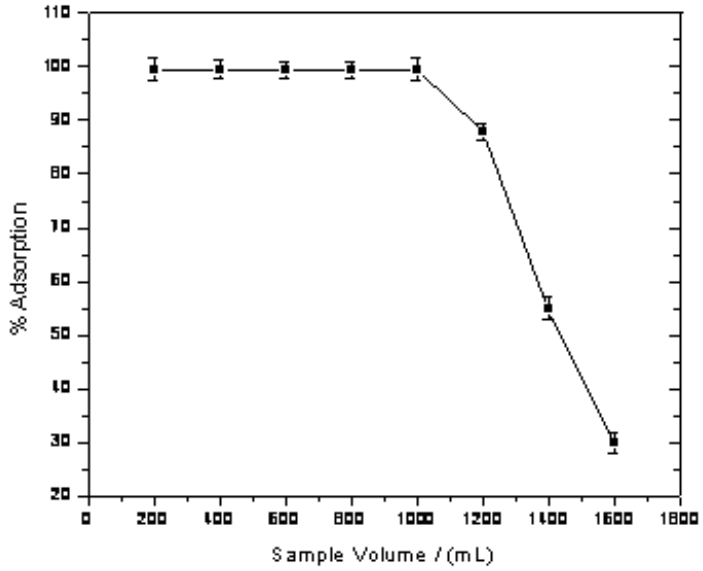

Figure 3.9 Effect of sample volume in the column study

(viii) Optimum Flow Rate and the Amount of Amberlite XAD 1180 Loaded on the Column

A flow rate of 5 mL min^{-1} was maintained for maximum column efficiency and the adsorption of chromium was quantitative. At higher flow rates, there was a decrease in the column adsorption efficiency and this could probably be ascribed to the lesser contact time between the sample solution and the amine impregnated resin matrix. The column adsorption efficiency was a maximum when the resin amount was in the range (2.0 to 3.0) g up to 1 L sample volume. However, when the resin amount was less than 2.0 g, the column efficiency was found to be good at lower sample volumes.

(ix) Regeneration of the Adsorbent Column

The recovery of chromium(VI) adsorbed onto the column was tried using sodium hydroxide, ascorbic acid, sodium nitrite and sodium sulfite respectively. [48,49] Even though, ascorbic acid, nitrite and sulfite were effective in reducing chromium(VI), the desorption was found to be a maximum with 10 mL of 3 moL L^{-1} sodium hydroxide as the eluent. The desorption efficiency increases in the order sodium nitrite (75 %) < ascorbic acid (88.6 %) < sodium sulfite (90 %) < sodium hydroxide (99.5 %)

respectively. In this process, the adsorbed chromium(VI) is brought into the aqueous solution as sodium chromate (Figure 3.10) and the concentration of the chromium was estimated spectrophotometrically

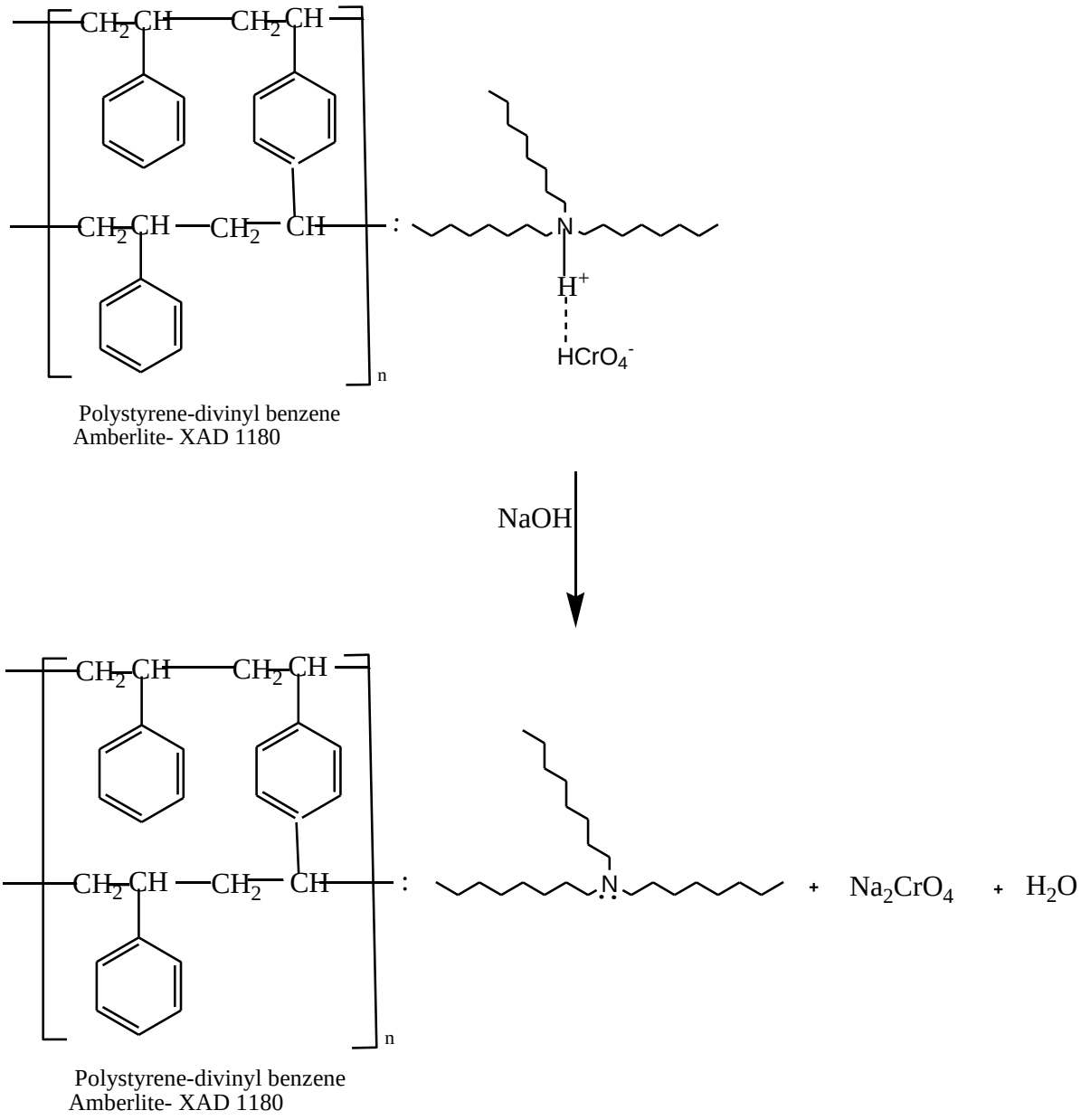

Figure 3.10 Recovery of Chromium(VI) with NaOH

The desorption was confirmed through FT-IR (Figure 3.2C) and powder XRD (Figure 3.3C) studies. The prominent peaks obtained after adsorption showed that the of chromium(VI) peak had disappeared after elution using sodium hydroxide and restored the pattern of the original adsorbent, thereby confirming the quantitative desorption.

(x) Stability of the Column

The stability of the Amberlite XAD 1180 column was tested using 100 μg mL^{-1} chromium(VI) maintaining a sample volume of 1 L. The adsorbed chromium(VI) was eluted using 10 mL of 3 moL L^{-1} sodium hydroxide. The column could be used with good precision (relative standard deviation 2.0 %) for 15 cycles without reduction in the performance efficiency.

(xi) Effect of Diverse Ions

The effect of various cations and anions that are commonly present in the real effluents were investigated independently at 1000 μg mL^{-1} concentration. Cations such as Fe(II, III), and Mn(II) caused significant reduction (Figure 3.11A) in the adsorption of chromium(VI). Among the anions, chloride, nitrate and phosphate caused a marginal decrease in the adsorption efficiency (Figure 3.11B) of chromium(VI). There is no appreciable interference from Ni(II), Ca(II), Mg(II), Hg(II) and Zn(II) ions. Under the given experimental conditions, these ions do not form any stable ion-pair with the protonated amine for competition with the hydrochromate for the active sites in the adsorbent. However, in the presence of excess chloride concentration, it is possible that Ni(II), Hg(II) and Zn(II) could form tetrahalo complexes which would compete with $HCrO_4^-$ for adsorption causing a decrease in the selectivity. The selectivity decreases in the presence of Mn(II) since manganese in the +2 oxidation state could reduce Cr(VI) to Cr(III) in an acidic medium

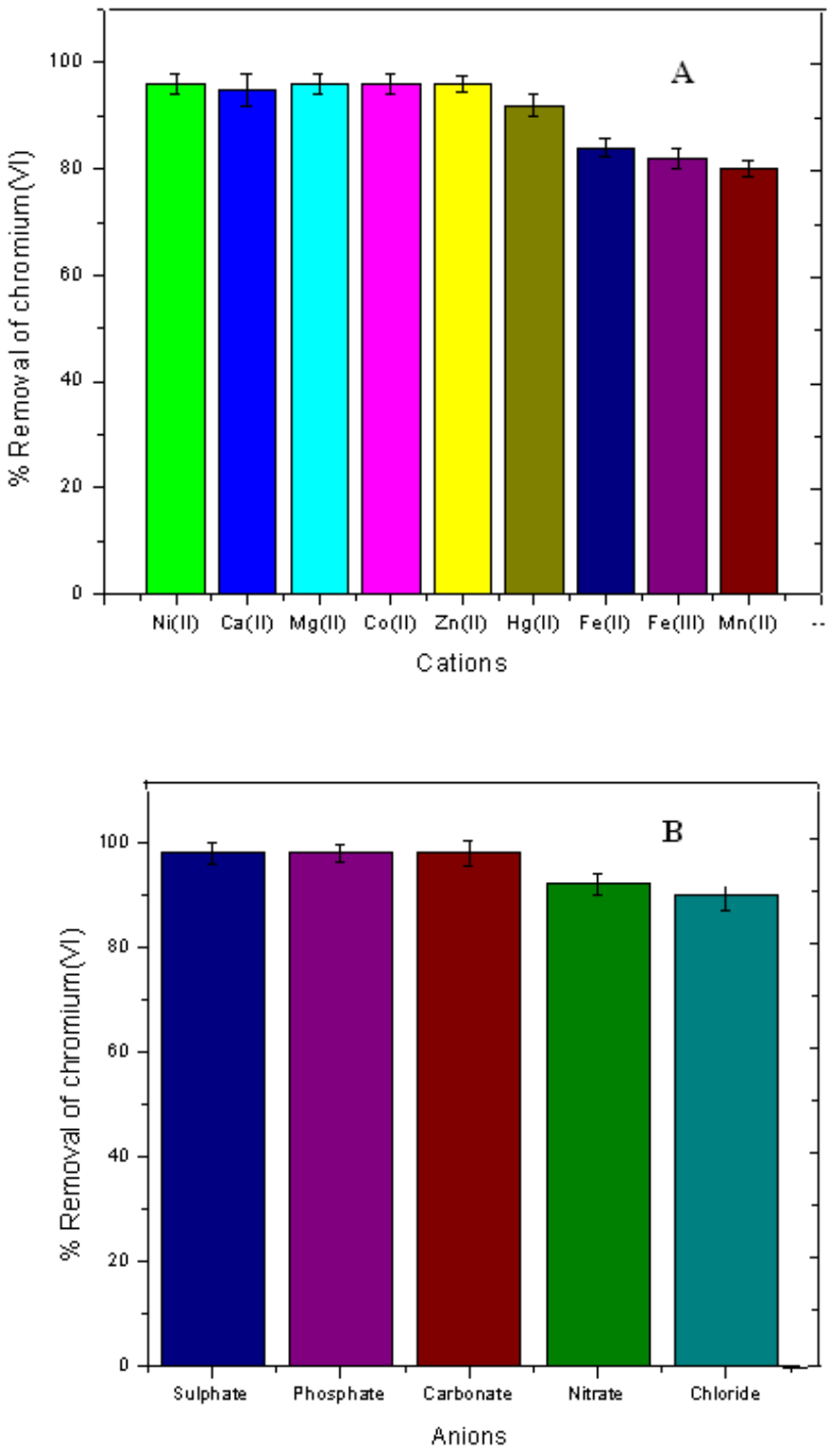

Figure 3.11 Effect of (A) diverse cations on the removal of Cr(VI) (B) diverse anions on the removal of Cr(VI)

(xii) Recovery of Total Chromium in Synthetic Effluents

The applicability of the proposed method was tested in synthetic effluents of three different compositions. The synthetic samples were prepared in such a way so as to match the approximate composition of real effluents. Cr(III) was also one of the constituents in the synthetic mixture and it was oxidized to Cr(VI) and the total chromium concentration was maintained in the level (100 to 700) μg mL^{-1}. The results are presented in Table 3.4. In the presence of chloride, cations such as Hg(II), Zn(II), Mn(II) and Fe(III) caused a reduction in the recovery of total chromium. This may be ascribed to the fact that all these ions can form stable chloro complexes, which might vie with the oxo-anion chromate for ion-pair formation with the protonated amine.

Table 3.4. Recovery of total chromium in various synthetic effluents

Sample	Composition in μg mL^{-1}	Recovery of total Cr / (%)
Synthetic Effluent -A	SO_4^{2-}(1000), NO_3^-(500), PO_4^{3-}(1000), Cl^- (1000), Cu^{2+}(1000), Zn^{2+} (500), Fe^{3+}(250), Mg^{2+}(1000), Ca^{2+}(1000), Hg^{2+} (500), Total Cr (100)	94.3±0.5
Synthetic Effluent - B	Fe^{3+}(700), SO_4^{2-}(500), Ca^{2+}(1000), Cu^{2+}(500), NO_3^-(250), Cl^- (1000), Mg^{2+}(1000), Hg^{2+}(1000), Mn^{2+} (750), Zn^{2+} (1000), Total Cr (700)	90.1±0.2
Synthetic Effluent - C	Fe^{3+}(150), SO_4^{2-}(1000), Ca^{2+}(1000), Cu^{2+}(250), NO_3^-(250), Cl^- (500), PO_4^{3-}(500), Mg^{2+} (1000), Total Cr (500)	99.5±0.2

(xiii) Removal of Chromium from Real Tannery and Electroplating Wastewater Effluents

The applicability of the method was finally tested for the removal of chromium from a real tannery waste water sample collected from Tamil Nadu, India. The sample was green in color at alkaline pH and stored in a polythene bottle. It is well known that the major constituent of tannery effluent is Cr(III), since it is the species used in leather tanning. Trace amounts of Cr(VI) are also likely to be present due to some oxidizing agents used in the tanning process. The organic matter is destroyed using an appropriate amount of a HNO_3-H_2SO_4 mixture.[50] A known volume of the effluent was taken and loaded onto the adsorbent column under alkaline conditions where Cr(III) is selectively retained. At higher pH, Cr(III) exists as $Cr(OH)_2^+$ and $Cr(OH)^{2+}$ species respectively. [51] In alkaline medium, the amine acts as an electron donor and facilitates effective interaction with the above mentioned positively charged Cr(III) species. Hence, Cr(III) is effectively retained at higher pH. The resulting solution is acidified to pH 3 and passed through another column containing the amine impregnated resin where Cr(VI) is selectively retained. The process is illustrated schematically in Figure 3.12. The separated Cr(III) and Cr(VI) could be eluted using H_2SO_4 and NaOH respectively. The total chromium concentration was determined spectrophotometrically. An overall removal efficiency of 99.3 % could be attained by the proposed method. An electroplating waste water sample was obtained from a small scale electroplating unit near Bangalore, India. The sample was brown in color and stored in a polythene bottle. The chromium present in the electroplating waste water sample was oxidized to Cr(VI) with alkaline peroxide and then loaded onto the adsorbent column.[52] The pH was maintained at 2 and the adsorbed chromium was eluted quantitatively using NaOH. An overall removal efficiency of 98.5 % could be attained by the proposed method.

3.2.4 Conclusions

The proposed method illustrates the high potential of a polystyrene-divinyl benzene based sorbent impregnated with a long chain amine for the removal of chromium. The polymeric sorbent is efficient and could endure the treatment in both acidic and alkaline media. The adsorption kinetics is fast, and follows a pseudo second order model and is also in accordance with the Langmuir adsorption isotherm model with an adsorption capacity of 171.82 mg g^{-1}.

The study of the thermodynamic parameters showed that the adsorption process decreases with an increase in temperature. Column studies proved that the system could tolerate a large sample volume (1 L) with effective separation from a synthetic mixture of various ions. Cr(VI) could be effectively removed at acidic pH based on the electrostatic attraction of the hydrochromate anion with the protonated amine, whereas Cr(III) was retained in the column at alkaline pH due to the interaction of the amine with $Cr(OH)_2^+$ and $Cr(OH)^{2+}$ species. The adsorbed chromium in the respective oxidation states could be recovered from the column using sulfuric acid and sodium hydroxide respectively, without any appreciable loss in the performance efficiency for 15 cycles. The validity of the proposed method is very well illustrated for the separation of chromium in real effluent samples with average removal efficiency greater than 98 %

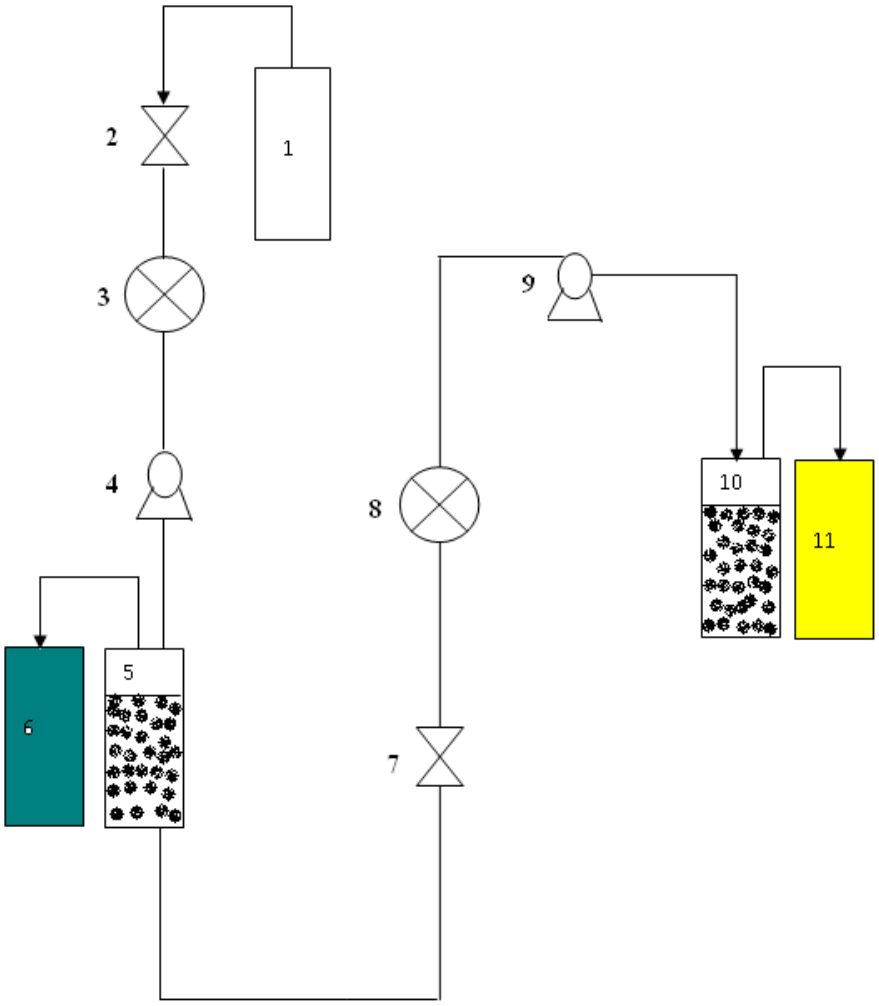

1. Feed water
2. Valve
3. pH adjustment [Alkaline Medium]
4. Peristaltic pump
5. Adsorbent column [Adsorption of Cr(III)]
6. Collection tank [Desorbed Cr(III)]
7. Valve
8. pH adjustment [Acidic Medium]
9. Peristaltic pump
10. Adsorbent column [Adsorption of Cr(VI)]
11. Collection tank [Desorbed Cr(VI)]

Figure 3.12 schematic diagrams for treating tannery effluent

Enhanced adsorption of chromium using n-octylamine impregnated amberlite xad-4 polymeric sorbent

3.3.1 Introduction

This chapter discusses an enhanced adsorption methodology for the detoxification of chromium using n-octylamine impregnated Amberlite XAD-4 polymeric sorbent. Macroporous polystyrene divinyl benzene based resins are known for their excellent surface characteristics for the effective adsorption of metals. Solid phase extraction offers considerable advantage in terms of treatment of large sample volume and high enrichment factor.[53] Activated carbon from various sources have been explored for the adsorption of chromium.[54,55] Silica [56] and alumina[57] based materials have also proved their utility as effective sorbents. Sorbents derived from biomass[58] and composite chitosan[59] based sorbents have also proved to be very useful for the adsorption of chromium. In addition, ion-exchange resins [60]and chemically modified polymeric resin [61,62] also offer considerable advantages for heavy metal removal in terms of their good selectivity and adsorption capacity. Solvent impregnated resins stabilized by coating with vinyl sulfone cross linked polyvinylalcohol have been utilized for the removal of chromium in Cr^{6+} oxidation state.[63] Amine impregnated microspheres prepared from polysulfone and polyvinyl pyrrolidine as additive have been evaluated for the extraction efficiency of chromium(VI).[64] Macroporous sorbents such as the above mentioned resins are known to possess good surface characteristics for the effective adsorption of metals.[65-67] The present investigation demonstrates the potential of a polystyrene divinyl benzene based polymeric resin (Amberlite XAD-4) as an effective sorbent for the removal of chromium. To the best of our knowledge, literature study shows that the ability of XAD-4 (polystyrene divinyl benzene polymeric resin) impregnated with long chain aliphatic primary amine has not been tested for the detoxification of chromium from industrial effluents.

3.3.2 Experimental Section

(i) Adsorbent Preparation

The preparation of the sorbent was carried out in a simple two stage process. In the first stage, an appropriate amount of the polymeric sorbent was taken in a round bottom flask containing 15 mL of propanone as the solvent medium. This was followed by the addition of 0.02 mol L^{-1} n-octylamine in the similar solvent medium and stirred for a time period of 9 hours at room temperature. Propane-2-one has been reported to be a fine solvent medium for the good dispersion of the macroporous resin.[62,68] The format for the preparation of the adsorbent is given in Figure 3.13. The amine extractant is transferred from the liquid phase to the solid matrix and a good dispersion of the sorbent is obtained. The resulting solution was filtered and the solid adsorbent was comprehensively characterized by various analytical methods. The separated solid adsorbent was dried and used for the batch study.

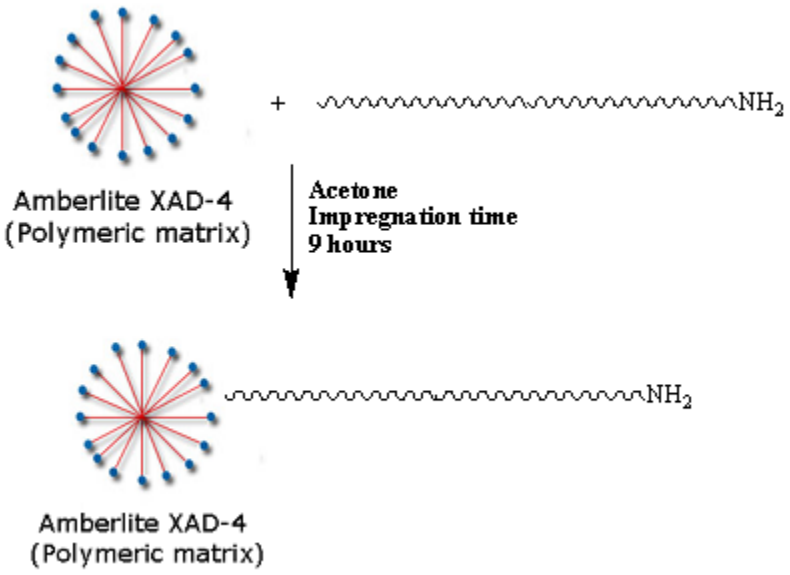

Figure 3.13. Conceptual illustration of amine impregnation Amberlite XAD-4 resin

(ii) Adsorption Procedure

The preliminary adsorption studies were carried out by the batch method. An appropriate quantity of the polymeric sorbent was shaken with 50 mg $L^{-1}$of Cr(VI), maintaining a pH 2.5 at 25^{o}C. The solution was separated from the adsorbent and the metal ion uptake at different time intervals and the concentration of chromium was measured as its chelate with diphenylcarbazide [69] at a wavelength maximium of 540 nm.

3.3.3 Results and Discussion

(i) Characterization of the Polymeric Sorbent

Powder X ray diffraction is an important analytical tool in the solid phase extraction. The XRD patterns show (Figure 3.14) sharp distinct peaks after the adsorption of chromium(VI) matching to 2θ values 31.65^0 and 45.71^0 with pointed increase in the intensity of the peaks after adsorption on the polymeric sorbent.[34] The adsorption of Cr(VI) in the pores of the Amberlite XAD-4 polymeric matrix shows a consistent distribution in the surface morphology. The polymeric sorbent before impregnation resin is a porous and rough structure with a active sites favorable for chromium(VI) adsorption. However, when n-octyl amine is impregnated with Amberlite XAD-4 polymeric matrix, the SEM images shows the appearance of shiny particles over the surface of adsorbent which is attributed to the effective adsorption and uniformity in the morphology on the adsorbent surface. This was evident from the distinct changes in the SEM images before and after the adsorption of chromium (Figure 3.15A, B). The BET surface area of the adsorbent material was found to be 406.82 m^2 g^{-1} and pore volume 1.046 cm^3 g^{-1}. The existence of chromium(VI) on the solid matrix was further evident from the Energy dispersive X ray spectrum analysis as well defined peak (Figure 3.16). Fourier transform Infrared spectroscopy (FT-IR) is another important analytical technique which gives information about the participation of various functional groups in the adsorption process. The characteristic vibrational stretching frequency bands were observed corresponding to the polymeric resin and the primary amine (Figure 3.17 A, B). The IR spectra of protonated amines are known to exhibit a strong band in the region 2300-2800 cm^{-1} and this depends on the nature of the anionic species in the acid.[32] Two prominent bands for

the protonation of the aliphatic primary amine were observed after the adsorption of chromium on the solid matrix. A distinct band at 2426 cm^{-1} further authenticates the protonation of the primary amine in acidic medium. The protonated primary amine group, RNH_3^+, where R is the octyl group, also shows asymmetric and symmetric deformation mode of vibration in the region 1500-1600 cm^{-1}.[70] The presence of a characteristic band at 899 cm^{-1} ($\nu_{Cr=O}$) in hydrochromate ion provides further validation to the ion-pair formation. [33,71] The solid state ^{13}C NMR spectrum recorded for the adsorbent in various forms showed further evidence for the adsorption of chromium. Distinct peaks which are characteristic of the Amberlite XAD-4 resin were observed and the chemical shifts were in accordance with values reported in literature for the polystyrene divinyl benzene resin.[72] The chemical shift of carbon attached to electronegative element like nitrogen is known to cause de shielding effect and hence appears downfield in the ^{13}C NMR spectrum. After the adsorption of chromium, a further downfield shift is observed in the NMR spectrum of the polymeric sorbent. This variation in the chemical shift of the carbon attached to nitrogen atom in the primary amine from 59.9 ppm to 62.3 ppm is evident in the NMR spectrum obtained after the adsorption of chromium on the polymeric sorbent and this is indicative of the fact that protonated nitrogen is the binding site for hydrochromate ion (NH_3^+---$HCrO_4^-$).This supports the fact the hydrochromate ion is bonded to the primary amine through electrostatic attraction (Figure 3.18A, B). The schematic representation for this observation is given in Figure 3.19. The removal efficiency of chromium essentially is dependent on nature of the amine and the polymeric matrix respectively.[62]

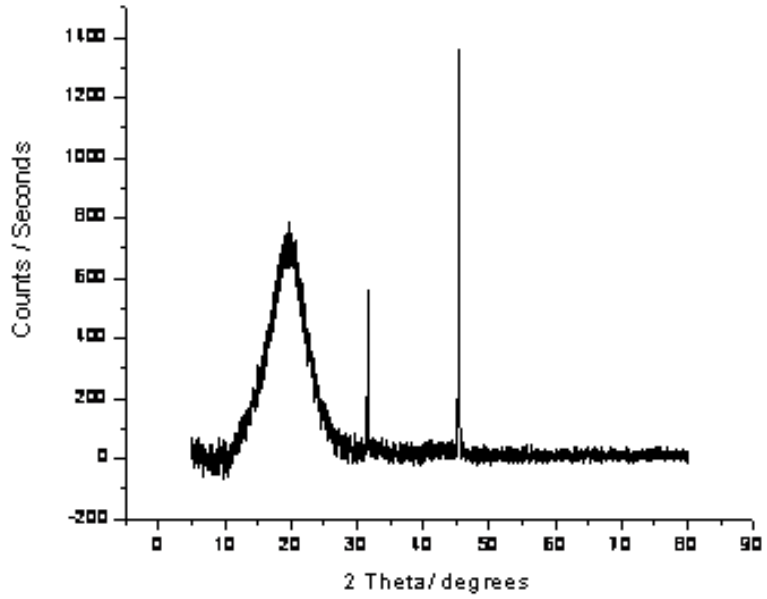

Figure 3.14. Powder–XRD pattern showing characteristic of chromium adsorption

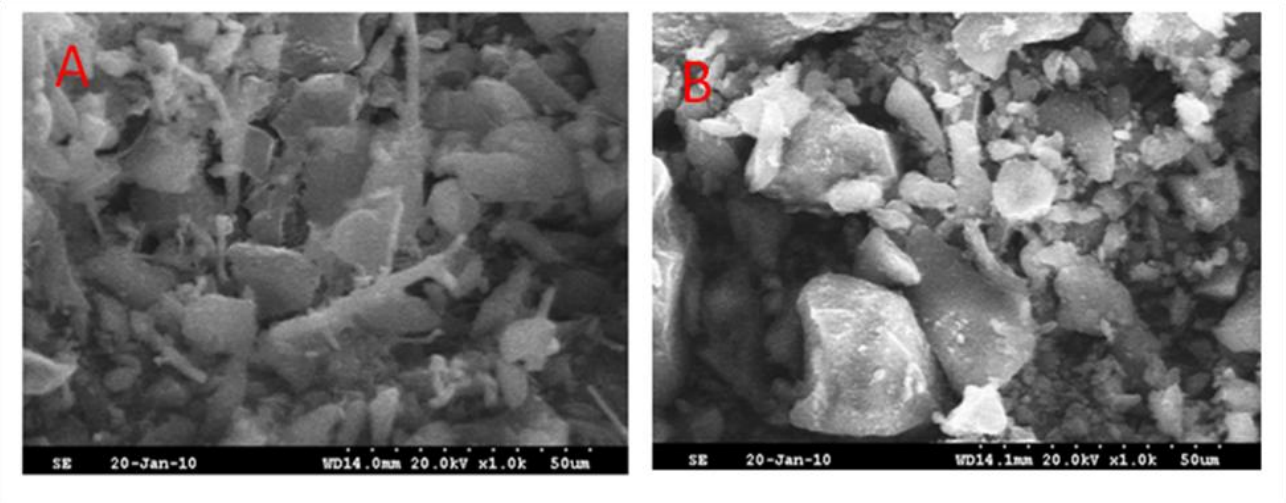

Figure 3.15 SEM images (A) sorbent (B) after chromium(VI) adsorption

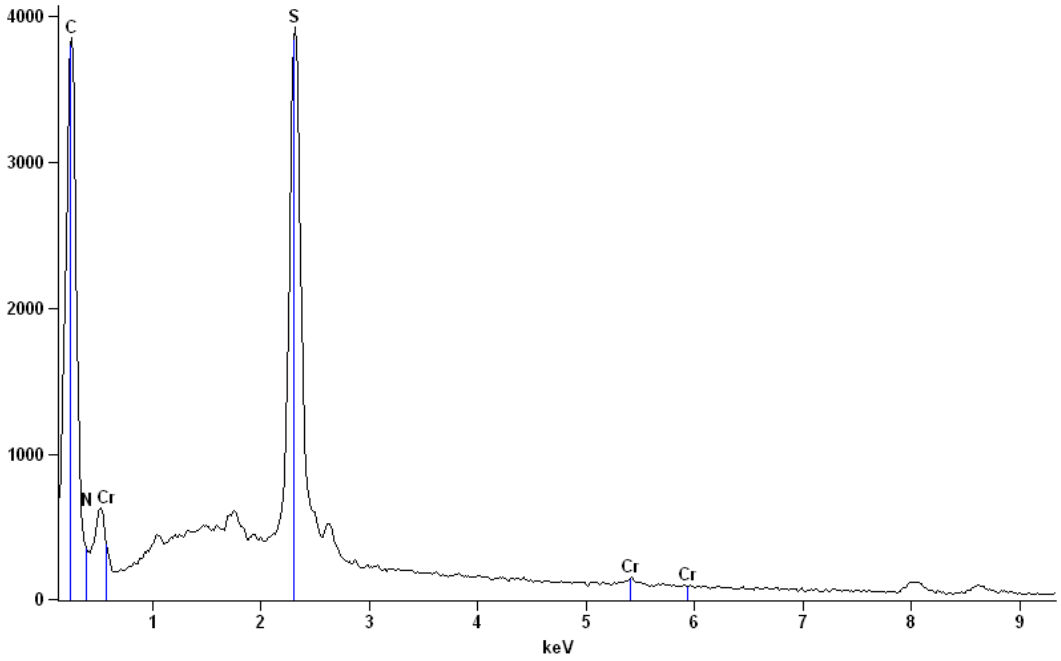

Figure 3.16 EDX spectrum of the after adsorbed chromium(VI)

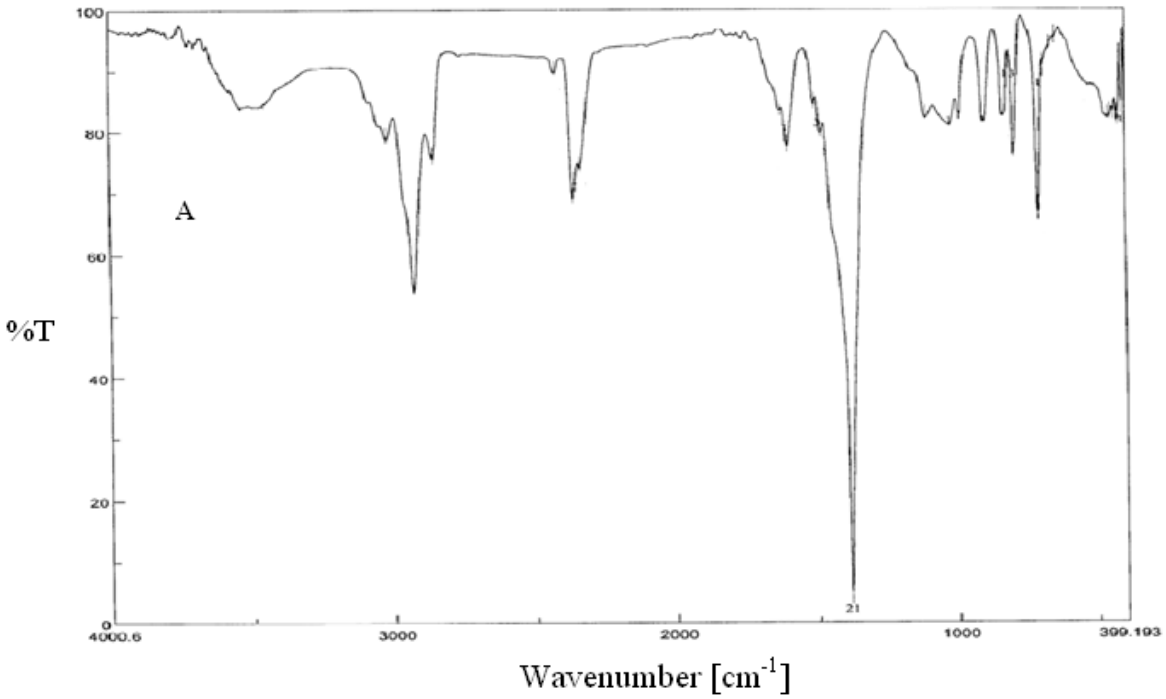

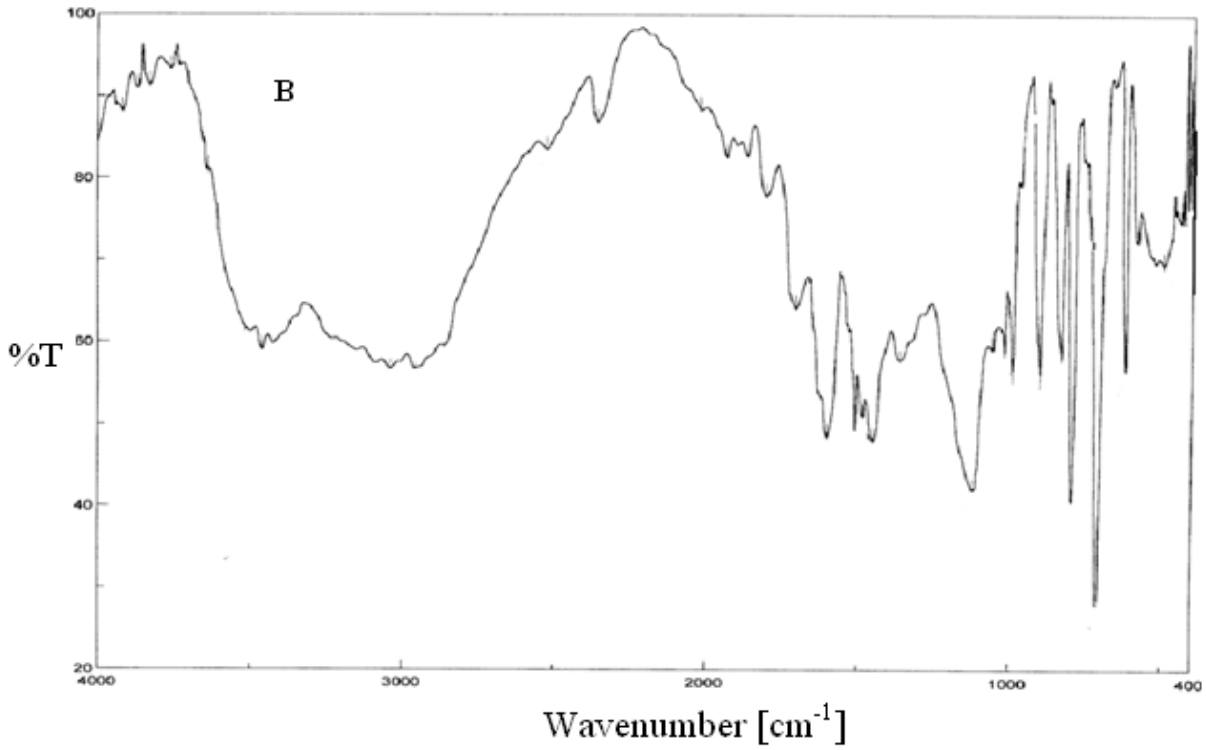

Figure 3.17. FT-IR Spectrum of (A) Adsorbent (B) after the adsorption of chromium(VI)

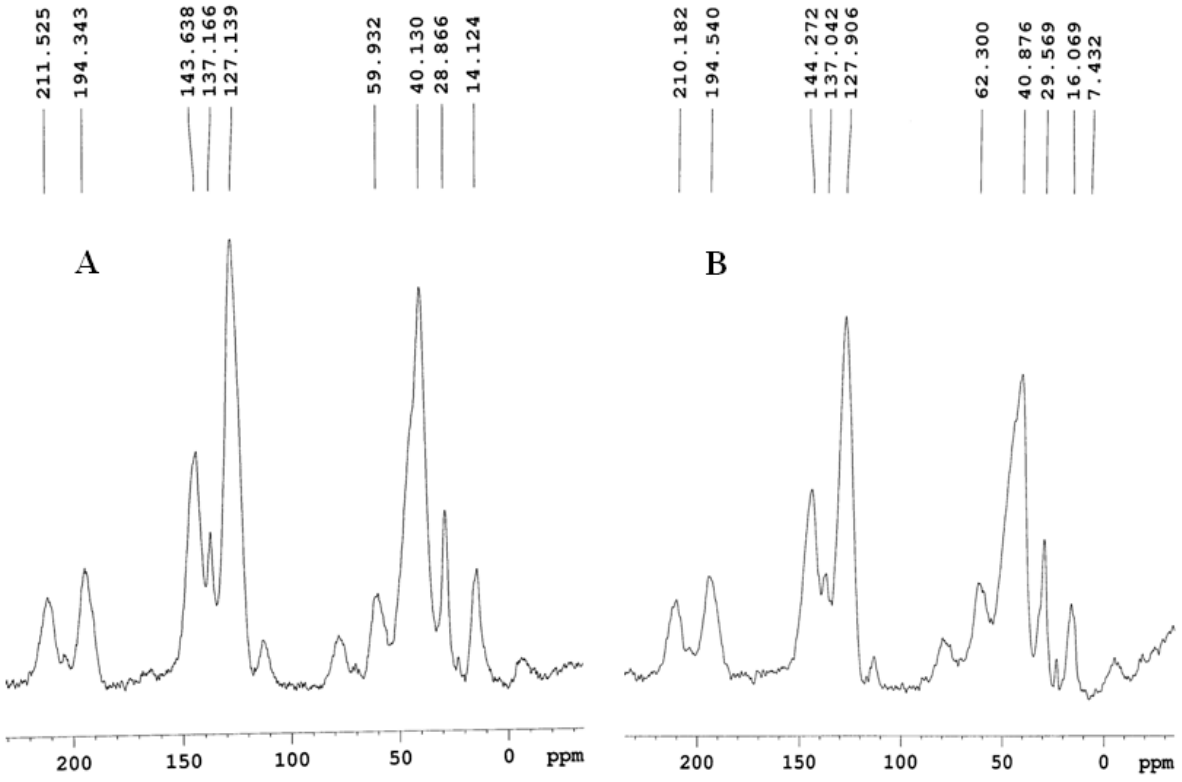

Figure 3.18 ^{13}C NMR spectrum (A) adsorbent (B) after adsorption of chromium(VI)

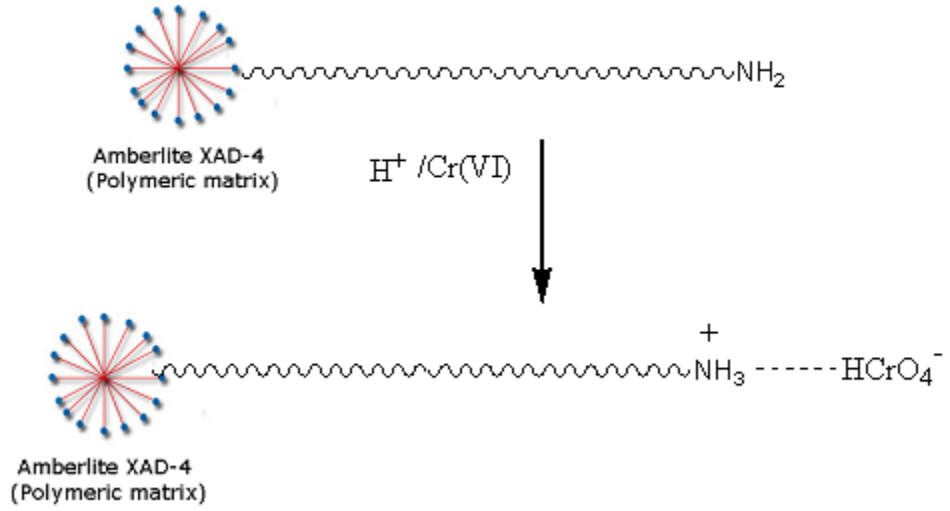

Figure 3.19 Conceptual illustration showing the adsorption of chromium in the amine impregnated polymeric sorbent

(ii) Consequence of pH and Adsorbent Dosage on the Adsorption of Chromium

The effect of pH on the adsorption was considered by adding 0.3g of adsorbent to 25 mL of 10 mg L^{-1} Cr(VI) at pH 2.5. This mixture was equilibrated for 30 min at 25 °C and a known volume of the solution was separated from the adsorbent, and the residual concentration of Cr(VI) was measured spectrophotometrically. In acidic medium, the $–NH_2$ group of n-octylamine is protonated as NH_3^+, which forms an ion-association complex with hydrochromate ion. Although, Cr(VI) can exist as hydrochromate and dichromate ion at low pH[73] it is the hydrochromate species that forms an ion-pair with n-octylamine. This fact has been confirmed through the FT-IR study as mentioned before from the characteristic Cr=O peak at 899 cm^{-1}. The electrostatic stabilization of the bound $HCrO_4^-$ to the NH_3^+ cation is in accordance with the FT-IR data. On the basis of the above observations, the optimum pH for the quantitative solid phase extraction of chromium was found to be in the range 2 to 3.5. At weakly acidic and alkaline pH conditions, the percentage adsorption was found to decrease since at higher pH, the species CrO_4^{2-} does not form a stable ion-association complex with the amine. As a result, the electrostatic forces between the adsorbate and adsorbent weaken and this leads to a decrease in the percentage adsorption of chromium(VI). The effect of adsorbent dosage on Cr(VI) removal was investigated by varying the amount of adsorbent from 0.1 to 1.0g with the initial concentration of 10 mgL^{-1}. The removal efficiency of chromium increases with increasing amount of adsorbent and then reaches its upper limit at 0.3g of adsorbent. At low adsorbent dosage, the active sites accessible for adsorption are inadequate in comparison to the concentration of Cr(VI), thereby resulting in reduction of the removal efficiency. When the amount of adsorbent is higher than 0.3g the adsorption sites are saturated and further increase in adsorbent dosage does not cause any appreciable increase in the removal efficiency of chromium(VI). The adsorption of Cr(VI) on the polymeric sorbent was found to be quantitative when the amount of the sorbent is in the range 0.1-0.3g in 25 mL sample volume used for the batch experiments.

3.3.4 Optimization of Analytical Procedure

(i) Isotherm Study

Freundlich[39] and Langmuir[38] are the most commonly used isotherms to study various adsorbent−adsorbate systems in solid phase extraction. Essentially, the Langmuir isotherm model assumes that adsorption takes place on certain fixed sites of the polymeric resin matrix and that the adsorbent layer is unimolecular in thickness. The maximum adsorption capacity q_o and the energy of adsorption b were found to be 75.93 mg g^{-1} and 0.1501 L mg^{-1} respectively. The good adsorption capacity shows that there is effective electrostatic interaction between Cr(VI) as $HCrO_4^-$ with the protonated amine (NH_3^+) in acidic medium on the surface of the polymeric resin sorbent. The Langmuir isotherm model also gives another important parameter, R_L given by the expression $R_L = 1/ (1 + b.C_0)$ facilitates to appreciate the adsorption system. It has been proved in many adsorption systems that the value of R_L in the range 0 to 1 signifies fine adsorption.[40] In the present investigation, the value of R_L for the adsorption of chromium on the polymeric sorbent was found to be 0.118 indicating efficient adsorption under the given experimental conditions. The Freundlich isotherm, an empirical equation, describes the adsorption of organic and inorganic species on a wide range of adsorbents. The Freundlich model proposes adsorption with a heterogeneous energetic distribution of active sites, accompanied by interactions between adsorbed molecules. In the present investigation, these two widely used isotherm models were applied to study the adsorption behavior of chromium(VI) on the polymeric sorbent (Figure 3.20A,B). A plot of log q_e versus log C_e gave a straight line with regression coefficient 0.98. The value of n (which is an index of adsorption) in the range 1-10 signifies good adsorption. In the present study, n which denotes the intensity of adsorption was found to be 1.66 and this is indicative of the fact that there is strong affinity between the hydrochromate anion and the protonated amine on the polymeric resin matrix. The adsorption capacity K_F obtained from the Freundlich equation was found to be 10.47 $mg^{1-1/n}$ g^{-1} $L^{1/n}$ Although, the correlation coefficient is similar in both types of isotherms, the experimental data demonstrate better adherence to Langmuir isotherm model in view of the higher adsorption capacity value.

(ii) Thermodynamics of Adsorption

The study of thermodynamics of the adsorption process was studied by conducting the batch experiments at four different temperatures. The change in the Gibbs free energy is related to the logarithm of the equilibrium constant and the values of ΔH^o and ΔS^0 are obtained from the slope and intercept of the Van't Hoff plot of $\ln K_c$ against 1/T. [45,46] For an endothermic reaction, the slope is negative and for an exothermic reaction the slope is positive and the equilibrium constant decreases with increase in temperature. The adsorption of Cr(VI) was more pronounced at room temperature and decreased at higher temperature range. This is indicative of the fact that the adsorbate–adsorbent interactive forces become weak at higher temperature. Hence, higher temperature is not favourable for the adsorption process. The ΔG^0 value at 298 K was found to be -10.92 kJ mol^{-1}. However, as the temperature increased, the free energy values become less negative. This indicates that adsorption is favorable at 298 K rather than the higher temperature range (Table 3.5). The equilibrium constant K_c is obtained from the ratio of the equilibrium concentration of the chromium(VI) on the adsorbent and in the solution. Assuming that ΔH^0 is constant over the temperature range studied, the Van't Hoff plot of $\ln K_c$ against 1/T is obtained and shown in Figure 3.20C. The ΔS^0 and ΔH^0 value were found to be -136.39 J $mol^{-1}K^{-1}$ and -51.57 kJ mol^{-1}, and this indicates reduction in the randomness at the sorbent-solution interface and the exothermic nature of adsorption. When an aqueous solution of the Cr(VI) is added to the polymeric adsorbent, the water molecules surround the hydrophobic polymeric host matrix and this cage effect is responsible for the decrease in entropy of the system.

(iii) Adsorption Kinetics and Intraparticle Rate Constant

Adsorption kinetics is quite important for the evaluation of the effectiveness of an adsorbent. At equilibrium, the uptake of chromium is governed by the rate at which it is transported from the surface to the pores of the adsorbent. The kinetic parameters for the adsorption of Cr(VI) were determined by using pseudo first-order[41] and pseudo second-order equations.[42] The second order rate constant was found to be 0.29 g mg^{-1} min^{-1} which is obtained from the plot of t/q_t versus t (Figure 3.20D). The value of $q_{e\,(exp)}$ and $q_{e\,(calc)}$ was found to be 6.12 mg $g^{-1}$and 6.20 mg g^{-1} at 50 mg L^{-1} concentration of Cr(VI).

The close agreement between the experimental and calculated value was in accordance with second order kinetic model. Essentially, in the adsorption process mass transfer from the bulk to the surface of the solid matrix transports the metal ion. It is possible that Cr(VI) could diffuse into the polymeric sorbent and in order to verify whether diffusion is the only rate determining step.[43] The intraparticle rate constant was found to be 0.114 mg $g^{-1}min^{-1/2}$ which is obtained from the slope of the plot of q_t against $\sqrt{t}$ (Figure 3.21E). The plot has a non-zero intercept and this indicates the fact that diffusion is not the only aspect that controls the mechanism of adsorption.[44]

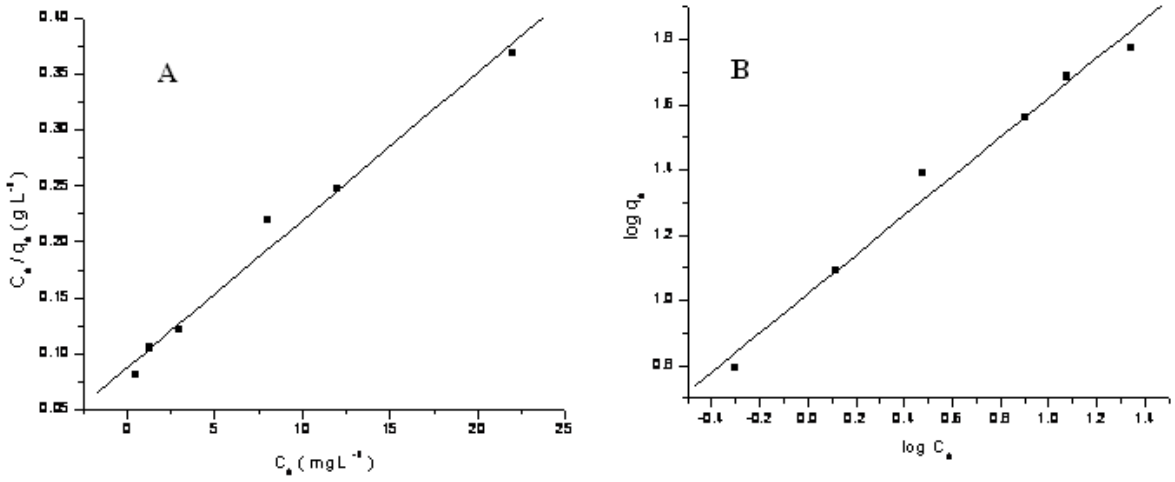

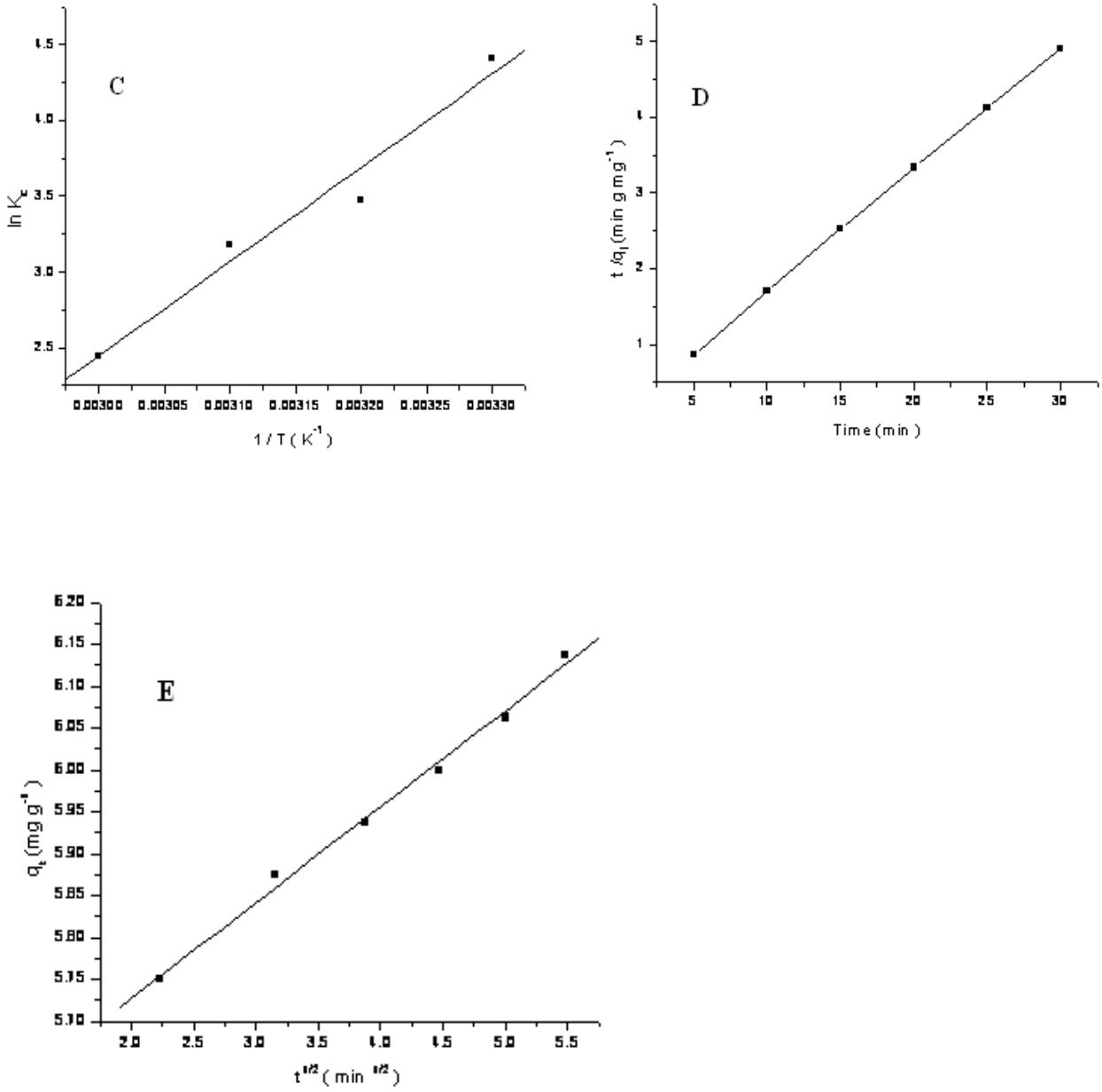

Figure 3.20 (A)Langmuir isotherm (B)Freundlich (C)Relationship of $\ln K_c$ vs 1/T (D) pseudo–second-order plot (E) Intraparticle diffusion

Table 3.5. Equilibrium constant and free energy change obtained at various temperatures

Temperature in Kelvin	Kc	ΔG^0 (kJ mol^{-1})
298	82.33	-10.92
308	32.33	-8.90
318	24	-8.40
328	11.5	-6.66

(iv) Column Adsorption Study

After optimizing the various parameters in batch mode, column study was performed to assess the removal of chromium from a larger sample volume. A known weight (3.5g) of the adsorbent was dispersed with 30 mL Milli-Q water and then loaded into a glass column (length 30 cm, i.d 1.5 cm). The column was plugged with cotton at the bottom for effective support to the resin and the polymeric sorbent was packed to a height of 3cm. A 300 mL volume of 10 mg L^{-1} chromium(VI) solution (pH 2.5) was loaded on the column packed with the adsorbent at a flow rate of 4 mL min^{-1}. The amount of chromium adsorbed was measured spectrophotometrically using the standard diphenylcarbazide method. The column adsorption efficiency was quantitative up to 600 mL sample volume.

(v) Regeneration and Reusability of the Polymeric Sorbent

In any solid phase extraction method, regeneration of the sorbent is a vital study to assess the performance efficiency of the solid matrix. In the present investigation, since the adsorption was effective in acidic medium, the desorption study was tried under alkaline condition using NaOH as the eluent.[26,62] The recovery of chromium(VI) was quantitative with 5 mL of 2 mol L^{-1} NaOH. This was confirmed by measuring the concentration of chromium(VI) in the eluate spectrophotometrically after complexation

with diphenylcarbazide. The mechanism of desorption is illustrated in Figure 3.21, where the eluent splits the interactive force existing between the adsorbent and the adsorbate and releases Cr(VI) as its sodium salt in the aqueous phase. The sorbent could be used for 9 adsorption-desorption cycles with good precision and efficiency. Beyond 9 cycles, there was a decrease in the recovery of chromium by 15%.

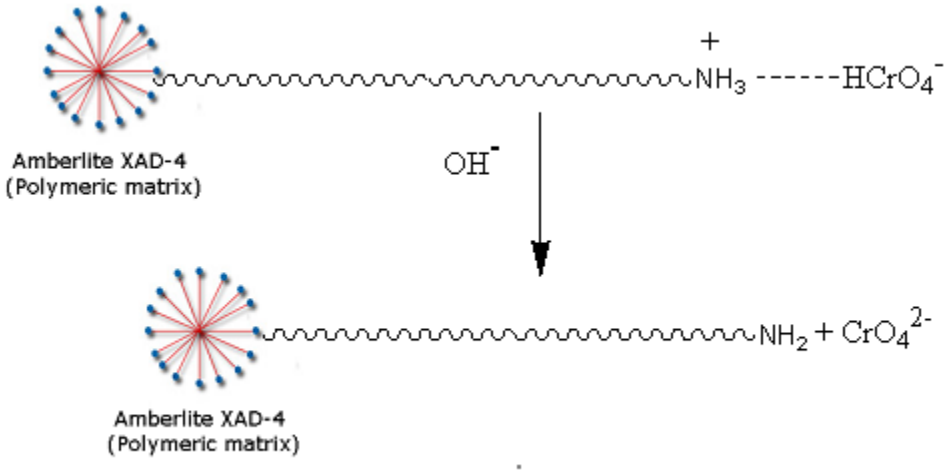

Figure 3.21. Recovery of chromium with sodium hydroxide

(vi) Characterization of the Regenerated Sorbent

The characteristic band in FT-IR for Cr=O (899 cm^{-1}) was not observed in the solid sorbent (Figure 3.22) after elution with NaOH. The CPMAS ^{13}C NMR also showed the absence of peak at 69.5 ppm, characteristic of the protonation of the nitrogen attached to carbon in the aliphatic primary amine (Figure 3.23). All the above observations confirm the quantitative desorption of chromium(VI) with sodium hydroxide as the eluent.

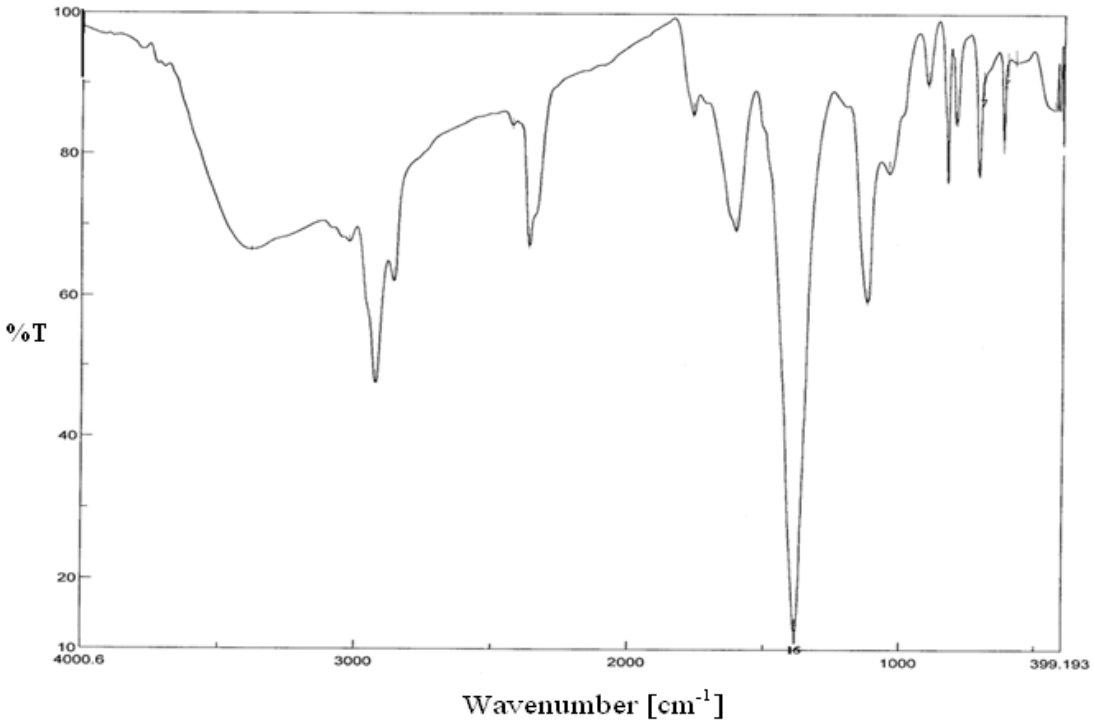

Figure 3.22. FT-IR spectrum of after desorption of chromium(VI)

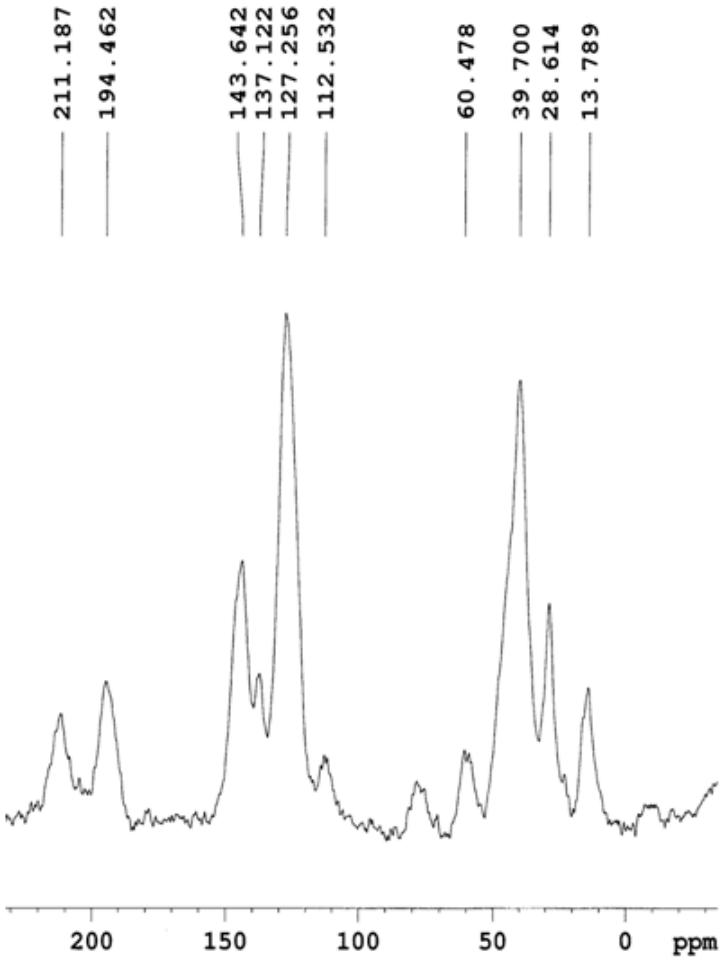

Figure 3.23. ^{13}C NMR spectrum obtained on desorption with NaOH

(vii) Application to Study the Removal of Chromium from Wastewater Sample obtained from Tannery

Prior to applying the proposed method to real effluents, the effect of certain commonly present ions in the waste water sample was studied from an aqueous solution containing 100 mg L^{-1} total chromium and anions such as Cl^- , NO_3^-, SO_4^{2-} at 600 mg L^{-1} respectively. The effect of anions was studied in particular, since they could also have competitive adsorption with the hydrochromate ion by ion-pair formation with the protonated amine. The pH was maintained at 2.5 and the mixture was passed through the column. The adsorption was found to be quantitative and hence the amine impregnated polymeric sorbent was tested for the removal of chromium from a leather tannery effluent, where chromium (III) is used in the tanning process.[50] The distinct

characteristics of the tannery waste water sample procured from a nearby industry are given in Table 3.6. A 50 mL volume of the tannery effluent was diluted to 250 mL and after destruction of the organic matter with nitric acid-sulfuric acid mixture, the sample was oxidized with alkaline peroxide to convert all chromium (III) to chromium (VI). The sample was loaded on the adsorbent column at a pH value of 2.5, where the chromium was quantitatively retained as $HCrO_4^-$ ----NH_3^+ in the column. The flow chart for the removal of total chromium is given in Figure 3.24. The adsorbed chromium could be quantitatively recovered using sodium hydroxide with an average removal efficiency of 99.5%.

Safe disposal of the recovered chromium (VI)

Since, Cr(VI) is a potential carcinogen, care should be taken for the proper disposal. The desorbed Cr(VI) was reduced to Cr(III) and collected separately. This was used for the ongoing remediation studies in our lab pertaining the separation of Cr(III) and Cr(VI).

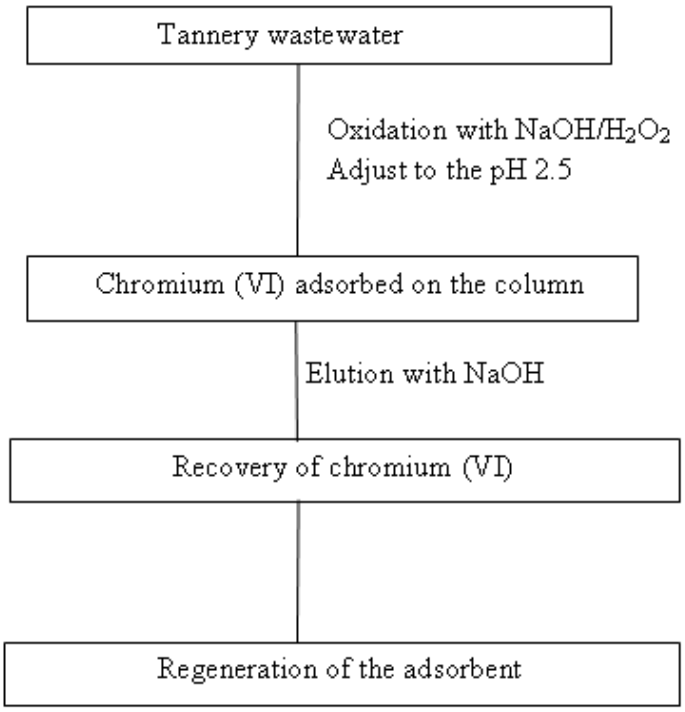

Figure 3.24. Flow chart for the adsorption and recovery of chromium(VI) from tannery effluent

3.3.5 Conclusion

In conclusion, the present investigation has demonstrated the ability of aliphatic primary amine impregnated polymeric sorbent for the effective detoxification of chromium. Amberlite XAD-4 proved to be an effective host for the impregnation of the n-octylamine as the guest. The removal efficiency depends on the nature of the amine impregnated in the resin matrix. The adsorption process was in accordance with the pseudo second order kinetic model and the thoroughly characterized adsorbent had a maximum adsorption capacity of 75.93 mg g^{-1}. The column study illustrated the potential of the adsorbent to remove chromium from a sample volume of 600 mL. The study of adsorption thermodynamics indicated the adsorption process to be spontaneous at room temperature. The adsorbent could be effectively regenerated and reused for 9 adsorption-desorption

Table 3.6. Characteristics of tannery effluent

Sl. No	Composition	Concentration (mg L^{-1})*
1	Color	Green
2	pH	8.23
3	Total dissolved solids	1510
4	Total Suspended solids	315
5	COD	1260
6	BOD	579
7	Chloride	2580
8	Sulfate	1280
9	Nitrate	706
10	Phosphate	226
11	Lead	1.6
12	Zinc	3.2
13	Iron	7.8
14	Manganese	1.2
15	Total Chromium	262

*All values are in mg L^{-1} except Sl. No.1 and 2.

Reference

1. Li, Y.; Long, C.; Tao, W.; Li, A.; Zhang, Q. *J. Chem. Eng. Data* **2010,** *55*, 3147.
2. Azanova, V. V.; Hradil, J. *React. Funct. Polym.* **1999**, *41*, 163.
3. Podlesnyuk, V. V.; Hradil, J.; Kralova, E. *React. Funct. Polym.* **1999**, *42*, 181.
4. Kunin, R. Porous Polymers as Adsorbents-A review of Current Practice, Rohm and Haas Company: Philadelphia, PA, **1980.** p163.
5. Tsyurupa, M. P.; Davankov, V. A. *React. Funct. Polym.* **2002**, *53*, 193.
6. Long, C.; Li, A. M.; Wu, H. S.; Zhang, Q. X. *Colloids Surf, A* **2009**, *333*, 150.
7. Lederer, M. *J. Chromatogr.***1958,** 314.
8. Warshawsky, South African Patent Application 71/5637, **1971.**
9. R. R. Grinstead, Report by the Dow Chemical Company., On Contract No. 14-12-808 to the Water Quality Office of US Environmental Protection Administration, January **1971.**
10. Warshawsky, A. *Talanta* **1974,** *21*, 624.
11. Warshawsky, A. Berkovitz, H. *Trans. Inst. Min. Metall. Sect. C* **1979,** *88*, 36.
12. Warshawsky, A.; Kalir, R.; Berkovitz, H. *Trans. Inst. Min. Metall. Sect. C* **1979,** *88,31*.
13. Warshawsky, A.; Marinsky, J. A.; Marcus, Y. Ion Exchange and Solvent Extraction, vol. 8, Marcel Dekker, New York, **1981,** p. 229
14. Rajesh, N.; Manikandan, G. *SpectrochimActa* **2008**, *70*, 754.
15. Kebiche-Senhadji, O.; Tingry, S.; Seta, P.; Benamo, M. *Desalination* **2010,** *258*, 59.
16. Trochimczuka, A.W.; Kabay, N.; Arda, M.; Streat M. *React. Funct. Polym.* **2004**, *59*, 1.
17. Raji, C.; Anirudhan, T. S. *Water Res.* **1998,** *32*, 3772.
18. Lakshmipathiraj, P.; Bhaskar Raju, G.; Raviatul Basariya, M.; Parvathy, S.; Prabhakar, S. *Sep. Purif. Technol.* **2008,** *60*, 96.
19. Mohan, D.; Pittman, C. U., Jr. *J. Hazard. Mater.* **2006,** *137*, 762.

20. Wang, X. S.; Chen, L. F.; Li, F. Y.; Chen, K. L.; Wan, W. Y.; Tang, Y. J. *J. Hazard. Mater.* **2010,** *175,* 816.
21. Park, D.; Lim, S. L.; Yun, Y. S.; Park, J. M. *Bioresour. Technol.* **2008,** *99,* 8810.
22. Saygi, K. O.; Tuzen, M.; Soylak, M.; Elci, L. *J. Hazard. Mater.* **2008,** *153,* 1009.
23. Neagu, V. *J. Hazard. Mater.* **2009,** *171,* 410.
24. Kabay, N.; Cortina, J. L.; Trochimczuk, A.; Streat, M. *React. Funct. Polym.* **2010,** *70,* 484.
25. Mahmoud, M. E.; Hafez, O. F.; Alrefaay, A.; Osman, M. M. *Desalination* **2010,** *253,* 9.
26. Qureshi, I.; Memon, S.; Yilmaz, M. *J. Hazard. Mater.* **2009,** *164,* 675.
27. Soylak, M.; Karatepe, A. U.; Elci, L.; Dogan, M. *Turk. J. Chem.* **2003,** *27,* 235.
28. Narin, I.; Kars, A.; Soylak, M. *J. Hazard. Mater.* **2008,** *150,* 453.
29. Saitoh, T.; Nakane, F.; Hiraide, M. *React. Funct. Polym.* **2007,** *67,* 247.
30. Juang, R. S. *Proc. Natl. Sci. Counc., Repub. China* **1999,** *23,* 353.
31. Mendham, J.; Denney, C.; Barnes, J. D.; Thomas, M. Vogel's Textbook of Quantitative Chemical Analysis, Pearson Education Asia: Singapore, **2002.**
32. Li, H.; Li, Z.; Liu, T.; Xiao, X.; Peng, Z.; Deng, L. *Bioresour. Technol.* **2008,** *99,* 6271.
33. Hoffmann, M. M.; Darab, J. G.; Fulton, J. L. *J. Phys. Chem. A* **2001,** *105,* 1772.
34. Lin, C. K.; Chen, J. N.; Lin, C. C. *J. Hazard. Mater.* **1997,** *56,* 21.
35. Aravindhan, R.; Madhan, B.; Raghava Rao, J.; Unni Nair, B.; Ramasami, T. *Environ. Sci. Technol.* **2004,** *38,* 300.
36. Albino Kumar, P.; Ray, M.; Chakraborty, S. *J. Hazard. Mater.* **2007,** *143,* 24.
37. Cabatingan, L. K.; Agapay, R. C.; Rakels, J. L. L.; Ottens, M.; Vander wielen, L. A. M. *Ind. Eng. Chem. Res.* **2001,** *40,* 2302.
38. Langmuir, I. *J. Am. Chem. Soc.* **1918,** *40,* 1361.
39. Freundlich, H. M. F. Z. Phys. Chem. **1906,** *57,* 385.
40. Hall, K. R.; Eagleton, L. C.; Acrivos, A.; Ver Meulen, T. *Ind. Eng. Chem. Fundam.* **1966,** *5,* 212.
41. Lagergren, S. *K. Sven. Vetenskapsakad. Handl.* **1898,** *24,* 1.

42. Ho, Y. S. *J. Hazard. Mater.* **2006,** *136,* 681.
43. Onal, Y.; Basar, C. A.; Eren, D.; Ozdemir, C. S.; Depci, T. *J. Hazard. Mater.* **2006,** *128,* 150.
44. Weber, W. J.; Morris, J. C. *J. Sanit. Eng. Div., Am. Soc. Civ. Eng.* **1963,** *89,* 31.
45. Bulut, E.; Ozacar, M.; Sengil, I. A. *Microporous Mesoporous Mater.* **2008,** *115,* 234.
46. Jiang, M. Q.; Wang, Q. P.; Jin, X. Y.; Chen, Z. L. *J. Hazard. Mater.* **2009,** *170,* 332.
47. Bermejo, R.; Ruiz, E.; Acien, F. G. *Enzyme Microb. Technol.* **2007,** *40,* 927.
48. Kalidhasan, S.; Rajesh, N. *J. Hazard. Mater.* **2009,** *170,* 1079.
49. Kalidhasan, S.; Sricharan, S.; Ganesh, M.; Rajesh, N. *J. Chem. Eng. Data* **2010, 55,** 5627.
50. Balasubramanian, S.; Pugalenthi, V. *Talanta* **1999,** *50,* 457.
51. Albino Kumar, P.; Ray, M.; Charkraborty, S. *Chem. Eng. J.* **2009,** *149,* 340.
52. Santhana Krishna Kumar, S. Kalidhasan, V. Rajesh, N. Rajesh, *Ind. Eng. Chem. Res.* **2012,** *51,* 58.
53. Khan, A. A.; Muthukrishnan, M.; Guha, B. K. *J. Hazard. Mater.* **2010**.*174*, 444.
54. Mohan,D.; Singh,K. P. *Water. Res.* **2002**, *36,* 2304.
55. Khezami, L.; Capart, R. *J. Hazard. Mater.* **2005**, *123*, 223.
56. Hassanien, M. M.; Sherbini, K. S. A. E. *Talanta* **2006**, *68*, 1550.
57. Sharma, Y.C.; Srivastava, V.; Mukherjee, A. K. *J. Chem. Eng. Data* **2010**, *55,* 2390.
58. Anjana, K.; Kaushik, A.; Kiran, B.; Nisha, R. *J. Hazard.Mater.* **2007**, *148,* 383.
59. Boddu V. M.; Abburi, K.; Talbott, J. L.; Smith, E. D. *Environ. Sci. Technol.* **2003**, *37,* 4449.
60. Carmona, M.; Warchoł, J.; Lucas, D. A.; Rodrigue, F. J. *J. Chem. Eng. Data* **2008**, *53,* 1325.
61. Kabay, N.; Arda, M. Trochimczuk, A.; Streat, M. *React. Funct. Polym.* **2004**, *59,* 15.

62. Rajesh, N.; Krishna Kumar, A. S.; Kalidhasan, S.; Vidya Rajesh. *J. Chem.Eng. Data* **2011**, *56*, 2295.
63. Kabay, N.; Arda, M.; Trochimczuk, A.; Streat, M. *React. Funct. Polym.* **2004**, *59*, 9.
64. Ochoa, N. A.; Illanes, C.; Marchese, J.; Basualto, C.; Valenzuela, F. *Sep. Purif. Technol.* **2006**, *52*, 39.
65. Lee, D.W.; Eum, C. H.; Lee, I. H.; Jeon, S. *J. Anal. Sci.* **1988**, *4*, 505.
66. Yalcin, S.; Apak, R. *Inter. J. Environ. Anal. Chem.* **2006**, *86*, 915.
67. Rajesh, N.; Jalan, R.K.; Hotwany, P. *J. Hazard. Mater.* **2008**, *150*, 723.
68. Saha, B.; Gill, R.J.; Bailey, D.G.; Kabay, N.; Arda, M. *React. Funct. Polym.* **2004**, *60*, 223.
69. Clesceri, L.S.; Greenberg, A.E.; Eaton, A.D. In Standard Methods for the Examination of Water and Wastewaters, American Public Health Association: Washington, DC, **1998**.
70. Darder, M.; Colilla, M.; Ruiz-Hitzky, E. *Chem. Mater.* **2003**, *15*, 3774.
71. Shahawi, M. S. E.; Hassan, S. S. M.; Othman, A. M.; Zyada, M. A.; Sonbathi, M. A. E. *Anal. Chim. Acta* **2005**, *534*, 319.
72. Law, R.V.; Sherrington, D. C.; Snape, C. E. *Macromolecules* **1997**, *30*, 2868.
73. Hena, S. J. Hazard. Mater. **2010,** *181*, 474.

Long Chain Amine and Biopolymer Modified Sodium Montmorillonite for the Removal of Chromium and Mercury

4.1 Introduction

This chapter deals with the adsorption of mercury and chromium by modification of the sodium form of montmorillonite with trioctylamine/dodecylamine followed by its application to coal fly ash sample and tannery wastewater. The use of clays as sorbents to remove contaminants has gained considerable attention since they are relatively cost effective than other materials such as activated carbon and zeolite. The Na^+-type of montmorillonite, is a 2:1 layered silicate that swells in aqueous medium. The inner layer is composed of an octahedral sheet of the general form $M_{2-3}(OH)_6$ (where M is typically Al^{3+}), which is sandwiched between two SiO_4 tetrahedral sheets.[1] The replacement of Al^{3+} for Si^{4+} in the tetrahedral layer and Mg^{2+} or Zn^{2+} for Al^{3+} in the octahedral layer results in a net negative charge on the clay surfaces. The charge imbalance is offset by exchangeable cations such as H^+, Na^+ or Ca^{2+} on the layer surfaces. In aqueous solutions, water is intercalated into the interlamellar space of montmorillonite, leading to an expansion of the minerals. Clays as such with a negative surface charge have weak affinity for heavy metal ions. Modification with surfactants have been widely utilized to alter the surface properties of the swelling clays in order to improve the sorption ability.[2,3] Some of the previous studies have also focused on using cationic surfactants to adsorb organic compounds e.g. the sorption of phenol on HDTMAB (hexadecyltrimethyammonium bromide)-modified montmorillonite[4]. In addition, the sorption of Cr(VI) oxyanions on CTABr modified montmorillonite has been reported.[4] In fact, the modification mechanism depends on the nature of clays (degree of swelling, layer structure) and surfactants (molecular size). Haggerty and Bowman[5] reported that amine surfactants are too large to enter the internal position of clay and sorption of the amines only occurs on the clay's external exchange sites. Relatively few studies have been reported for sorption of heavy metal cations on clays modified with anionic surfactants such as sodium dodecylsulfate. In order to adsorb metal cations and form complexes, the clay surface must possess negatively charged sites or there should be a replacement of weakly held counter-ions in the solution. Sorption of metal cations on

anionic surfactant modified clays is due to the formation of a surface-cation complex.[6-9] The research on heavy metal–clay mineral surface interactions is still of great interest in view of their toxicity .[10-18]

The first part of this chapter deals with an enhanced method for the adsorption of mercury by impregnation of trioctylamine onto sodium montmorillonite clay matrix.

The second part of this chapter deals with the adsorption of chromium by impregnation of dodecylamine onto sodium montmorillonite clay matrix.

The final part of this chapter deals with

(i) Application of cellulose-clay composite biosorbent toward the effective adsorption of chromium from industrial wastewater and

(ii) Microwave assisted preparation and characterization of biopolymer-clay composite material and its application for chromium detoxification from an industrial effluent.

Study on the adsorption of mercury as tetrachloromercurate(II)anion with trioctylamine modified sodium montmorillonite

4.2.1 Introduction

This chapter deals with a meticulous study on the adsorption of mercury as tetrachloromercurate(II) anion with trioctylamine modified sodium montmorillonite as the adsorbent.. Clay materials have evoked substantial interest in varied applications. Clays are known for their utility as low cost and well-organized adsorbents in view of their chemical and mechanical stability, high specific surface area, and structural properties.The indefatigable quest in the journey towards exploring effective adsorbents has witnessed a plethora of methods and materials for the detoxification of heavy metals including mercury.[19] The lacunae with some of the existing adsorbent materials needs to be addressed in terms of the adsorption capacity, regenerability etc. In this regard, chemically modified clay materials prove to be a viable and attractive alternative as effective adsorbents for toxic heavy metals.[20] Mercury is regarded as one of the most toxic metals in atmospheric and aqueous systems because of its ability to bioaccumulate in the food chain.[21] The pollution of mercury arises from various industrial sources such as coal combustion[22] electronics manufacturing plants, sulfide ore roasting and chlor-alkali industry.[23] Therefore, effective treatment of the wastewater containing mercury is very important. Many techniques involving liquid- liquid extraction[24] and solid phase extraction [25,26] have been in vogue for the treatment of wastewater containing mercury. Adsorbents such as thiol functionalized clays,[27] thiourea modified chitosan,[28] barbital immobilized chitosan,[29] thiol-functionalized mesostructured silica,[30] free and monolayer protected silver nanoparticles[31] are known for their efficacy in the removal of mercury.

In addition to the quaternary ammonium cations such as CTABr[32] long chain amines such as trioctylamine[33] can also be effectively intercalated in the interlayer of the clays. Thiol ligands loaded onto organophilic sodium montmorillonite has been studied for the voltammetric determination of mercury.[34] The intercalation of protonated pyridinium derivatives in the montmorillonite clay matrix has been utilized in the development of amperometric sensors for mercury.[35] To the best of our literature survey, there are no

reports on the application of trioctylamine modified sodium montmorillonite for the solid phase extraction of mercury. This chapter deals with the modification of the sodium form of montmorillonite with trioctylamine and the resulting interaction with mercury followed by its application toward the adsorption and detoxification from a coal fly ash sample.

4.2.2. Experimental Section

(i) Adsorbent Preparation

The sodium form of the montmorillonite clay was prepared from montmorillonite as described previously in literature.[36] An 8.6 mL volume of 0.02 mole trioctylamine in 3 mol L^{-1} HCl medium was added to 4 g of the sodium montmorillonite suspended in 15 mL acetone. [37] The acidic medium ensures the protonation of trioctylamine thereby rendering the clay surface organophilic. Further, the contents were stirred magnetically for 10 hours. The mixture was centrifuged, washed and the centrifugate was verified to ascertain the presence of chloride ion by the silver nitrate test. The absence of turbidity in the aqueous phase ensures the complete exclusion of chloride. The amine modified adsorbent material was dried in a hot air oven at 80^{o}C for 8 hours prior to the batch adsorption experiments. The prepared adsorbent was well characterized using various analytical techniques.

(ii) Adsorption Studies

The batch experiments were performed by equilibrating 0.2 g of the amine modified clay adsorbent material with a known volume (V) (25 mL of 100 mg L^{-1} Hg(II) solution) at 1.0 mol L^{-1} NaCl concentration adjusted to pH 3.0 in an orbital incubator shaker supplied by Biotechnics, India for varying time intervals and the concentration of Hg(II) in the solution phase was estimated by the standard Cold Vapour-Atomic Absorption Spectrophotometric (CV-AAS) technique.[38]

(iii)Column Study

For the scale up of the process, a packed bed glass column (3 cm diameter, 30 cm length) was filled with 4.5 g of the amine-modified adsorbent. The packing height was fixed at 4

cm. At a flow rate of 8 mL min^{-1} and pH 3.0, a 100 mL volume of 10 mg L^{-1} Hg(II) was transferred to the adsorbent column and the concentration of mercury in the solution phase was ascertained through CV-AAS technique. The adsorption of mercury as tetrachloromercurate(II) anion on the packed bed organophilic clay adsorbent column was quantitative (99.4± 0.2%) and this was confirmed with three replicate measurements.

4.2.3. Results and Discussion

(i) Characterization of Trioctylamine Modified Sodium Montmorillonite by FT-IR Spectroscopy

In the FT-IR spectrum (Figure 4.1) characteristic bands corresponding to the various functionalities in the amine modified sodium montmorillonite were observed at 3625 cm^{-1} (ν_{O-H}), 2927 cm^{-1} (ν_{C-H}), 1639 cm^{-1} (δ_{O-H}), 1029 cm^{-1} (ν_{Si-O}), 469 cm^{-1} (ν_{Mg-O}) and 618 cm^{-1} (ν_{Al-O}) respectively.[39] The stretching vibrational frequency as a result of the protonation of the tertiary amine (ν_{NH^+}) was observed at 2463 cm^{-1} [40] The deformation peak (δ_{N-H^+}) in the protonated trioctylamine is obtained at 1377 cm^{-1}. [41,42] After the adsorption of mercury as $HgCl_4^{2-}$, with the positively charged amine, the (ν_{NH^+}) shifts to 2484 cm^{-1}. This shift to a higher frequency implies that the tertiary nitrogen in the protonated amine is effective in its interaction with the tetrachloromercurate(II) anion in the clay matrix. The FT-IR study of the adsorbent material indicates that $HgCl_4^{2-}$ (guest) anion is effectively relocated from the aqueous phase to the organophilic clay (host) by means of an interesting host-guest electrostatic interaction with the protonated tertiary amine.

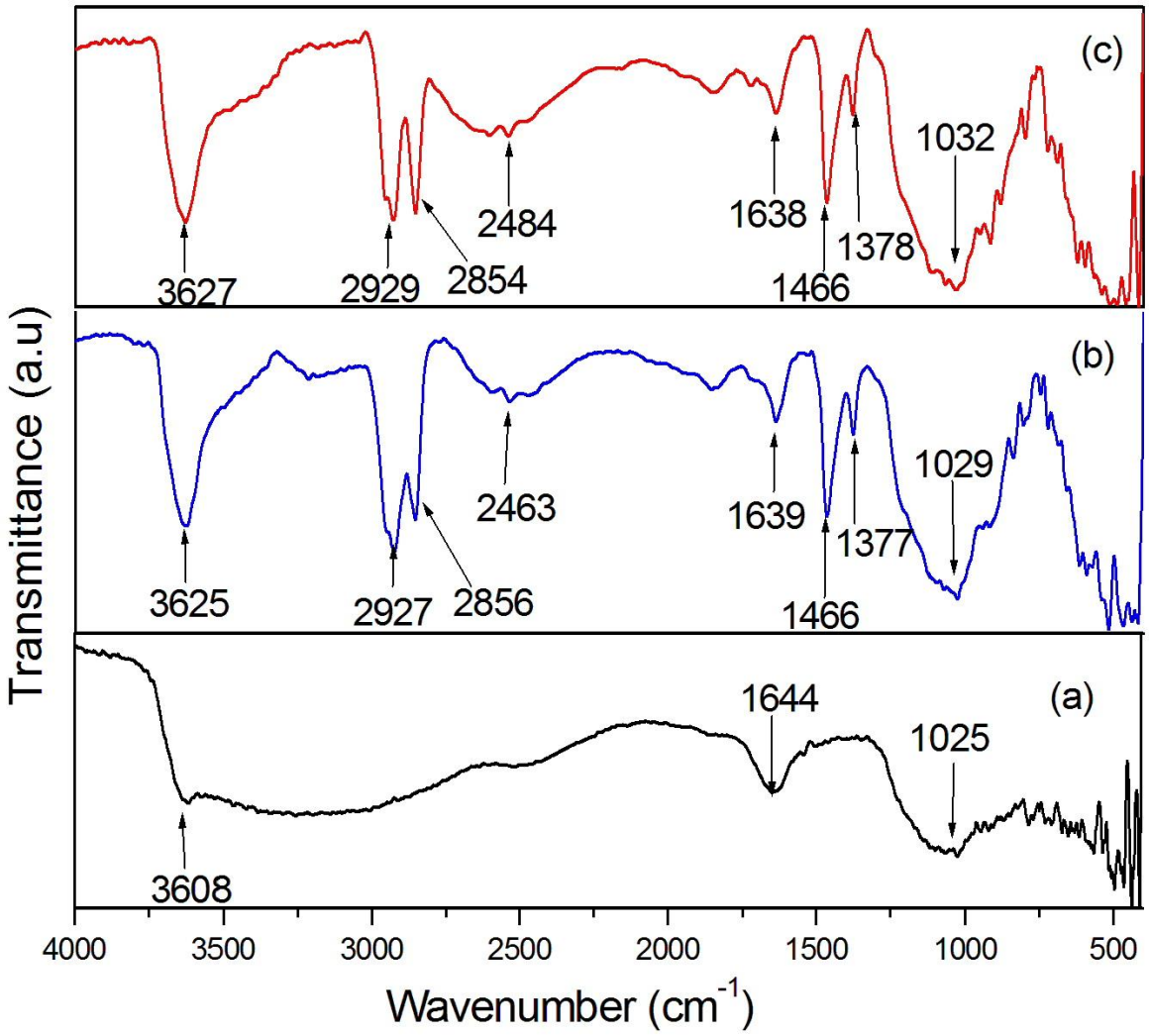

Figure 4.1. FT- IR Spectrum of (A) Na-MMT (B) amine impregnated Na-MMT (C) after adsorption of mercury

(ii)Surface Morphological Changes and Energy Dispersive X ray Spectrum of the Adsorbent Material

The surface morphology of the adsorbent material was studied through the images obtained by optical microscopy. The optical microscopy image for the amine modified adsorbent material (Figure 4.2A) was obtained by spreading a thin layer of the adsorbent on a glass slide. After the adsorption of Hg(II), few drops of diphenylthiocarbazone was added as a spot reagent to the adsorbent material and the image was recorded as mentioned above. Diphenylthiocarbazone is an excellent reagent known to chelate mercury in acidic medium[43] and the complexation occurs through the sulfur and nitrogen atoms in the ligand. Distinct morphological changes were evident prior and after the adsorption of mercury. The red colored spots (Figure 4.2B) obtained after adsorption indicates the effective chelation between Hg(II) and diphenylthiocarbazone in acidic medium. The adsorption of mercury on the surface of the trioctylamine intercalated onto the montmorillonite clay was also confirmed through the energy dispersive X ray (EDX) spectral analysis (Figure 4.3). The EDX spectrum indicates the presence of adsorbed mercury (in the range 1-2 keV) and other elemental peaks such as C, O, N, Mg, Na, Al and Si characteristic of the adsorbent at different regions in the spectrum.[44]

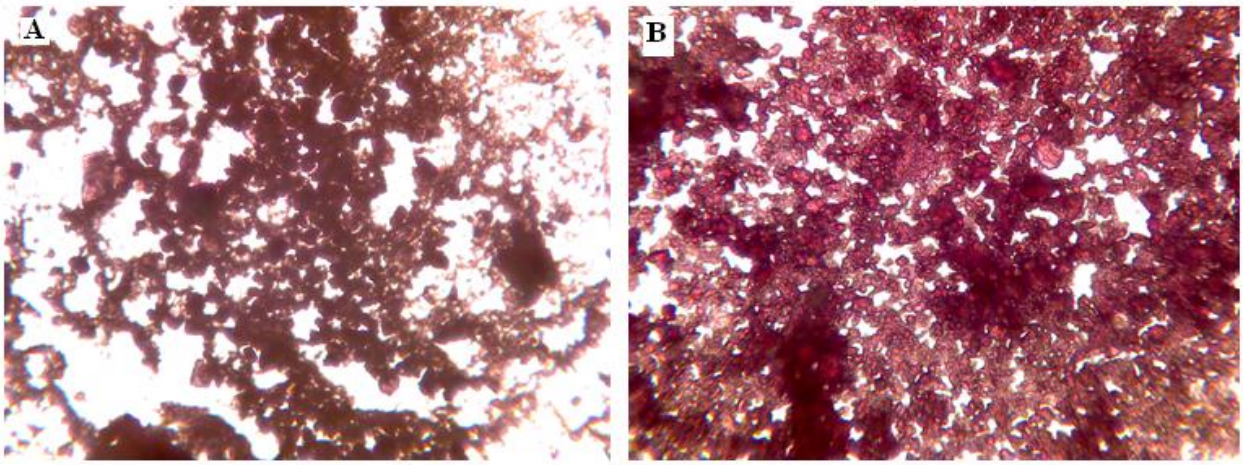

Figure 4.2. Optical microscopy images (A) amine modified sodium montmorillonite (B) after mercury adsorption on the sorbent

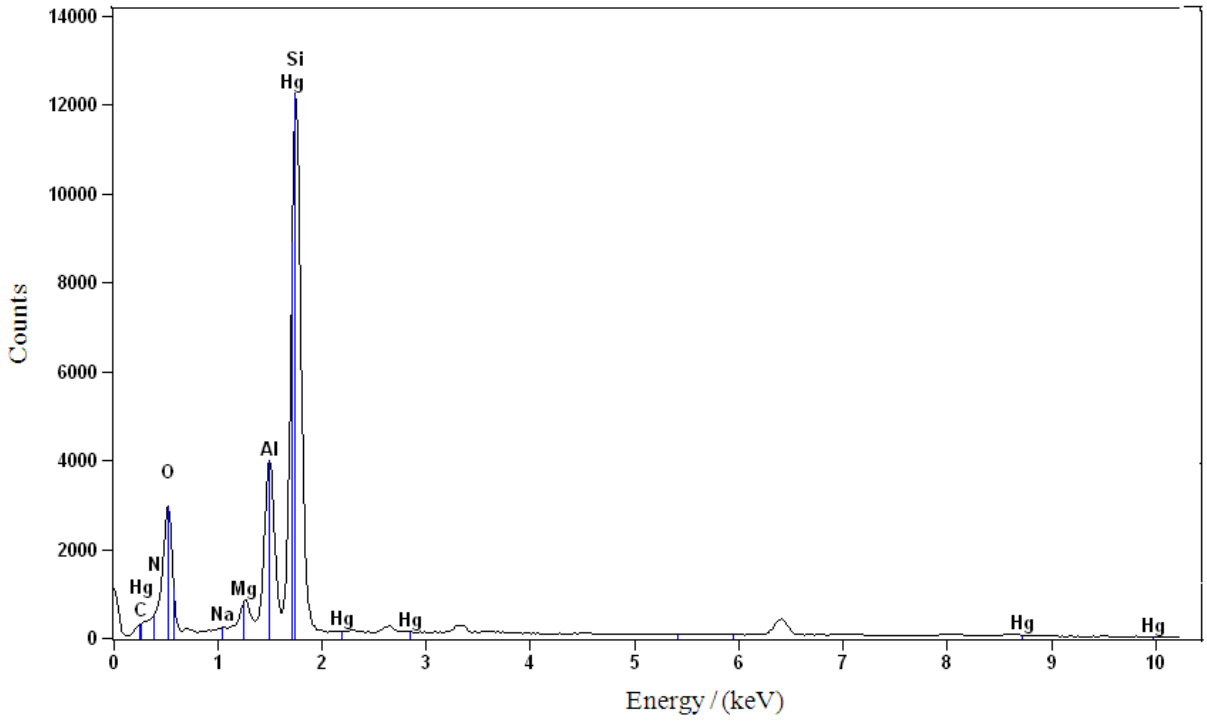

Figure 4.3. EDX spectrum of the adsorbed mercury on the organophilic clay

(iii)X Ray Diffraction Studies of the Amine Modified Clay Adsorbent

The XRD studies on the adsorbent before and after the adsorption of mercury leads to some interesting observations. Since, an adsorption process might lead to some structural changes in the adsorbent material (in terms of amorphous or crystalline nature), it is vital to assess this phenomenon from the distinct XRD patterns of the adsorbent in various forms. The XRD pattern of sodium montmorillonite prior to the modification with trioctylamine shows sharp and meaningful diffraction peaks at 2θ values (Figure 4.4A) corresponding to 6.07^0 (001), 8.99^0, 19.81^0 (100), 25.53^0, 26.61^0(103), 31.24^0 and 35.10^0 (006) respectively.[33,45] After treatment with trioctylamine in acidic medium (Figure 4.4B), the peaks are shifted to lower 2θ values such as 4.52^0, 8.53^0, 19.50^0, 26.14^0 and 34.64^0 respectively. This shift could be ascribed to the intercalation the protonated amine in sodium montmorillonite. The XRD pattern of the unmodified clay sample clearly shows reflections corresponding to (001) peak [46,47] at d = 14.92 Å which is characteristic of montmorillonite. After modification with trioctylamine the interlayer spacing increases from 14.92 Å to 20.21 Å. This increase of 5.28 Å is attributed to the effective

intercalation of trioctylamine in the clay layer. After the adsorption of mercury as its tetrachlormercurate(II) anion with the protonated amine, the peaks (Figure 4.4C) sharpen further with a shift in the 2θ values corresponding to 4.8^0, 8.87^0 and 19.84^0 respectively. [48,49] This indicates clearly that there is an effective electrostatic interaction between the protonated amine and the tetrachlorcomplex of mercury in the clay matrix. Furthermore, the sharp peaks also indicate the crystalline nature of the adsorbent material in various forms.

(iv) Surface area and Barrett-Joyner- Halenda (BJH) Pore size Distribution

The surface area of the amine modified adsorbent material obtained from N_2 adsorption-desorption study was found to be 20.15 m^2 g^{-1}. This type IV isotherm indicates the mesoporous nature of the adsorbent material (Figure 4.5A). A pore size of 1.92 nm corresponding to a maximum pore volume of 0.12 cm^3 g^{-1} was obtained from the Barrett-Joyner- Halenda (BJH) pore size distribution curve (Figure 4.5B) Literature evidence[50] also points to the fact that ultrastable mesoporous adsorbents as very effective for the removal of mercury ions. This is also corroborated from the supporting evidences such as XRD and EDX spectral analysis which clearly shows the presence of adsorbed mercury on the surface of the adsorbent. Furthermore, the ordered XRD pattern before and after the adsorption of mercury indicates that the mesoporous nature of the adsorbent is retained very well and hence this could be attributed to the effective interaction of mercury with the adsorbent surface.[50] The mesoporous nature of trioctylamine intercalated onto the montmorillonite clay and the fine surface area is indicates the effectiveness in the interaction of tetrachlormercurate(II) anion with the amine modified clay surface.

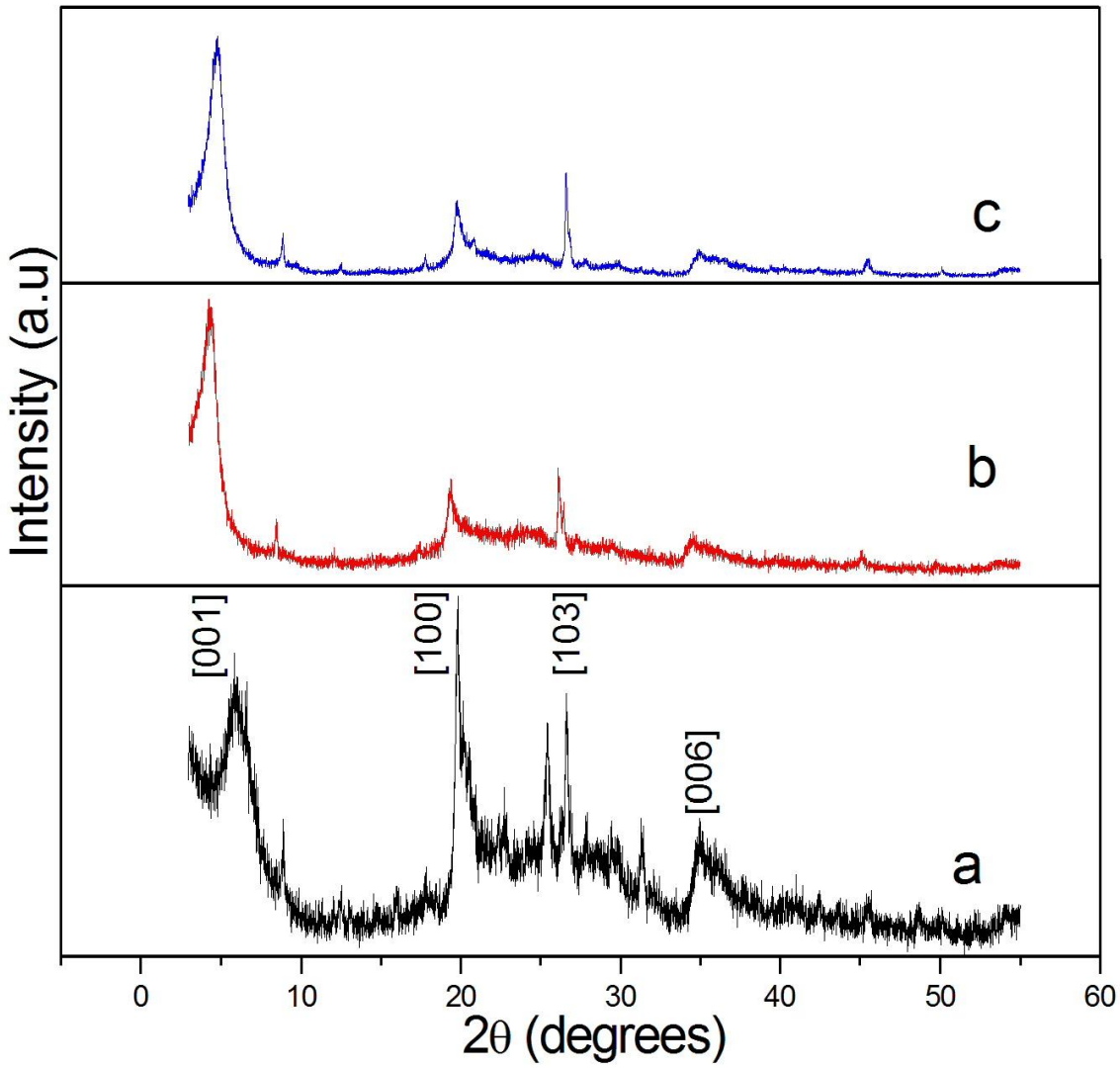

Figure 4.4. XRD pattern (A) Na-MMT (B) amine modified Na-MMT adsorbent (C) After mercury adsorption

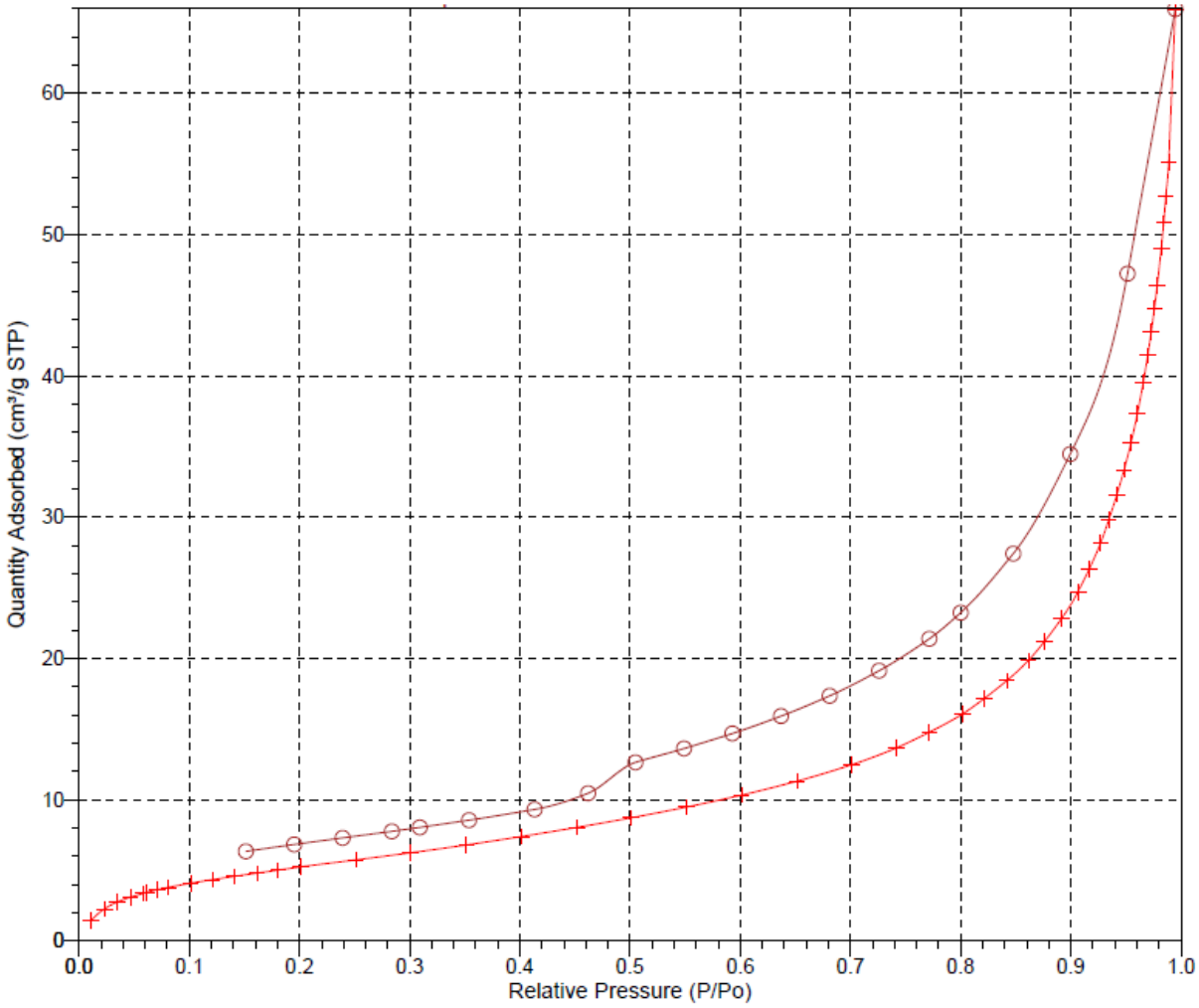

Figure 4.5 (A) Nitrogen adsorption and desorption isotherm

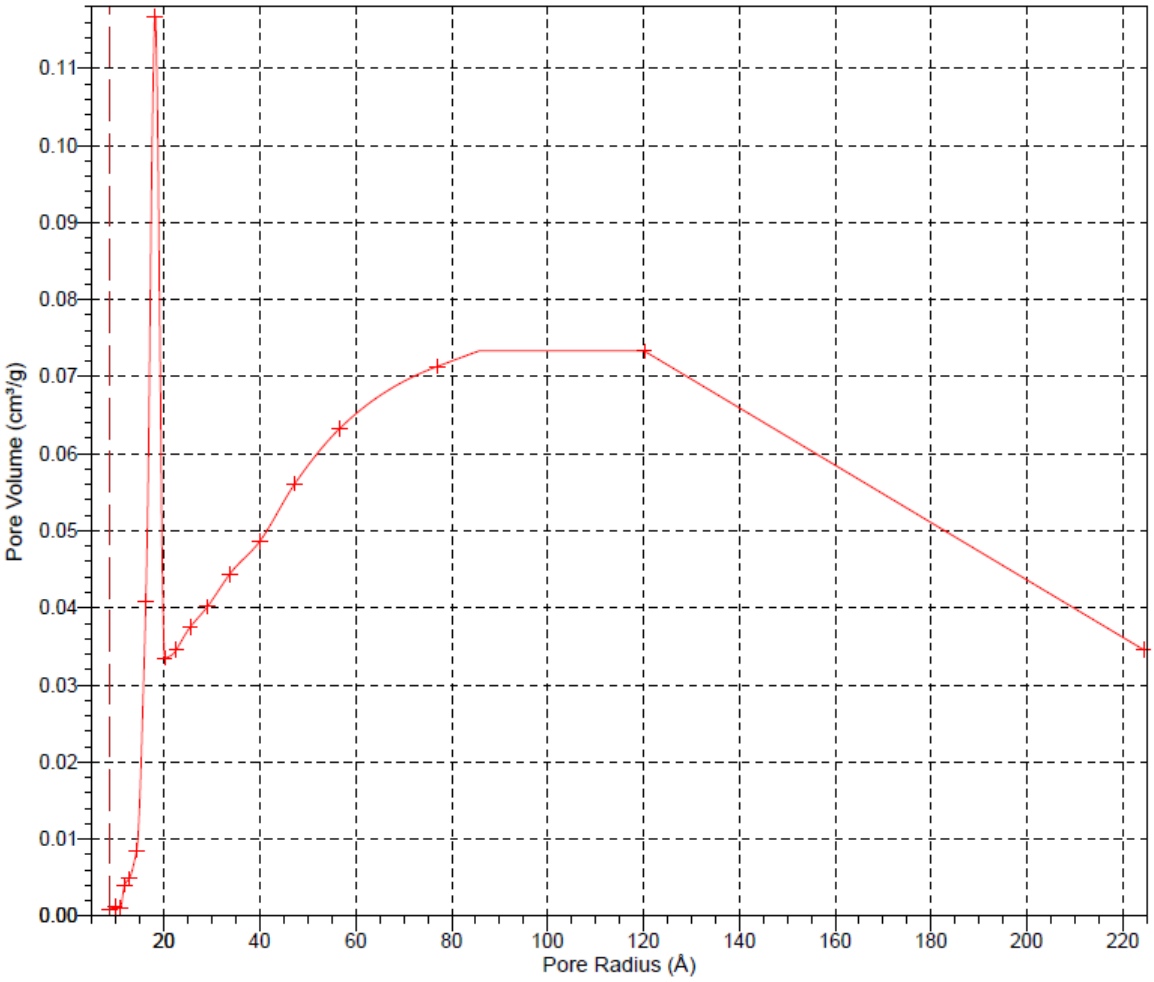

Figure 4.5 (B) BJH pore distribution curve

(v) pH dependence and the Mechanism of Adsorption

The optimization of pH is a significant factor in adsorption study. The pH was varied from 2 to 9.5. The favorable pH for the adsorption of Hg(II) was observed in weakly acidic medium (2.5-3.5). Beyond pH 3.5, there is a decrease in the percentage adsorption of mercury. At a concentration greater than 0.5 mol L^{-1} NaCl, the tetrachloromercurate anion is the predominant species.[51] Among the various possible chloro complexes of mercury, the tetrachloro complex has a high stability constant value[51] and the stepwise formation of the various chloro complexes of mercury with the respective log K (formation constant) values are given below.

$$Hg^{2+} + Cl^{-} \rightleftharpoons HgCl^{+} \qquad \log K_1 = 6.74 \qquad (1)$$

$$Hg^{2+} + 2Cl^{-} \rightleftharpoons HgCl_2 \qquad \log K_2 = 13.22 \qquad (2)$$

$$Hg^{2+} + 3Cl^{-} \rightleftharpoons HgCl_3^{-} \qquad \log K_3 = 14.07 \qquad (3)$$

$$Hg^{2+} + 4Cl^{-} \rightleftharpoons HgCl_4^{2-} \qquad \log K_4 = 15.07 \qquad (4)$$

It is quite obvious that the fourth step in the above is characterized by a high formation constant value. The selective adsorption of tetrachloromercurate(II) anion in the interlayer of the clay matrix results from an energetically favorable electrostatic interaction between the protonated amine and $HgCl_4^{2-}$ anion. The silanol groups in the clay surface could be protonated in acidic medium[52] and this further enhances the electrostatic interaction between tetrachloromercurate(II) anion and the clay surface. In addition, van der Waals interaction could also be possible between the trioctylamine and the clay surface, thereby leading to a good compactness [53] and captivity of $HgCl_4^{2-}$ and the protonated amine in the interlayer. The schematic representation for this interaction is given in Figure 4.6. Indeed, the organophilic clay matrix acts as an effective host to the guest (i.e. tetrachloromercurate(II) anion) species in the pH range 2.5 to 3.5. At low concentration of chloride (<0.5 mol L^{-1}) and in the pH range 2-5, the predominant mercury species are $HgCl_2$ and $HgCl_3^{-}$, while the $HgCl_4^{2-}$ anion prevails at chloride concentration (>0.5 mol L^{-1}) in the pH range 2-5. Hg(II) undergoes hydrolysis to HgOHCl and $Hg(OH)_2$ in the pH range 6-8 and 9-10 respectively.[54,55] Furthermore, at alkaline pH, formation of $HgOH^{+}$, $Hg(OH)_2$ species[51] also leads to a reduction in percentage adsorption. The above mentioned hydroxyl species, could compete for the active adsorption species in the clay matrix and hence affect the adsorption of mercury as its anionic tetrachlorocomplex. The pK_a of trioctylamine[56] is 3.5 at pH values <4, in aqueous acidic medium, the existence of trioctylammonium cation is more favourable. The protonation of amine is facile in the pH range 2-3.5. In basic medium where the pH is greater than pK_a, the amine gets deprotonated and hence the percentage adsorption of mercury decreases. At pH value greater than 4, the solvation of $HgCl_4^{2-}$ with

trioctylamine is more probable and hence the adsorption decreases at higher pH. Tertiary amines are protonated at lower pH values[57] and hence the electrostatic interaction is effective, whereas at higher pH values, the electrostatic repulsion between the anionic chloro complex and the deprotonated amine leads to the decrease in the adsorption of mercury. At higher pH, the deprotonation of $SiOH^+$ group,[52] in the clay surface as SiO^- might also lead to the decrease in the amount of mercury adsorbed as the tetrachloromercurate(II) anion on the clay surface. The various steps involved in the mechanism could be categorized as a) Protonation of the amine b) Interaction of the amine with sodium montmorillonite c) Adsorption of mercury as its tetrachloromercurate(II) anion. These interactions are illustrated through the following equations:-

Step 1. Protonation of trioctylamine

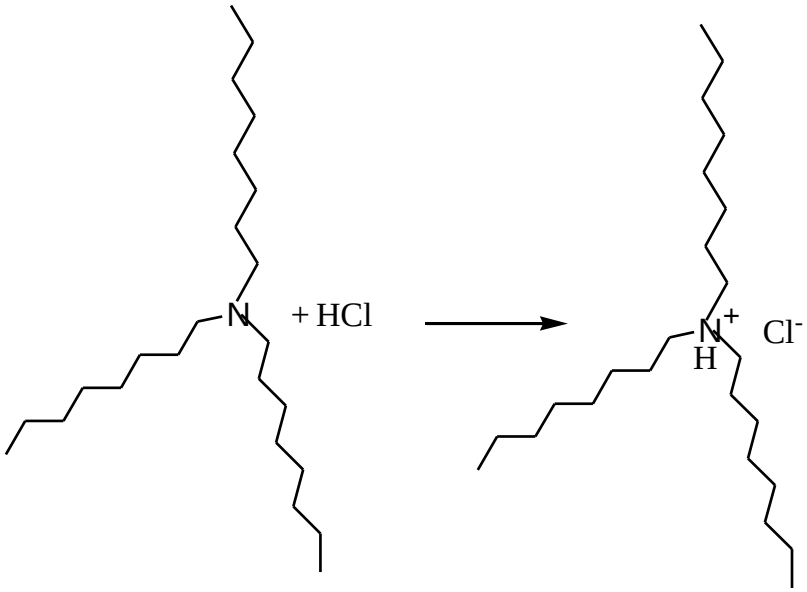

Step 2. Interaction of sodium montomorillonite with protonated trioctylamine

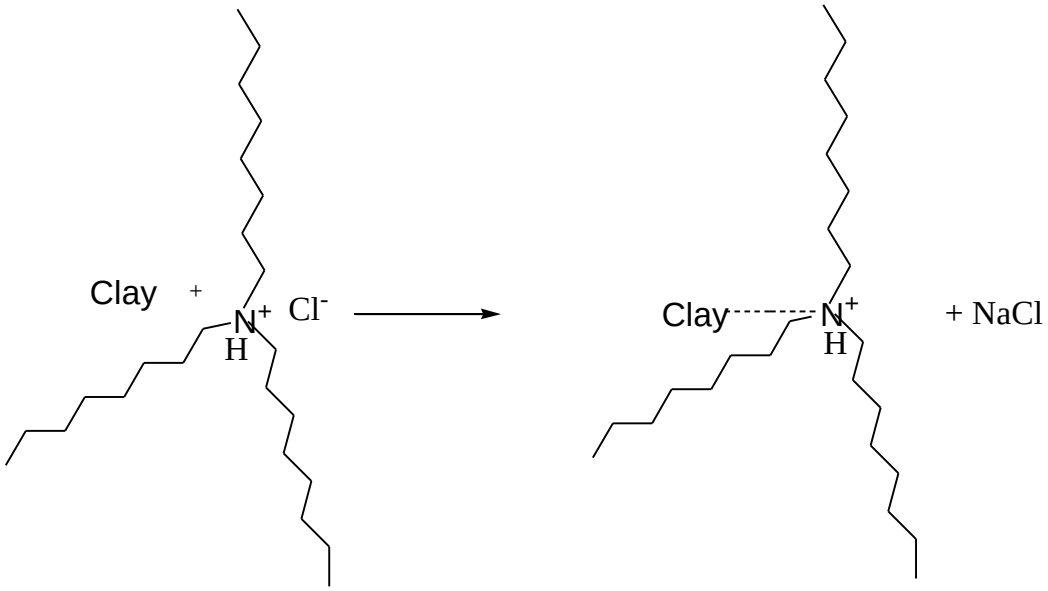

Step 3. Adsorption of mercury in the clay matrix

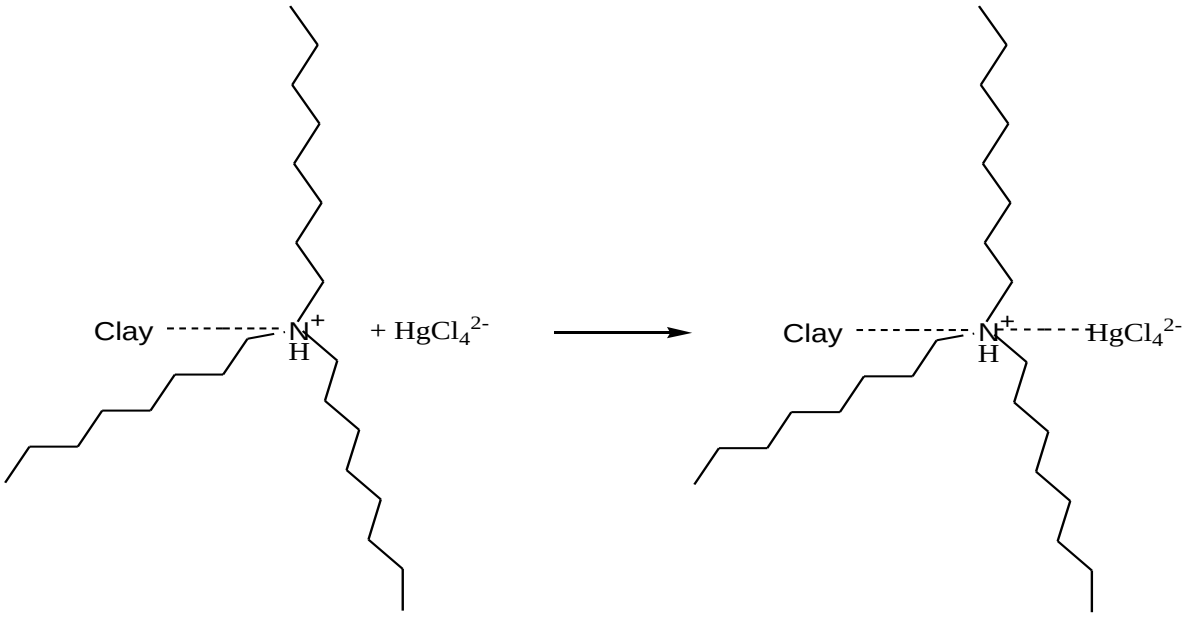

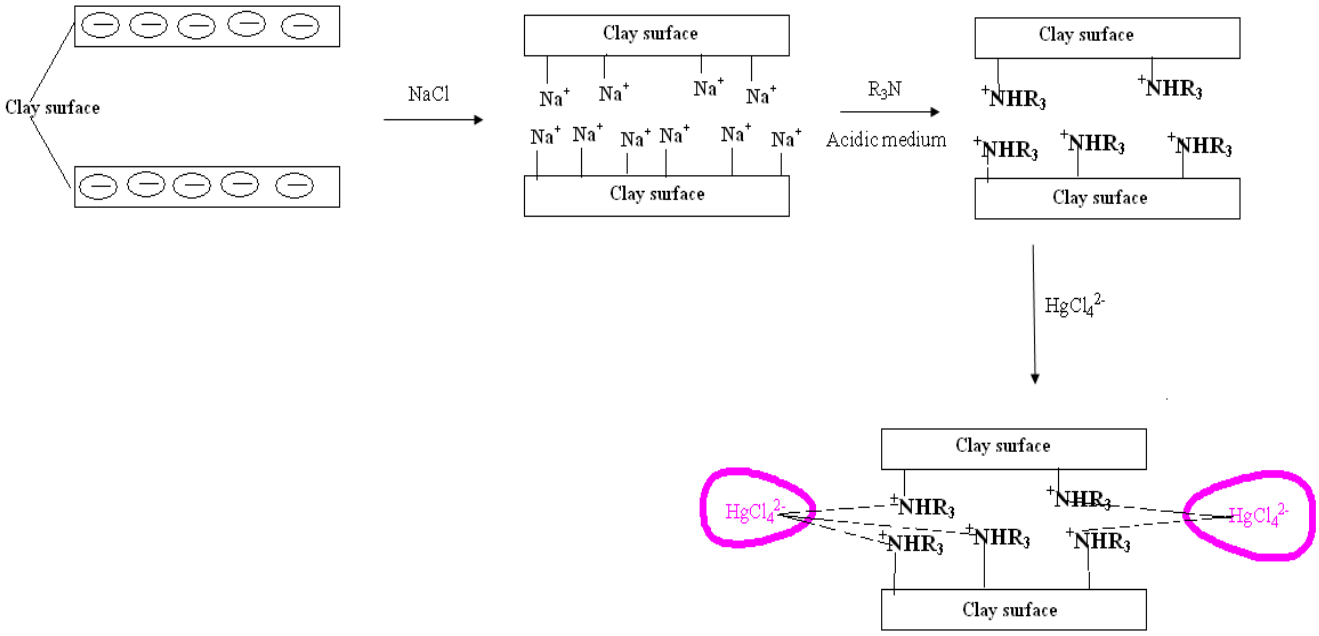

Figure 4.6. Conceptual illustration showing the interaction of tetrachloromercurate(II) anion with the protonated amine in clay matrix

4.2.4 Optimization of Analytical Parameters

(i) Effect of the Amount of the Adsorbent Material

In the batch experiments, the amount of the adsorbent material was varied in the range (0.05 to 0.5) g. The amount of mercury adsorbed as an ion-pair of tetrachloromercurate(II) anion with the protonated amine was found to be maximium (99.2 ±0.03%) in the range (0.2 to 0.3) g in 25 mL sample volume. The available adsorption sites and the surface area increases by varying the adsorbent dose and therefore results in the increase in percentage adsorption of mercury. Although, the percentage adsorption increases with increase in adsorbent dose, the amount of mercury adsorbed per unit mass decreases. This fact is supported from the trend in % adsorption which shows a sharp increase initially and later attains its maximum at 0.2g of the adsorbent (Figure 4.7). The decrease in adsorption capacity with increase in adsorbent dose is attributed to unsaturation of adsorption sites in the process of adsorption.

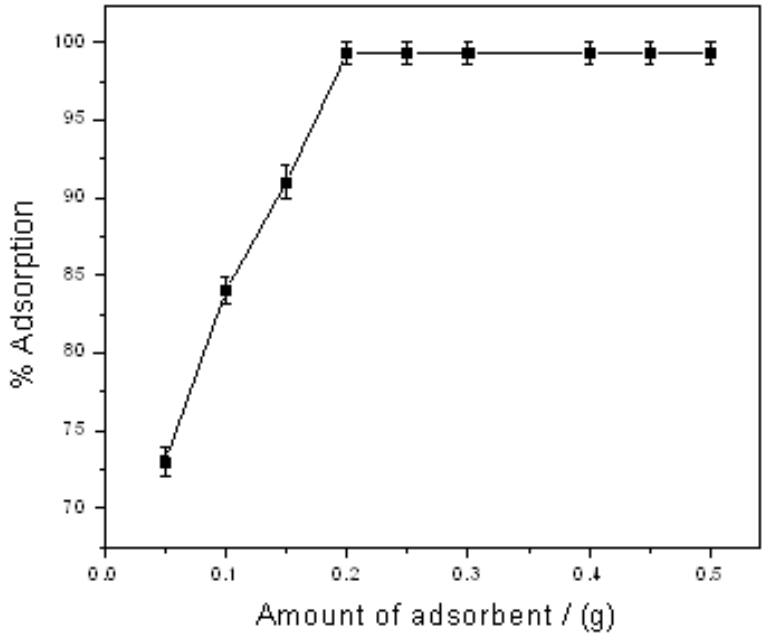

Figure 4.7. Amount of adsorbent

(ii) Study of Various Isotherm Models

A variety of isotherm models was employed to study the effectiveness of the adsorbent-adsorbate interaction. Langmuir isotherm[58] is one of the commonly used empirical isotherm models which take into account the uniformity in the adsorbent surface with a monolayer. From the plot of C_e/q_e against C_e, the maximum adsorption capacity, q_o (mg g^{-1}) of Hg(II) and the constant b are obtained from the slope and intercept respectively. The constant b is attributed to the affinity between the amine modified adsorbent and mercury. These isotherm parameters are given in Table 4.1. Furthermore, the Langmuir isotherm model also relates a dimensionless parameter R_L to the concentration of mercury C_o and b. The values greater than 1 is an indication of an unfavorable isotherm and R_L equal to zero is accounted for a totally irreversible isotherm.[59] In the present system, the R_L value is obtained in the range 0-1 (0.0848, C_o=100 mg L^{-1}) and this implies that there is a strong interaction between the tetrachloromercurate(II) anion and

the protonated amine in the clay matrix. Another extensively employed empirical isotherm model to study the adsorption process from aqueous solution is the Freundlich model[60] which relates q_e and C_e. . At low concentration of the adsorbate, the extent of adsorption varies linearly with concentration, whereas at higher levels it becomes independent of the concentration. A good adsorbent material is characterized by n value in the range 1-10. From the slope and intercept obtained through the logarithmic plot of q_e against C_e, the constants K_F and n were found to be 16.95 mg $^{1-1/n}$ g $^{-1}$ L $^{1/n}$ and 1.806 respectively (Table 4.1). The adsorption mechanism and the interaction between mercury and the amine modified adsorbent surface can be understood through yet another isotherm model known as the Dubinin–Radushkevich isotherm.[61] The nature of the adsorption mechanism is ascertained from the E_{DR} values. The mean free energy value lower than 8 kJ mol^{-1} is indicative of physical adsorption. In the present system, involving the electrostatic interaction between tetrachloromercurate(II) anion and the organophilic clay surface, a value of 1.23 kJ mol^{-1} was obtained and this is attributed to the physical adsorption. The R-P model includes the attributes of Langmuir and Freundlich isotherms. The Redlich–Peterson model relates the constants A, B and an exponent g to the amount of mercury adsorbed at equilibrium q_e. It has been observed in many adsorption systems that the value of g lies between 0-1. The slope and intercept of the plot gives the parameters g and B respectively (Table 4.1). The value of g was found to be 0.845 (near to 1) and this shows that the system could adhere to the Langmuir isotherm model.The Temkin isotherm model is based on the assumption that the adsorption energy decreases linearly with the surface coverage. The linear plot of q_e versus lnC_e gives the constants *A* and *B*. Elovich model is based on the fact that the adsorption sites increase exponentially with adsorption, thereby leading to a multilayer adsorption. The respective isotherm parameters can be obtained from the slope and the intercept of the plot ln (q_e/C_e) against q_e and these are given in Table 4.1.

(iii) Statistical Treatment of the Individual Isotherm Models

The suitability of an isotherm model to understand the present adsorption system is best assessed through the statistical analysis of the experimental and calculated data obtained

through the various isotherm models. Regression coefficient (r^2) is one parameter which helps us to find out the fit to the best possible model. However, this needs to be substantiated by calculating the average percentage error (APE) in each of these isotherm models. The APE is essentially the standard deviation which takes into account the difference in the summation of the experimental and calculated q_e values and the number of experimental data points, N. The APE can be expressed mathematically as

$$APE\ (\%) = \frac{\sum_{i=1}^{N} \left| \left((q_e)_{experimental} - (q_e)_{calculated} \right) / (q_e)_{experimental} \right|}{N} X\ 100 \qquad (5)$$

The regression coefficient in case of Langmuir and Freundlich models were close to 1 (0.98) and the APE in case of the above isotherm models were found to be 7.2 and 8.4 % respectively. The lower APE indicates good adherence to Langmuir model and furthermore, the respective isotherm data plots of q_e against C_e which is L shaped in accordance with Giles classification[62] also shows a better fit to the Langmuir isotherm in terms of the good proximity to the experimental and calculated data points (Figure 4.8A). Moreover, the maximum adsorption capacity for mercury (140.84 mg g^{-1}) was obtained in the case of the Langmuir isotherm model. The APE in the other isotherm models was quite large and with lower correlation coefficient values. The level of significance of regression coefficient is also given by the p value and the standard deviation. Taking into cognizance all these observations, the Langmuir isotherm model supports the data obtained in the study of the interaction between the tetrachlorocomplex of mercury and the protonated amine in the clay matrix.

(iv) Adsorption Kinetics

The adsorption data were fitted to the first order and pseudo second order kinetic equations. These equations relate the amount of mercury adsorbed q_t at time t and at equilibrium $q_{e.}$ [63,64] The plot of log (q_e-q_t) against t (Figure 4.8B) and t/q_t against t (Figure 4.8C) gives the kinetic parameters. The experimental data shows a good fit to the pseudo second order model owing to the higher regression coefficient value. In addition, the chi square value obtained from the second order model was found to be lower as compared to the first order kinetic data. Furthermore, the $q_{e\ calculated}$ and $q_{e\ exp}$ values were found to be

12.48 mg g^{-1} and 12.40 mg g^{-1} in agreement with the second order model. This proximity in the values (Table 4.2) further confirms the suitability of the second order kinetics to the adsorption data. The transport of the tetrachlormercurate(II) anion from the solution phase to the surface of the adsorbent could be controlled by film or external diffusion, pore and surface diffusion.[70] In addition, there is also a likelihood of intraparticle diffusion of the metal ion from the bulk into the pores of the adsorbent material, which is generally a slow process. The intraparticle diffusion is studied using the well known Weber Morris [65] intraparticle diffusion model, which relates the amount of Hg(II) adsorbed at time t to the intraparticle diffusion rate constant k_{int}. A plot of q_t vs $\sqrt{t}$ gives a straight line (Figure 4.8D) and the intraparticle rate constant as obtained from the slope was found to be 0.155 mg g^{-1} $min^{-1/2}$. Since, q_t increases with the time of adsorption t, initially the external surface diffusion could influence the kinetics followed by intraparticle diffusion as the rate-determining step.[66] The Weber-Morris plot does not pass through the origin and hence we can conclude that in addition to intraparticle diffusion, the boundary layer effect also could influence the kinetics in the adsorption of the tetrachloromercurate(II) anion in the interlayer of the organophilic clay matrix.

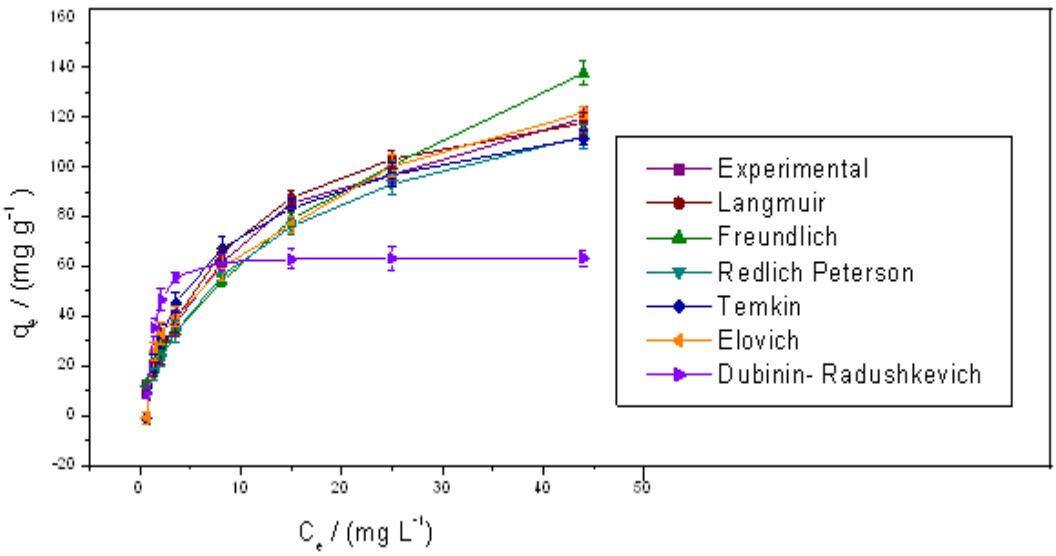

Figure 4.8. (A) Plot of q_e against C_e

Table 4.1. Adsorption isotherm parameters

Sl. No	Isotherm model	Parameters	Values
1	Langmuir	q_o (mg g^{-1})	140.84
		b (L mg^{-1})	0.1079
		R_L	0.0848
		r^2	0.98
		APE (%)	7.2
2	Freundlich	K_F (mg $^{1-1/n}$ g^{-1} $L^{1/n}$)	16.95
		n	1.806
		r^2	0.98
		APE (%)	8.4
3	Dubinin Radushkevich	q_m (mg g^{-1})	63.41
		β (mol^2 kJ^{-2})	0.3299
		E (kJ mol^{-1})	1.23
		r^2	0.63
		APE (%)	45.2
4	Redlich Peterson	g	0.845
		B (L mg^{-1})	0.2025
		A (L g^{-1})	15.196
		r^2	0.74
		APE (%)	18.69

5	Temkin	B	26.280
		A (L mg^{-1})	1.595
		b (J $mole^{-1}$)	94.27
		r^2	0.96
		APE (%)	23.9
6	Elovich	q_m (mg g^{-1})	60.35
		K_E (L mg^{-1})	0.337
		r^2	0.96
		APE (%)	25.74

Table 4.2. Kinetic parameters for the adsorption of mercury(II)

C_o	q_e	Second order rate constant	Regression coefficient	First order rate constant	Regression coefficient
mg. L^{-1}	mg g^{-1}	k_2 /(g mg^{-1} min^{-1})	R_1^2	k_1 / (min^{-1})	R_2^2
100	12.48	0.1175	0.99	0.0108	0.90

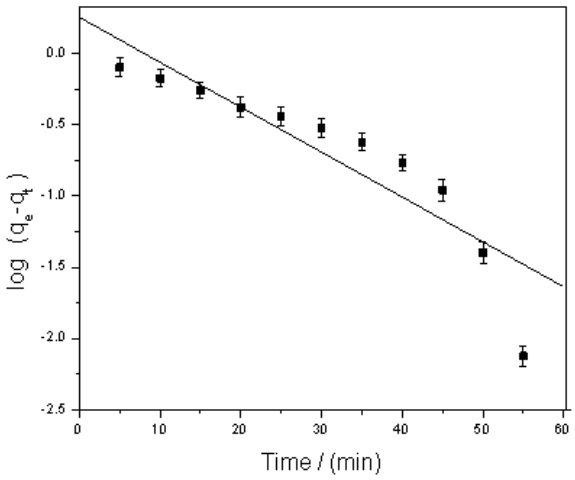

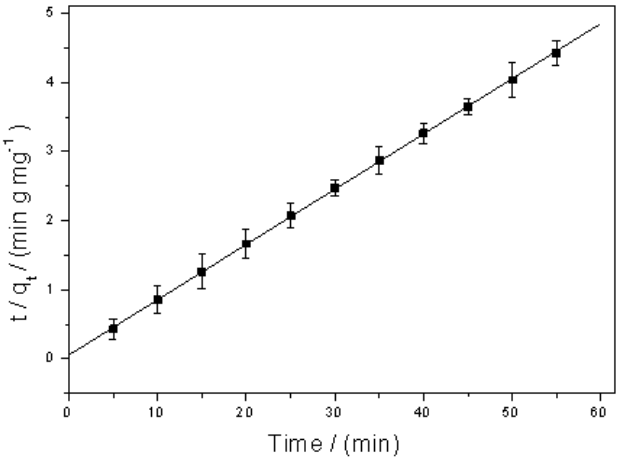

Figure 4.8. (B) Pseudo first order kinetic plot (C) Pseudo second order kinetic plot

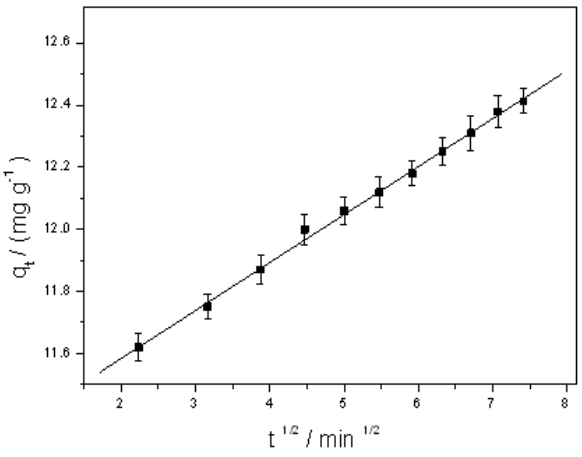

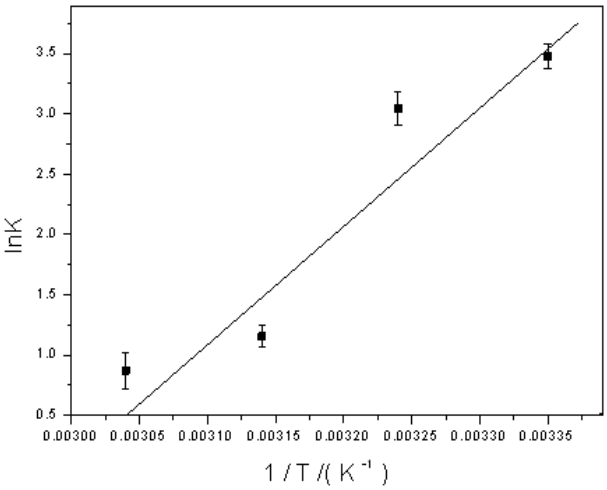

Figure 4.8. (D) Plot of q_t against time (E) Van't Hoff plot

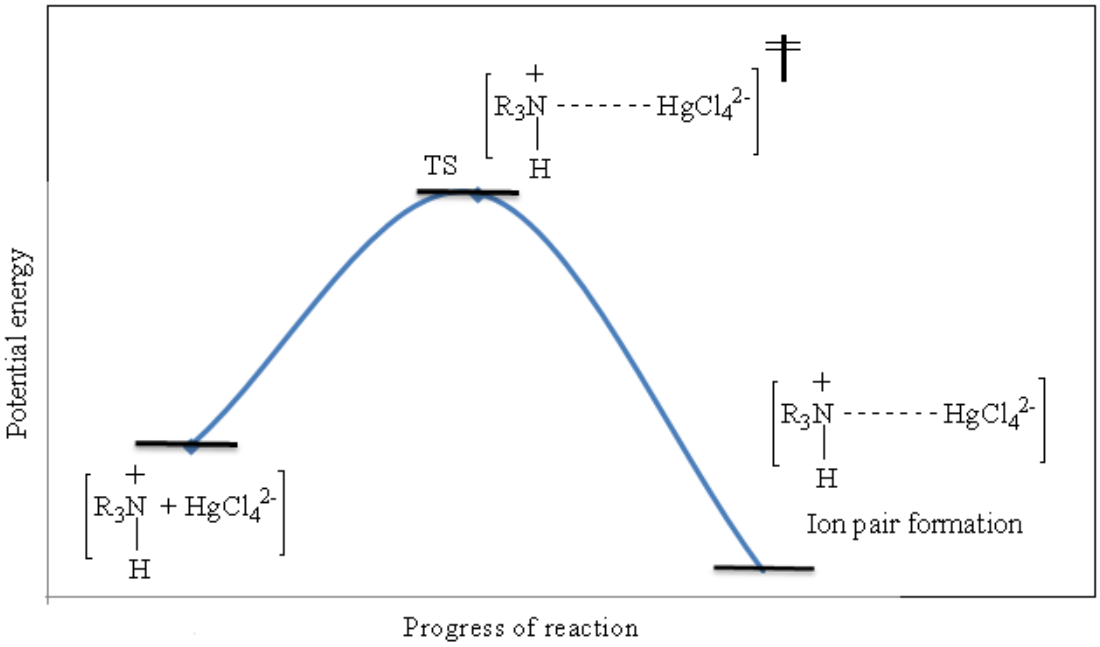

Figure 4. 9. Energy profile of the ion-pair formation

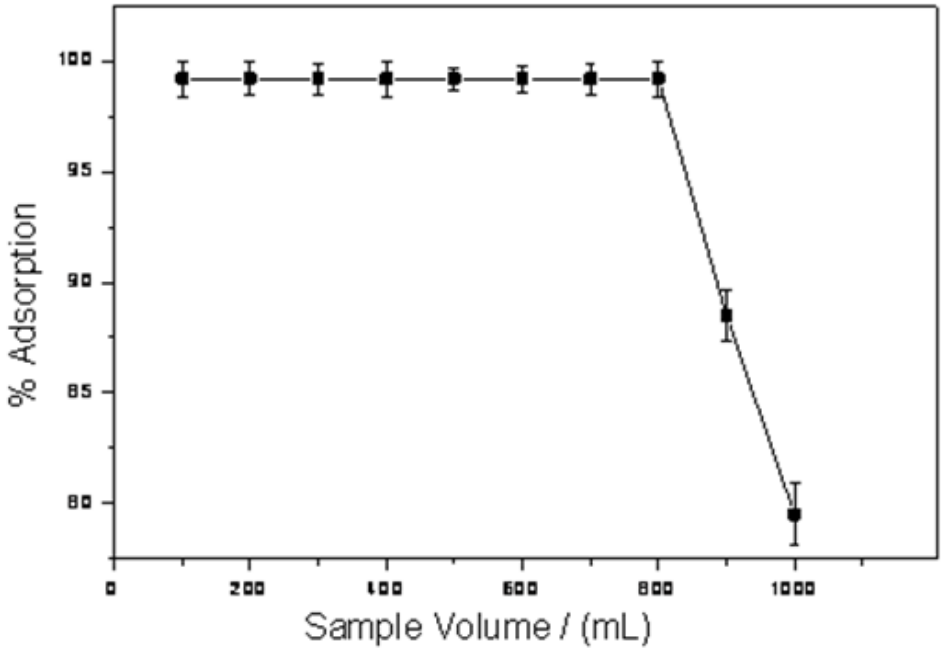

Figure 4.10. Sample breakthrough volume study

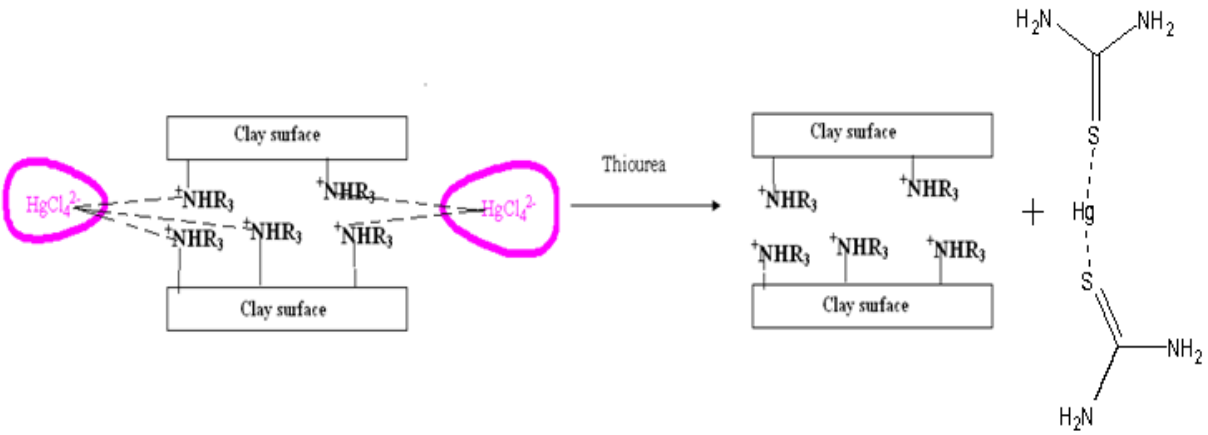

Figure 4.11. Regeneration of adsorbent

Table 4.3. Thermodynamic parameters for the adsorption of mercury

Temperature/ (Kelvin)	Concentration / (mg L^{-1})	ΔG^0 / (kJ mol^{-1})	ΔS^0 / (J mol^{-1} K^{-1})	ΔH^0 / (kJ mol^{-1})
298	100	-8.612	-233.15	-78.09
308	100	-5.225		
318	100	-3.04		
328	100	-2.37		

(v) Thermodynamics of Adsorption

The thermodynamics of adsorption were studied at 298, 308, 318 and 328 K respectively in order to obtain the Gibb's free energy (ΔG^0), enthalpy (ΔH^0) and entropy (ΔS^0) changes in the overall process. These parameters are obtained through the classical Van't Hoff equations[67] The equilibrium constant K is obtained from the ratio of concentration of Hg(II) adsorbed on the amine modified adsorbent to that in the solution. The endothermic or exothermic nature of the adsorption process is reflected through the positive and negative values of ΔH^0. The thermodynamic parameters, ΔH^0 and ΔS^0 were obtained from the slope and intercept of the plot of lnK against 1/ T (Figure 4.8E). The negative values of ΔG^0 imply a spontaneous physical adsorption process and the respective thermodynamic parameters are given in Table 4.3. The negative free energy (ΔG^0) values confirm the effectiveness of the electrostatic interaction between $HgCl_4^{2-}$ and the protonated amine. The overall free energy of adsorption (ΔG_{ads}) could arise from a combination of this electrostatic force of attraction as well as possible interaction between the positively charged amine and the oxygen framework in the clay surface

$$\Delta G_{\text{adsorption}} = \Delta G_{\text{electrostatic}} + \Delta G_{\text{van der Waals}} \qquad (6)$$

The fact that ΔH is negative is an interaction of the exothermic nature of adsorption and enthalpy factor is predominant at lower temperature than the entropy. The adsorption is enthalpically more favourable at lower temperature and this is also obvious from the free energy values obtained at these temperatures. The ΔG^0 values decrease with increase in temperature (298-328K) with negative entropy and enthalpy changes during the adsorption process. The overall enthalpy and entropy of adsorption could be visualized as a summation of the enthalpy and entropy due to the amine modified clay and the tetrachloromercurate(II) anion.

$$\Delta H_{\text{adsorption}} = \Delta H_{\text{(amine modified clay)}} + \Delta H_{HgCl_4^{2-}} \qquad (7)$$

$$\Delta S_{\text{adsorption}} = \Delta S_{\text{(amine modified clay)}} + \Delta S_{HgCl_4^{2-}} \qquad (8)$$

$$\Delta G_{\text{adsorption}} = \Delta H_{\text{adsorption}} - T\,(\Delta S_{\text{amine modified clay}} + \Delta H_{HgCl_4^{2-}}) \qquad (9)$$

As a matter of fact, these enthalpy and entropy factors play an interesting role in ion-pair interactions. Since $\Delta G < 0$, $\Delta S < 0$, and $\Delta H < 0$, with $K > 1$, $T < \Delta H_{ads} / \Delta S_{ads}$ and hence in accordance with the Le-Chatlier principle, an increase in temperature would not favor the adsorption process (as the process is exothermic). When $HgCl_4^{2-}$ and the positively charged amine come in proximity to form an ordered transition state, there is a decrease in the translational entropy of the system.

$$HgCl_4^{2-} + R_3\overset{+}{N}H \longrightarrow \left[HgCl_4^{2-}\text{----------}R_3\overset{+}{N}\text{-}H\right]^{\ddagger} \longrightarrow HgCl_4^{2-}\text{---------}R_3\overset{+}{N}\text{-}H \qquad (10)$$

This could also be schematically illustrated by plotting the potential energy against the progress of the reaction (Figure 4.9). This leads to the decrease in randomness at the solid solution interface, with decrease in the activation energy barrier and the interionic distance.[53] It is this sort of compactness that eventually results in negative entropy change during the adsorption process. The permeation of the tetrachloromercurate(II) anion from the bulk to the interlayer of the clay matrix results in strong electrostatic interaction with the positively charged amine. The ability of the tetrachloromercurate(II) anion to permeate the head group ($-N^+H$) of trioctylamine is also in accordance with the Hofmeister series[68] for simple anions ($Cl^- > NO_3^- > Br^- > I^-$). The Hofmeister series for anions play important role in understanding the effective interaction with the surrounding water molecules. Multiple charged ions with high charge density such as $HgCl_4^{2-}$ are classified as kosmotropic[69] and are well hydrated, whereas singly charged large size ions are chaotropic and are poorly solvated. In this regard, even though the long chain protonated trioctylamine is singly charged (R_3N^+H), and bulky, it is not really chaotropic in view of its hydrophobic hydration.[69] As a result, we can visualize the amine species to exhibit certain degree of kosmotropicity as well. Kosmotropes, being structure makers[69] have good interaction with water molecules, resulting in negative $\Delta S_{hyd.}$ Furthermore, the entropy of hydration also includes the contribution from electrostatic and van der Waals interaction.

$$\Delta S_{hyd} = \Delta S_{electrostatic} + \Delta S_{van\ der\ Waals} \quad (11)$$

$$\Delta S_{ads} = \Delta S_{electrostatic} + \Delta S_{hyd} + \Delta S_{van\ der\ Waals} \quad (12)$$

Hence, in addition to the strong electrostatic interaction between $HgCl_4^{2-}$ and the protonated amine, the tetrachloromercurate(II) anion and the kosmotropic amine are also solvated or hydrated which leads to a considerable order thereby resulting in a negative entropy change. The van der Waals interaction of the ions with the solvent also affect the entropy change in the adsorption process. At low temperatures, the tetrachlormercurate(II) anion could be solvated effectively. Nevertheless, as a trade of between solvation and electrostatic interaction, effectiveness of ion-association between the $HgCl_4^{2-}$ and the protonated amine is of considerable importance in the adsorption mechanism. The chain length of alkylamine is also an important factor[53] that causes this entropy change arising as a result of the protonation of the amine. Hence, the interplay of solvation effect and electrostatic interaction fosters good interaction for the effective adsorption of Hg^{2+} as its tetrachloromercurate(II) anion in the clay matrix. This leads to a negative entropy change during the adsorption process. The fact can be further substantiated by considering the free energy changes associated with sodium montmorillonite, trioctylamine (TOA) and tetrachlormercurate(II) anion respectively. The change in the free energy can be expressed as the difference in the enthalpy and the entropy changes of the respective components as follows

$$\Delta G_{(sodium\ form\ clay)} = \Delta H_{(sodium\ form\ clay)} - T\Delta S_{(sodium\ form\ clay)} \quad (13)$$

$$\Delta G_{TOA} = \Delta H_{TOA} - T\Delta S_{TOA} \quad (14)$$

$$\Delta G_{HgCl_4^{2-}} = \Delta H_{HgCl_4^{2-}} - T\Delta S_{HgCl_4^{2-}} \quad (15)$$

$$\Delta G_{adsorption} = \Delta H_{adsorption} - T\,(\Delta S_{(sodium\ form\ clay)} + \Delta S_{TOA} + \Delta S_{HgCl_4^{2-}}) \quad (16)$$

The interaction of the protonated amine (NH^+) with the negatively charged tetrachloromercurate ion is characterized by a negative value of enthalpy and entropy. The overall entropy contribution arises from the individual entropy changes disassociated with the clay and amine. Hence, the summation, $\sum(\Delta S_{(sodium\ form\ of\ clay)} + \Delta S_{TOA} + \Delta S_{HgCl_4^{2-}})$ becomes largely negative reflecting the decreased randomness at the adsorbent-solution

interface. Overall, the physico-chemical adsorption process is enthalpy driven rather than the entropy effect. The average energy of activation, obtained from the expression[70] $E_a = \Delta H_{ads} + RT$ was found to be -75.48 kJ mol^{-1} this indicates the exothermic nature of adsorption.

(vi) Effect of Sample Breakthrough Volume in Column Study

Clays are known to swell or expand when they are in contact with aqueous solution and the extent of swelling is dependent on the sample volume. The adsorption of Hg(II) is quantitative up to a 800 mL sample volume (Figure 4.10) at 10 mg L^{-1}concentration of Hg(II). Above 800 mL, there is a decrease in the percentage adsorption of mercury. This could be attributed to a considerable expansion in the packed bed column[42] and as a consequence, the close packing of the adsorbent is disturbed in the column. Hence, the retention of mercury as its tetrachloromercurate(II) anion with the protonated amine in the column is not quantitative beyond 800 mL sample volume. As low as 10 ppb of mercury could be adsorbed effectively in the column. Furthermore, the adsorption is also quantitative at an optimized flow rate of 8 mL min^{-1} which ensures effective contact between the mercury(II) and the adsorbent. The performance of an adsorbent is also expressed in terms of the rate at which the adsorbent bed gets exhausted. The rate of exhaustion of the adsorbent bed is given by the ratio of the mass of the adsorbent to the maximum sample volume.[71] On a laboratory scale, with 4.5 g of the adsorbent, at 10 mg L^{-1} concentration of Hg(II), the exhaustion rate of the adsorbent is 5.6 g L^{-1}. A lower value of the exhaustion rate signifies the effectiveness of the adsorbent column. Hence, it is possible that on an industrial scale, with an increase in the amount of the adsorbent in the column, the upper limit for the sample volume would also enhance correspondingly.

(vii) Desorption Studies

The regeneration of adsorbent is an important aspect to be examined in an adsorption process. A 100 mL volume of 10 mg L^{-1} Hg(II) was loaded on the adsorbent column at a flow rate of 5 mL min^{-1}. The desorption of mercury was studied individually using 15 mL of 1.0 mol L^{-1} of potassium iodide, potassium bromide and hydrogen bromide

respectively. Bromide and iodide are known to form stable tetraiodo and tetrabromo complexes[72] and hence compete with tetrachloromercurate(II) anion for the effective sites in the adsorbent matrix as well as the protonated amine. In view of the competing ability of these two halides with chloride for the protonated amine the adsorption of mercury in the column is affected and hence it is probable that some amount of mercury could be released in the aqueous phase. Furthermore, in aqueous solution the E^o (standard reduction potential) of I_2/I^- , Br_2/Br^- and Cl_2/Cl^- are +0.54V, +1.09V and +1.36V respectively.[73] Hence, in aqueous acidic medium it is also highly probable that bromide and iodide can be oxidized easily and hence elute the mercury also as covalent HgI_2 and $HgBr_2$ in the aqueous phase. As a result, the interaction of tetraiodo and tetrabromo complexes with the protonated amine is not quantitative as compared to the tetrachloromercurate(II) anion. This leads to the partial elution of mercury with bromide and iodide into the aqueous phase. Since, bromide and iodide were not effective in quantitative elution, thiourea was tried as an alternative organic complexing agent for mercury(II). In the proposed methodology, we found that 10 mL of 2.0 mol L^{-1} thiourea was effective in quantitative desorption (99 ±0.3%) of mercury in the eluate. Although, the tetrachloromercurate(II) anion has a high stability constant (log K= 15.07), the addition of thiourea leads to a weakening of interaction between $HgCl_4^{2-}$ and the adsorbent. Since Hg^{2+} is a typical soft acid, it has very good affinity towards sulfur containing ligands like thiourea.[74] Thiourea forms a 1:2 complex with Hg(II), thereby bringing down the mercury to the aqueous phase and regenerating the adsorbent (Figure 4.11). The order of elution with the above tested reagents were found to be thiourea (99.3%) > potassium iodide (79%) > potassium bromide (62%) > hydrogen bromide (49 %). The adsorbent could be reused for 10 adsorption-desorption cycles without any noticeable decrease in the performance efficiency of the column.

(viii) Impact of Co-existing Ions

The effect of diverse ionic constituents (Figure 4.12) was investigated in order to study their impact on the adsorption efficiency of mercury. A 100 mL volume of 10 mg L^{-1} Hg(II) was mixed individually with varying concentrations of these ions and loaded on the column. The amount of mercury adsorbed was ascertained to study the extent of

interference of these species. At lower concentration (150 mg L^{-1}) the high diffusion barrier[75] could prevent these ions to enter the interlayer of the clay matrix and hence do not compete with $HgCl_4^{2-}$ for the effective adsorption sites. At higher concentration (300 mg L^{-1}), the relaxation in this diffusion barrier leads to the competing ability of ions such as zinc, cobalt, cadmium, nickel, copper and lead by forming their respective chlorocomplexes[42] thereby causing a decrease in the percentage adsorption of mercury. At 300 mg L^{-1} level, ions such as bromide and iodide interfere by decreasing the adsorption of mercury. These ions compete with chloride for the effective adsorption sites in the clay matrix as well as the protonated amine, as their respective tetrabromo /iodomercurate(II) complexes. In acidic medium, it is also probable that bromide and iodide would be preferably oxidized which may further decrease the percentage adsorption of mercury. Similarly, anions such as sulfate and phosphate could also interfere by competing with chloride for the ion-pair formation with the protonated amine.

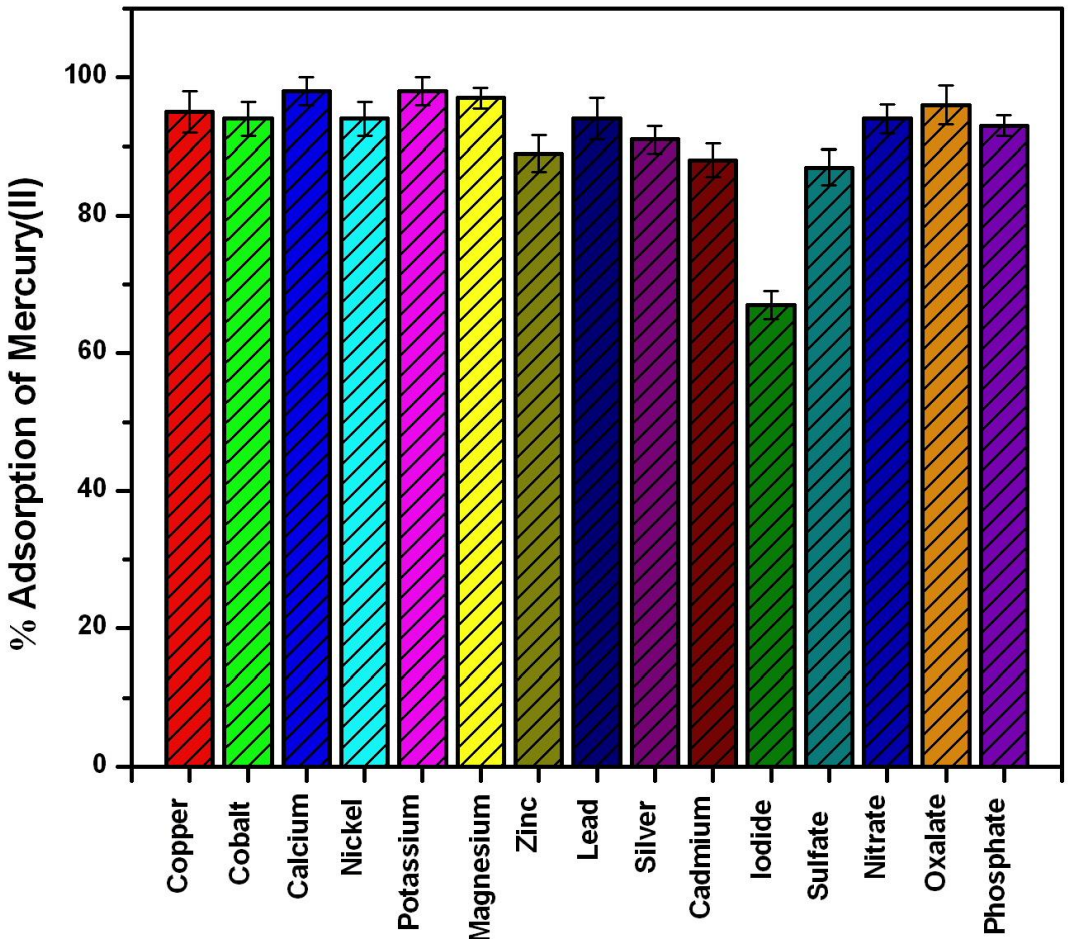

Figure 4.12. Effect of diverse ionic constituents

(ix) Application to Study the Removal of Mercury from a Coal Fly Ash Sample

Fly ash is an important source of mercury pollution generated in thermal power plants and comprises of fine particles that rise with the flue gases.[22] In addition to mercury, some of the major metallic constituents present in fly ash include aluminum, iron, manganese, chromium, arsenic and lead.[76] The fly ash sample was collected from a thermal power plant. 5 g of the sample was taken and pretreated using HF-HNO_3-H_2SO_4 mixture[76] the resulting mixture was filtered and made up to a known volume. Hg(II) was adsorbed on the column as tetrachlormercurate(II) anion with the organophilic clay

adsorbent material. The adsorption of mercury was quantitative and this was ascertained from the analysis of mercury in the aqueous phase using cold vapor atomic absorption technique. The amine modified clay adsorbent was effective in the removal of mercury from the fly ash sample and furthermore, the adsorbed mercury could also be desorbed quantitatively using thiourea. The concentration of mercury in the fly ash sample was found to be 0.23 ± 0.02 µg g^{-1} obtained as the average of three replicate determinations.

4.2.5 Conclusions

In conclusion, this work has established the effectiveness of interaction between tetrachloromercurate (II) anion and trioctylamine in acidic medium. The sorption kinetics favors the pseudo second order kinetic model and a maximium adsorption capacity of 140.84 mg g^{-1} in concurrence with the Langmuir isotherm. The adsorption process is consistent with the mechanism involving the electrostatic interaction between the tetrachloromercurate(II) anion and the protonated amine in the clay. The thermodynamically favorable adsorption process is driven by negative enthalpy and entropy changes respectively. The adsorbent material could be effectively regenerated using thiourea and the method could be scaled to a sample volume of 800 mL. As low as 10 ppb of mercury could be effectively adsorbed in the column. Finally, the method has proved to be successful in the adsorption of mercury from coal fly ash, which is a vital source of mercury pollution.

Application of dodecylamine modified sodium montmorillonite as an effective adsorbent for hexavalent chromium

4.3.1 Introduction

This chapter deals with the potential application of dodecylamine modified sodium montmorillonite as an effective adsorbent for hexavalent chromium. Clay materials are well suited for heavy metal adsorption in view of their excellent surface area and cation exchange capacity. The clay minerals (e.g. montmorillonite) always contain negative charges on their layers because of the isomorphous substitution of the central atoms in the octahedral/tetrahedral sheet by cations of lower valence. These negative charges have to be compensated by inorganic cations (e.g., Na^+ and Ca^{2+}). These inorganic cations are exchangeable and can be replaced with organic cations, and the resulting materials are denoted as organoclays.[77-79] The organoclays show high affinity toward hydrophobic organic compounds (HOCs) and they can be used as sorbents for HOC's [80] and heavy metals. [81,82] A viable approach toward improved sorbing properties of natural clays, i.e., in terms of maximum adsorption capacity as well as of selectivity, relies on incorporation of organic moieties into the clay interlamelar structure. Organoclays formed by intercalation of organic ligating groups into the interlamelar space of clays have been shown to be improved heavy metal sorbents. Pyrophyllite modified with amino groups was shown to have improved sorbing capacity for Pb^{2+}. [83] Recently modification of montmorillonites with various organic molecules like dithiocarbamate was reported.[84] Improved adsorption of Pb was achieved by an –SH-exchanged montmorillonite [85]or –SH-exchanged sepiolite.[86] An –SH or $–NH_2$ functionalized layered magnesium phyllosilicate material showed improved sorption in the following order: $Hg^{2+} > Pb^{2+} > Cd^{2+}$.[87] The harmful effect due to the various heavy metals is an issue being addressed by environmental chemists and engineers for many years. Chromium is definitely not an exception, whose toxicity as a carcinogen in its highest oxidation state (+6) is a serious concern. We need to combat this problem by developing viable adsorbents with excellent sorption potential. Cost-effective adsorbents such as dolomite,[88] hazelnut carbon,[89] lignocellulose,[90] and zeolites [91] are known for their good adsorptive capacity. The uptake

of hexavalent chromium using parthenium weeds[92] also shows good potential for adsorption. Clays are characterized by their excellent cation exchange capacity and good surface area for effective adsorption of heavy metals and water treatment. [93,94] Montmorillonite is a typical 2:1 smectite clay that can be converted to its sodium form by treatment with sodium chloride and further the sodium ion in the interlayer can be substituted with organoammonium cations [94] and certain long chain amines such as dodecylamine.[95] Recently, Surfactant modified sodium montmorillonite and tannin immobilized activated clay [96,97] has been utilized for the adsorption of hexavalent chromium. cellulose-clay [98] and chitosan-clay [99,100] composites have very good adsorption capacity for chromium. The simultaneous adsorption of phenol and hexavalent chromium on natural red clay modified with HDTMA is another method that has been reported recently.[101] Long chain amine modified clay materials have not been explored to its full potential towards the remediation of heavy metals. This chapter deals with the interaction mechanism of hexavalent chromium with dodecylamine modified sodium montmorillonite and its potential towards the remediation of tannery wastewater.

4.3.2 Experimental Section

(i) Adsorbent Preparation

Montmorillonite was first converted to its sodium form by treatment with NaCl as mentioned already in literature.[36] A 17 mL volume of 0.1 mole dodecylamine in 2.5 mol L^{-1} HCl was added to 4 g of the sodium montmorillonite in 15 mL acetone.[102] The acidic medium results in the protonation of dodecylamine and the surface of the clay becomes organophilic. The mixture was stirred magnetically for 12 hours, centrifuged, washed and the centrifugate was checked with $AgNO_3$ for the presence of chloride. The dodecylamine modified adsorbent material was dried in a hot air oven at 80^oC for 8 hours before proceeding to the batch adsorption studies.

(ii) Adsorption procedure

The batch adsorption study was conducted using an orbital incubator shaker (Biotechnics, India) at room temperature for varying time intervals with 25 mL of 10 mg L^{-1} chromium(VI) and 0.5 g of dodecylamine modified sodium montmorillonite adsorbent

material maintaining a pH of 2.5 in the solution. The concentration of chromium left in the solution was determined by the standard spectrophotometric method using diphenylcarbazide as the complexant for chromium.[38] Diphenylcarbazide reacts with Cr(VI) in acidic medium to give a red-violet complex at 540 nm. The color intensity is proportional to the concentration of Cr(VI) in the solution.

4.3 3. Results and Discussion

(i) Characterization of the Polymeric Sorbent

The FT-IR pattern (Figure 4.13) shows the presence of distinct peaks attributed to the symmetric O-H stretching at 3608 cm^{-1}, Si-O stretching at 1025 cm^{-1}, Al-Fe-OH deformation at 837 cm^{-1} Si-O deformation at 719 cm^{-1}, Si-O out of plane vibration at 620 cm^{-1} and Al-O-Si deformation at 554 cm^{-1} respectively.[98] The N-H deformation and C-N stretching were observed at approximately 1644 cm^{-1} and 1305 cm^{-1}.The characteristic antisymmetric and symmetric stretching frequency of the N-H bond of primary amine was observed close to 3251 and 3188 cm^{-1}.[102] The appearance of two bands at 2924 and 2854 cm^{-1} are characteristic of symmetric and asymmetric CH_2 stretching in dodecylamine.[103] Since, the amine modification is done in HCl medium, the primary amine gets protonated ($^{+}NH_3$) with the appearance of a peak at 2247 cm^{-1}. [104] The existence of Cr(VI) as hydrogentetraoxochromate(VI) anion in the pH range 2.5-3.5 is known from earlier reports and accordingly the perceivable changes in the IR spectrum in the range 750-900 cm^{-1} relate to the Cr=O and Cr-O bonds respectively, [98,105] The negatively charged hydrogentetraoxochromate ($HCrO_4^-$) and the protonated dodecylamine interact via an electrostatic force of attraction in the clay matrix as evident from the FT-IR spectral features. The appearance of characteristic new peaks at 811 cm^{-1} (Cr = O) and at 774 cm^{-1} (Cr - O) validate the electrostatic interaction.

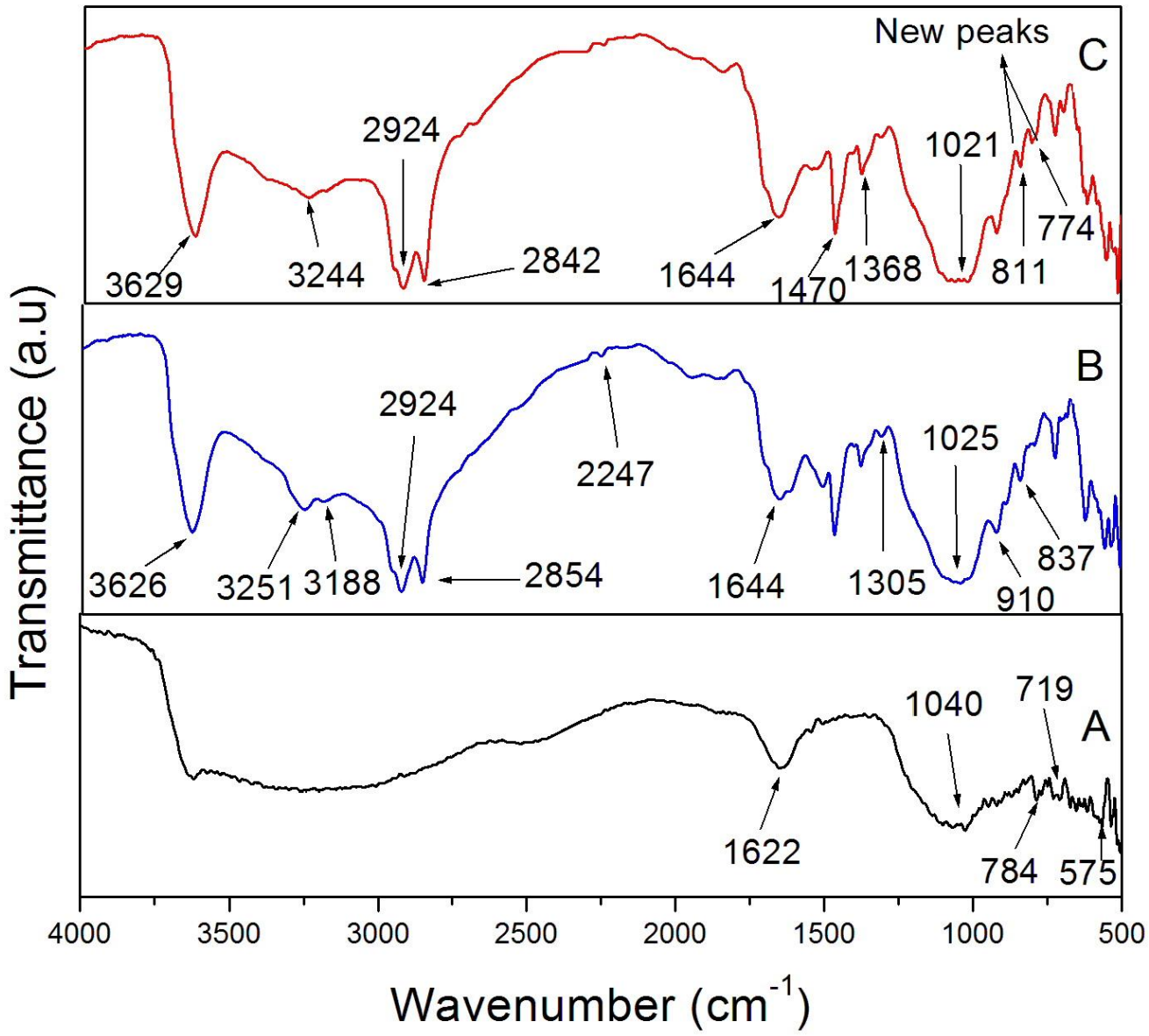

Figure 4.13. FT-IR spectrum (A) Na-MMT (B) dodecylamine modified Na-MMT (C) adsorption of chromium(VI)

(ii) XRD, Nitrogen Adsorption, SEM and EDS Studies

Sodium montmorillonite shows sharp reflections (Figure 4.14) at 2θ values corresponding to 5.79^0, 8.92^0 19.80^0, 22.73^0, 25.46^0, 26.54^0 and 34.98^0 [106] which is a typical feature ascribed to a certain degree of crystallinity in montmorillonite. After treatment with dodecylamine in HCl medium, the 2θ values shift to 16.02^0, 17.74^0, 22.05^0 and 33.45^0. The reflections corresponding to (100) peak of montmorillonite is observed at d= 4.481Å. After modification with the amine, the interlayer spacing increases to 5.529Å. This increase in the basal spacing by 1.048Å is attributed to the effective intercalation of the protonated amine in the interlayer. New peaks emerged at 23.47^0 and 51.23^0 which highlight the effective adsorption of chromium onto the adsorbent.[107] The effectiveness of adsorption is reflected in the surface area and the mesoporous nature of the dodecylamine-modified adsorbent. The N_2 adsorption-desorption (Figure 4.15A) study of the adsorbent results in a type IV isotherm[108] with a surface area of 23.18 m^2 g^{-1}. The Barrett-Joyner- Halenda (BJH) pore size distribution curve (Figure 4.15B) yields a pore radius 9.0 nm matching to a maximum pore volume of 0.16 cm^3 g^{-1}. The porous surface with an intense morphology is observed in the SEM images (Figure 4.16) of the dodecylamine-modified adsorbent. The adsorption of hydrogentetraoxochromate(VI) on the adsorbent matrix is obvious from the change in the surface morphology as a shiny agglomerated ball shaped structure. The EDS analysis (Figure.4.17) also shows peaks at various regions corresponding to the elements in the dodecylamine modified sodium montmorillonite adsorbent. The peak due to chromium adsorption is obtained in the range 0-1 keV and 5-6 keV which establishes the fact that the adsorption occurs effectively on the organophilic clay surface. [98,109,110]

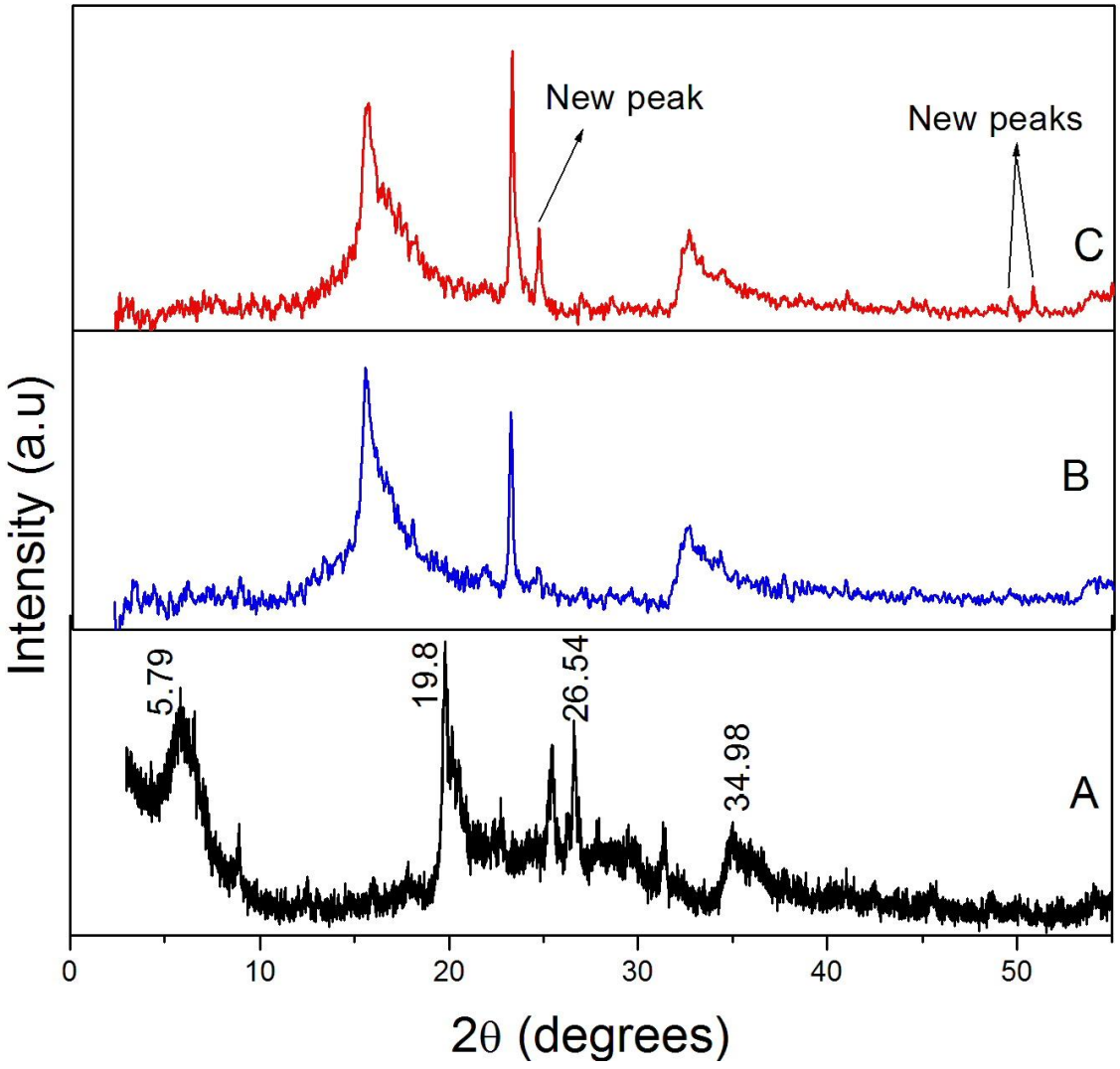

Figure. 4.14. XRD pattern (A) Na-MMT (B) dodecyl amine modified Na-MMT (C) After chromium(VI) adsorption

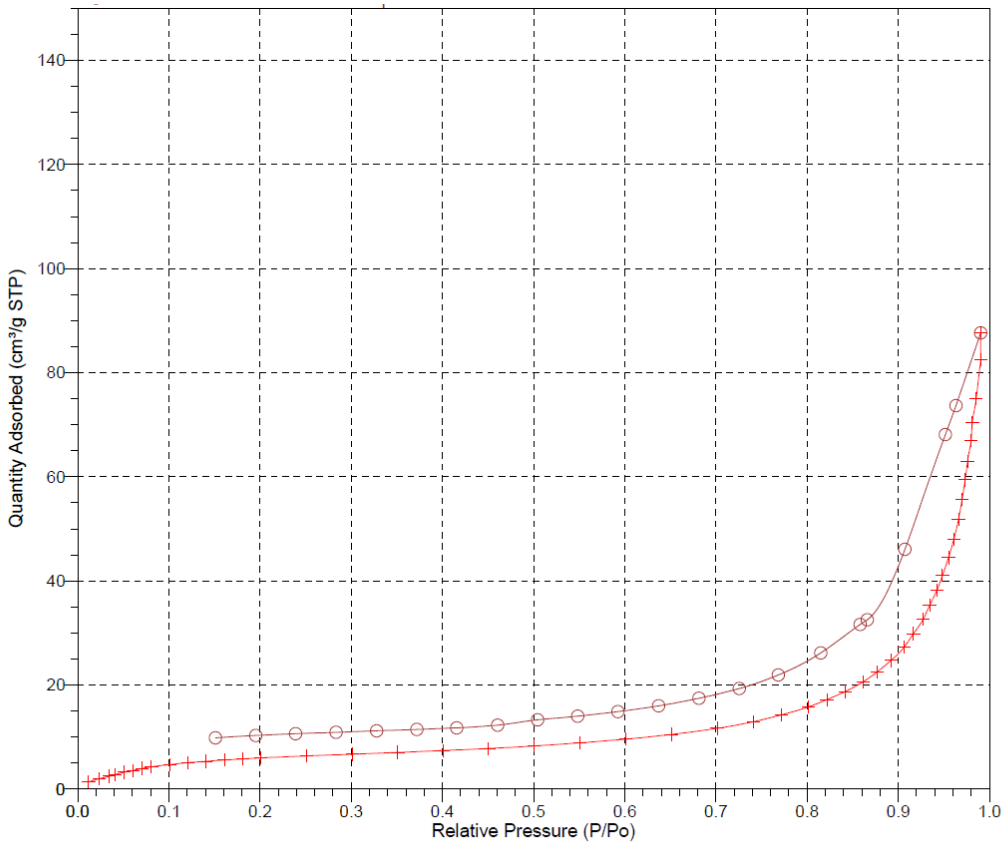

Figure 4.15A. Nitrogen adsorption-desorption isotherm

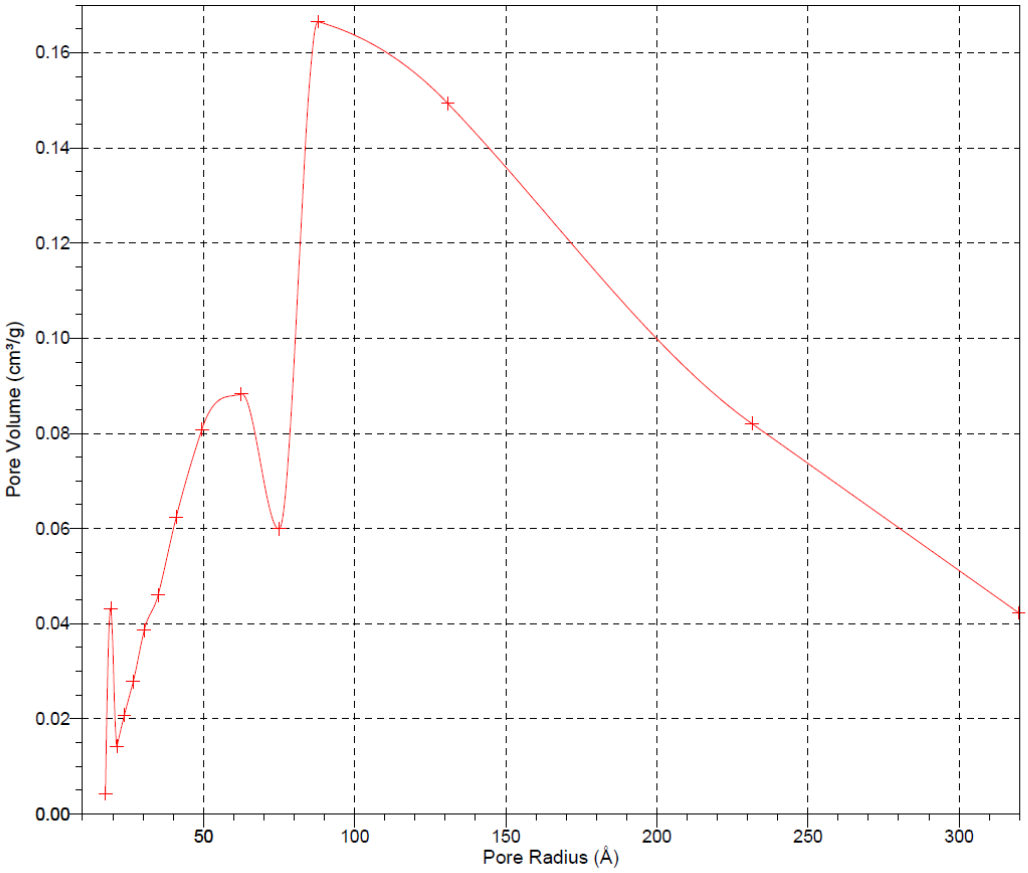

Figure 4.15B. Pore distribution curve

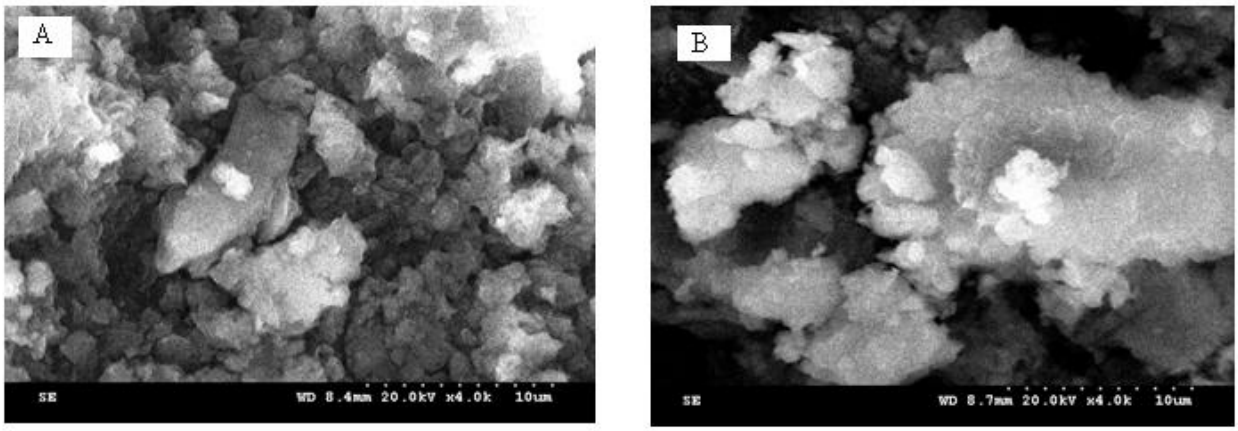

Figure 4.16. SEM Images (A) dodecylamine modified Na-MMT
(B) after chromium(VI) adsorption

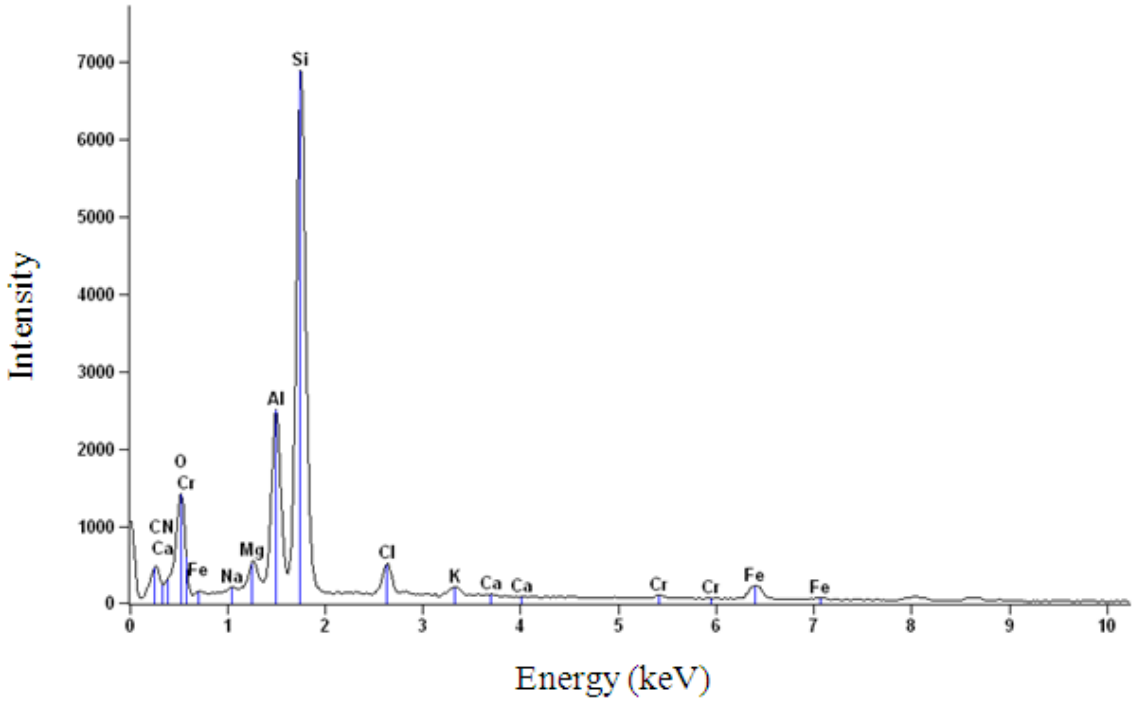

Figure 4.17 EDS spectrum after adsorption of hexavalent chromium

(iii)Adsorption Mechanism

The influence of pH is a key parameter that needs to be optimized in any adsorption process. In the present system, the pH conducive for the quantitative adsorption of chromium(VI) was observed in the pH range 2.0-3.5. In the pH range 2.5 to 3.5, Cr(VI) exists in solution primarily as hydrogentetraoxochromate(VI) anion, whereas the dichromate ($Cr_2O_7^{2-}$) and the tetraoxochromate(VI) species exist at highly acidic (<2.0) and alkaline pH (>7) respectively. Hence, depending on the pH the equilibrium between the chromium (VI) species can be represented as [39]

$$H_2CrO_4 \rightleftharpoons H^+ + HCrO_4^- \qquad K_1 = 0.16 \qquad (17)$$

$$HCrO_4^- \rightleftharpoons H^+ + CrO_4^{2-} \qquad K_2 = 3.2 \times 10^{-7} \qquad (18)$$

$$2HCrO_4^- \rightleftharpoons Cr_2O_7^{2-} + H_2O \qquad K_3 = 33.1 \qquad (19)$$

The electrostatic interaction between hydrogentetraoxochromate(VI) and the positively charged dodecylamine is more probable in acidic medium. Moreover, Cr(VI) is a hard acid and nitrogen is a hard base and therefore we can anticipate effective interaction between the protonated amine and hydrogentetraoxochromate(VI) anion. The mechanism is illustrated schematically (Figure 4.18), which indicates the protonation of the amine and the surface hydroxyl groups of the clay in HCl medium followed by the ion-pair interaction of $HCrO_4^-$ anion with the protonated amine. Hydrogen bonding is also likely between the protonated nitrogen in the primary amine and the OH groups in the clay (NH_3^+…..OH) surface. The contribution due to the OH_2^+ groups in the clay is given by surface complexation. Surface complexation facilitates in understanding the mechanism of adsorption of ionic species on charged surfaces and the process involves coordination reaction at active surface sites as well as electrostatic interaction between the protonated amine and hexavalent chromium. The pH corresponding to the point of zero charge (pH_{pzc}) was found to be 3.62 (Figure 4.19). At pH less than the pH_{pzc}, the amine as well as the surface OH groups in the clay is protonated [111,112] and interact through an electrostatic force of attraction with $HCrO_4^-$ anion. Beyond pH 3.5, there is a gradual decrease in the percentage of chromium (VI) adsorbed on the clay surface. Primary amines are protonated at low pH wherein, the electrostatic interaction is effective

[113] while at higher pH values, the repulsion between the hydrogentetraoxochromate(VI) anion and the deprotonated amine would result in a decrease in the amount of chromium adsorbed. At higher pH, the deprotonation of $SiOH^+$ group [52,114] in the montmorillonite clay surface as SiO^- could also exert an influence in reducing the adsorption capacity of hexavalent chromium. The amount of chromium adsorbed was best (>98%) with 0.5 g of the adsorbent used in the batch study. Above this weight, the saturation of the active sites in the organophilic clay surface results in maximizing the amount of chromium(VI) adsorbed as hydrogentetraoxochromate(VI) anion.

4. 3 4. Optimization of Analytical Procedure

(i) Study of Various Isotherm Models

The adsorption process was studied using six distinct isotherm models. Langmuir isotherm [58] is one such well-studied monolayer adsorption model in many adsorption systems. In the above expression, the constant b refers to the adsorption energy. In the present adsorption system, the value of q_o and b were found to be 23.69 mg g^{-1} and 0.109 L mg^{-1} respectively as obtained from the slope and intercept of the plot of C_e/q_e against C_e (Figure 4.20A). The value of R_L for the adsorption of tetraoxyhydrochromate(VI) anion on the dodecylamine modified montmorillonite adsorbent was found to be 0.47, which is an indication of the effectiveness of the adsorbent-adsorbate interaction. The second well-known isotherm is the Freundlich model [60] which again relates q_e, C_e, K_F and n respectively. The constants K_F and n given in Table 4.4 were obtained from the slope and intercept of the plot of $\log q_e$ against $\log C_e$ (Figure 4.20B). The value of n in the range 1-10 is another benchmark to assess the good adsorbent-adsorbate interaction. The value of n was found to be 2.02, which is a reflection of the effectiveness of the electrostatic interaction. The adsorption mechanism and the interaction between chromium and the amine modified adsorbent surface can be understood through yet another isotherm model known as the Dubinin–Radushkevich isotherm.[61] The nature of the adsorption mechanism (Figure 4.20C) is ascertained from the E_{DR} values. The mean free energy value lower than 8 kJ mol^{-1} is indicative of physical adsorption. In the present system, involving the electrostatic interaction between hydrogen tetraoxochromate(VI) anion and the organophilic clay surface, a value of 0.54 kJ mol^{-1} was obtained and this is attributed to

the physical adsorption. The R-P model includes the attributes of Langmuir and Freundlich isotherms. The Redlich–Peterson model relates the constants A, B and an exponent g to the amount of chromium adsorbed at equilibrium q_e. It has been observed in many adsorption systems that the value of g lies between 0-1. The slope and intercept of the plot gives (Figure 4.20D) the parameters g and B respectively (Table 4.4). The value of g was found to be 0.86 (near to 1) and this shows that the system could adhere to the Langmuir isotherm model. The linear plot of q_e versus $\ln C_e$ gives the Temkin constants A and B. The variation of adsorption energy and the Temkin equilibrium constant can be calculated from the slope (Figure 4.20E) and the intercept of the plot q_e versus $\ln C_e$. The respective Elovich isotherm parameters can be obtained from the slope and the intercept of the plot (Figure 4.20F) of $\ln (q_e/C_e)$ against q_e and these are given in Table 4.4.

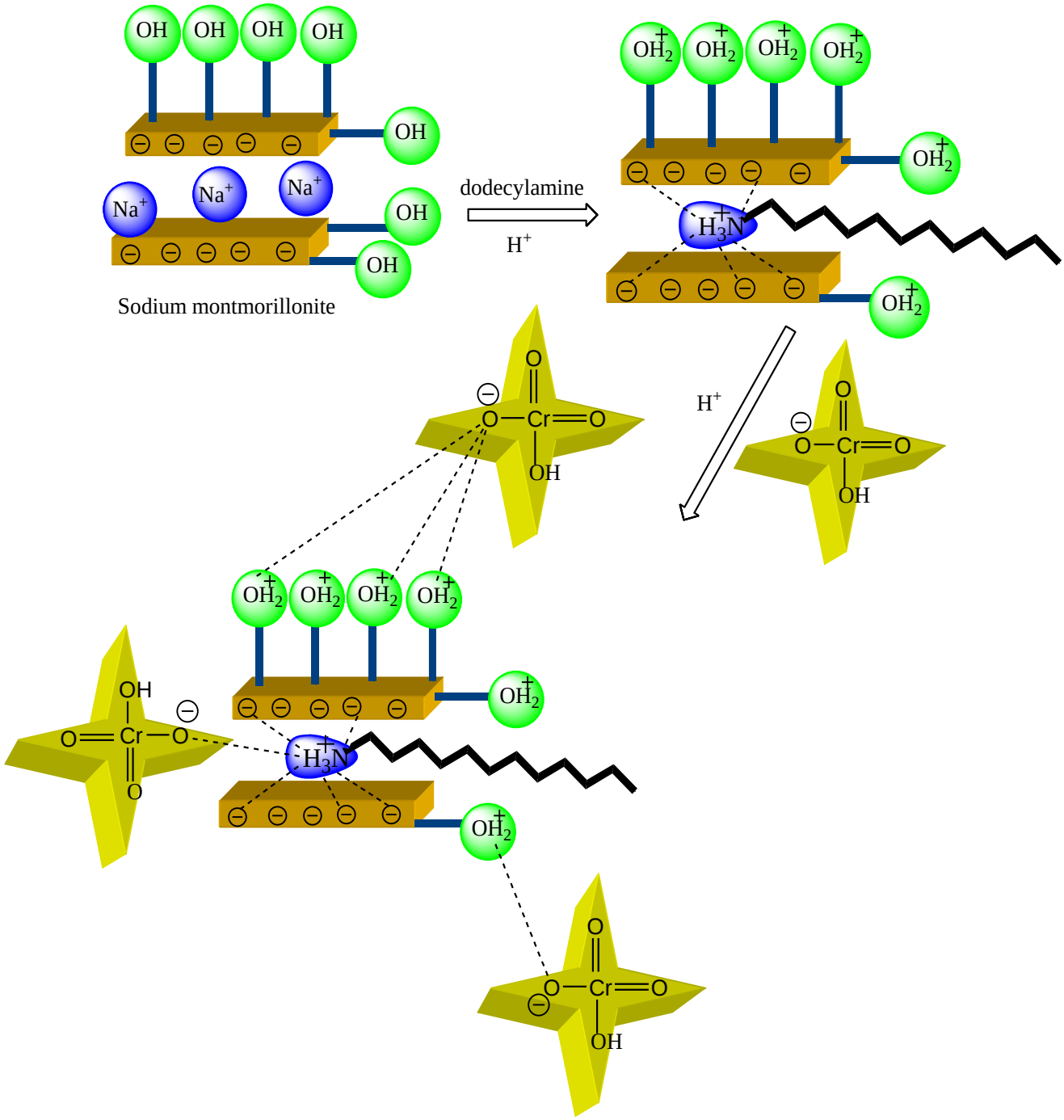

Figure 4.18 Illustration of the interaction hydrogentetraoxochromate(VI) anion and protonated amine in the clay surface

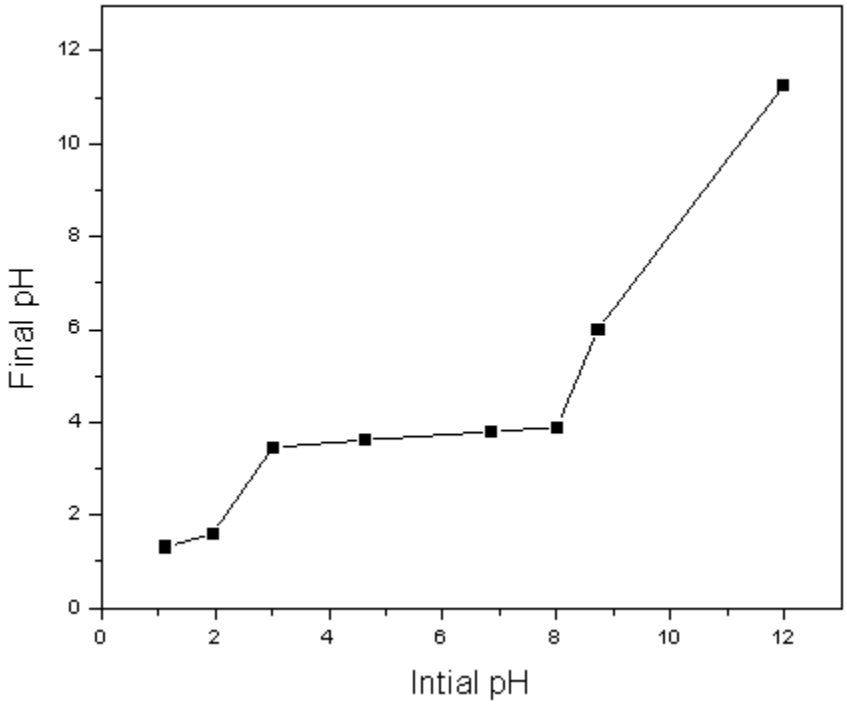

Figure 4.19. Point of zero charge (pH_{pzc})

Table 4.4. Various adsorption isotherm parameters

Isotherm	Constants	Values
Freundlich	K_F (mg $^{1-1/n}$ g^{-1} $L^{1/n}$)	3.27
	n	2.02
	r^2	0.98
Langmuir	q_o (mg g^{-1})	23.69
	b (L mg^{-1})	0.109
	R_L	0.47
	r^2	0.86
Dubinin Radushkevich	q_m (mg g^{-1})	13.897
	β (mol^2 kJ^{-2})	1.7085
	E (kJ mol^{-1})	0.5409
	r^2	0.74
Temkin	B	3.1294
	A (L mg^{-1})	4.4545
	b (kJ $mole^{-1}$)	0.79
	r^2	0.78
Redlich Peterson	g	0.86
	B (L mg^{-1})	0.1845
	A (L g^{-1})	2.5964
	r^2	0.95
Elovich	q_m (mg g^{-1})	8.3542
	K_E (L mg^{-1})	0.5726
	r^2	0.69

(ii) Kinetic Models and Intraparticle Diffusion

The kinetic data were evaluated using the Lageregen first order and pseudo second order kinetic equations.[63,64] The kinetic constants can be obtained from the plot of t/q_t (Figure 4.21A) and log (q_e-q_t) (Figure 4.21B) against different time intervals. The equilibrium adsorption capacity (q_e) obtained experimentally (1.23 mg g^{-1}) correlates with the second order kinetic model (1.34 mg g^{-1}). The regression coefficient obtained from this model was also higher (Table 4.5) thereby leading to the conclusion that the experimental data fits well with the second order kinetics. The adsorption process in general could involve the following stages. a) Transport of the hydrogentetraoxochromate(VI) anion from the bulk aqueous phase through a liquid film, surrounding the external surface of the amine modified adsorbent. b) Diffusion of the oxoanion into the pores of the adsorbent c) Adsorption on the surface of the dodecylamine modified adsorbent. The rate of adsorption would depend on the slowest or the rate determining step,[66] which is usually either film or intraparticle diffusion. Intraparticle diffusion (Figure 4.21C) is generally observed at higher concentration of Cr(VI) and a weak adsorbent-adsorbate interaction, whereas film diffusion is prevalent at lower Cr(VI) concentration and a good adsorbent-adsorbate interaction.

(iii) Adsorption Thermodynamics

The feasibility of the adsorption process is best studied from the free energy (ΔG^0), entropy (ΔS^0) and enthalpy (ΔH^0) changes respectively. In order to determine these parameters the adsorption study was performed at four different temperatures. The equilibrium constant for adsorption (K) is obtained from the ratio of the concentration of hydrogentetraoxochromate (VI) anion adsorbed on the clay surface to that in the aqueous phase. Using the K value, the free energy of adsorption is obtained using the relation as mentioned in chapter 2. The free energy of adsorption was found to be negative at all temperatures, with decrease in the K values at higher temperature range (Table 4.6 3). The entropy and enthalpy of adsorption is obtained from the familiar Van't Hoff equation [67] and the plot of lnK against the reciprocal of temperature (Figure 4.21D). The ΔH^0 and ΔS^0 were also found to be negative (Table 4.6) which leads to the conclusion that the

adsorption process is indeed exothermic with decreased randomness at the adsorbent-adsorbate interface. The above mentioned thermodynamic parameters are all dependent on the nature of interactions between the hydrogentetraoxochromate(VI) anion and the dodecylamine modified sodium montmorillonite. Since, the protonated amine and the hydroxyl groups on the clay surface are involved in the dominant electrostatic interaction with $HCrO_4^-$ anion, it is reasonable to approximate the thermodynamic parameters primarily as

$$\Delta G_{ads}, \Delta H_{ads}, \Delta S_{ads} = f \text{ (electrostatic interaction)} \qquad (20)$$

The facile approach of the hydrogentetraoxochromate(VI) anion from the bulk to the protonated primary amine in the solid adsorbent results in a rigid electrostatic interaction in the clay interlayer as shown in Fig. 5. This leads to an overall reduction in the entropy of adsorption. Hence, the enthalpically beneficial adsorption process coupled with the negative free energy and entropy governs the overall interaction of chromium(VI) with the dodecylamine modified sodium montmorillonite.

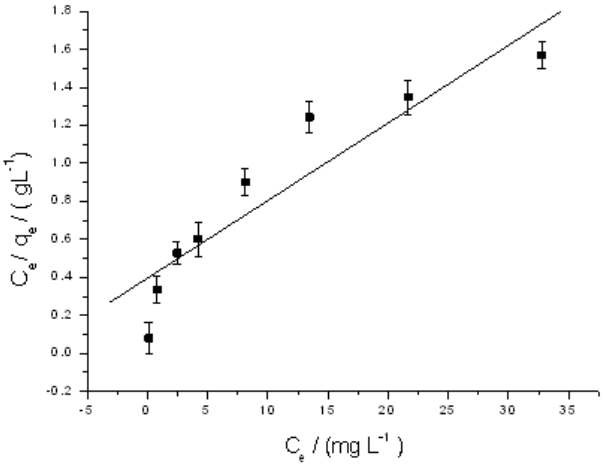

Figure 4.20A. Langmuir isotherm

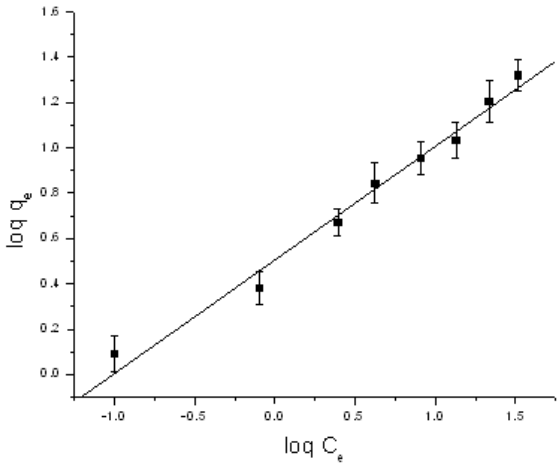

Figure 4.20B. Freundlich isotherm

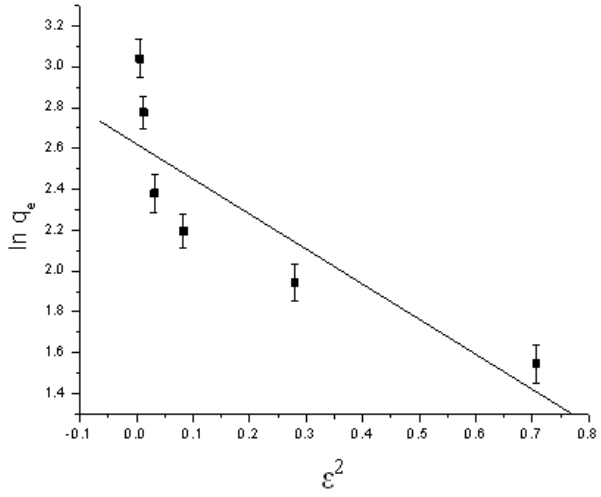

Figure 4.20C. Dubinin–Radushkevich isotherm

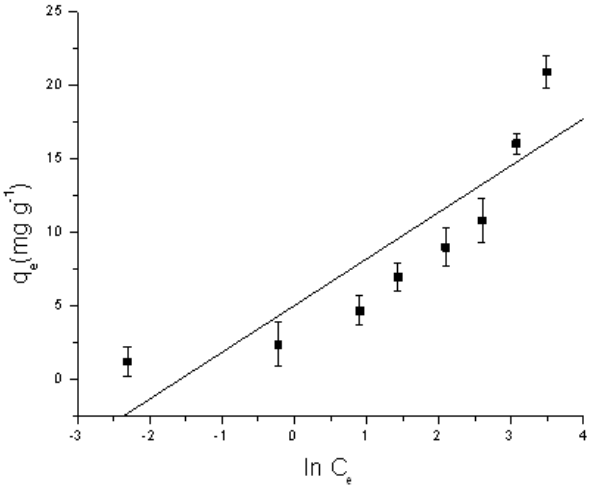

Figure 4.20D. Temkin isotherm

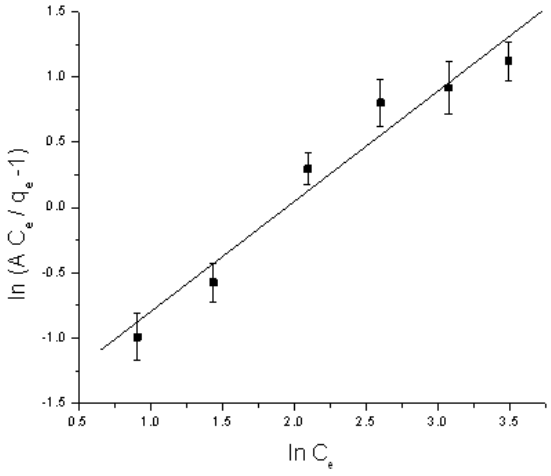

Figure 4.20E. Redlich–Peterson isotherm

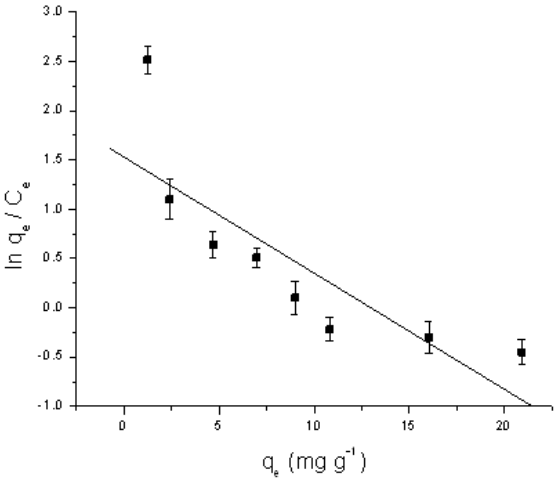

Figure 4.20F. Elovich isotherm

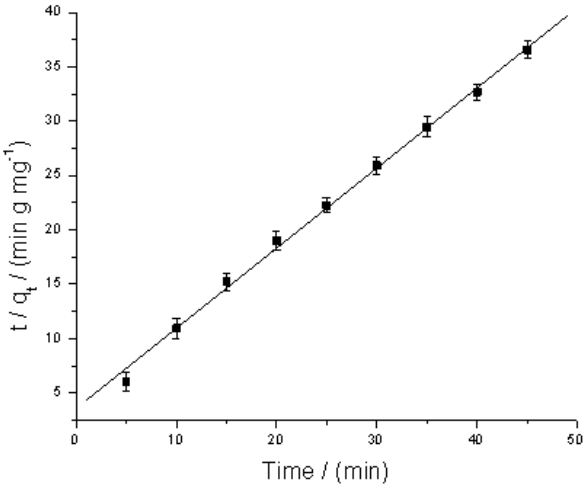

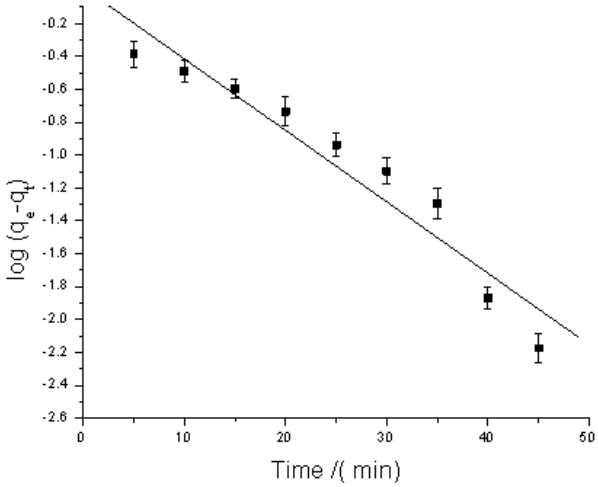

Figure 4.21A. Pseudo second order kinetics

Figure 4.21B. Pseudo first order kinetics

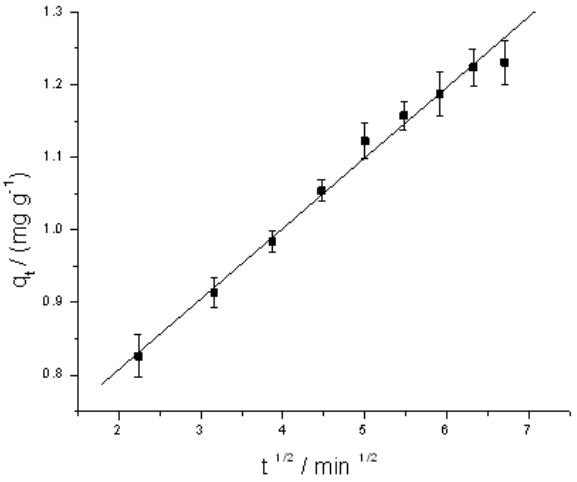

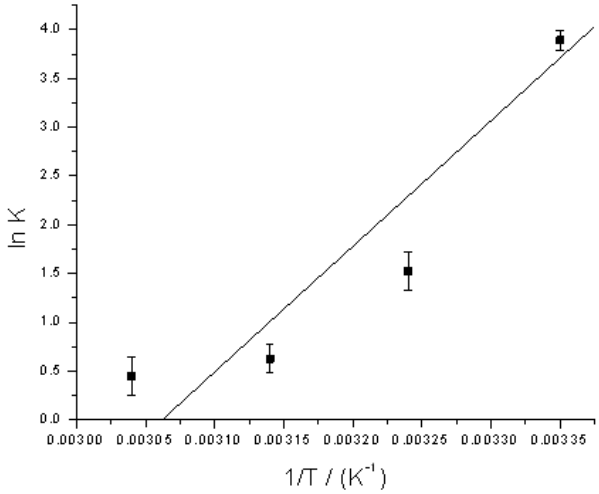

Figure 4.21C. Iintraparticle diffusion

Figure 4.21D. Van Hoff Plot

Table 4.5. Respective kinetic constants for the adsorption of hexavalent chromium

Rate constant k_2/(g mg^{-1} min^{-1})	Regression coefficient (r^2)	Weber-Morris rate constant k_{int}/(mg g^{-1} $min^{-½}$)	Rate constant k_1 / (min^{-1})	Regression coefficient (r^2)
0.2337	0.99	0.09	0.1001	0.92

Table 4.6. Thermodynamic quantities obtained from adsorption studies at different temperatures

Temperature / (Kelvin)	ΔG^0/ (kJ mol^{-1})	ΔS^0/ (J mol^{-1} K^{-1})	ΔH^0/ (kJ mol^{-1})
298	-9.642	-278.63	-91.50
308	-3.903		
318	-1.662		
328	-1.219		

(iv) Column Adsorption Study

On a laboratory scale, a glass column (3 cm diameter, 30 cm length) was packed with 2.5 g of the dodecylamine modified adsorbent. The packing height was set at 3 cm. At a flow rate of 7 mL min^{-1} adjusted with a peristaltic pump and an optimized pH 2.5, a 250 mL volume of 10 mg L^{-1} Cr(VI) was loaded onto the adsorbent column. The amount of hexavalent chromium adsorbed in the column was found by measuring its concentration

in the solution phase spectrophotometrically using diphenylcarbazide as the complexant. The adsorption of chromium as hydrogentetraoxochromate(VI) anion on the organophilic clay adsorbent column was quantitative (99.0±0.72%) as established with three replicate studies. With 10 mg L^{-1} chromium (VI), the adsorption process was effective up to a sample volume of 300 mL (Figure 4.22.). The interactive affinity between chromium and the positively charged primary amine decreased at higher sample volumes leading to a decrease in the adsorption efficiency. As we have illustrated in our earlier studies [98] clay materials swell when in contact with water and at larger volume this phenomena is more prominent. The swelling ability of clays at higher volume would enlarge the adsorbent bed resulting in their decreased affinity towards the metal ion. The adsorbent exhaustion rate[115] (AER) as an index for the assessment of the column adsorption efficiency. AER is defined as the ratio of the mass of adsorbent to the sample volume and in the present adsorption system, the adsorbent exhaustion rate was found to be 8.3 g L^{-1}, which is reasonably good for a laboratory column operation.

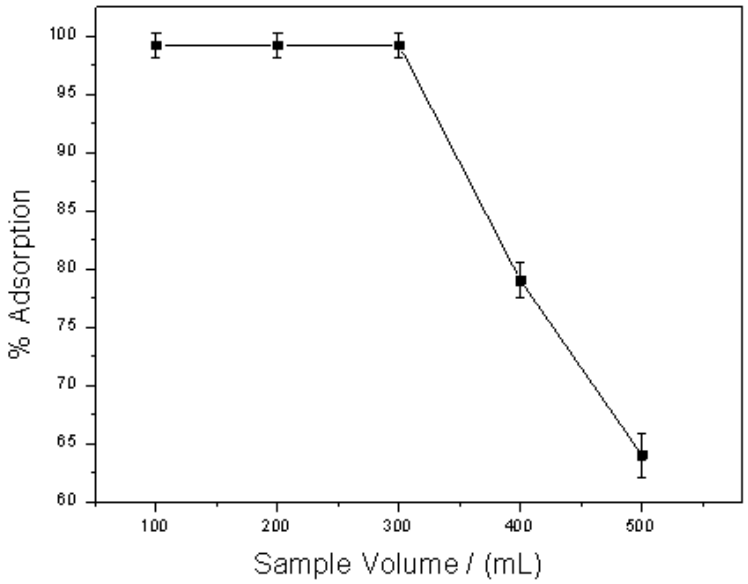

Figure 4.22. Sample volume variation

(v)Adsorbent Regeneration

The regeneration of the adsorbent was effective (99.4% elution) with 10 mL of 1.0 mol L^{-1} NaOH as the eluent. The performance of the adsorbent was very good with an elution efficiency of >90% for 4 adsorption-desorption cycles. Beyond 4 cycles, the removal efficiency decreases gradually by about 10%. The data pertaining to the above is presented in Figure 4.23. The mechanism involves the weakening of the existing electrostatic affinity between the hydrogentetraoxochromate(VI) anion and the protonated primary amine (Figure 4.24). As a consequence, the alkaline medium disturbs the equilibrium and hence the hexavalent chromium is removed quantitatively as its sodium salt in the eluate.[98] After four cycles, the percentage elution of chromium (VI) decreases which could be ascribed to the exchange of sodium ion with the protonated amine. This could lead to the competition of Na^+ for the hexavalent chromium as well as the amine. Hence, the adsorption capacity decreases beyond 4 cycles leading to a reduction in the amount of chromium eluted as sodium chromate in the aqueous phase.

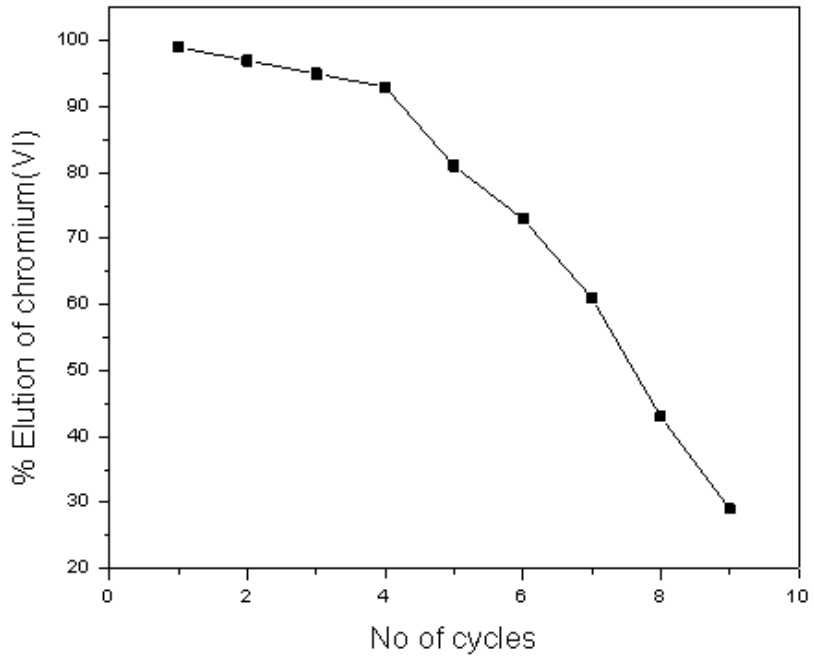

Figure 4.23. Adsorbent regeneration

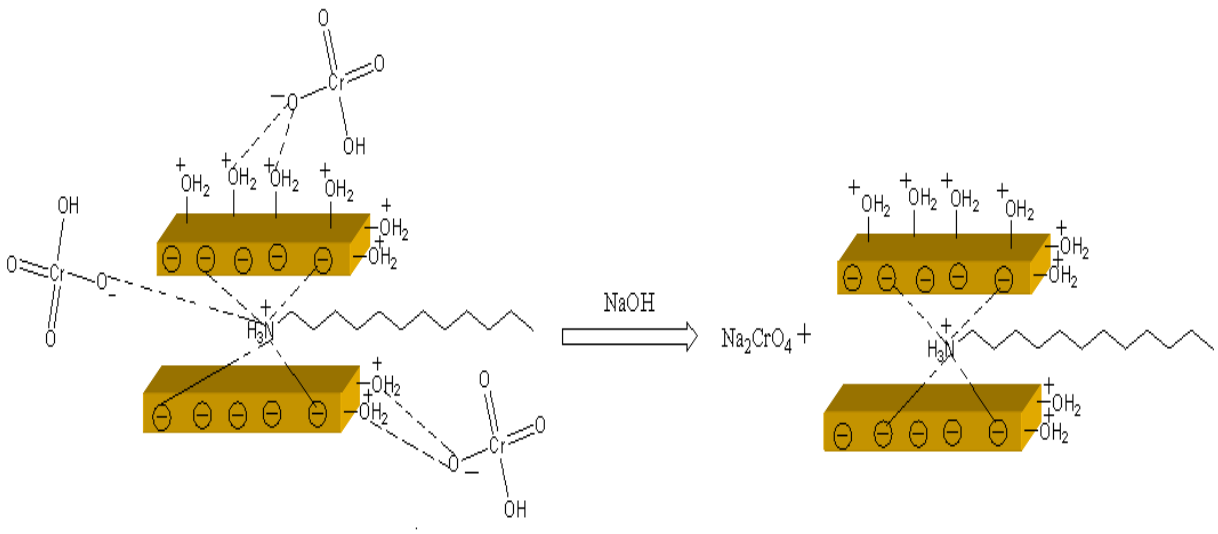

Figure 4.24. Mechanism of adsorbent regeneration with sodium hydroxide

(vi) Adsorption and Regeneration Dynamics

The adsorption and regeneration dynamics are important in a column study. The flow rate and packing height are two important aspects which affect the percentage adsorption of chromium. The interaction of hydrogentetraoxochromate(VI) anion with the protonated amine depends on the contact time of the adsorbate with the adsorbent. The results presented in Table 4.7 indicate that an optimum flow rate of 7 mL min^{-1} and a column packing height 3 cm is well suited for effective adsorption of chromium(VI) from a 200 mL sample volume. The effective contact between the hydrogentetraoxochromate(VI) anion and the adsorbent is enhanced at lesser flow rates with a packing height of 3 cm. Similarly, a regeneration flow rate of 4 mL min^{-1} with the same bed height ensures the successful elution of Cr(VI) with sodium hydroxide as the eluent.

(vii) Application to Real Sample Treatment

After optimizing the vital column parameters, the interference of certain major ionic constituents that might affect the adsorption of chromium(VI) were examined. The ions studied were similar to those present in a real tannery wastewater sample. Calcium and magnesium ions did not cause any interference even at 500 mg L^{-1} level. Other common

cations such as copper and zinc had a tolerance limit of 150 mg L^{-1}. Serious interference was observed with iron (especially in its lower oxidation state) at 100 mg L^{-1} level. The reason could be ascribed to the reduction of Cr(VI) to Cr(III) [98,116] thereby decreasing the adsorption efficiency. Among the anions, chloride, sulfate and nitrate interfered at concentrations above 200 mg L^{-1} level. These negatively charged anionic species compete for the prime adsorption sites in the adsorbent through their ability to also interact with the protonated primary amine. A 100 mL volume of the concentrated tannery wastewater sample was diluted to 250 mL before pretreatment in order to avoid the interference from the major ionic constituents in the adsorption of chromium. A 2.5 g of the adsorbent material was packed in a glass column (3.0 cm in diameter and 30 cm in length) to a height of 3 cm. The pretreatment procedure [98,116] involved the oxidation of the organic matter with HNO_3-H_2SO_4 mixture. The pretreated sample was subjected to oxidation with hydrogen peroxide in NaOH medium so as to ensure the total oxidation of chromium to its highest oxidation state (+6). The pH was adjusted to the required value (2.5) for column adsorption. The effectiveness of chromium adsorption was evident from its quantitative retention in the column. The schematic illustration of the treatment of the effluent sample is given in Figure 4.25, showing the adsorption process as well as the regeneration of the column. The values obtained after treatment (Table 4.8) showed that the adsorbent had a total chromium removal efficiency of 98.8% which validates the method.

Table 4.7 Adsorption and regeneration dynamics

Sl. No	Initial concentration (mg/ L)	Column packing height (cm)	Adsorption flow rate (mL/min)	% Adsorption of chromium	Regeneration flow rate (mL/min)	%Elution of chromium
1	10	3	7	99.1± 0.4	4	99.2± 0.2
2	10	3	10	93.4 ± 0.6	6	96.8± 0.3
3	10	3	12	87.0± 0.2	8	91.0± 0.5

Table 4.8. Tannery wastewater treatment

Sl. No	Sample	Total chromium present during collection (mg /L)	Total chromium removed by proposed method (mg /L)	Efficiency (%)
1	Tannery waste water	238.0	232.0	98.8 ±0.5

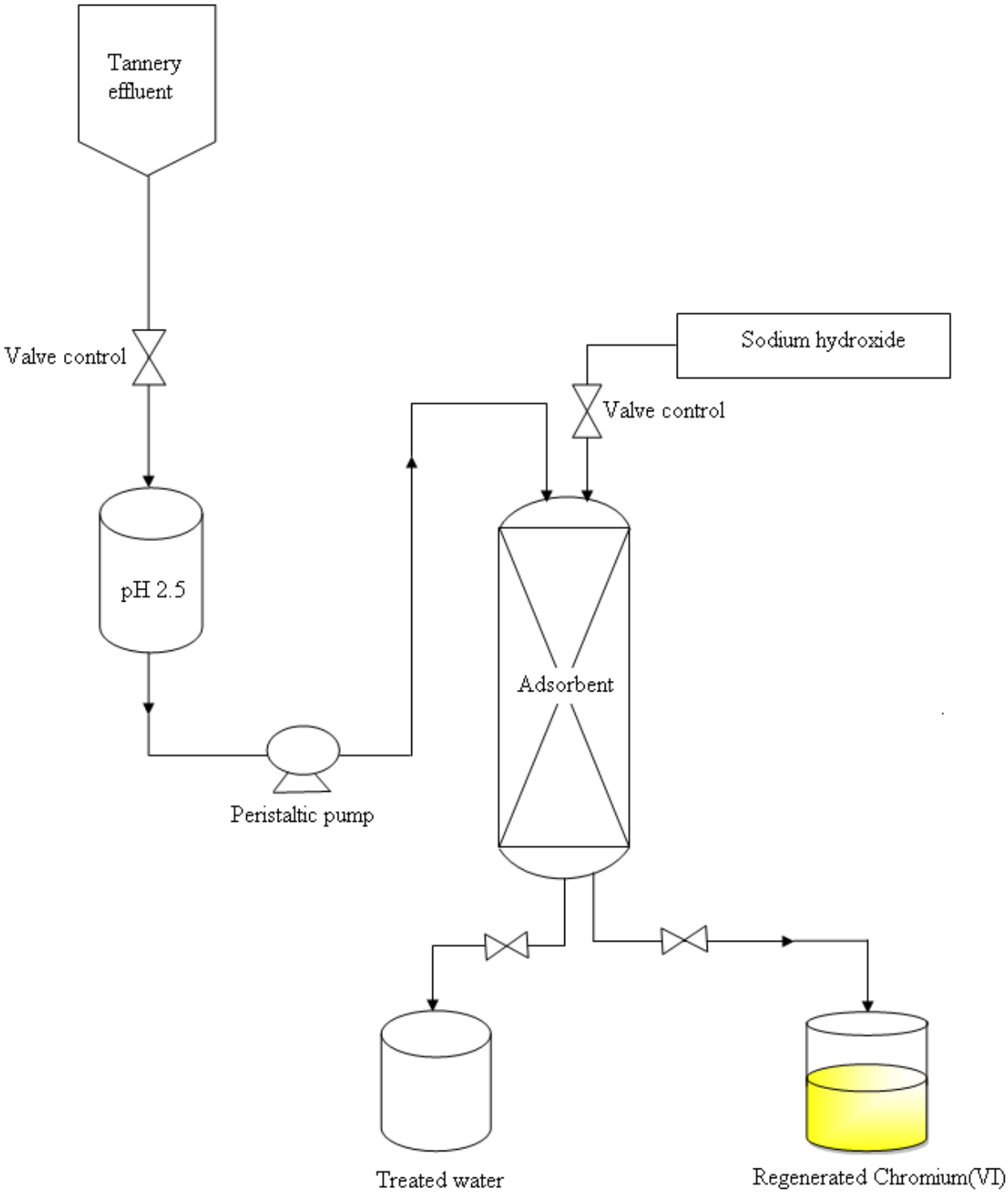

Figure 4.25. Scheme illustrating the adsorption of chromium from a tannery effluent

4.3.5 Conclusions

The dodecylamine modified sodium montmorillonite adsorbent has proved to be very effective in the solid phase extraction of hexavalent chromium. Freundlich and Redlich-Peterson isotherm models gave higher regression coefficient values and the electrostatic interaction of hydrogentetraoxochromate(VI) anion with the protonated primary amine is supported by a Langmuir adsorption capacity of 23.69 mg g^{-1}. The second order kinetic model and the thermodynamically favorable exothermic adsorption process further strengthen the efficacy of this adsorbent. A sample volume of 300 mL could be tolerated on a laboratory scale with 10 mg L^{-1} concentration of Cr(VI). Furthermore, the regeneration of the adsorbent is possible using sodium hydroxide as the eluent. The practical application in detoxifying chromium from a tannery wastewater sample highlights the potential of this dodecylamine modified clay adsorbent material for environmental remediation.

Cellulose-clay composite biosorbent towards the effective adsorption and removal of chromium

4.4.1 Introduction

This chapter deals with the application of cellulose-clay composite biosorbent towards the effective adsorption and removal of chromium. Clays are known for their excellent sorption properties toward metal cations.[117] Clay minerals, such a montmorillonite, play an important role in determining the availability and transport of metals species in soil and sediments [117] The unique features of clays for trapping of pollutants from the environment [118] include their high specific surface area associated with their small particle size (less than 2 μm)[118] The impact of heavy metal pollution has led to the search for biodegradable and cost effective adsorbent materials in order to alleviate the associated hazards caused to the environment. Chromium is not an exception and is known to be carcinogenic in the +6 oxidation state. Solid phase extraction is an effective methodology for heavy metal adsorption.[119] Adsorbents such as agricultural waste biomass,[120] Natural materials which are cost effective and biodegradable are also known for their efficacy in wastewater treatment.[121-123] Chitosan based composite biosorbents[124,125] are known for their good adsorption capacity towards chromium. Montmorillonite clays are naturally hydrophilic which makes them inadequately suited to interact with most polymer matrices. The organophilic clays ensure better compatibility with the biopolymer and is intended to separate the silicate layers for the effective interaction with cellulose.[126] The sodium ions in the clay can be exchanged with organo ammonium cations and to the best of our knowledge, there is no literature evidence on the application of cellulose-sodium montmorillonite clay composite for the detoxification of chromium from wastewater. The following sections present an interesting interaction between surfactant modified sodium montmorillonite (NaMMT) and cellulose biopolymer followed by its application towards the adsorption and remediation of chromium from chrome tannery wastewater sample.

4.4.2. Experimental Section

(i) Preparation of Cellulose –NaMMT Composite Adsorbent

The NaMMT clay was prepared from montmorillonite as described earlier in literature.[36] A 0.001 mol L^{-1} CTABr solution was prepared by appropriate dilution with Milli Q water. 6 g of the sodium form of the clay was suspended in 20 mL acetone. A 100 mL volume of 0.001 mol L^{-1} cetyltrimethylammonium bromide was added to the clay suspension. The selection of an appropriate solvent for effective swelling and dispersion of clay is an important aspect to be considered.[127,128] The contents were stirred magnetically for 8 hours. The mixture was centrifuged and the centrifugate was discarded. The solid material was washed with water until it was free from bromide (confirmed through the $AgNO_3$ test) and then dried overnight at 80 ^{0}C. 3 g of cellulose powder was taken and added slowly to the prepared organophilic NaMMT (as a suspension in 20 mL acetone) and the resulting mixture was stirred for 12 hours at a temperature of 60 ^{0}C. The resulting composite adsorbent was washed with Millipore water and dried in a hot air oven for 6 hours and used for further studies.

(ii) Adsorption Study

The batch adsorption studies were conducted by equilibrating 0.5 g of the the adsorbent material with 25 mL of 20 mg L^{-1} chromium(VI) solution at pH 5.0 in an orbital incubator shaker (Biotechnics, India) for varying time intervals and the concentration of chromium in the solution phase was estimated by the standard spectrophotometric method.[129]

4.4.3 Result and Discussion

(i) FT-IR Characterization and Mechanism of Biopolymer-Clay-Chromium Interaction

The FT-IR spectrum (Figure 4.26) showed characteristic bands corresponding to the various functional groups in cellulose[130] and NaMMT. A strong band at 3379 cm^{-1} is ascribed to O-H stretching and that at 2902 cm^{-1} is attributed to the C-H stretching in cellulose. The band at 1635 cm^{-1} could be ascribed to the H-OH bonding in water. A

strong peak at 1063 cm^{-1} arises from the C-O-C pyranose ring skeletal vibration. The peaks characteristic of NaMMT were observed at 794 cm^{-1} (Si-O stretching of quartz and silica), 694 cm^{-1}(Si-O deformation), 611 cm^{-1} (Al-O and Si-O out of plane vibration), 543 cm^{-1} (Al-O-Si deformation), 489 cm^{-1} (Si-O-Fe deformation) and 470 cm^{-1} (Mg-O deformation) respectively.[131,132] There exists an interesting molecular interaction between the surfactant modified NaMMT and the cellulose biopolymer. The central point to take cognizance is that the hydroxyl groups in the biopolymer play a pivotal role in this interaction. The quaternary ammonium cation present in CTABr interacts with the cellulose hydroxyl group in the form of a weak electrostatic attraction. There are considerable amendments in the spectral features after the adsorption of hexavalent chromium and the change is more obvious in the O-H region of the FT-IR spectrum. Hexavalent chromium exists primarily as hydrochromate ion ($HCrO_4^-$) and dichromate ($Cr_2O_7^{2-}$) in acidic medium.[133] The hydrochromate anion is the prime species in weakly acidic medium. The cellulose-clay composite material is now involved in the ensuing interaction with chromium(VI) as hydrochromate anion. The hydrochromate ion forms an ion-pair with the positively charged nitrogen of the surfactant molecule and this interaction is more pronounced than the interaction that exists between the quaternary ammonium cation and the hydroxyl groups of the biopolymer. This fact is also substantiated through the appearance of characteristic Cr=O and Cr-O peaks at 913 cm^{-1} and 765 cm^{-1} respectively.[134] We have also demonstrated the operation of a similar mechanism in our earlier study involving the interaction of ionic liquid in a cellulose matrix.[135] Hydrogen bonding interaction is also probable between the hydroxyl protons in cellulose and the oxygen atoms in the hydrochromate anion. The conceptual graphic illustration of the mechanism involved in the interaction between chromium and the biopolymer-clay adsorbent surface is shown in Figure 4.27. Furthermore, it is also probable that the silanol groups in clay could be protonated as $SiOH^{2+}$ in acidic medium[136] and this would further reinforce the interaction of hydrochromate anion with the positively charged composite adsorbent surface.

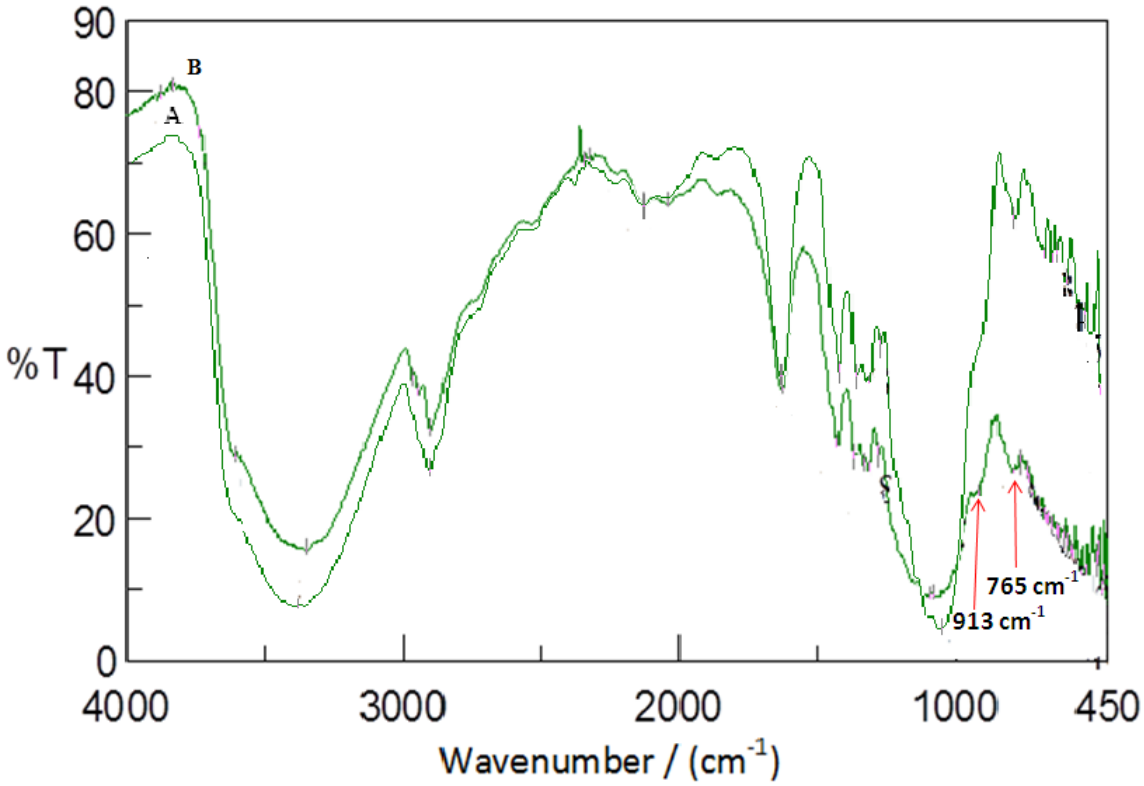

Figure 4. 26. FT-IR spectrum of (a) adsorbent (b) after adsorption of chromium(VI)

(ii) Energy Dispersive X-ray Spectrum (EDX) and Powder X-ray Diffraction (XRD) Analysis of the Cellulose-Clay Composite Material

The adsorption of chromium on the surface of the cellulose-clay composite was authenticated from the EDX spectrum (Figure 4.28) which shows the presence of adsorbed chromium along with the other major elemental peaks such as C,N,O, S and Si respectively. The peak for silicon is ascribed to the Si-O present in montmorillonite and the sulfur peak could originate from the sulfuric acid medium used for maintaining the pH of the medium. Depending on the amount of the added clay, the silicate layers would

be either dispersed or exfoliated in the composite.[126] The XRD pattern of the composite material shows sharp and pointed diffraction peaks (Figure 4.29A) at 2θ values corresponding to 6.25^0, 8.8^0, 18.14^0, 20.73^0 and 22.79^0 which indicates the crystalline nature of the polymeric composite with certain degree of exfoliation.[137] The noteworthy sharp peaks also signifies the ordered distribution of clay layers in the biopolymer composite. The surface modification of the clays makes them more organophilic and this provides an enhanced interaction with the biopolymer cellulose resulting in a fine dispersion in the matrix. Interestingly, the crystalline nature of the composite is not disturbed after the adsorption of chromium and the new sharp peaks obtained at 2θ values corresponding to 39^0 and 42.47^0 are attributed to the adsorption of chromium (Figure 4.29B) which concurs with the reported values in literature.[138]

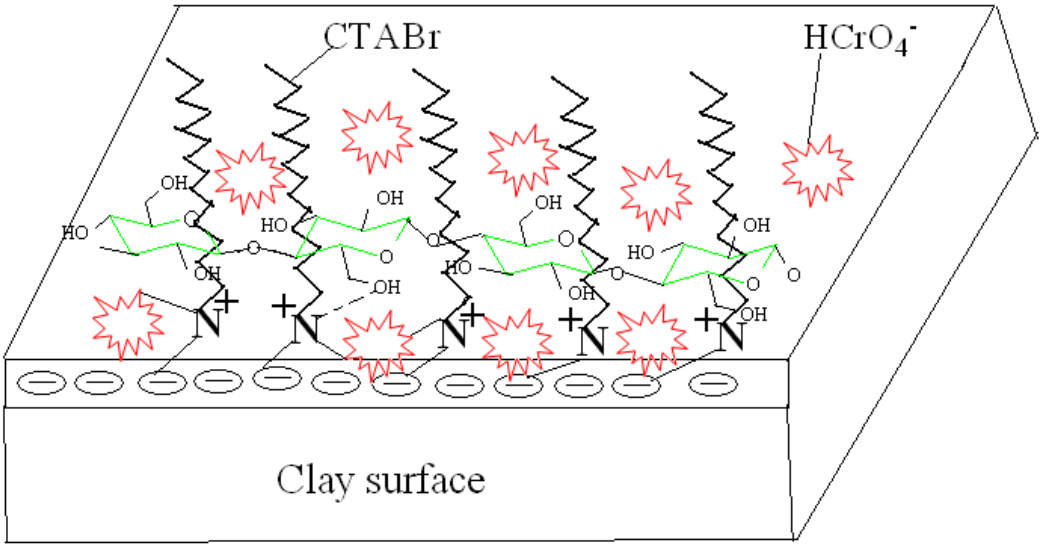

Figure 4. 27. Conceptual illustration showing the interaction of hydrochromate ion with the biopolymer–clay

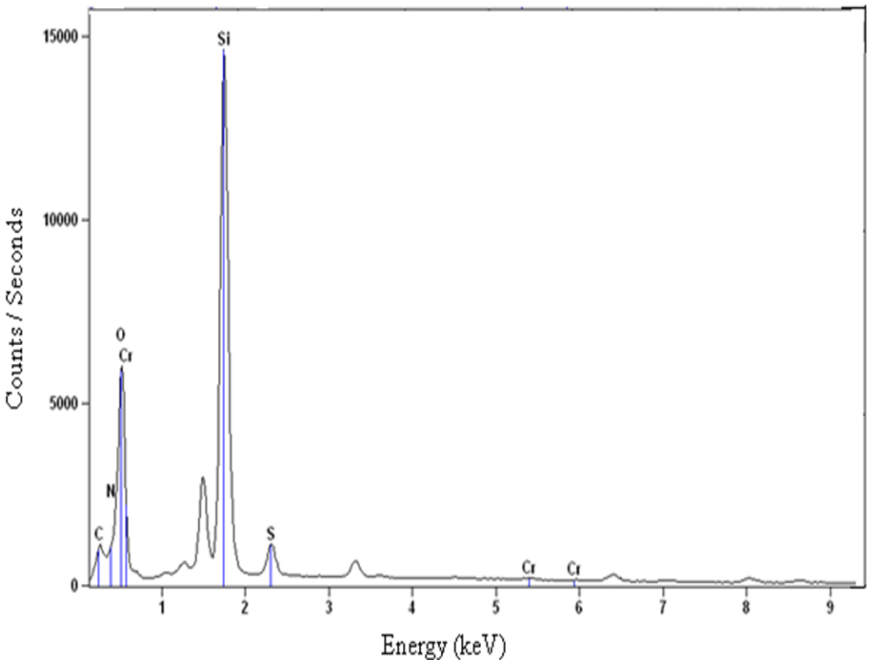

Figure 4.28. EDX spectrum of the adsorbed Cr(VI) on the adsorbent material

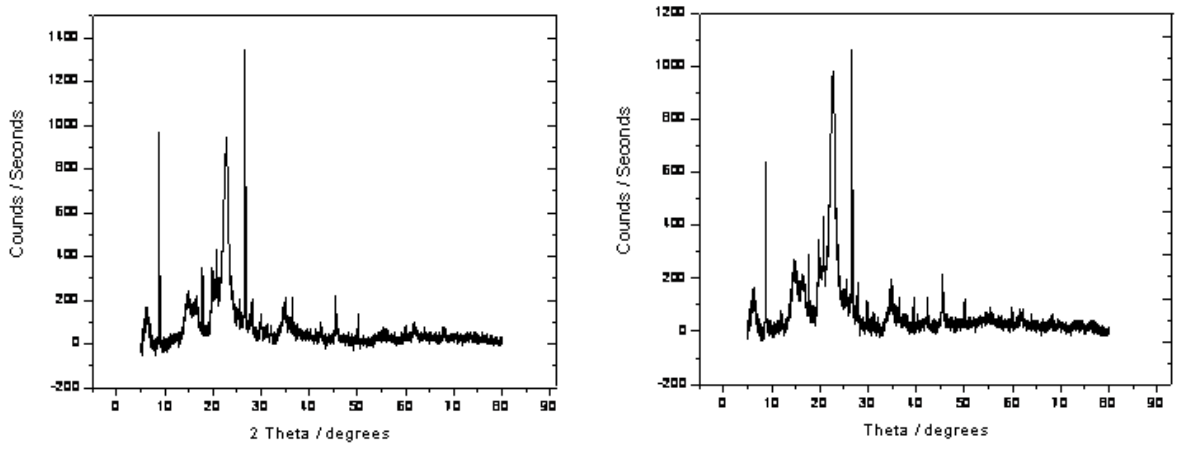

Figure 4.29. XRD pattern (A) adsorbent (B) after chromium(VI) adsorption

(iii) Nitrogen Adsorption Isotherm Study, Pore Size Distribution

The BET surface area of the material obtained from N_2 adsorption isotherm was found to be 87.09 m^2 g^{-1}. The shape of the isotherm indicates the mesoporous nature of the cellulose-clay composite material[139] The Barrett-Joyner-Halenda (BJH) pore size distribution curve (Figure 4.30A) for the composite adsorbent material provides a pore size of 1.8 nm at a maximum pore volume of 0.31 cm^3 g^{-1}. The adsorption hysteresis relates to the Type IV isotherm (Figure 4.30B). The mesoporous nature of the cellulose-clay composite, nano pore size, and the good surface area is an indication of effective adsorption of chromium on the polymeric adsorbent.

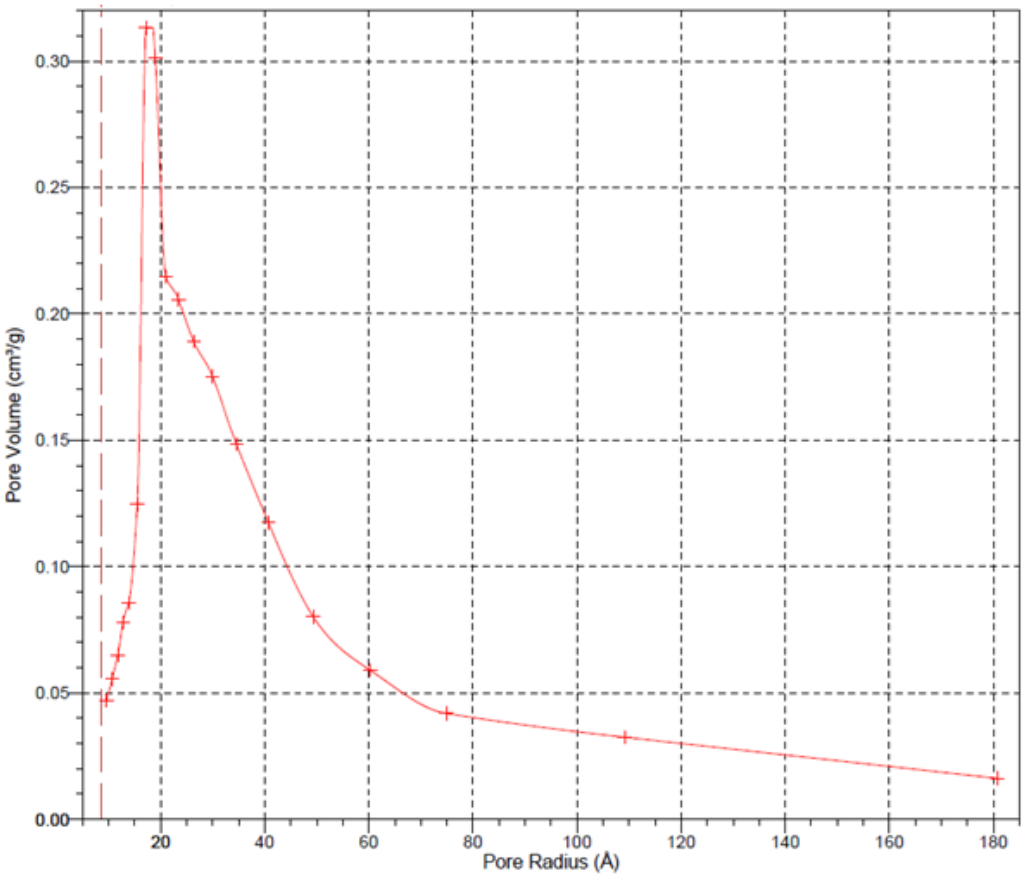

Figure 4.30(A) BJH Pore distribution curve

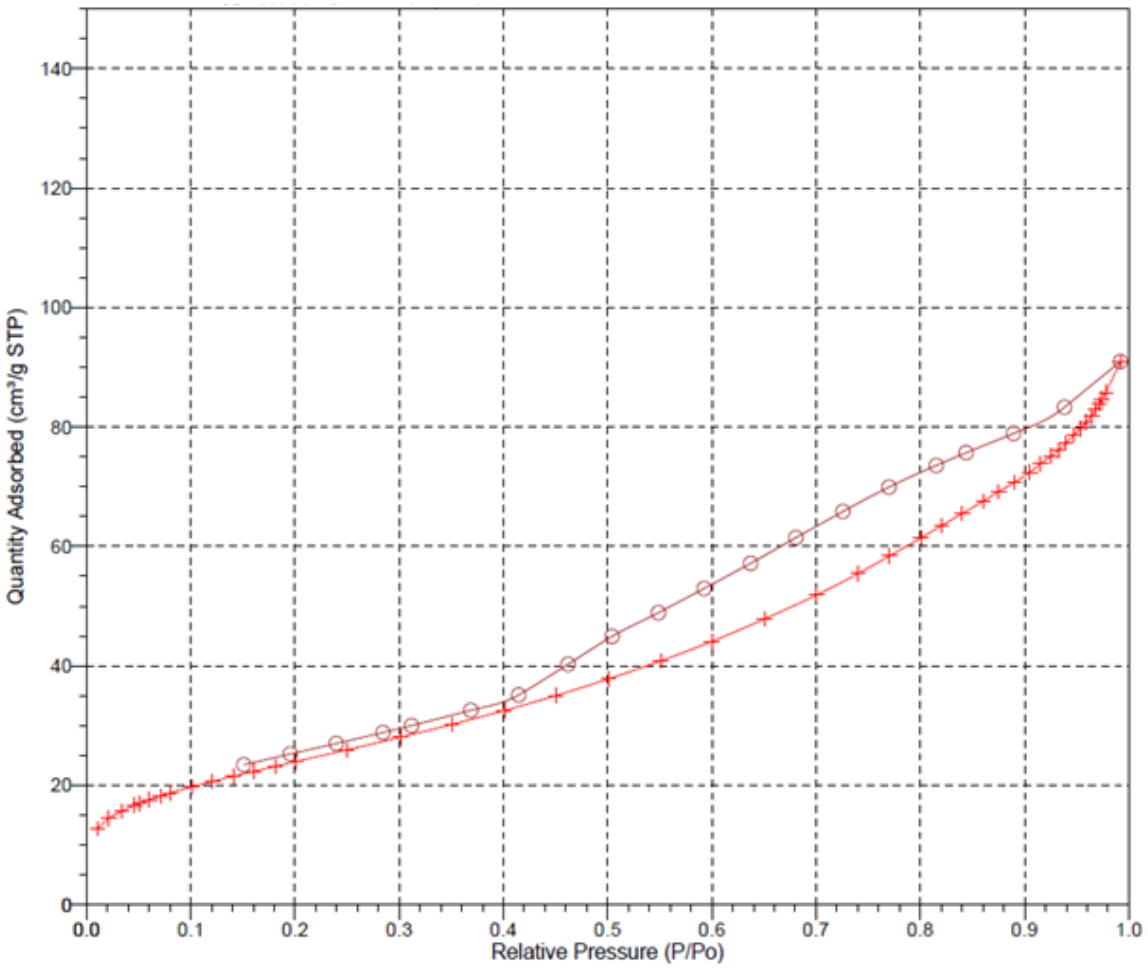

Figure 4.30(B). Nitrogen adsorption and desorption isotherm

(iv)Optimization of pH

The optimization of pH is a significant factor in the adsorption study. Hexavalent chromium can exist in various forms such as $HCrO_4^-$, CrO_4^{2-} and $Cr_2O_7^{2-}$ depending on the pH and concentration of the aqueous phase.[140] In the pH range 3.8-5.5, Cr(VI) exists in solution primarily as hydrochromate ($HCrO_4^-$) anion, whereas the dichromate ($Cr_2O_7^{2-}$) anion predominates at lower pH values. The favorable pH for the adsorption of Cr(VI) was observed in weakly acidic medium (3.8-5.5). In weakly acidic medium, the hydrochromate ion forms an ion-pair with the positively charged biopolymer composite

surface as evidenced by the FT-IR study. The hard acid soft base (HSAB) principle is a very useful model to explain a variety of complexation reactions. According to Pearson's classification,[141] chromium is categorized as a hard acid and nitrogen is classified as a hard base. Hence, we can expect good interaction between the positively charged nitrogen and negatively charged hydrochromate anion. In the case of hard acids such as chromium, the energy difference between the acceptor and donor orbital level is quite large and hence the bonding is strongly electrostatic in nature. Beyond pH 5.5, there is a decrease in the percentage adsorption of chromium. This could be attributed to the deprotonation of the surface hydroxyl groups in the biopolymer composite, which causes the decrease in adsorption.[136] Similarly, at higher pH the competition of the hydroxide anion with the hydrochromate anion for the effective adsorption sites could also lead to a reduction in the percentage adsorption of chromium. Three replicate measurements yielded a maximum adsorption of 99.6 ± 0.2 % at the optimized pH and it is the $HCrO_4^-$ species which is associated as an ion pair with the biopolymer-organophilic clay adsorbent followed by the hydrogen bonding interaction with the hydroxyl groups of cellulose.

(v) Amount of Adsorbent

The amount of adsorbent used in the batch study was varied in the range 0.1-1.0 g. The percentage adsorption was found to be maximium (99.5 ± 0.3 %) with three replicate measurements when the amount of adsorbent was in the range 0.5-0.6 g in 25 mL sample volume. The initial increase in adsorption is attributed to the strong electrostatic attraction between the hydrochromate anion and the biopolymer clay adsorbent. Beyond 0.6 g, there was no appreciable increase in the percentage adsorption, which indicates the saturation of the active adsorption sites in the biopolymer composite.

(vi) Adsorption Isotherm Studies

Langmuir isotherm model is commonly used to describe the relationship between the equilibrium concentration of the adsorbate and the amount adsorbed on the surface of the adsorbent. This isotherm is essentially based on three assumptions: a) Adsorption is essentially monolayer coverage. b) All the sites are equivalent with surface uniformity. c)

There is negligible interaction between the adsorbed molecules and the ability of a molecule to adsorb at a particular site is independent of the occupancy of the adjacent sites. The assumptions b and c imply that ΔH_{ads} is identical for all sites and is independent of the degree of surface coverage. The surface interaction of chromium with the composite adsorbent can be represented as

$$X + S \rightleftharpoons XS \qquad (21)$$

where X and S represent the chromium and the biopolymer clay composite surface and XS refers to the chromium adsorbed on the adsorbent. The Langmuir isotherm model is utilized to calculate the maximum adsorption capacity which is a measure of amount of the metal ion adsorbed per unit weight of the adsorbent. The maximium adsorption capacity was obtained by fitting the experimental data to Langmuir isotherm model,[58] which assumes monolayer adsorption. The maximum adsorption capacity, q_o and the constant b are obtained from the slope and intercept of the plot of C_e/q_e against C_e (Figure 4.31A). The values indicate good affinity of the hydrochromate anion towards the composite adsorbent material. The regression coefficient obtained from this plot was found to be 0.99 and the respective isotherm parameters are given in Table 4.9. The applicability of this isotherm model is evident from the good correlation obtained through the above plot. An R_L value of zero indicates irreversible adsorption while values greater than 1 indicate unfavorable adsorption. It has been well established in many adsorption systems that the value of R_L in the range 0 to 1 serves as an index to constructive adsorption. The value of R_L for the adsorption of chromium on the cellulose-clay composite material was found to be 0.3178 and this indicates the effectiveness of interaction between $HCrO_4^-$ and the adsorbent surface under the optimized experimental conditions.

(vii) Freundlich Isotherm

The Freundlich isotherm[60] takes into account the logarithmic decrease in the energy of adsorption with increasing surface coverage and this is attributed to the surface heterogeneity. The values of K_F and n were obtained from the slope and intercept of the logarithmic plot of q_e vs C_e (Figure 4.31B) and the results are presented in Table 4.9. The

plot is linear with a regression coefficient of 0.99. The Freundlich constant n lies between 1-10 for a favorable adsorption process and a larger value of n implies effective interaction between adsorbent and the adsorbate

(viii) Dubinin–Radushkevich Isotherm

The Dubinin–Radushkevich isotherm[61] (D-R) is analogous to the Langmuir isotherm but it does not assume a homogeneous surface or a steady adsorption potential. The D-R isotherm helps in calculating the adsorption energy and the nature of the adsorption mechanism involved in the interaction between chromium and the adsorbent surface. The values of β and q_m were obtained from the slope and intercept of the plot of $\ln q_e$ versus ε^2 (Figure 4.31C) and the results are presented in Table 4.9. The regression coefficient value was found to be 0.83. The adsorption energy, E can also be expressed as $-(2\beta)^{-0.5}$and the positive value of E indicates an endothermic adsorption. The adsorption energy was found to be 1.379 kJ mol^{-1} and this indicates that the electrostatic interaction between the hydrochromate anion and polymeric adsorbent is endothermic and higher temperatures favour the adsorption process.

(ix) Chi Square Test for the Adsorption Isotherms

The values of the regression coefficient above 0.9 indicate that the experimental data could fit into Langmuir and Freundlich isotherm models. Hence, the chi square test was adopted in order to find the suitability of an isotherm that fits best with the experimental data. The chi-square test is essentially the sum of the squares of the differences between the experimental and calculated data (obtained from the respective isotherm models) with each squared difference divided by the corresponding data obtained by calculation. The chi square test[142] can be expressed mathematically as

$$\chi^2 = \Sigma\ (q_{e\ exp} - q_{e\ cal})^2 / q_{e\ cal} \qquad (22)$$

where $q_{e\ cal}$ (mg g^{-1}) is the amount of chromium(VI) adsorbed at equilibrium obtained by calculating from the respective isotherm models and $q_{e\ exp}$ (mg g^{-1}) is the value obtained experimentally The value of χ^2 would be of a smaller magnitude if the data obtained from a particular isotherm model is in close concurrence with the experimental values.The

results from Table 4.9 indicate lower χ^2 values for Langmuir isotherm model showing that the experimental data correlates well with the Langmuir isotherm. This was also further verified from the respective isotherm data plots of q_e against C_e . The L shaped adsorption isotherms are in accordance with the classification of Giles [62] which indicates a good correlation to the Langmuir type isotherm as shown in Figure 4.31D. The initial increase is attributed to the effective interaction between the hydrochromate anion and the adsorbent and the plateau signifies the saturation of the adsorption sites.

(x) Kinetics of Adsorption

The kinetic parameters were evaluated using the well-known first order and pseudo second order models. [63],[64] The slope and intercept obtained from the plots of log (q_e-q_t) and t/q_t against t (Figure 4.316E &F) gives the respective kinetic parameters. The adsorption data is in good concurrence with the pseudo second order model due to the higher regression coefficient (Table 4.10). The q_e values obtained experimentally and from the second order kinetic model were found to be 1.16 mg g^{-1} and 1.21 mg g^{-1} respectively. The close correlation between the experimental and calculated values authenticates the applicability of second order kinetic model in the adsorption of chromium.The overall rate of adsorption of chromium on the biopolymer-clay adsorbent could be influenced by the following three steps: a) film or surface diffusion where the Cr(VI) is transported from the bulk solution to the external surface of the adsorbent. b) intraparticle or pore diffusion, where the adsorbate molecules move into the interior of the adsorbent particles and c) adsorption of chromium ion on the interior sites of the adsorbent. Since, the adsorption step happens quite rapidly it is assumed that it does not bear significant influence on the adsorption kinetics. Hence, the overall rate of adsorption could be controlled by surface or intraparticle diffusion. The Weber–Morris[65] intraparticle diffusion model has often been used to determine whether intraparticle diffusion is the rate-determining step. According to this model, a plot of q_t versus $t^{0.5}$ should be linear if intraparticle diffusion is involved in the adsorption process and if the plot passes through the origin then intraparticle diffusion is the only rate-limiting step. This plot is linear and the slope gives the intraparticle rate constant k_{int} and the non-zero intercept (Figure 4.31G) points to the fact that diffusion is not the only phenomenon that

controls the adsorption of the metal ion on the cellulose-clay composite material. Furthermore, the hysteresis between the nitrogen adsorption and desorption isotherms (Figure 4.30B) also indicate that intra particle diffusion is not the only rate controlling mechanism [66] operating in the adsorption of chromium on the polymeric adsorbent.

(xi) Thermodynamics of Adsorption

The adsorption thermodynamics was studied at varying temperatures and the respective thermodynamic parameters such as the free energy, enthalpy and entropy changes were obtained from the following equations where ΔH^0 and ΔS^0 are enthalpy and entropy changes, R is the universal gas constant (8.314 J mol^{-1} K^{-1}) and T is the absolute temperature (Kelvin). The equilibrium constant K is obtained from the ratio of concentration of Cr(VI) adsorbed on the composite material to that in the solution. The values of ΔH^0 and ΔS^0 were calculated from the slope and intercept of the Van't Hoff plot of lnK against 1/ T and equation 12 was used to calculate the Gibb's free energy[67] (ΔG^0). The spontaneity of adsorption process is ascertained from the equilibrium constant K and the Gibb's free energy values. The results are presented in Table 4.11 and the negative free energy value implies a spontaneous adsorption process. The magnitude of ΔH^0 gives information about the adsorption mechanism and for physical adsorption, ΔH^0 is generally less than 80 kJ mol^{-1} while for chemical adsorption the value lies in the range 80 and 400 kJ mol^{-1}. The equilibrium constant increases with temperature and this is reflected in the free energy values obtained at higher temperatures. Higher temperatures favour the adsorption process as evident from these values. The entropy of adsorption was found to be positive and this is indicative of increased randomness at the adsorbent-solution interface. The positive value of enthalpy change indicates the endothermic reaction between the adsorbent and the adsorbate. The energy is manifested in weakening the interaction between N^+ in CTABr and the hydroxyl groups of cellulose and strengthening the subsequent electrostatic interaction between the positively charged nitrogen and the hydrochromate anion respectively. These data demonstrate the effectiveness of the cellulose-clay composite material as an useful adsorbent for chromium(VI). When the clay matrix is dispersed in the solvent medium, the molecules

tend to be disordered in order to accommodate the cellulose polymeric chains. The process involves a gain in the translational entropy resulting in the separation of the clay layers. This leads to a positive entropy change during the adsorption process. This fact can be further substantiated by considering the free energy changes associated with cellulose, NaMMT and chromium. The change in the free energy can be expressed as the difference in the enthalpy and the entropy changes of the respective components as follows

$$\Delta G_{\text{cellulose}} = \Delta H_{\text{cellulose}} - T\Delta S_{\text{cellulose}} \quad (23)$$

$$\Delta G_{\text{Na MMT}} = \Delta H_{\text{Na MMT}} - T\Delta S_{\text{Na MMT}} \quad (24)$$

$$\Delta G_{Cr} = \Delta H_{Cr} - T\Delta S_{Cr} \quad (25)$$

$$\Delta G_{\text{adsorption}} = \Delta H_{\text{adsorption}} - T\Delta S_{\text{adsorption}} \quad (26)$$

$$\Delta G_{\text{adsorption}} = \Delta H_{\text{adsorption}} - T\,(\Delta S_{\text{cellulose}} + \Delta S_{\text{NaMMT}} + \Delta S_{Cr}) \quad (27)$$

The interaction of hard cation (N^+) with the negatively charged hydrochromate oxoanion is characterized by a positive value of enthalpy and entropy. The overall entropy contribution arises from the individual entropy changes associated with the biopolymer, clay and cellulose. Hence, the summation ($\Delta S_{cellulose} + \Delta S_{NaMMT} + \Delta S_{Cr}$) becomes largely positive reflecting the increased randomness at the adsorbent-solution interface. Furthermore, the fact that $T\Delta S > \Delta H$ shows that the physico-chemical adsorption process is entropically driven rather than the enthalpy effect. The large entropy and the positive enthalpy contribution ($\Delta H > 0$) is attributed to the decrease in the hydration of the ions.[143] The positive entropy change is related to the release of the water molecules leading to an increase in the total degrees of freedom attributed to the effective interaction between the hydrochromate anion and the polymeric adsorbent. The energy of activation (E_a) at various temperatures can be calculated using the relation $E_a = \Delta H^0_{ads} + RT$ for adsorption from solutions.[70] The average energy of activation was found to be 92.63 kJ mol $^{-1}$ and the positive value of E_a indicates the endothermic nature of adsorption.

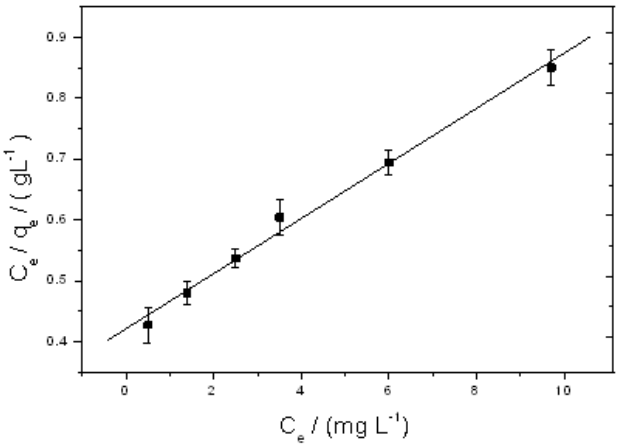

Figure 4.31. (A) Langmuir isotherm

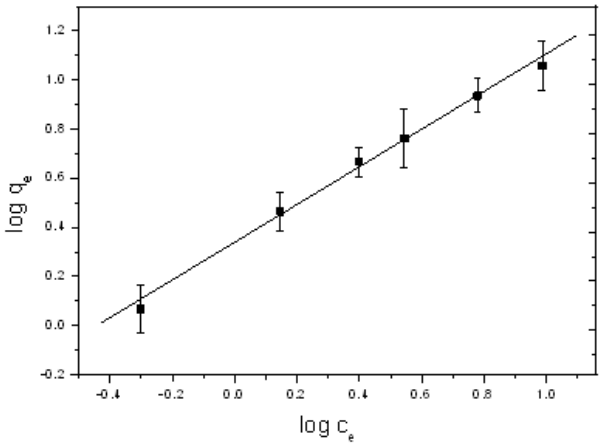

Figure 4.31. (B) Freundlich isotherm

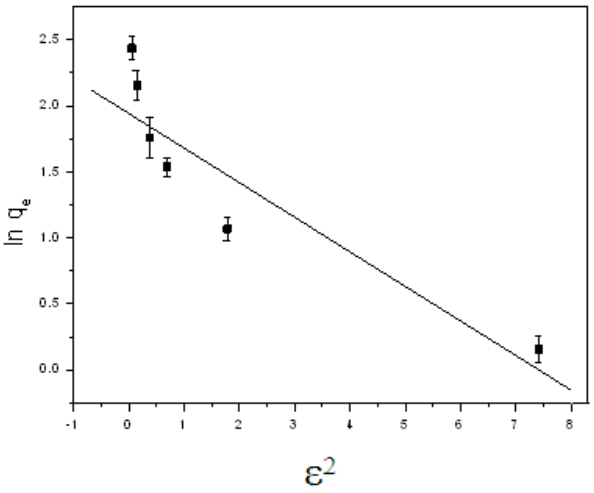

Figure 4.31. (C) Dubinin–Radushkevich isotherm

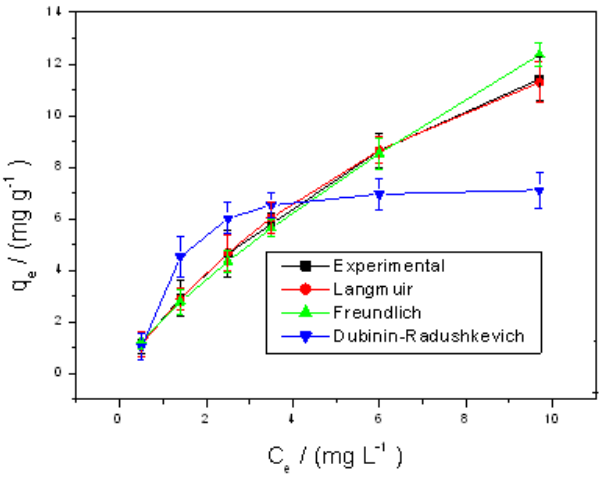

Figure 4.31. (D) Plot of q_e vs C_e

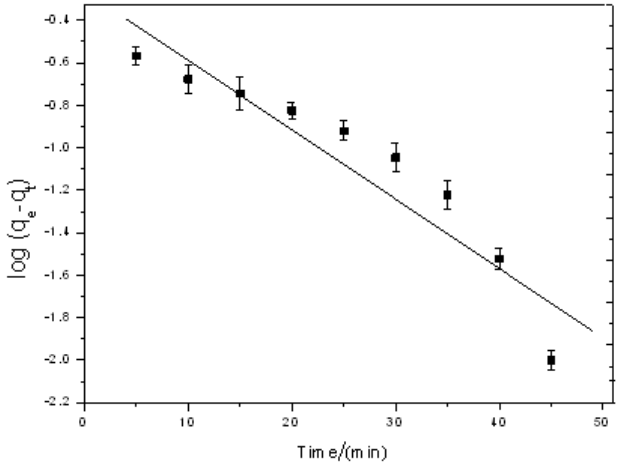

Figure 4.31. (E) Pseudo first order kinetic plot

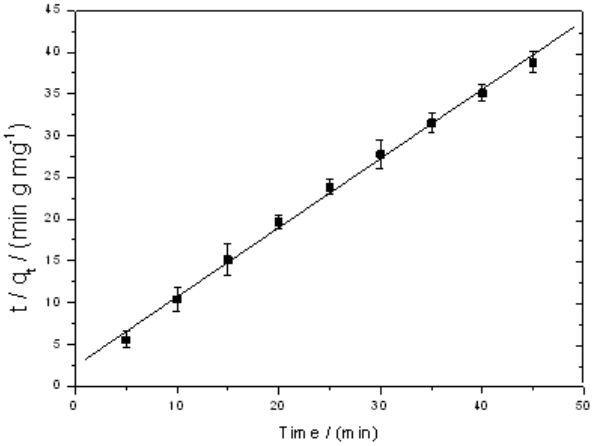

Figure 4.31. (F) Pseudo second order plot

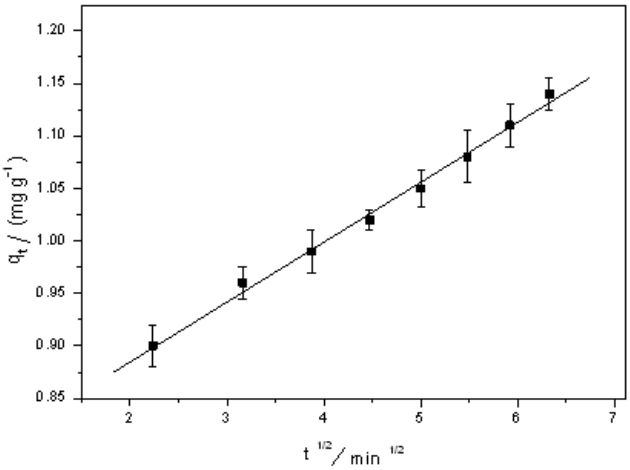

Figure 4.31. (G) Plot of q_t vs square root of time

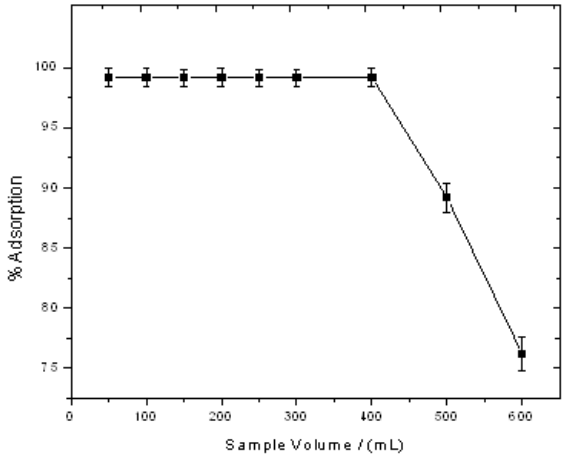

Figure 4.31. (H) Effect of sample volume

(xii) Column Study

After optimizing the parameters in batch study, the applicability of the composite adsorbent material was examined for the detoxification of chromium from a larger sample volume. A glass column 2.5 cm in diameter and 30 cm in length was used for the column adsorption study. 3.5 g of the adsorbent material was packed in the glass column to a height of 5 cm. A known volume (250 mL) of 100 mg L^{-1} Cr(VI) was transferred to the column at a flow rate of 6 mL min^{-1}. Cr(VI) was effectively adsorbed on the column at pH 4.0 and this was ascertained spectrophotometrically from the concentration of chromium in the solution phase.

(xiii) Effect of Sample Volume

The effect of sample volume for the adsorption of chromium(VI) on the biopolymer clay composite adsorbent was investigated in the range (100 to 600) mL maintaining an overall concentration of 100 mg L^{-1}. As can be seen from Figure 4.31H, it is evident that the adsorption of chromium is quantitative till a 400 mL sample volume with a preconcentration factor of 50. The amount of the adsorbent, bed height and diameter of the column play a pivotal role in the performance of the column.[8] On loading the column with a higher aqueous sample volume, the degree of swelling in the biopolymer clay composite adsorbent increases and results in the expansion of the adsorbent bed. This would create some voids in the column by disturbing the effective packing and hence the adsorption of chromium decreases beyond a 400 mL sample volume.

(xiv) Optimum Flow rate and Bed height of the Column

The flow rate and bed height are two vital parameters which affect the percentage adsorption of chromium. The interaction of hydrochromate with the biopolymer adsorbent depends on the contact or residence time of the adsorbate with the adsorbent. The results presented in Table 4.12 indicate an optimum flow rate of 5 mL min^{-1} and a bed height greater than 3 cm ensures quantitative adsorption of chromium(VI) from aqueous solution. At low flow rates, there exists an effective contact between the hydrochromate anion and the adsorbent. Similarly, a low bed height also results in lesser adsorption of chromium since the amount of the adsorbent used in the packing of the

column is insufficient for the complete retention of chromium. A flow rate of 5 mL min^{-1} was maintained for maximum column efficiency and effective retention of chromium. At higher flow rates, there was a decrease in the column adsorption efficiency and this could be ascribed to the lesser contact time between the sample and the biopolymer-clay composite adsorbent.

(xv) Regeneration and Reusability of the Biopolymer Clay Composite Adsorbent

The regeneration of adsorbent is important from a greener perspective and hence it is imperative to look for effective and non-toxic eluents for the quantitative recovery of chromium. Considering the above aspect, reagents such as sodium hydroxide as well as reducing agents like sodium sulfite and ascorbic acid were examined for effective desorption. These reagents have also proved their efficacy in some of our earlier studies.[98,100,135,144] pertaining to the removal of chromium. Ascorbic acid was quite effective in reducing Cr(VI) to the less toxic Cr(III). Nevertheless, the recovery was only 85% with 15 mL of the eluent and a larger volume (2 x10 mL) of the reagent was required for quantitative desorption of chromium as Cr(III). The overall mechanism of this reduction is well established and is recognized to proceed through a Cr(IV) intermediate.[144] In the proposed methodology, we found that with three replicate measurements, an 8 mL volume of 3 mol L^{-1} sodium hydroxide was effective in the quantitative elution (99 ± 0.3 %) of chromium (VI) as sodium chromate in the eluate (Figure 4.32). The adsorbent could be reused for 10 adsorption-desorption cycles with good efficiency. Beyond 10 cycles, the repeated use of acidic and alkaline medium for the adsorption and desorption of chromium(VI) decreased the performance efficiency of the column. This could be attributed to the decrease in the effective interaction between the adsorbent and the adsorbate due to the non-availability of active sites for adsorption.

(xvi) Interference of Diverse Ions

In order to apply the solid phase extraction methodology to real effluent samples, it is essential to study the interfering effect of diverse ions that are usually associated with these effluents. The effect of diverse ions were studied at 50 mg L^{-1} Cr(VI) concentration, maintaining a sample volume of 250 mL. Ions such as Ca^{2+} and Mg^{2+} did not cause any

interference up to 800 mg L^{-1} level. Lower concentrations of anions (< 500 mg L^{-1}) such as chloride, nitrate and sulfate did not affect the quantitative adsorption of chromium. However, considerable interference was observed due to the cations such as Co^{2+}, Mn^{2+}, Ni^{2+}, Cu^{2+}, Zn^{2+}, Fe^{2+}, Fe^{3+} and Hg^{2+} at 600 mg L^{-1} level in the presence of 750 mg L^{-1} chloride. The results presented in the bar diagram (Figure 4.33) illustrates the above fact and this could be attributed to the order of stability of the chloro complexes of these metal ions. The stability of the high spin complex chloro-anions[145] follows the order Ni^{2+} < Mn^{2+} < Co^{2+} < Cu^{2+} < Fe^{3+} < Zn^{2+} . Iron in the +2 oxidation state could act as a reducing agent and interferes by reducing the Cr(VI) to Cr(III) . The negatively charged high spin metal complexes could contend with the hydrochromate anion for the active sites in the biopolymer-composite adsorbent thereby leading to a decrease in the percentage adsorption of chromium. A similar phenomena arising from the competing nature of the halocomplexes has also been observed in our earlier studies pertaining to the removal of chromium. Anions such as chloride, nitrate and sulfate could also directly compete with the hydrochromate anion for the effective adsorption sites at higher concentrations (>500 mg L^{-1}) causing a reduction in the percentage adsorption of chromium.

(xvii) Application to a Real Industrial Effluent

The performance of the composite material was investigated for the detoxification of chromium from a chrome tannery leather effluent. The chrome tan waste liquor at the time of collection was green in color with a pH value of 6.5 and it is the basic chromium sulfate which is used in tanning of the leather. The distinct characteristics of the effluent sample procured from a leather tannery unit are given in Table 4.13. Prior to the adsorption, it is essential to destroy the organic components present in the sample and this was achieved by treatment with nitric acid-sulfuric acid mixture. The Cr(III) present in the sample is oxidized to the +6 oxidation state using hydrogen peroxide in alkaline medium.[135,144] A 100 mL volume of the concentrated effluent sample was diluted to 500 mL and a known volume of the diluted effluent (300 mL) was passed through the glass column packed with the adsorbent by maintaining the optimum pH required for the adsorption of Cr(VI). Five replicate measurements ensured effective adsorption of chromium (97.5 ± 0.25 %) and this

was confirmed through the spectrophotometric determination of chromium in the treated effluent. In the diluted effluent sample, anions such as chloride, nitrate, sulfate and commonly present cations such as calcium, magnesium, zinc, copper etc did not cause any appreciable reduction in the removal efficiency of chromium. After the effective adsorption and removal of chromium from the effluent sample, the regeneration of the column was also effective with sodium hydroxide as the eluent.

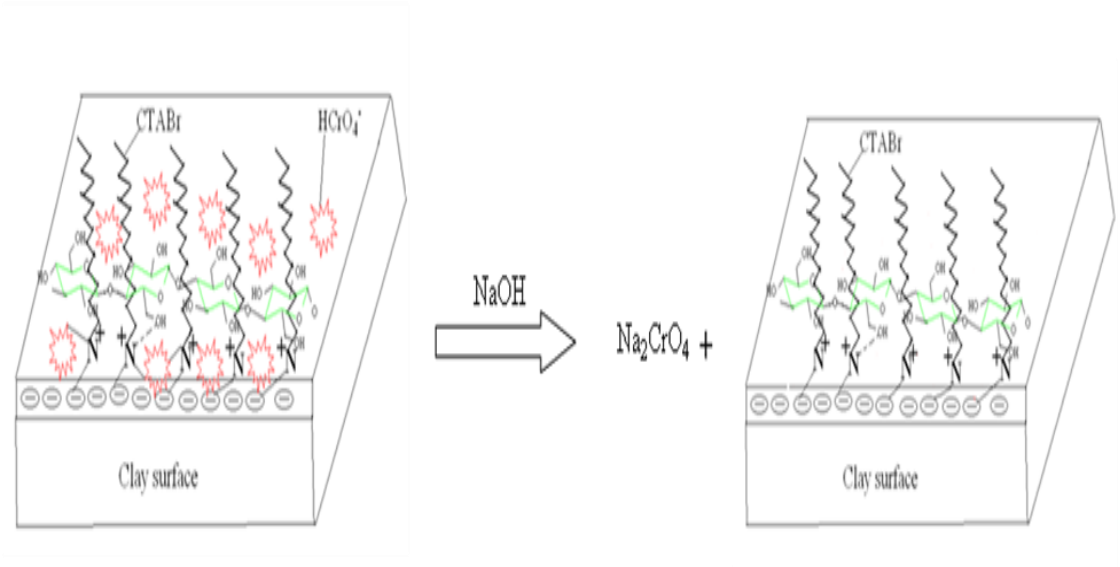

Figure 4.32. Conceptual illustration showing the regeneration of the adsorbent

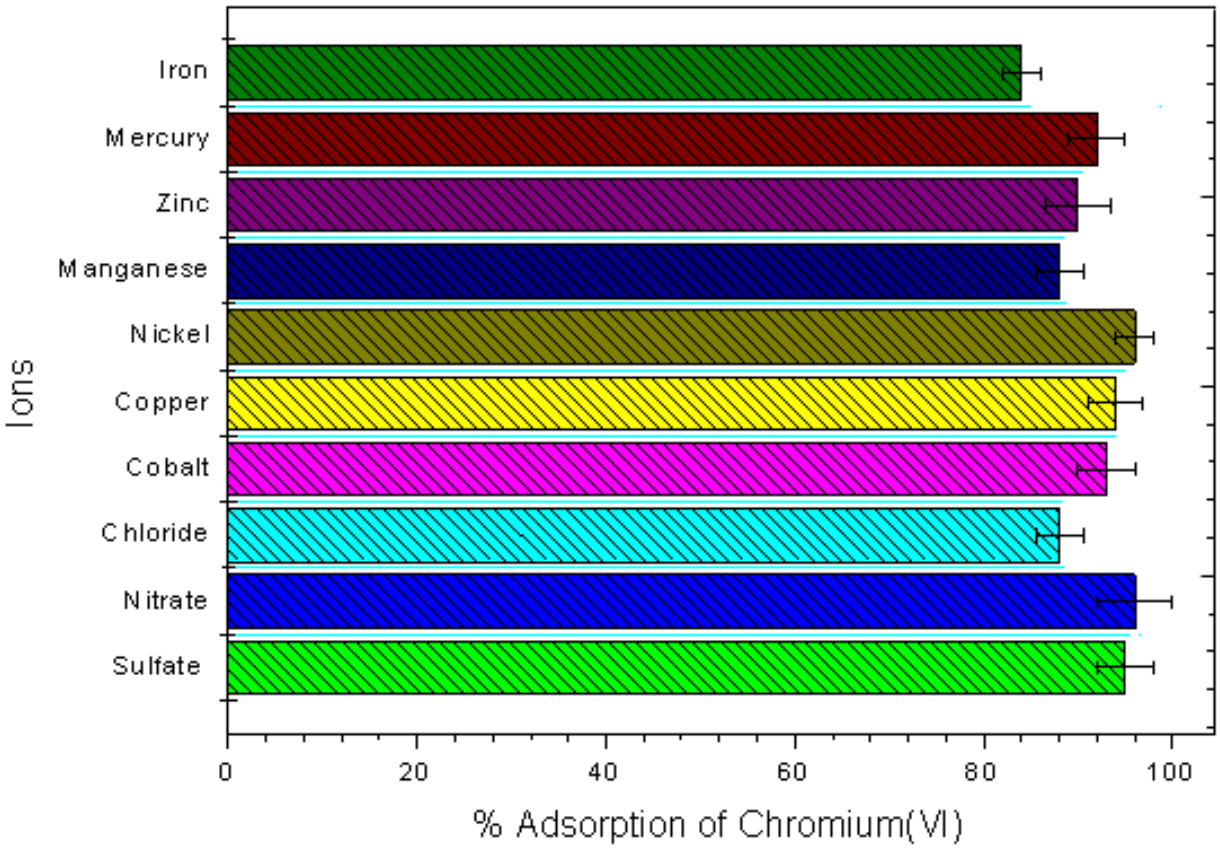

Figure 4.33. Effect of diverse ions

4.4.4 Conclusions

In conclusion, the interaction between the cellulose and NaMMT has demonstrated the potential application of a biopolymer composite material for the effective adsorption of chromium. The biopolymer composite exhibits an adsorption capacity of 22.2 mg g^{-1} and the experimental data showed a good fit to the Langmuir adsorption isotherm model. The spontaneity of adsorption was ascertained from the thermodynamic properties and the experimental data showed excellent adherence to second order kinetics. The mesoporous nature of the material was established from the nitrogen adsorption isotherm study and there is no significant change in the crystalline nature of the composite adsorbent after the adsorption of chromium. A sample volume of 400 mL could be quantitatively treated by column method at 100 mg L^{-1} concentration of Cr(VI) with a preconcentration factor of 50. The efficiency of the method is well illustrated in terms of regeneration of the composite material in a facile manner. The adsorbent could be reused with quantitative recovery for 10 cycles and its applicability to detoxify chromium from wastewater has shown good prospects in addressing the global environmental concern for heavy metal pollution.

Table 4.9. Adsorption isotherm parameters

Langmuir					Freundlich				Dubinin Radushkevich				
q_o (mg g^{-1})	b (L mg^{-1})	R_L	r^2	χ^2	K_F (mg $^{1-1/n}$ g^{-1} $L^{1/n}$)	n	r^2	χ^2	q_m (mg g^{-1})	β (mol^2 kJ^{-2})	E (kJ mol^{-1})	r^2	χ^2
22.2	0.1073	0.31	0.9	0.01	2.1458	1.29	0.99	0.10	7.22	0.263	1.379	0.83	0.78

Table 4.10. Kinetic parameters and intra-particle rate constant for chromium(VI) adsorption

First order rate constant k_1 / (min^{-1})	R_1^2	Second order rate constant k_2 / (g mg^{-1} min^{-1})	R_2^2	Intra particle rate constant k_{int} / (mg g^{-1} $min^{-½}$)
0.0723	0.88	0.2817	0.99	0.0575

Table 4.11. Thermodynamic parameters for the adsorption of chromium(VI)

Temperature / (Kelvin)	ΔG^0/ (kJ mol^{-1})	ΔS^0 / (J mol^{-1} K^{-1})	ΔH^0/ (kJ mol^{-1})
298	-3.434	313.02	90.07
308	-6.455		
318	-9.685		

Table 4.12. Optimization of bed height and flow rate in column studies

S. No	Initial concentration (mg L^{-1})	Bed height (cm)	Flow rate (mL min^{-1})	Adsorption (%)
1.	50	3	5	94.3 ± 0.3
		5	5	99.5 ± 0.2
		8	5	99.5 ± 0.3
2.	50	5	2	99.5 ± 0.4
		5	5	99.5 ± 0.3
		5	10	97.0 ± 0.2

Table 4.13. Characteristics of chrome tan waste liquor

Constituents	Concentration (mg L^{-1})
Total Dissolved solids	1270
Zinc	5.2
Copper	3.5
Iron	7.2
Manganese	1.0
Nickel	1.1
Chloride	1520
Cadmium	0.5
Sulfate	840
Lead	1.2
Carbonate	17.0
Nitrate	560
Phosphate	320
Total Chromium	190

Microwave assisted preparation and characterization of biopolymer-clay composite material and its application for chromium detoxification

4.5.1 Introduction

This chapter deals with microwave assisted preparation and characterization of biopolymer clay composite material and its application for chromium detoxification from industrial effluent. Over the last decade, polymer–clay nanocomposites have been the subject of much research interest. The cationic biopolymer chitosan (poly-β(1,4)-2- amino-2-deoxy-D-glucose) can be intercalated in Na+-montmorillonite through cationic exchange and hydrogen bonding processes, the resulting nanocomposites showing interesting structural and functional properties.[146] Due to its properties, such as high mechanical strength, hydrophilic character, good adhesion and non-toxicity, chitosan is usually applied as food additive, supporting material for chromatography and chelating polymer for heavy metals removal.[147-149] Chitosan is an interesting gluosamine biopolymer with free amino groups available for interaction with metals.[150] Potato starch-silica nanobiocomposite is known for its excellent adsorption for heavy metal cadmium from aqueous solution. [151] Biopolymers deserve special attention for their potential application in waste water treatment.[152] Cellulose modified with β-cyclodextrin and quaternary ammonium groups has been recently reported for the effective adsorption of chromium.[153] However, with a view to enhance the adsorption capacity and to detoxify chromium from real industrial effluents, an unconventional methodology is proposed using surfactant modified NaMMT clay material and chitosan. Surfactant modification of clays is essential for effective compatibility between the hydrophilic clay and the biopolymer.[154] Upon treatment with long chain quaternary ammonium cations, the clays acquire organophilic character. CTABr is an excellent choice for such surface modification, where the alkyl ammonium cation replaces the Na^+ in the clay matrix.[155] The surface hydroxyl groups in clay can be protonated and this could also serve as a source of electrostatic interaction with the hydrochromate oxyanion.

Nanocomposites based on the intercalation of chitosan, a cationic natural polymer, in Na^+ montmorillonite are bidimensional nanostructured materials provided of anionic exchange sites ($–NH_3^+X^-$). This fact is due to the special arrangement of the biopolymer as a bilayer when the amount of intercalated chitosan is higher than the cationic exchange capacity (CEC) of the clay. The high affinity between the chitosan and the montmorillonite clay substrate is the basis of the high stability of the intercalated biopolymer against desorption or degradation, and, in consequence, of the long-term stability.

4.5.2 Experimental Section

(i) Preparation of Surfactant Modified Sodium Montmorillonite (NaMMT)

The MMT clay (6 g approx) was mixed with 200 mL of 1.0 mol L^{-1} NaCl and the mixture was stirred magnetically for 18 hours.[36] The resulting suspension was centrifuged and the supernatant discarded. The clay suspension was washed several times with Milli-Q water until no precipitate was observed in the filtrate with $AgNO_3$. This ensures the removal of chloride ions completely. The prepared NaMMT was dried and a small quantity of methanol (5 mL) was added so as to craft the clay less sticky and adaptable.[127] The sodium form of the clay was stirred magnetically with 100 mL of 0.01 mol L^{-1} CTABr for 6 hour. The mixture was centrifuged and the solid was washed with water and tested with $AgNO_3$ for the absence of bromide in the solution phase.

(ii) Microwave Assisted Preparation of the Composite Material

About 3 g of chitosan was dissolved in 10 mL of 1 % v/v acetic acid and the pH was adjusted to 5.0 with NaOH solution. 6 g of the surfactant modified NaMMT clay material was dispersed in 10 mL of methanol and the chitosan solution was slowly added to the clay suspension and stirred magnetically for about 5 min to ensure homogeneity. The mixture was then irradiated under microwave conditions for 30 min with 1 minute time interval. Every minute, a small quantity of methanol was added, made as a paste and further irradiated with MW. This process was continued for 30 min and the prepared composite material was dried in hot air oven at 120^oC for 6 hours. The composite material was then characterized by various analytical techniques and used subsequently for the adsorption of chromium.

(iii) Batch Adsorption Studies

The batch adsorption was studied by equilibrating 0.5 g of the composite material in a conical flask containing 70 mg L^{-1} Cr(VI). The pH of the medium was maintained at 5.0 and the reaction mixture was equilibrated in orbital incubator shaker at room temperature at 150 rpm at various time intervals and the amount of chromium(VI) adsorbed was calculated by measuring the concentration of chromium left in the aqueous solution spectrophotometrically after complexation with diphenyl carbazide in acidic medium.[38]

4.5.3 Results and Section

(i) Characterization of the Chitosan-Clay Composite by FT-IR spectroscopy

The infra red spectrum of the Chitosan-NaMMT (Figure 4.34A, B) shows the combination of characteristic absorptions due to chitosan and the clay material as reported earlier in literature. [131,146,155] The FT-IR spectrum shows the following characteristic bands: 3627 cm^{-1}(O-H stretching), 3445 cm^{-1} (Hydrogen bonded water), 1645 cm^{-1} (O-H deformation). The band corresponding to 1867 cm^{-1} could be ascribed to the ν_{CO} stretching frequency of acetate ions associated with chitosan.[146] In addition, distinct bands are observed at 833 cm^{-1} (Al-Fe-OH deformation) 800 cm^{-1}(Si-O stretching) 694 cm^{-1} (Si-O deformation) 613 cm^{-1} (Al-O and Si-O out of plane) 577 cm^{-1}(Al-O-Si deformation), 1472 (N–H bending), 1377 cm^{-1} (C-H bending) and 1051 cm^{-1} (C–O stretching) respectively. There is a considerable modification in the spectral features after the adsorption of chromium(VI), Hexavalent chromium exists principally as hydrochromate ion ($HCrO_4^-$) in weakly acidic medium. The vibrational bands at 1557 cm^{-1} corresponding to N-H deformation mode in chitosan are shifted towards lower frequency with also considerable reduction in the peak intensity after the adsorption of chromium. This indicates that the free amino group in chitosan plays an important role in the mechanism.[146] The primary amine group is protonated and the NH_3^+ cation is electrostatically bound to $HCrO_4^-$ in acidic medium. This fact is also confirmed through the characteristic Cr=O peak at 916 cm^{-1}.[42, 105]

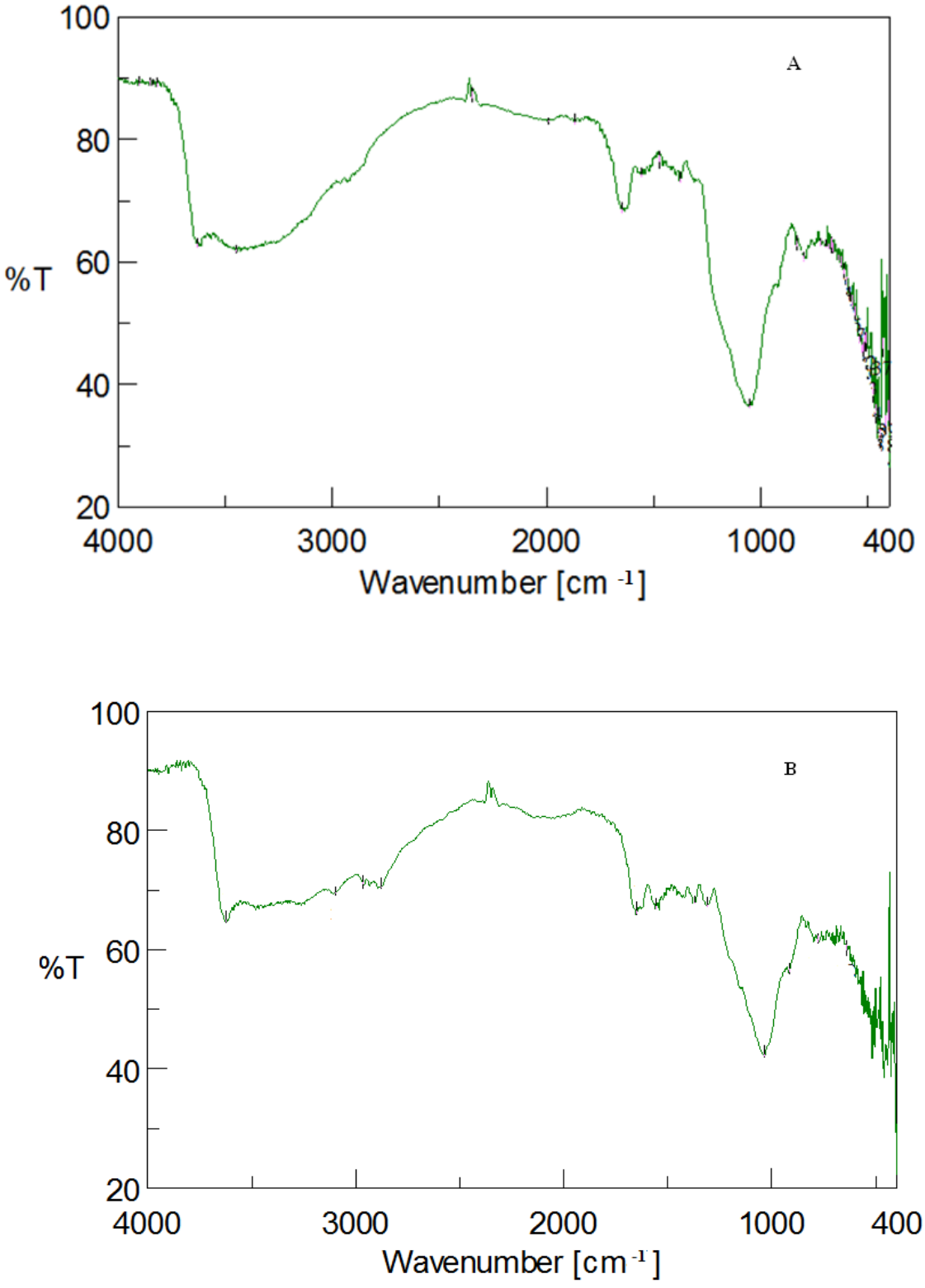

Figure 4.34. FT-IR spectrum of (A) adsorbent (B) after chromium(VI) adsorption

(ii) Powder XRD, SEM and EDX Analysis of the Composite Material

The wide angle X ray diffraction (WAXRD) of the composite material shows sharp and symmetric diffraction peaks (Figure 4.35A, B) at 2θ values corresponding to 8.84^0, 17.88^0, 19.70^0, 26.92^0 which is indicative of the crystalline and exfoliated nature of the material. Considerable degree of exfoliation is known in polar polymers. The SEM images (Figure 4.36A, B) also show good difference in the surface morphology after the adsorption of chromium with the appearance of glossy particles on the surface of the adsorbent. The intercalative or exfoliated nature of the polymer composite depends on the amount of the added clay. When the amount of added clay is less, the silicate layers would be dispersed or exfoliated in the polymeric matrix. The organophilicity of the clays leads to a better interaction with the biopolymer chitosan, resulting in a good dispersion and tendency to exfoliate in the matrix. The significant sharp peaks at higher 2θ values indicate a relatively more ordered distribution of clay layers in the biopolymer composite. At lower angles ($<10^0$) peak sharpening is slightly reduced and this could reflect a less ordered morphology.[33] After the adsorption of chromium, the crystallinity of the composite material is retained with the appearance of a new sharp peak at 2θ value corresponding to 35.20^0 which is characteristic of chromium adsorption and this is in close agreement with the earlier reported value in literature.[107] The adsorption of chromium on the surface of the composite material was confirmed from the energy dispersive X ray spectrum (Figure 4.37) which shows the presence of chromium (observed in the range 5-6 keV) with the other elemental constituents.

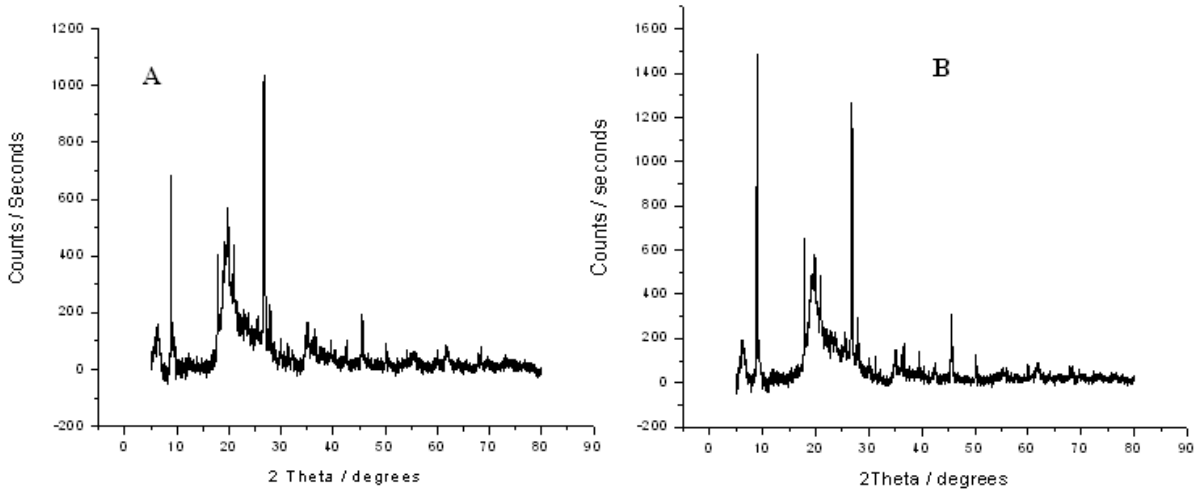

Figure 4.35 Powder XRD pattern of the (A) adsorbent (B) after chromium(VI) adsorption

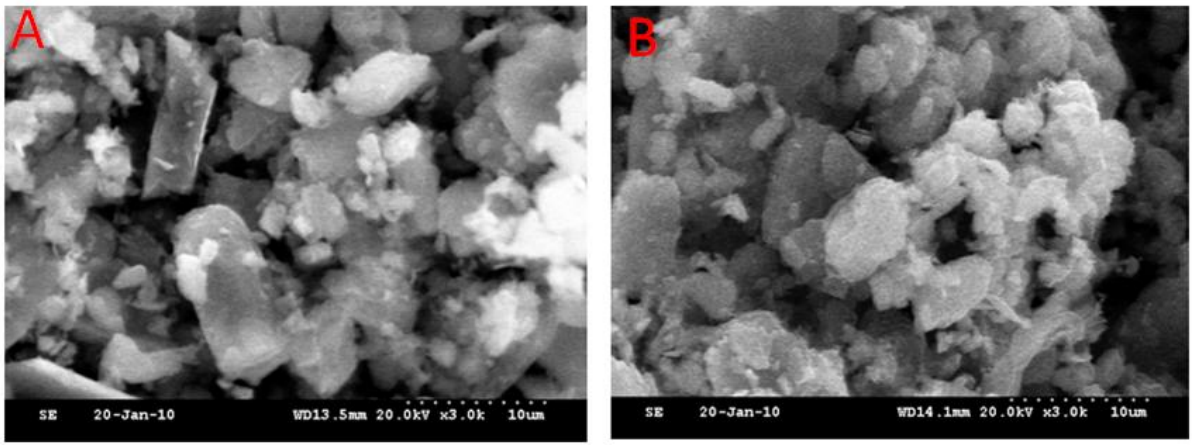

Figure 4.36 SEM image of the (A) adsorbent (B) after chromium(VI) adsorption

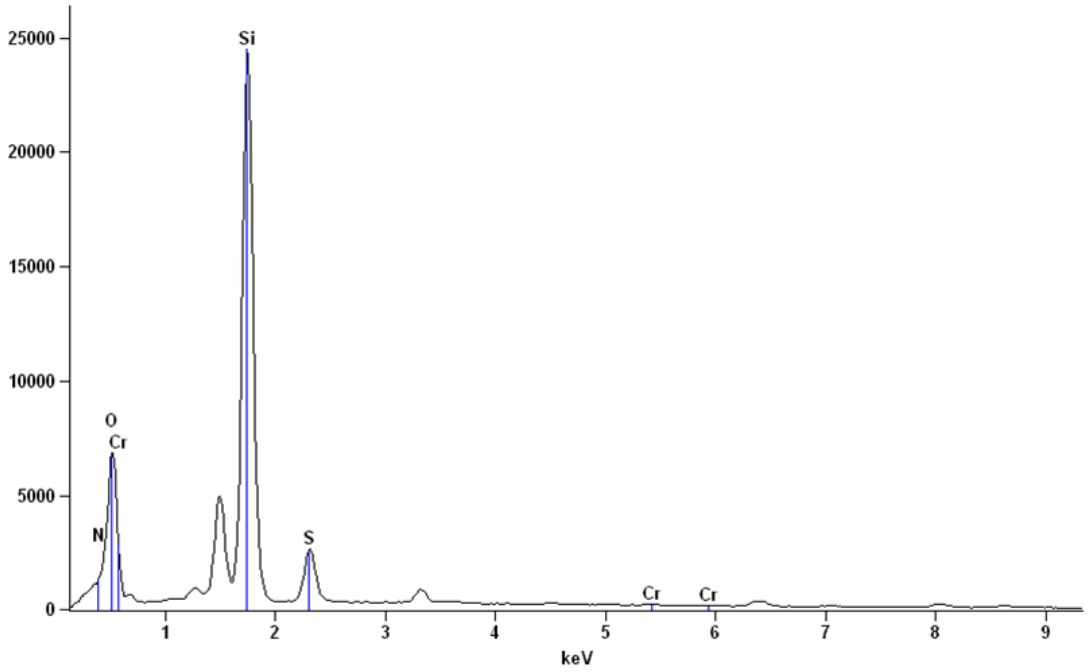

Figure 4.37 EDS spectrum of the adsorbed Cr(VI) on the composite material

(iii) Adsorption Hysteresis

The adsorption hysteresis can be classified as Type IV isotherm with an inflexion at P/Po= 0.4 (Figure 4.38A). The shape of the isotherm indicates the mesoporosity in the composite material. The Barret-Joyner-Halenda (BJH) pore size distribution curve (Figure 4.38B) for the composite adsorbent material gives a pore size of 3.5 nm at maximum pore volume of 0.16 cm^3g^{-1}. The BET surface area of the material obtained from N_2 adsorption was found to be 52 m^2 g^{-1}. The effective surface area, mesoporous nature of the composite material and the nano pore size reflect the effectiveness in the adsorption of chromium.

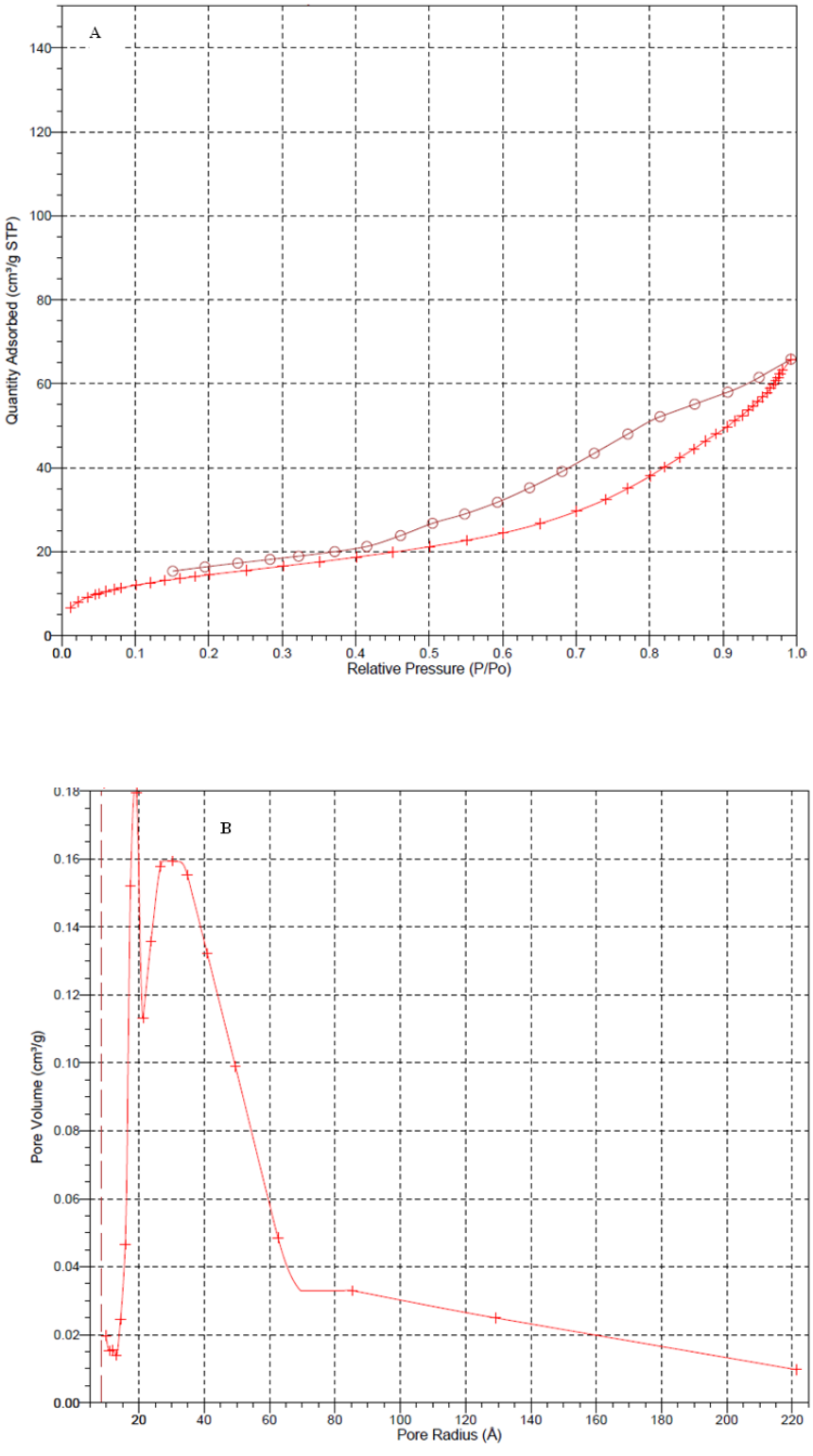

Figure 4.38 (A) Nitrogen adsorption and desorption isotherm (B) BJH pore distribution curve.

(iv) Optimization of pH and Mechanism of Adsorption

The optimization of pH is an important factor in sorption studies. The optimium pH for the adsorption of Cr(VI) was found to be in the range 4-5 which corresponds to a weakly acidic medium. As mentioned earlier, in weakly acidic medium the hydrochromate ion forms an ion-pair with the protonated amine group in chitosan and this has also been substantiated by the IR study. It is also possible that in acidic medium, the surface hydroxyl groups in clay can be protonated and this could also serve as a source of electrostatic interaction with the hydrochromate oxyanion. Beyond pH 5 the percentage adsorption decreases and at alkaline pH there is a considerable decrease in the adsorption of chromium. This could be attributed to the deprotonation of the surface hydroxyl groups in the composite material which causes the decrease in adsorption.

(v) Effect of Amount of Adsorbent

The amount of the composite adsorbent was varied from 0.2 g to 1.0 g with a constant initial concentration of 70 mg L^{-1} and agitation time of 40 min. The extent of adsorption (%) enhanced with increase in the amount of adsorbent. The availability of increasing number of active adsorption sites ensured the enhanced uptake of chromium(VI). This is a common phenomenon in adsorption, when the number of active sites or the effective surface area is increased. The quantitative adsorption efficiency (>99 %) was attained with 0.5 g of the composite adsorbent material. However, beyond 0.5 g the % adsorption is constant, due to the saturation of effective adsorption sites for the retention of Cr(VI).

(vi) Adsorption Isotherm

The experimental data were fitted into the Langmuir and Freundlich isotherm models. [58,60] The maximum adsorption capacity, q_o and the constant b (Figure 4.39A) were found to be 133 mg g^{-1} and 0.0884 L mg^{-1} respectively. The Langmuir isotherm model also provides another vital parameter, R_L, a dimensionless constant expressed as $1/ (1 + b.C_0)$. It is known in many adsorption systems that the value of R_L in the range 0 to 1 signifies favorable adsorption.[59] In the present investigation, the value of R_L for the adsorption of chromium on the composite material was found to be 0.1391 and this indicates effective adsorption under the optimized experimental conditions. The well known Freundlich isotherm K_F and n are the Freundlich constants which indicate the adsorption capacity

and the adsorption intensity respectively. The constants K_F and n were found to be 11.51 L g^{-1} and 1.4355 obtained from the slope and intercept of the plot of log q_e against log C_e (Figure 4.39B). The regression coefficients obtained from the Langmuir and Freundlich plots were found to be 0.99 and 0.98 respectively and this indicates the applicability of both these isotherm models to the experimental data.

(vii) Kinetics of Adsorption

The rate of adsorption increased with time and reached its maximum at 40 min. The first order and pseudo second order models were used to fit the experimentally obtained adsorption data. [63,64] The plot of t/q_t versus t (Figure 4.39C) and log $(q_e–q_t)$ versus t (Figure 4.39D) gives the kinetic parameters. The adsorption data was well in agreement with the pseudo second order model in view of the higher regression coefficients (Table 4.14). Moreover, the q_e value obtained from the second order model and the q_e value obtained experimentally were found to be 8.125 mg g^{-1} and 8.779 mg g^{-1} respectively. The close agreement between the experimental and calculated values further confirms the applicability of the second order kinetics. A plot of q_t against the square root of time gives a straight line with a definite intercept (Figure 4.39E). This plot is linear and the slope gives the intraparticle rate constant $k_{int.}$[65] The nonzero intercept indicates that diffusion is not the only process that controls the adsorption of the metal ion on the composite material. Boundary layer control could also reflect on the adsorption process. This fact is consistent with the literature reports on similar phenomena observed in various other adsorbent-adsorbate interactions.[66]

(viii) Sorption Thermodynamics

The free energy, enthalpy and entropy change associated with the adsorption process was obtained from the sorption thermodynamics at different temperatures. The well known Van't Hoff equation[67] also relates the equilibrium constant with enthalpy and entropy changes as a function of temperature. The equilibrium constant values were obtained at various temperatures and a plot of $\ln K_c$ against 1/T (Figure 4.39F) gives the corresponding thermodynamic parameters. The free energy values were found to be ascendingly negative with rise in temperature. The negative free energy is a good indication of spontaneous adsorption. The enthalpy change (ΔH^0) was found to be

positive which indicates the endothermic nature of adsorption (Table 4.15). The endothermic nature of adsorption has also been reported earlier for chromium adsorption using kaolinte clay in the absence of biopolymer. The entropy of adsorption (ΔS^0) was also found to be positive and this is indicative of increased randomness at the adsorbent-solution interface. These facts demonstrate the efficacy of the composite material as an useful material for chromium(VI) adsorption.

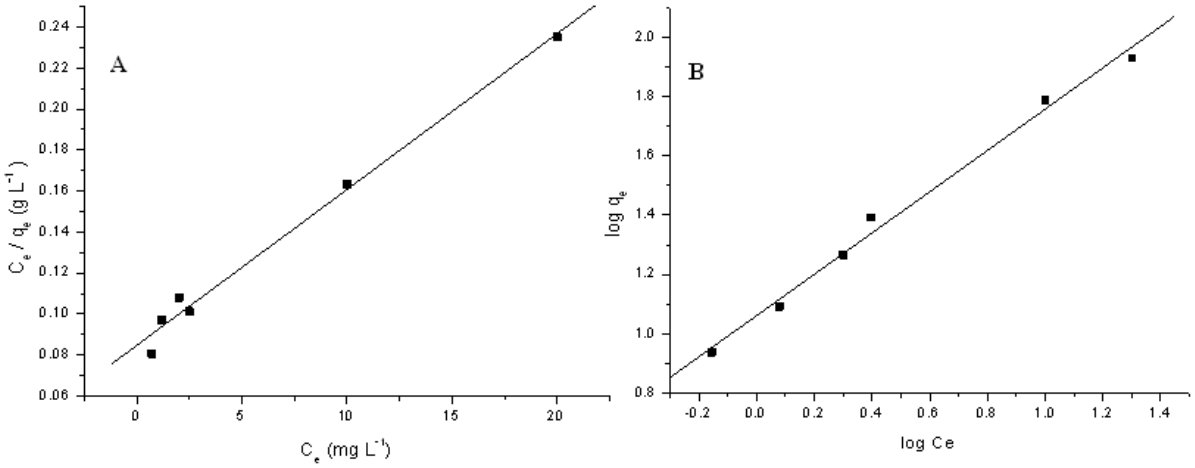

Figure 4.39 (A) Langmuir isotherm (B) Freundlich isotherm

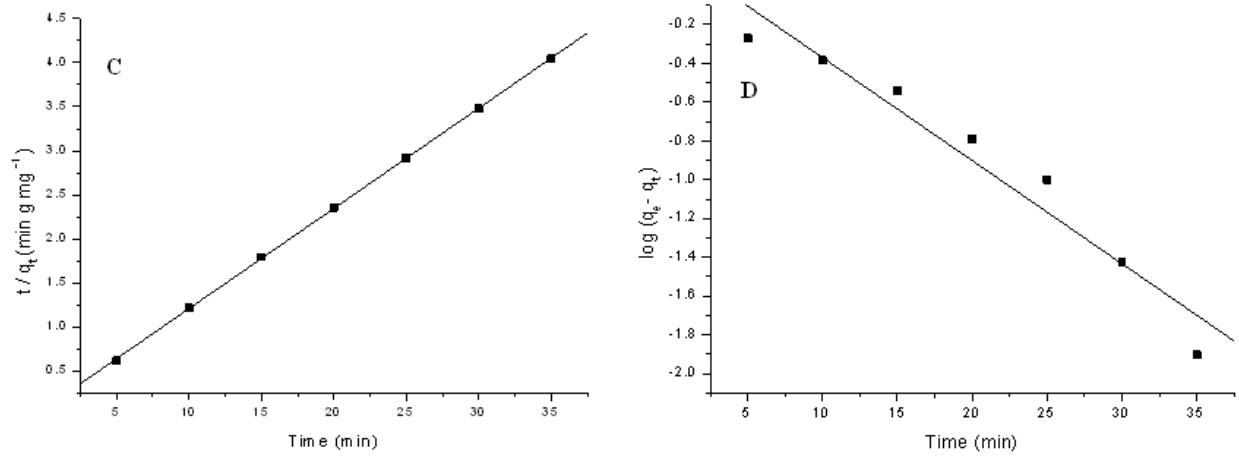

Figure 4.39 (C) Pseudo second order kinetics (D) Pseudo first order kinetic plot

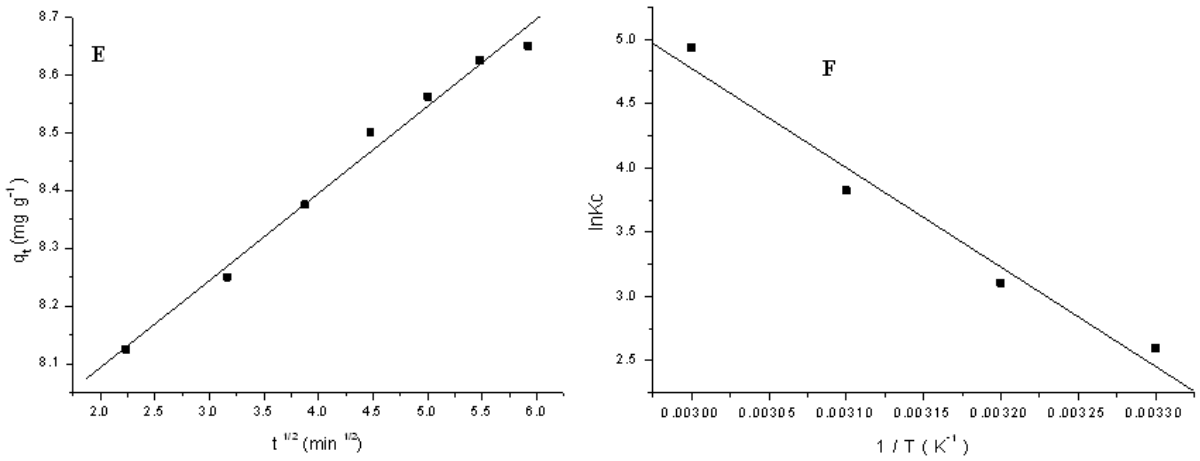

Figure 4.39 (E) Plot of qt vs square root of time (F) Van't Hoff plot

(ix) Scale up to a Larger Sample Volume

The above mentioned study of various optimized parameters has demonstrated the applicability of the material for detoxification of chromium from a larger sample volume. The polymeric composite was packed in a small glass column upto a height of 4 cm. A known volume of 150 mg L^{-1} Cr(VI) was transferred into the column at a flow rate of 4 mL min^{-1}. Cr(VI) was effectively retained on the column at pH 5.0 and this was confirmed by measuring the concentration of chromium spectrophotometrically in the solution phase. A maximium breakthrough volume of 500 mL could be achieved by this column study at 150 mg L^{-1} concentration of Cr(VI).

(x) Regeneration of the Composite Material

The regeneration of the composite material is an important fact that needs to be considered in the adsorption process. Since, Cr(VI) is toxic and carcinogenic, it is advisable to convert the chromium in +6 oxidation state to the less toxic +3 state. The adsorbed Cr(VI) could be effectively reduced with 0.1 mol L^{-1} sodium sulfite as well as 0.2 mol L^{-1} ascorbic acid respectively. These well-known reducing agents [42, 98,144] were found to be equally effective in the reduction of Cr(VI) with >99 % efficiency thereby regenerating the sorbent.

(xi) Application to a Real Industrial Effluent

The performance of the composite material was tested for chromium detoxification from a leather tannery effluent. The effluent sample which contains Cr(III) as its major constituent(in addition to the organic matter) was oxidized to the +6 oxidation state using hydrogen peroxide in alkaline medium.[42] The organic constituents were decomposed initially by boiling the sample with nitric acid-sulfuric acid mixture. A known volume of the effluent (300 mL) was passed through the glass column containing the composite material at pH 5.0. The composite material could retain chromium quantitatively and the regeneration of the column was also equally effective.

4.5.4 Conclusions

In conclusion, the chitosan-NaMMT clay composite prepared under microwave conditions has proved to very effective in the adsorption and removal of chromium from a large sample volume. The biopolymer composite exhibits an adsorption capacity of 133 mg g^{-1} and interestingly the crystallinity of the composite material was retained after adsorption of chromium. The mesoporous nature and the nano pore size prove to be a value addition for the retention of chromium. The study of the sorption thermodynamics indicates spontaneity and the endothermic nature of adsorption. The material could also be regenerated by using simple reducing agents, thereby making the process eco-friendly and benign.

Table 4.14. Kinetic parameters for the sorption of chromium (VI) on the composite material

q_e (mg g^{-1})	k_2 (g mg^{-1} min^{-1})	Regression coefficient	k_1 (min^{-1})	Regression coefficient	k_{int}
8.125	0.1968	0.99	0.1222	0.98	0.1509

Table 4.15. Thermodynamic data for the adsorption of chromium (VI) on the composite material

Temp (K)	Conc.(mg L^{-1})	Equilibrium constant (K)	Free energy change (ΔG^0 k Jmol^{-1})	Entropy change (ΔS^0J $mol^{-1}K^{-1}$)	Enthalpy change (ΔH^0 k J mol^{-1})
300	70	22.33	-7.74	276.09	76
310	70	45.66	-9.84		
320	70	139	-13.12		

References

1. Zhu, L.; Ren, X.; Yu, S. *Environ. Sci. Technol.* **1998,** *32*, 3374.
2. Krishna, B.S.; Murty, D. S. R.; Prakash, B. S. J. *J. Colloid Interf. Sci.* **2000,** *229*, 230.
3. Juang, R. S.; Wu, F. C.; Tseng, R.L. *Environ. Sci. Technol.* **1997,** *18*, 535.
4. Huh, J. I.; Song, D.I.; Jeon, Y.W. *Sep. Sci. Technol.* **2000,** *35*, 243.
5. Haggerty, G. M.; Bowman, R. S. *Environ. Sci. Technol.* **1994,** *28*, 452.
6. Zhang, Z. Z.; Sparks, D. L.; Scrivner, N. S. *Environ. Sci. Technol.* **1993**, *27*, 1625.
7. Lin, S. H.; Juang. R. S. *J. Hazards. Mater.* **2002,** *92*, 315.
8. Bhattacharyya, K. G.; Gupta, S. S. *Sep. Purif. Technol*. **2006**, *50*, 388.
9. Vengiris, T.; Binkiene, R.; Sveikauskaite, A. *Appl. Clay Sci*. **2001**, *18*, 183.
10. Zhang, Z. Z.; Sparks, D.L. *Soil Sci. Am. J.* **1996**, *60*, 1750.
11. Mellah, A.; Chegrouche, S. *Water Res*. **1997**, *31*, 621.
12. Malakul, P.; Srinivasan, K. R.; Wang, H.Y. *Ind. Eng. Chem. Res.* **1998,** *37*, 4296.
13. Lin, S. H.; Juang, R.S. *J. Hazard. Mater.* **2002**, *92*, 326.
14. Abollino, O.; Aceto, M.; Malandrino, M.; Sarzanini, C.; Mentasti, E. *Water Res.* **2003**, *37*, 1619.
15. Kaya, A.; Oren, A.H. *J. Hazard. Mater*. **2005**, *125*, 183.
16. Krikorian, N.; Martin, D. F. *J. Environ. Sci. Health. Part A* **2005**, *40*, 601.
17. Ozdemir, G.; Yapar, S. *J. Hazard. Mater.* **2009**, *166*, 1307.
18. Ozdemir, G.; Limoncu, M. H.; Yapar, S. *Appl. Clay Sci.* **2010,** *48*, 319.
19. Camel, V.; *Spectrochim. Acta. B* **2003**, *58*, 1177.
20. Bhattacharyya, K. G.; Gupta, S. S. *Ind. Eng. Chem. Res.* **2006**, 45, 7232.
21. Chumchal, M. M.; Rainwater, T. R.; Osborn, S. C.; Roberts, A. P.; Abel, M. T; Cobb, G. P.; Smith, P. N.; Bailey, F. C. *Environ. Toxicol. Chem.* **2011**, *30*, 1153.
22. Liu, Y.; Kelly, D. J.; Yang, H.; Lin, C. C. H.; Kuznicki, S. M.; Xu, Z. *Environ. Sci. Technol.* **2008**, *42*, 6205.
23. Vieira, R. S.; Beppu, M. M. *Water Res.* **2006**, *40*, 1726.
24. De Mendoncca Fabrega, F.; Mansur, M. B. *Hydrometallurgy* **2007**, *87*, 83.

25. Mahmoud, M. E. *Anal. Chim. Acta*.**1999**, *398*, 297.
26. Xiong, C.; Yao, C. *Chem. Eng. J*. **2009**, *155*, 844.
27. Mercier, L.; Detellier, C. *Environ. Sci. Technol.* **1995**, *29*, 1318.
28. Wang, L.; Xing, R.; Liu, S.; Cai, S.; Yu., H.; Feng., J.; Li, R.; Li, P.*Int. J. Biol. Macromol.* **2010**, *46*, 524.
29. Kushwaha, S.; Sreedhar, B.; Padmaja, P. *J. Chem. Eng. Data* **2010**, *55*, 4691.
30. Billinge, S. J. L.; Mckimmy, E. J.; Shatnawi, M.; Kim, H. J.; Petkov, V.; Wermeille, D.; Pinnavaia., T. J. *J. Am. Chem. Soc.* **2005**, *127*, 8492.
31. Bootharaju, M. S.; Pradeep, T. *J. Phys. Chem. C* **2010**, *114*, 8328.
32. Krishna, B. S.; Murthy, D. S. R.; Jai Prakash, B. S. *Appl. Clay Sci*. **2001**, *20*, 65.
33. Ahmad, M. B.; Hoidy, W. H.; Ibrahim, N. A. B.; Al-Mulla, E. A. J. *J. Eng. Appl. Sci.* **2009**, *4*, 184.
34. Dias Filho, N. L.; Do Carmo, D. R. *Talanta*. **2006**, *68*, 919.
35. Colilla, M.; Darder, M.; Aranda, P.; Ruiz-Hitzky, E. *Chem. Mater.* **2005**, *17*, 708.
36. Boufatit, M.; Ait-Amar, H. *Desalination.* **2007**, *206*, 300.
37. Mahadevaiah, N.; Venkataramani, B.; Jai Prakash. B. S. *Ind. Eng. Chem. Res.* **2008**, *47*, 1755.
38. Mendham, V. J.; Denny, R. C.; Barnes, J. D.; Thomas, M. J. K. *Pearson education, Singapore:* **2002**, *1*, 668.
39. Abou-El-Sherbini, K. S.; Hassanien, M. M. *J. Hazard. Mater.* **2010**, *184*, 654.
40. Li, H.; Li, Z.; Liu, T.; Xiao, X.; Peng, Z.; Deng, L. *Bioresour. Technol.* **2008**, *99*, 6271.
41. Cook, D. *Can. J. Chem.* **1965**, *43*, 3322.
42. Rajesh, N.; Krishna Kumar, A. S.; Kalidhasan, S.; Rajesh, V. *J. Chem. Eng. Data.* **2011**, *56*, 2295.
43. Rajesh, N.; Hari, M. S. *Spectrochim. Acta*. Part A **2008**, *70*, 1104.
44. Guo, Y.; Yan, N.; Yang, S.; Liu, P.; Wang, J.; Qu, Z.; Jia, J. *J. Hazard. Mater.* **2012**, 213-214, 62.
45. Khalil, H.; Mahajan, D.; Rafailovich, M. *Polym. Int.* **2005**, *54*, 423.
46. Mishra, M.; Bora, J. J.; Goswamee, R. L. *Appl. Clay Sci.* **2011**, *53*, 8.
47. Chang, P. H.; Li, Z.; Jiang, W. T.; Jean, J. S. *Appl. Clay Sci.* **2006**, *46*, 27.

48. Brigatti, M. F.; Colonna, S.; Malferrari, D.; Medici, L.; Poppi, L. *Appl. Clay Sci.* **2005**, *28*, 1.
49. Anirudhan, T. S.; Suchithra, P. S.; Divya, L. *Water, Air, Soil Pollut.* **2009**, *196*, 127.
50. De Canck, E.; Lapeire, L.; De Clercq, J.; Verpoort, F.; Van der Voort, P. *Langmuir*. **2010**, *26*, 10076.
51. Puanngam, M.; Unob, F. *J. Hazard. Mater.* **2008**, *154*, 578.
52. Behrens, S. H.; Grier, D. G. *J. Chem. Phys.* **2001**, *115*, 6716.
53. Gounder, R.; Iglesia, E. *Acc. Chem. Res.* **2012**, *45*, 229.
54. Yu, Y.; Addai-Mensah, J.; Losic, D. *Sci. Technol. Adv. Mater.* **2012**, *13*, 1.
55. Boszke, L.; Glosinska, G.; Siepak, J. *Pol. J. Environ. Stud.* **2002**, *11*, 285−298.
56. Cichy, W.; Schlosser, S.; Szymanowski, J. *J. Chem. Technol. Biotechnol.* **2005**, *80*, 189.
57. Cakara, D.; Kleimann, J.; Borkovec, M. *Macromolecules.* **2003**, *36*, 4201.
58. Langmuir, I. *J. Am. Chem. Soc.* **1918,** 40, 1361.
59. Hall, K. R.; Eagleton, L. C.; Acrivos, A.; Ver Meulen, T. *Ind. Eng. Chem. Fundam.* **1966,** *5*, 212.
60. Freundlich, H. M. F. *Z. Phys. Chem.* **1906,** *57*, 385.
61. Dubinin, M. M.; Radushkevich, L.V. *Proc. Acad. Sci. USSR Phys. Chem. Sect.* **1947,** *55* 331.
62. Giles, C. H.; Mckay, R. B. J. Bacteriol. 1965, 89, 390−397.
63. Lagergren, S. *K. Sven. Vetenskapsakad. Handl.* **1898,** *24*, 1.
64. Ho, Y. S. *J. Hazard. Mater.* **2006,** *136*, 681.
65. Weber, W. J.; Morris, J. C. *J. Sanit. Eng. Div., Am. Soc. Civ. Eng.* **1963,** *89*, 31.
66. Sengil, I. A.; Ozacar, M.; Turkmenler, H. *J. Hazard. Mater.* **2009,** *162*, 1046.
67. Donia, A. M.; Atia, A. A.; El-Boraey, H. A.; Mabrouk, D. *Sep. Purif.Technol.* **2006,** *49*, 64–70.
68. Zhang, Y.; Cremer, P. S. *Curr. Opin. Chem. Biol.* **2006,** *10*, 658.
69. Zhao, H. *J. Chem. Technol. Biotechnol.* **2006,** *81*, 877.
70. Abd El-Latif, M. M.; Ibrahim, A. M.; El-Kady, M. F. *J. Am. Sci.* **2010,** *6*, 267.

71. Onyango, M. S.; Leswifi, T. Y.; Ochieng, A.; Kuchar, D.; Otieno, F. O.; Matsuda, H. *Ind. Eng. Chem. Res.* **2009,** *48,* 931.
72. Arencibia, A.; Aguado, J.; Arsuaga, J. M. *Appl. Surf. Sci.* **2010,** *256,* 5453.
73. Atkins, P.; Paula, J. D. Elements of Physical Chemistry; Oxford University Press: New York, 2005
74. Shade, C. W. *Environ. Sci. Technol.* **2008,** *42,* 6604.
75. Bibby, A.; Mercier, L. *Chem. Mater.* **2002,** *14,* 1591.
76. Sushil, S.; Batra, V. S. *Fuel* **2006,** *85,* 2676.
77. Lo, I. M. C.; Yang, X. *J. Environ. Eng.* **2001**, *127,* 154.
78. Zhu, R.; Zhu, L. *J. Colloid Surface Sci.* **2008**, *322,* 27.
79. He, H.; Frost, R. L.; Bostrom, T.; Yuan, P.; Duong, L.; Yang, D.; Xi, Y.; Kloprogge, J. T. *Appl. Clay Sci.* **2006**, *31,* 262.
80. Yildız, N.; Gonulsen, R.; Koyuncu, H.; Calımlı, A. *Colloids Surf. A* **2005**, *260,* 87.
81. Karamanis, D.; Assimakopoulos, P. A. *Water Res.* **2007**, *41,* 1897.
82. Saha, U. K.; Taniguchi, S.; Sakurai, K.; *Soil Sci. Soc. Am. J.* **2001**, *65,* 694.
83. Lagadic, I. L.; Mitchell, M.K.; Payne, B.D. *Environ. Sci. Technol.* **2001,** *35,* 984.
84. Say, R.; Birlik, E.; Denizli, A.; Ersoz, A. *Appl. Clay Sci.* **2006**, *31*, 298.
85. Celis, R.; Hermosin, M.C.; Cornejo, J. *Environ. Sci. Technol.* **2000**, *34*, 4593.
86. Sheng, G.; Xu, S.H.; Boyd, S. A. *Soil Sci. Soc. Am. J.* **1999**, *63,* 73.
87. Tonle, I.K.; Ngameni, E.; Njopwouo, D.; Carteretc, C.; Walcarius, A. *Phys. Chem.* **2003**, *5*, 4951.
88. Albadarin, A.B.; Mangwandi, C.; Al-Muhtaseb, A.H.; Walker, G.M.; Allen, S. J.; Ahmad, M. N. M. *Chem. Eng. J.* **2012**, *179*, 193.
89. Kobya, M. *Adsorpt. Sci. Technol.* **2004**, *22*, 51.
90. Dupont, L.; Guillon, E. *Environ. Sci. Technol.* **2003**, *37*, 4235.
91. Zeng, Y.; Woo, H.; Lee, G.; Park, J. **2010**, *130*, 83.
92. Venugopal, V.; Mohanty, K. *Chem. Eng. J.* **2011**, *174*, 151.
93. Zhou, C. H. *Appl. Clay Sci.* **2010**, *48*, 1.
94. Jiang, J.Q.; Ashekuzzaman, S.M. *Curr. Opin. Chem. Eng.* **2012**, *1*, 1.

95. Akcay, G.; Yurdakoc, M. K. *Turkey J. Chem.***1999**, *23*, 105.
96. Brum, M.C.; Capitaneo, J. L.; Oliveira, J.F. *Miner. Eng.* **2010**, *23*, 270.
97. Li, W; Tang, Y.; Zeng, Y.; Tong, Z.; Liang, D.; Cui, W. *Chem. Eng. J.* **2012**, *193–194*, 88.
98. Santhana Krishna Kumar, A.; Kalidhasan, S.; Rajesh, V.; Rajesh, N. *Ind. Eng. Chem.Res.* **2012**, *51*, 58.
99. Pandey, S.; Mishra, S.B. *J. Colloid Interface Sci.* **2011**, *361*, 509.
100. Santhana Krishna Kumar, A.; Kalidhasan, S.; Rajesh, V.; Rajesh, N. *Adv. Mater. Lett.* **2011**, *2*, 383.
101. Płaska, A.G.; Majdan, M.; Pikus, S.; Sternik, D. *Chem. Eng. J.* **2012**, *179*, 140.
102. Chakraborty, S.; Sengupta, R.; Dasgupta, S.; Mukhopadhyay, R.; Bandyopadhyay, S.;Joshi, M.; Ameta, S.C. *J. Appl. Polym. Sci.* **2009**, *113*, 1316.
103. Zhang, L.; Xu, J.; Hou, G.; Tang, H.; Deng, F. *J. Colloid Interface Sci.* **2007**, *311*, 38.
104. Balomenou, G.; Stathi, P.; Enotiadis, A.; Gournis, D.; Deligiannakis,Y. *J. Colloid Interface Sci.* **2008,** *325,* 74.
105. G. Z. Kyzas, M. Kostoglou, N. K. Lazaridis, *Chem. Eng. J.* **2009,** 152, 440.
106. Mani, G.; Fan, Q.; Ugbolue, S.C.; Yang, Y. *J. Appl. Polym. Sci.* **2005**, *97*, 218.
107. Lin, C. K.; Chen, J.N.; Lin, C.C. *J. Hazard. Mater.* **1997**, *56*, 21.
108. Gonzalez, T.V.; Salazar, C.G.; de la Rosa, J.R.; Gonzalez, V.G. *J. Appl. Polym. Sci.* **2008**, *108* 2923.
109. Oztop, B.; Shahwan, T. *J. Colloid Interface Sci.* **2006**, *295*, 303.
110. Anandkumar, J.; Mandal, B. *J. Hazard. Mater.* **2009**, *168*, 633.
111. M. V. Lopez-Ramon, F. Stoeckli, C. Moreno-Castilla, F. Carrasco-Marin, *Carbon*, **1999,** *37*, 1215.
112. Stathi, P.; Papadas, I.T.; Tselepidou, A.; Deligiannakis, Y. *Global NEST J.* **2010**, *12*, 248.
113. Das, S. K.; Das, A.K.; Guha, A.K. *Environ. Sci. Technol.* **2007**, *41*, 8281.
114. Sharma, Y.C.; Singh, B.; Agrawal, A.; Weng, C.H. *J. Hazard. Mater.* **2008**, *151*, 789.

115. A. Santhana Krishna Kumar, S. Kalidhasan, V. Rajesh N. Rajesh, *Ind. Eng. Chem. Res.* 2012, 51, 11312.
116. S. Krishna Kumar, S. Kalidhasan, Vidya Rajesh, N. Rajesh, *J. Environ. Sci. Health: Part A.* **2011,** 46, 1598.
117. Bayens, B.; Bradbury, M.H. *J. Contam. Hydrol.* **1997**, *27*, 199.
118. Sposito, G. The Chemistry of Soils, Oxford Univ. Press, New York, **1989.**
119. Anirudhan, T. S.; Ramachandran, M. *Ind. Eng. Chem. Res.* **2008**, *47*, 6175.
120. Garg, U. K.; Kaur, M. P.; Garg, V. K.; Sud, D. *J. Hazard. Mater.* **2007**, *140*, 60.
121. Crini, G. *Prog. Polym. Sci.* **2005**, *30*, 38.
122. Park, D.; Lim, S. R.; Yun, Y. S.; Park, J. M. *Bioresour. Technol.* **2008**, *99*, 8810.
123. Unnithan, M. R.; Vinod, V. P.; Anirudhan, T. S. *Ind. Eng. Chem. Res.* **2004**, *43*, 2247.
124. Chauhan, D.; Sankararamakrishnan, N. *J. Hazard. Mater.* **2011**, *185*, 55.
125. Boddu, V. M.; Abburi, K.; Talbott, J. L.; Smith, E. D. *Environ. Sci. Technol.* **2003**, *37*, 4449.
126. Zeng, Q. H.; Yu, A. B.; Lu, G. Q.; Paul, D. R. *J. Nanosci. Nanotechnol.* **2005**, *5*, 1574.
127. Krishna, B. S.; Murthy, D. S. R.; Jai Prakash, B. S. *J. Colliod Interface Sci.* **2000**, *229*, 230.
128. Romero, R. B.; Leite, C. A. P.; Goncalves, M. D. C. *Polymer* **2009**, *50*, 161.
129. Clesceri, L. S.; Greenberg, E. Standard Methods for the Examination of Water and Wastewater; American Public Health Association: Washington, DC, **1998.**
130. Liu, C. F.; Sun, R. C.; Zhang, A. P.; Hua., M.; Ren., J. L.; Wang., X. A. *J. Agric. Food Chem.* **2007**, *55*, 2399.
131. Katti, K. S.; Sikdar, D.; Katti, D. R.; Ghosh, P.; Verma, D. *Polymer* **2006**, *47*, 403.
132. Liang, Z. M.; Yin, J.; Xu, H. J. *Polymer*. **2003**, *44*, 1391.
133. Suksabye, P.; Thiravetyan, P.; Nakbanpote, W.; Chayabutra, S. *J. Hazard. Mater.* **2007**, *141*, 637.

134. Singh, V.; Sharma, A. K.; Kumari, P.; Tiwari, S. *Ind. Eng. Chem. Res.* **2008**, *47*, 5267.
135. Kalidhasan, S.; Santhana Krishna Kumar, A.; Vidya, R.; Rajesh, N. *J. Colloid Interface Sci.* **2012**, 367, 398.
136. Hu, Q. H.; Qiao, S. Z.; Haghseresht, F.; Wilson, F. M. A.; Lu, G. Q. *Ind. Eng. Chem. Res.* **2006**, *45*, 733.
137. Ghosh, A. K.; Woo, E. M. *J. Mater. Chem.* **2004**, *14*, 3034.
138. O. E. Omotoso, D.G. Ivey, R. Mikula, *J. Hazard.Mater.* **1998,** *60*, 1.
139. Cai, G. B.; Zhao, G. Z.; Wang, X. K.; Yu, S. H. *J. Phys. Chem.* C **2010**, *114*, 12948.
140. Luo, P.; Zhang, J. S.; Zhang, B.; Wang, J. H.; Zhao, Y. F.; Liu, J. D. *Ind. Eng. Chem. Res.* **2011**, *50*, 10246.
141. Pearson, R. G. *J. Am. Chem.* Soc.**1963,** *85*, 3533.
142. Ho.Y. S. *Carbon* **2004,** *42*, 2113.
143. Shen, X. E.; Shan, X. Q.; Dong, D. M.; Hua, X. Y.; Owens, G. *J. Colloid Interface Sci.* **2009,** *330*, 1.
144. Stearns, D. M.; Wetterhahn, K. E. *Chem. Res. Toxicol.* **1994**, *7*, 219.
145. Anderson, R. Sample Pre-treatment and Separation-Analytical Chemistry by Open Learning; John Wiley & Sons: Singapore,**1987.**
146. Darder, M.; Ruiz-Hitzky, E. *J. Mater. Chem.* **2005,** *15*, 3913.
147. Park, J.W.; Park, M.-O.; Park, K. K. *Bull. Korean Chem. Soc.***1984,** *5*, 108.
148. Guibal, E.; Milot, C.; Eterradossi, O.; Gauffier, C.; Domard, A. *Int.J. Biol. Macromol.* **1999**, *24*, 49.
149. Tianwei, T.; Xiaojing, H.; Weixia, D. *J. Chem. Technol. Biotechnol.* **2001**, *76*, 191.
150. Wan Ngah, W. S.; Teong, L.C.; Hanafiah, M.A.K.M. *Carbohydr. Polym.* **2011,** *83,*1446.
151. Singh, V.; Singh, S. K.; Pandey, S.; Sanghi, R. *Adv. Mat. Lett.* **2010,** *1*, 40.
152. Crini, G. *Prog. Polym. Sci.* **2005,** *30*, 38.
153. Zhou, Y.; Jin, Q.; Zhu, T.; Akama, Y. *J. Hazard. Mater.* **2011,** *187,* 303.

154. Zeng, Q. H.; Yu, A. B.; Lu, G. Q.; Paul. D. R. *J. Nanosci. Nanotechnol*. **2005**, *5*, 1574.

155. Wenhua, L.; Guangjie, Z. *Forestry Studies in China*. **2004,** *6*, 54.

156. Monvisade, P.; Siriphannon, P. *Appl Clay Sci.* **2009,** *42*, 427.

Customized Biopolymer Sorbents and Graphene Oxide for the Adsorption of Chromium and Mercury

5.1 Introduction

The final chapter of the thesis deals with a novel and environmentally benign approach for the removal of chromium based on the impregnation of ionic liquid onto a biopolymer and exfoliated graphene oxide for the detoxification of chromium. Biopolymers as well as ionic liquids are known for their potential applications. In this chapter, we report the utility of chitosan as an excellent platform for impregnating the ionic liquid, tetraoctylammonium bromide by ultrasonication and its subsequent adsorption for chromium(VI). The effective mass transfer due to sonication coupled with the hydrogen bonding interaction between chitosan-ionic liquid and the electrostatic interaction involving the amino groups in chitosan and hexavalent chromium governs this three centre (3c) co-operative mechanism. The second method in this chapter deals with an interesting interaction between exfoliated graphene oxide (EGO), ionic liquid (IL) Aliquat -336 and hexavalent chromium. Graphene oxide was impregnated with the ionic liquid and the interaction primarily involves electrostatic affinity between the quaternary ammonium cation and surface hydroxyl groups in EGO. The IL-EGO combination functions as an effective adsorbent for hexavalent chromium. The IL-EGO adsorbent acts as a good host in welcoming the incoming guest, hydrochromate anion and several interesting interactions such as cation-π, electrostatic as well as anion-π could be conceptualized in this process. The final method in this chapter presents an interesting method for the adsorption of mercury involving its interaction with cellulose and mercaptobenzathiazole (MBT). We envisage a triangular interaction with cellulose acting as a host and MBT as guest in the first instance followed by the subsequent complexation of mercury with MBT. Thanks to the soft-soft interaction between Hg^{2+} and sulfur, that augments the effective complexation with MBT. Complexation, electrostatic and hydrogen bonding are the probable mechanistic interactions.The feasibility of the method

has been successfully demonstrated in the detoxification of chromium and mercury from industrial wastewater samples.

The first part of this chapter deals with the effective adsorption of hexavalent chromium through a three centre (3c) co-operative interaction with an ionic liquid and biopolymer

The second part of this chapter explores the interesting interaction between graphene oxide, Aliquat-336(a room temperature ionic liquid) and chromium(VI) for wastewater treatment

The third part of this chapter deals with the study of adsorption of Hg^{2+} through its appealing interaction with biopolymer cellulose and mercaptobenzathiazole.

Adsorption of Cr(VI) through a three centre co-operative interaction with an ionic liquid and chitosan

5.2.1 Introduction

This chapter deals with the application of chitosan as an excellent platform for impregnating the ionic liquid, tetraoctylammonium bromide by ultrasonication and its subsequent adsorption for chromium(VI). The effective mass transfer due to sonication coupled with the hydrogen bonding interaction between chitosan-ionic liquid and the electrostatic interaction involving the amino groups in chitosan and hexavalent chromium governs this three centre (3c) co-operative mechanism. The biodegradability and excellent stability coupled with the active binding sites makes them well suited for adsorption of heavy metals. Prominent among the biopolymers is chitosan, an N-deacetylated derivative of chitin, which is one of the most abundant biopolymer materials that finds heavy metal remediation.[1] The utility of chitosan derivatives for detoxification of wastewater has been reported.[2] Ngah et al [3,4] have studied the application of chitosan for the removal of copper and gold using cross linked chitosan beads. Cervera et al[5] have reported the adsorption of cadmium and chromium at 50 ppm level using alumina and chitosan. Chitosan/PVA hydrogel beads are known for their potential towards heavy metal adsorption.[6] Guibal[7] has reviewed the metal ion interactions with chitosan and the involvement of the hydroxyl groups and the protonated amino groups in strengthening the affinity towards the metal. Hu et al [8] have studied the kinetics and thermodynamics of chromium(VI) adsorption using ethylenediamine modified cross linked magnetic chitosan resin. More recently, chitosan-Fe nanoparticles[9] has shown good potential in the adsorption of chromium. Ngah et al[10] have also reviewed the adsorption of dyes and heavy metal interaction with chitosan composites. Literature survey revealed that the interaction of an ionic liquid, tetraoctylammonium bromide with biopolymers such as chitosan have not been explored for heavy metal adsorption. An excellent three centre co-operative interaction between this ionic liquid, chitosan and chromium(VI) followed by the study of various factors that affect the adsorption of chromium is discussed in the following sections.

5.2.2 Experimental Section

(i) Adsorbent Preparation

A known weight (3 g) of tetraoctylammonium bromide was dissolved in 15 mL methanol. 6 g of chitosan was taken in a round bottom flask and the dissolved ionic liquid was added dropwise and sonicated (Ultrasonic bath, Biotechnics, India) for 2 hours with a 15 min intermittent time interval. The resulting solution was filtered, washed with methanol and the filtrate was subjected to silver nitrate test to check the presence of bromide and the resulting ionic liquid impregnated chitosan was dried at room temperature and used for further adsorption studies. The ultrasonication ensures effective impregnation of ionic liquid and this was ascertained through a comprehensive physico-chemical characterisation of the adsorbent material.

(ii) Adsorption Procedure

A 25 mL volume of 20 mg L^{-1} chromium(VI) was equilibrated at pH 3.5 with 0.2 g of the ionic liquid impregnated biopolymeric adsorbent material in an orbital incubator shaker (Biotechnics, India) at room temperature for varying time period and the concentration of chromium in the solution phase was determined by the standard spectrophotometric method using diphenylcarbazide as the chelating reagent for chromium.[11] The quantitative adsorption of chromium (99.0 ± 0.3 %) was attained in 30 min, beyond which there was no perceptible increase thereby signifying the saturation of the active adsorption sites in the polymeric adsorbent.

5.2.3 Results and Discussion

(i) FT-IR Spectral Characterization

The FT-IR spectral analysis (Figure 5.1) showed distinct characteristic bands corresponding to O-H and N-H stretching vibrations at 3450 cm^{-1} and 3358 cm^{-1} respectively. The C–H and the C-O stretching were obtained at 2877 cm^{-1} and 1071 cm^{-1}respectively. The hydroxyl peak broadened with a corresponding shift to 3570 cm^{-1}. The N–H bending vibration at 1583 cm^{-1} is shifted to 1561 cm^{-1} after the impregnation with the ionic liquid. Similarly, the C-N bending vibration observed at 1375 cm^{-1} resulted in a shift to 1312 cm^{-1}.[12,13] These changes could be attributed to the effective interaction of the tetraoctylammonium cation with the hydroxyl group of chitosan in the

form of an intermolecular hydrogen bonding interaction. Indeed, the interaction of ammonium cation through hydrogen bonding interaction is an interesting phenomenon observed in host-guest interaction.[14,15] The essential point to realize is that the presence of amino groups in the biopolymer also plays a significant role in this interaction. Initially, the quaternary ammonium cation coordinates with the chitosan primary OH group through intermolecular hydrogen bonding. A considerable change is observed in the spectral features after the adsorption of chromium(VI). The change is quite prominent in the N-H region of the IR spectrum. Hexavalent chromium exists mainly as hydrogen chromate ($HCrO_4^-$) and dichromate ($Cr_2O_7^{2-}$) anionic species in acidic medium.[16] At the optimum pH (3-4) we observed characteristic new peaks in the IR spectrum which is attributed to Cr=O at 898 cm^{-1} and Cr-O at 777 cm^{-1} [17,18] respectively. All these changes are indicative of the fact the hydrochromate anion interacts electrostatically with the positively charged amino group (NH_3^+) of the biopolymer.

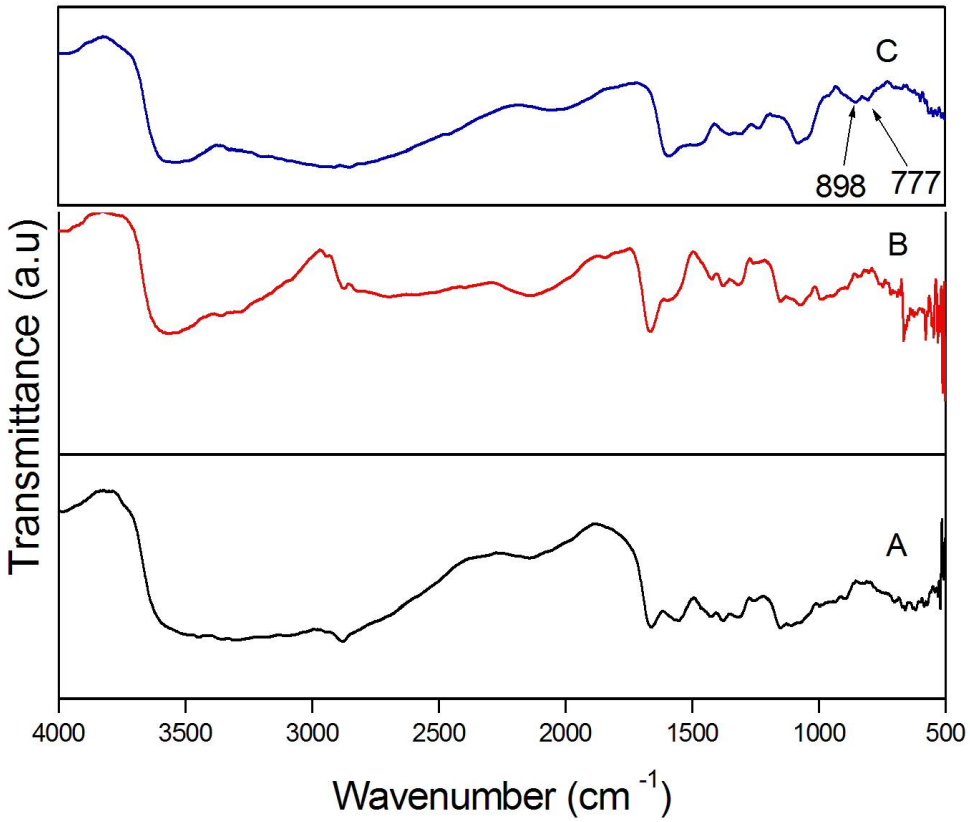

Figure 5.1. FT-IR Spectrum of (A) chitosan (B) Ionic liquid impregnated chitosan (C) after adsorption of chromium(VI)

(ii) Morphology of the Adsorbent using SEM and Optical Microscopy

The adsorbent material is porous with a dense and homogenous surface for the effective interaction of ionic liquid with chitosan. The effective hydrogen bonding interaction and the corresponding morphological changes in the adsorbent layer as evident from the shiny and bright spots in the SEM micrographs highlight the electrostatic affinity between the ionic liquid impregnated chitosan and the hexavalent chromium (Figure 5.2). To substantiate this further, optical microscopy images were also obtained for the ionic liquid impregnated chitosan adsorbent before and after the adsorption of chromium. The adsorbent was spread on a glass slide and the images were recorded at 4x magnification. The optical images indicate the voids where there is a potential possibility of interaction

of tetraoctylammonium cation with chromium. This was confirmed by taking the image after the adsorption of chromium by adding diphenylcarbazide as the color reagent to qualitatively identify the presence of chromium. The adsorbent morphology changed to a distinct red-violet color (Figure 5.3) and this testifies the fact that chromium is indeed adsorbed on the adsorbent surface by interacting with the protonated amine groups in the biopolymer matrix.

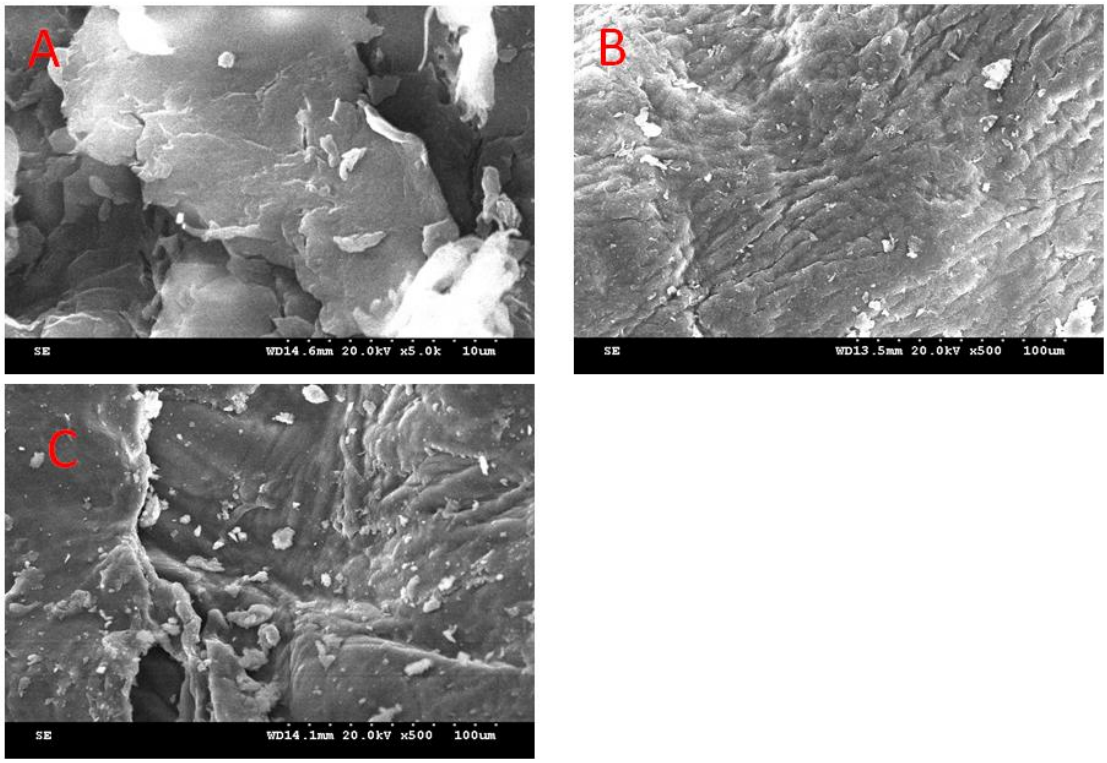

Figure 5.2. SEM images (A) chitosan (B) Ionic liquid impregnated chitosan (C) after adsorption of chromium(VI)

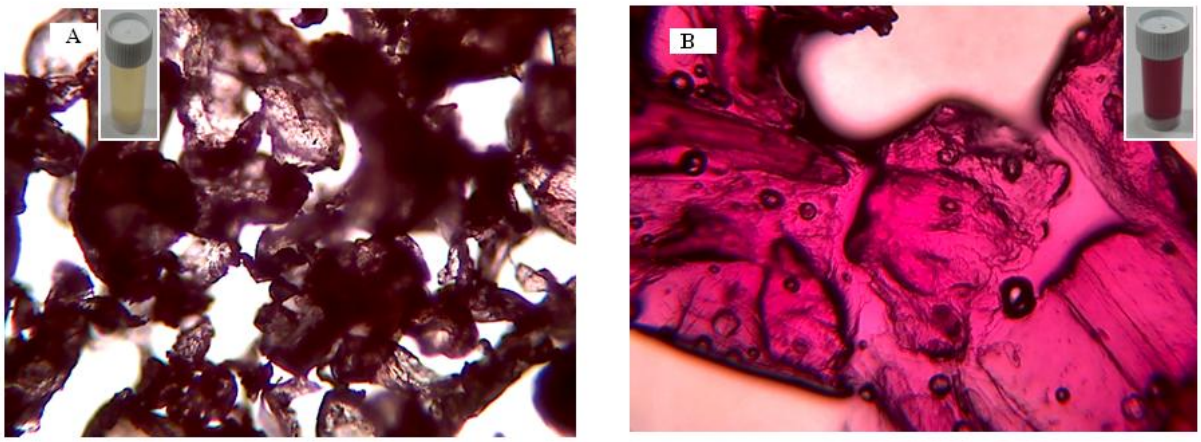

Figure 5.3. Optical images (A) Ionic liquid impregnated chitosan (B) after adsorption of chromium(VI) (inset: color developed as Cr(VI)-diphenylcarbazide complex)

(iii) XRD Studies

The X-ray diffraction spectra (Figure 5.4) of the chitosan indicate an amorphous nature in the 2θ range 20 to 25^0 attributed to the intramolecular hydrogen bonding interaction in the chitosan backbone. The characteristic peaks due to chitosan are observed at 2θ = 20.16^0.[19]After treatment with tetraoctylammonium bromide, there is a slight shift in the above value with decrease in the intensity. The intramolecular hydrogen bonding in the biopolymer and the intermolecular hydrogen bonding interaction of tetraoctylammonium cation with the chitosan backbone could be the reason for the decrease in crystallinity of this adsorbent material.[20] The interaction of hydrogen chromate with the protonated amine groups in chitosan results in the emergence of a new peak at 2θ=22^0 with retention in the amorphous nature of the adsorbent. [21,22]

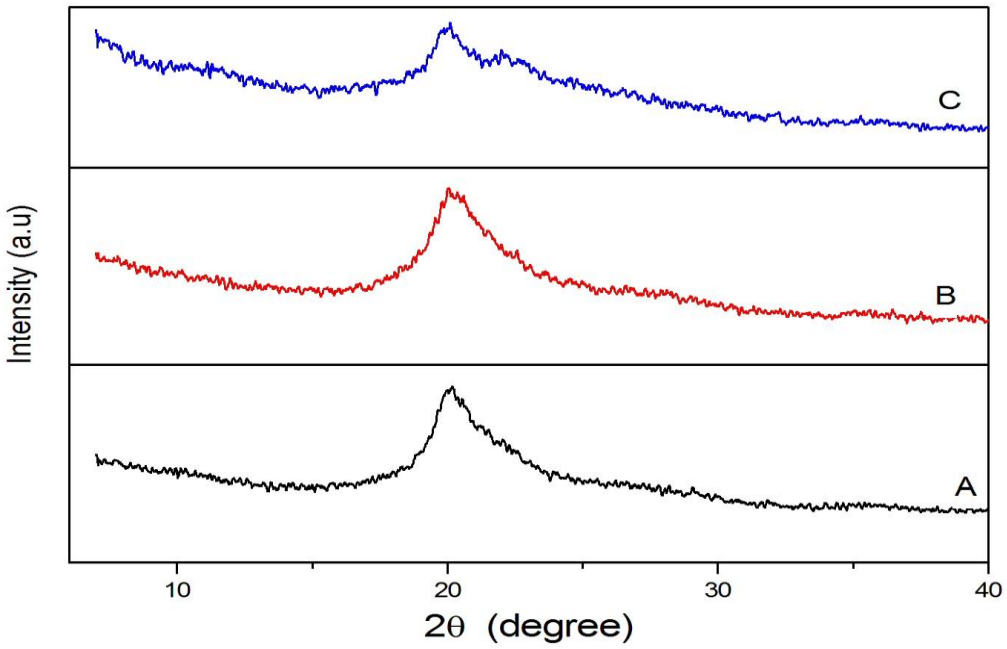

Figure 5.4. XRD pattern (A) chitosan (B) Ionic liquid impregnated chitosan (C) after adsorption of chromium(VI)

(iv) Effect of pH

Ultrasonication results in an effective transfer of the tetraoctylammonium bromide onto the chitosan biopolymer matrix. The formation and collapse of bubbles resulting in implosions [23] creates shock waves that help in the impregnation of the ionic liquid (guest) in the host (chitosan) matrix. In aqueous medium, depending on the pH, there exists a well-known equilibrium between the various oxyanions of chromium[24] as given below.

$$H_2CrO_4 \rightleftharpoons H^+ + HCrO_4^- \qquad \log K = -0.8 \qquad (1)$$

$$HCrO_4^- \rightleftharpoons H^+ + CrO_4^{2-} \qquad \log K = -6.5 \qquad (2)$$

$$2HCrO_4^- \rightleftharpoons Cr_2O_7^{2-} + H_2O \qquad \log K = 1.52 \qquad (3)$$

The optimum pH for the quantitative adsorption of chromium was observed in the range 3-4. In this pH range, the active binding sites in the ionic liquid and chitosan ensure a triangular interaction with the hexavalent hydrogen chromate oxy anion. Beyond pH 4.0, there is a decline in the percentage adsorption of chromium and this could be attributed to the deprotonation of the surface amino group and consequent competition of the

hydroxide ion for the active adsorption sites.[25] The interaction of chromium as hydrochromate anion in weakly acidic medium could also be inferred from the FT-IR spectral analysis as mentioned before. The tetraoctylammonium cation interacts with chitosan through hydrogen bonding followed by the electrostatic interaction of the hydrochromate anion with the protonated amine groups in chitosan. The schematic illustration depicting this interaction is given in Figure 5.5. This type of a co-operative host-guest interaction favors a kind of conformational adjustment and promotes the binding through a facile interaction between the three species.

5.2.4 Study of Various Isotherm Models

(i) Langmuir Isotherm

A widely used monolayer adsorption model which relates the maximum adsorption capacity (q_o) and the adsorption energy b in the linearized Langmuir expression.[26] The maximum adsorption capacity, q_o and the constant b obtained from the slope and intercept of the plot of C_e/q_e against C_e (Figure 5.6A) were found to be 63.69 mg g^{-1} and 0.0158 L mg^{-1} (Table 5.1) respectively with a regression coefficient of 0.95. An R_L value in the range 0 to 1 is an index to efficient adsorption.[27] The value of R_L for the adsorption of chromium (C_o=20 mg L^{-1}) on the ionic liquid impregnated polymeric sorbent material was found to be 0.7598 and this indicates the efficacy of the triangular interaction between the ionic liquid, chitosan and chromium(VI) under the optimized experimental conditions.

(ii) Freundlich isotherm

The Freundlich isotherm[28] is yet another useful model to study the adsorption from dilute solutions. A favorable adsorption tends to have Freundlich constant n between 1 and 10. A higher value of n (smaller value of 1/n) implies stronger interaction between the tetraoctylammonium cation, chitosan and hexavalent chromium. The logarithmic plot of q_e against C_e (Figure 5.6B) gives the constants K_F and n as 2.8727 $mg^{1-1/n}$ g^{-1} L^{-1} and 1.9685 respectively (Table. 5.1) with a regression coefficient of 0.94.

(iii) Redlich–Peterson (R-P) Isotherm

The Redlich–Peterson model relates the amount of chromium(VI) adsorbed at equilibrium q_e and the respective isotherm constants A, B and an exponent g given by the equation.[29] described in chapter 2. In an efficient adsorption process the value of g lies between 0-1. Furthermore, when the exponent g equals unity, the above expression reduces to the simple Langmuir isotherm equation. The parameters g and B are obtained from the slope and intercept of the plot (Figure 5.6C) respectively (Table 5.1). The value of g was found to be 0.744 and this shows that the adsorption data could fit well with the Langmuir isotherm model.

(iv) ***Dubinin–Radushkevich (D-R) Isotherm***

The adsorption mechanism and the interaction between hydrochomate anion and the ionic liquid impregnated biopolymer can be modeled through D-R isotherm.[30] This isotherm relates q_e, q_m (maximium adsorption capacity), adsorption energy (β) and Polanyi potential (Ɛ). From the slope and intercept of the plot of $\ln q_e$ versus ε^2 (Figure 5.6D) the parameters β and q_m (Table 5.1) can be obtained. In addition, the adsorption energy is related to the mean free energy E_{DR} of adsorption and in the present system, a mean free energy of adsorption of 0.2552 kJ mol^{-1} was obtained and this could be ascribed to the physical adsorption.

(v) Elovich and Temkin isotherm

The Elovich isotherm model[31] assumes that the adsorption sites increase exponentially with adsorption, resulting in multilayer adsorption. The slope and the intercept of the plot of ln (q_e/C_e) against q_e (Figure 5.6E) give the required isotherm parameters (Table 5.1). Temkin isotherm[32] parameters can be obtained from the linear plot of q_e versus $\ln C_e$ (Figure 5.6F, Table 5.1).

(vi) Uptake Kinetics

The uptake of metal ion by the adsorbent depends on the contact time and in this context, the study of the kinetics of adsorption is of considerable significance. The pseudo first order and second order kinetic models [33,34] were utilized to correlate the experimental data. Essentially, the models relate the amount of the metal ion adsorbed at equilibrium at various time intervals to the kinetic rate constants k_1 and k_2. The kinetic parameters

(Table. 5.2) are obtained from the respective plots (Figure 5.6 G,H). The higher regression coefficient obtained with the second order kinetics indicates that the experimental data shows a good fit to this model. The experimental and calculated equilibrium adsorption capacity (q_e) values were found to be 2.42 mg g^{-1} and 2.47 mg g^{-1} in accordance with the second order kinetics.

(vii) Intraparticle Diffusion

Diffusion processes such as film or external diffusion, pore and surface diffusion could also influence the transport of the hydrochromate anion from the bulk to the adsorbent surface. Intraparticle diffusion of the metal ion from the bulk into the pores of the adsorbent material is another process that could influence the uptake kinetics. The Weber Morris[35] intraparticle diffusion model is used to study this phenonema and this model gives the intraparticle diffusion rate constant k_{int} (Table 5.2) and also relates the boundary layer thickness (C). The fact that the Weber-Morris plot (Figure 5.6I) has an intercept value is attributed to the fact that boundary layer effect[36] also could influence the uptake kinetics of the hydrochromate anion from the bulk to the ionic liquid impregnated polymeric matrix.

(viii) Thermodynamics of Adsorption

The temperature effect on the adsorption of hexavalent chromium was studied in order to obtain the relevant thermodynamic parameters. The free energy of adsorption (ΔG^0) and the entropy and enthalpy changes ΔH^0 and ΔS^0 in the adsorption process are related by the Van't Hoff equations.[37] The equilibrium constant K is evaluated from the ratio of concentration of hydrochromate anion adsorbed on the ionic liquid impregnated chitosan adsorbent to that in the solution phase. The enthalpy and entropy changes are obtained from the slope and intercept of the plot of lnK against 1/ T (Figure 5.6J). The negative free energy change and the exothermic nature of the adsorption process (Table 5.3) indicate a spontaneous adsorption process. The ionic liquid impregnated chitosan would be conformationally oriented in such a manner so as to facilitate the effective interaction with the guest, hydrochromate anion. The ordered host-guest interaction results in the decreased randomness at the adsorption-liquid interface which is also obvious from the negative entropy change accompanying this process. It has been studied in several host-

guest complexation phenomena that the binding energies can be ascribed to contribution due to hydrophobic, hydrogen bonding, electrostatic, and van der Waals interactions.[38]

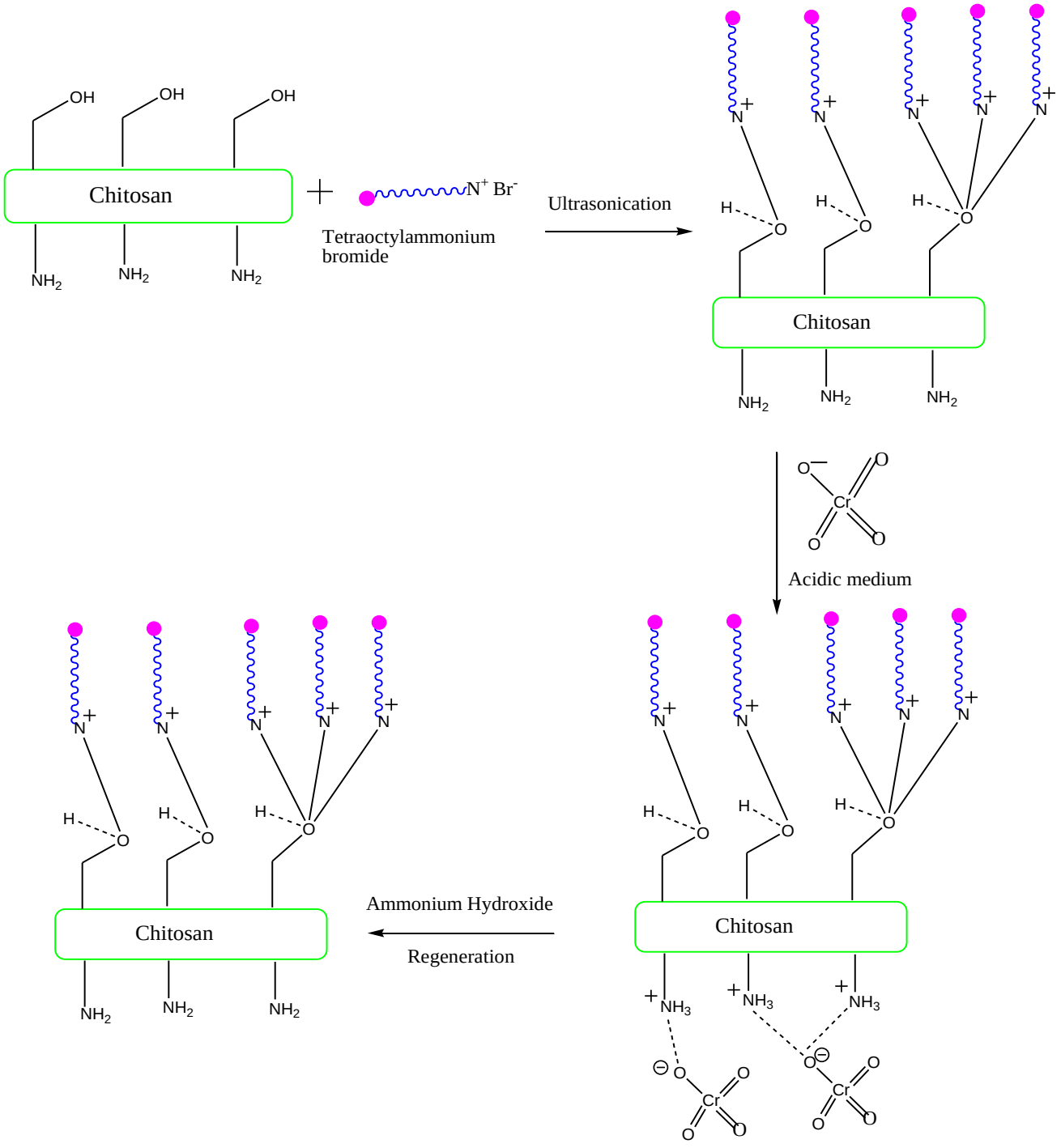

Figure 5.5. Conceptual illustration showing the interaction between ionic liquid, hydrogenchromate and chitosan

However, in the present system the free energy of adsorption involves essentially the contribution due to the intermolecular hydrogen bonding and the electrostatic interactions. The host-guest interaction would be visualized as a positive co-operative effect[39] between the ionic liquid (X), chitosan (Y) and the hydrochromate (Z) anion. The free energy, entropy and enthalpy changes associated with the interaction of X and Y could be represented by the following equations:-

$$\Delta G_{X-Y} = \Delta G_{X} + \Delta G_{Y} - \Delta G_{X-Y} \quad (4)$$

$$\Delta S_{X-Y} = \Delta S_{X} + \Delta S_{Y} - \Delta S_{X-Y} \quad (5)$$

$$\Delta H_{X-Y} = \Delta H_{X} + \Delta H_{Y} - \Delta H_{X-Y} \quad (6)$$

$$\Delta G_{X-Y} = \Delta H_{X-Y} - T\,\Delta S_{X-Y} \quad (7)$$

$$\Delta G_{ads} = \Delta G_{electrostatic} + \Delta G_{hydrogen\ bonding} \quad (8)$$

$$\Delta H_{ads} = \Delta H_{electrostatic} + \Delta H_{hydrogen\ bonding} \quad (9)$$

$$\Delta S_{ads} = \Delta S_{electrostatic} + \Delta S_{hydrogen\ bonding} \quad (10)$$

Overall, the adsorption is influenced by a combination of hydrogen bonding and electrostatic interactions. This is also illustrated in Fig.9 which shows that initially the active sites in chitosan (OH and NH_2) serve as an excellent platform to invite the tetraoctylammonium cation by non-covalent interaction in the form of hydrogen bonding. This is followed by the electrostatic interaction of the protonated amine groups in chitosan. In addition, it is plausible that there could be an additional affinity between the tetraoctylammonium cation and the hydrochromate anion in the form of a secondary electrostatic interaction manifested as hydrogen bonding between the hydrochromate anion and chitosan. This further augments the adsorption of hexavalent chromium from the aqueous phase.

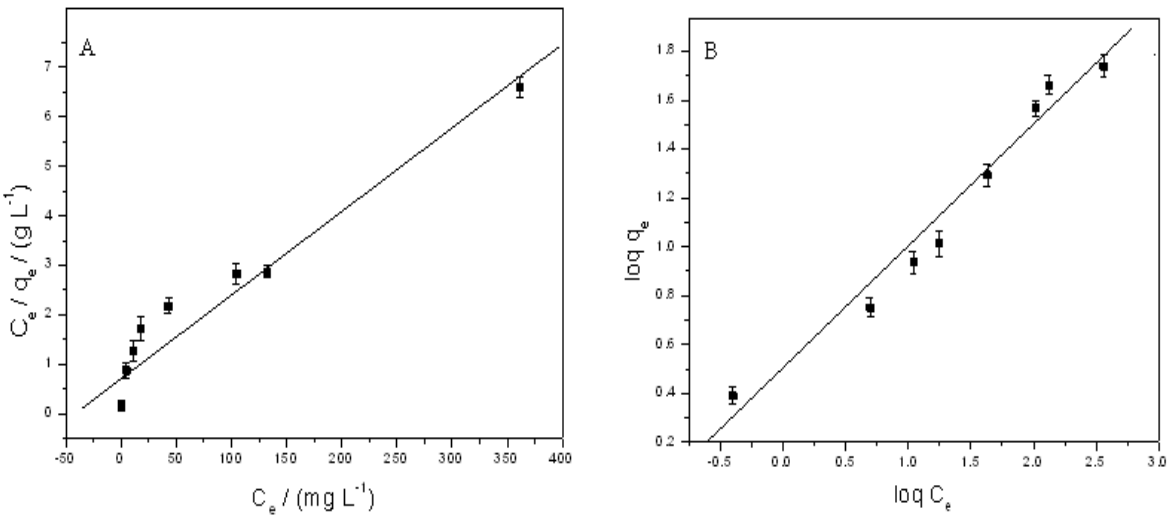

Figure 5.6. (A) Langmuir isotherm. (B) Freundlich isotherm

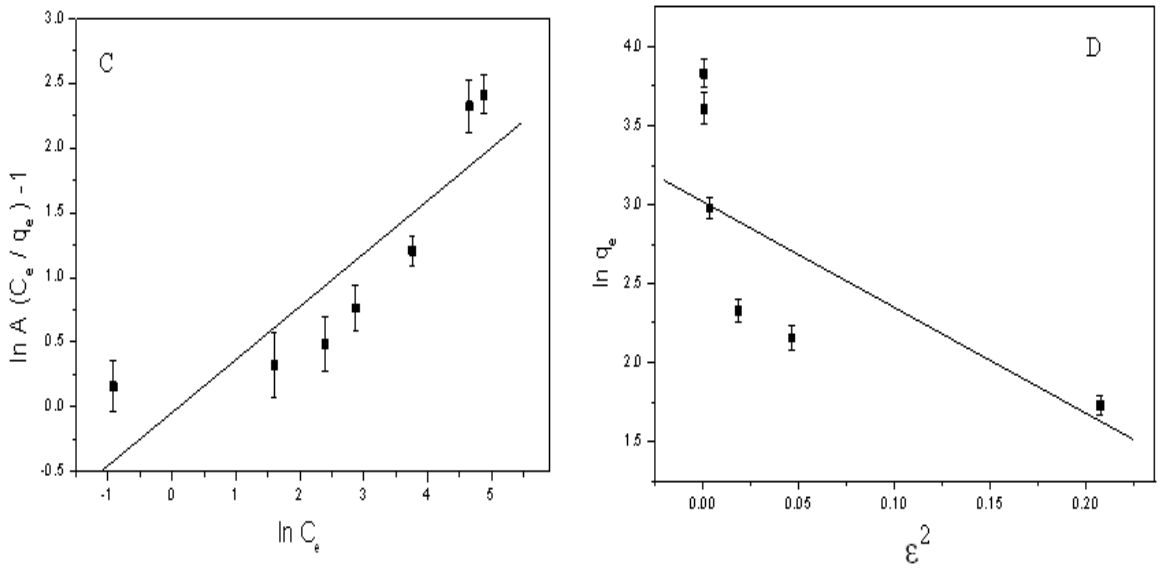

Figure 5.6. (C) Redlich–Peterson isotherm. (D) Dubinin–Radushkevich isotherm

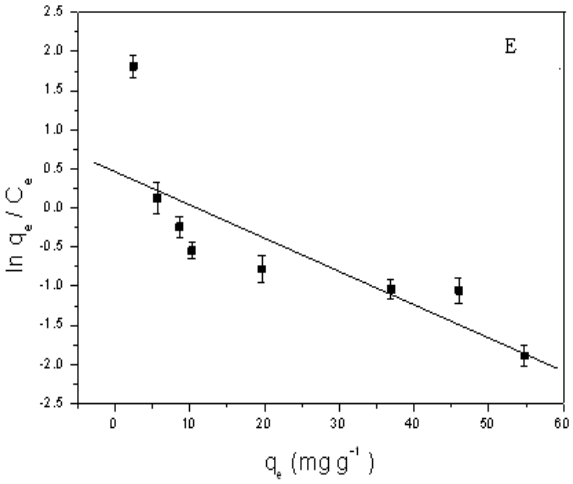

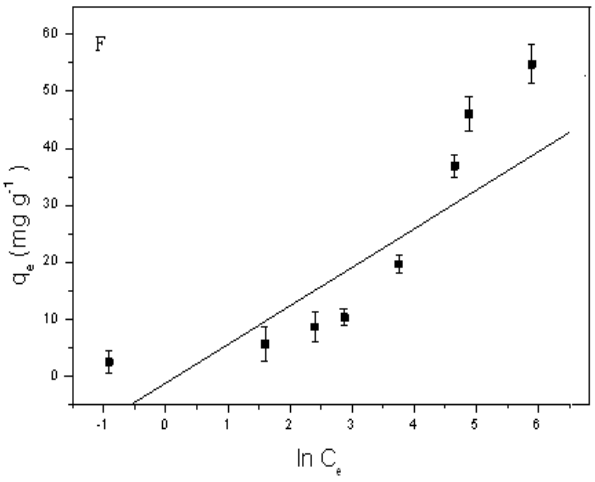

Figure 5.6. (E) Elovich isotherm (F) Temkin isotherm

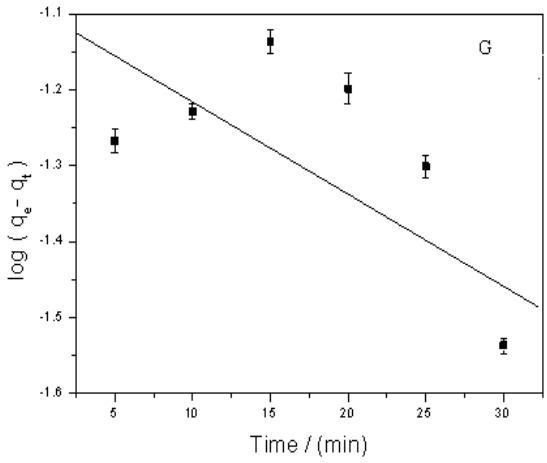

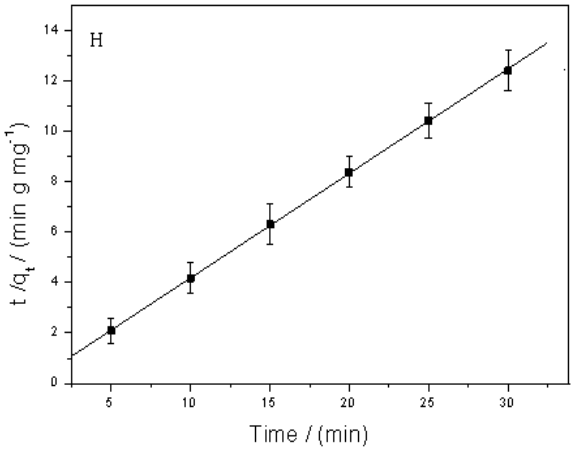

Figure 5.6. (G) Pseudo first order kinetic plot (H) Pseudo second order kinetic plot

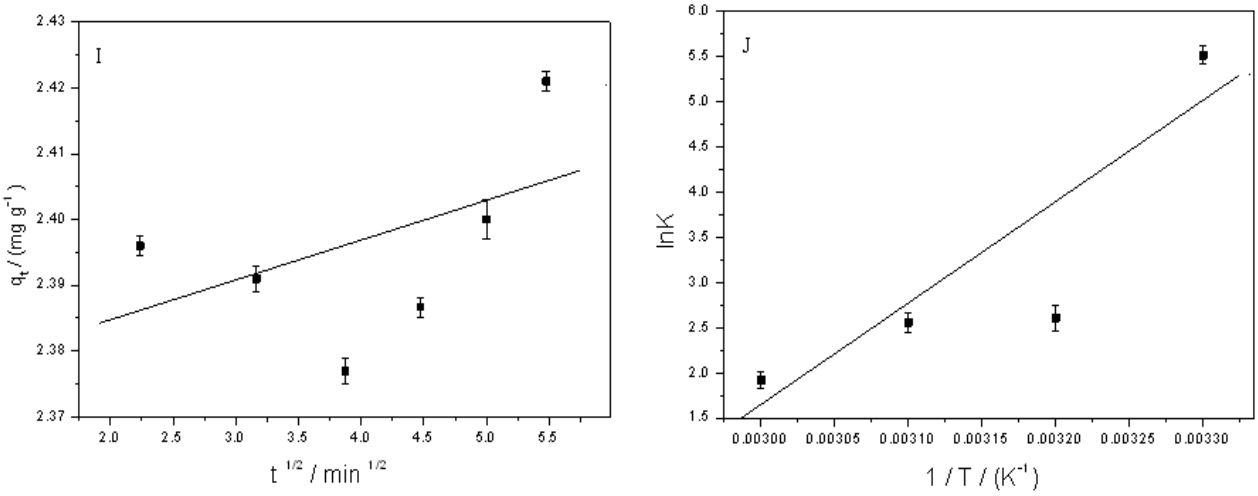

Figure 5.6. (I) Intra particle diffusion (J) Van't Hoff plot

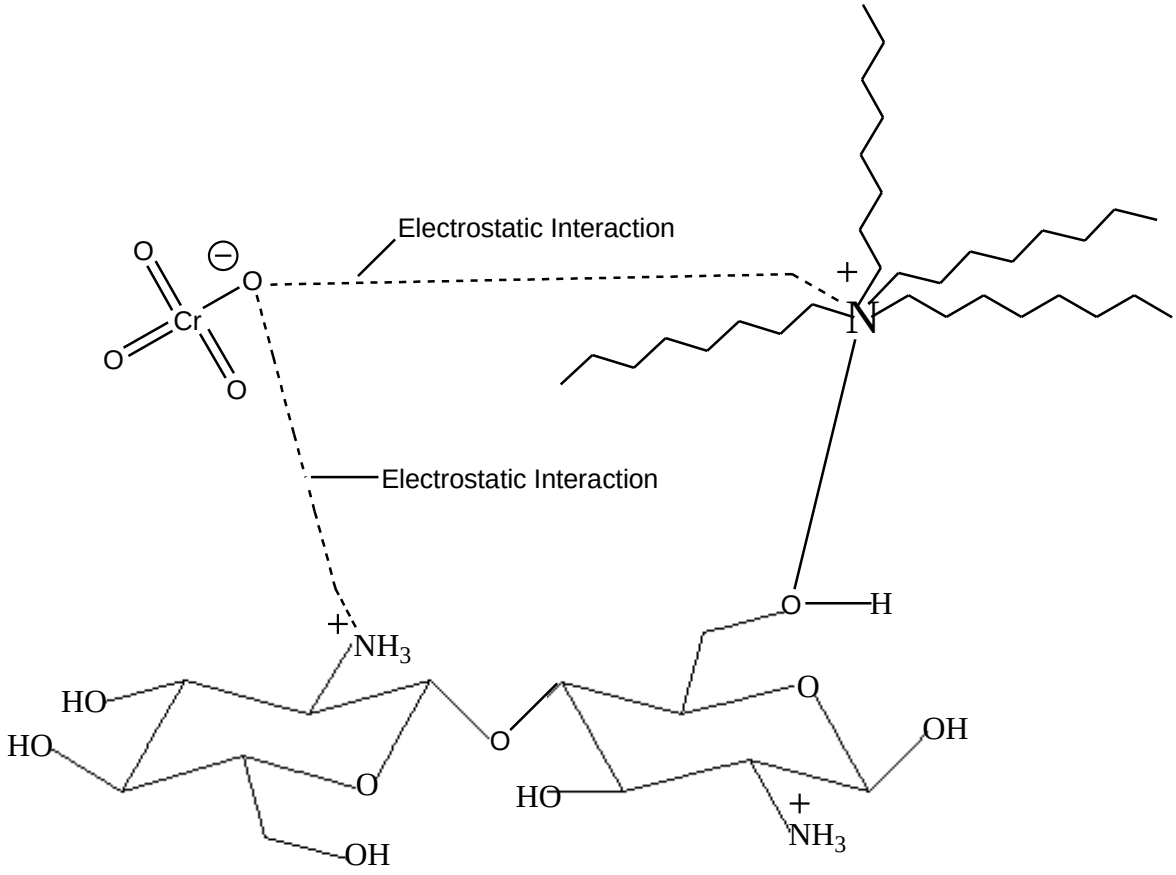

Figure 5.7. Schematic illustration depicting the co-operative interaction between ionic liquid, chitosan and hydrogen chromate anion

(ix) Amount of Adsorbent

The amount of adsorbent used in batch adsorption is also an important aspect that affects the adsorption capacity. The percentage adsorption reached an upper limit (99.0 ± 0.35 %) when the amount of adsorbent was in the range 0.2-0.3 g in 25 mL sample volume. The initial increase in adsorption is attributed to the strong electrostatic attraction between the hydrogen chromate anion and chitosan. Beyond 0.3 g, there was no observable rise in the percentage adsorption, which indicates the saturation of the active adsorption sites in the tetraoctylammonium bromide impregnated chitosan biopolymer matrix.

(x) Column Studies

A glass column (30 cm length) was filled with 2 g of the tetraoctylammonium bromide impregnated chitosan adsorbent upto a height of 2.5 cm. Maintaining a flow rate of 6 mL min^{-1} (which ensures effective contact between the hydrochromate anion and the biopolymer adsorbent) a 100 mL volume of 30 mg L^{-1} Cr(VI) was poured on to the adsorbent column and the concentration of chromium in the solution phase was measured spectrophotometrically by complexation with diphenylcarbazide. The adsorption of chromium(VI) on the adsorbent column was very efficient and quantitative (98.7 ± 0.2%) till a sample volume of 700 mL (Figure 5.8). At sample volumes greater than 700 mL, the adsorbent bed gets exhausted leading to a decline in the percentage adsorption. Indeed, this could be ascribed to the fact that larger sample volumes could result in an expansion or a spread out of the adsorbent bed [40,41] owing to the swelling of the chitosan impregnated with the ionic liquid. Hence, the expanded bed could be the reason for the reduction in the adsorption efficiency at higher sample volume. The regeneration of the adsorbent was examined using certain reducing agents such as sodium nitrite, sodium sulfite, ascorbic acid[18,41,42] and sodium metabisulfite which are recognized to reduce the hexavalent chromium to trivalent state. Reagents such as sodium hydroxide and ammonium hydroxide were also explored since they possess the ability to elute the hexavalent chromium to the respective sodium and ammonium salts. The elution of chromium(VI) was found to be in the order NH_4OH (98 %) > NaOH (75%) > ascorbic acid (63%) > sodium sulfite (49 %) >sodium metabisulfite (40%) > sodium nitrite (33%). The conceptual depiction of this elution process is given in Figure 5.9. Hence, it

can be concluded that ammonium hydroxide could elute chromium effectively as ammonium chromate in the aqueous phase.

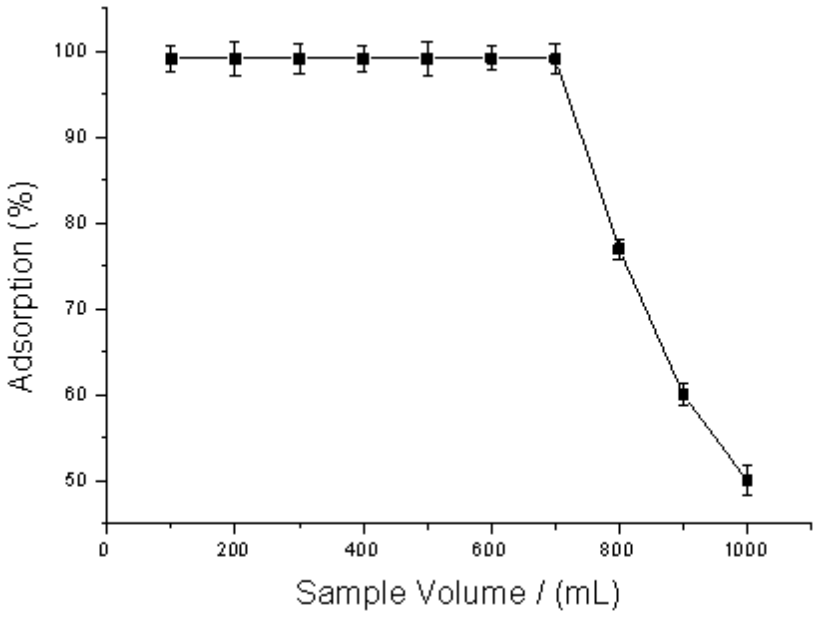

Figure 5.8. Effect of sample volume variation

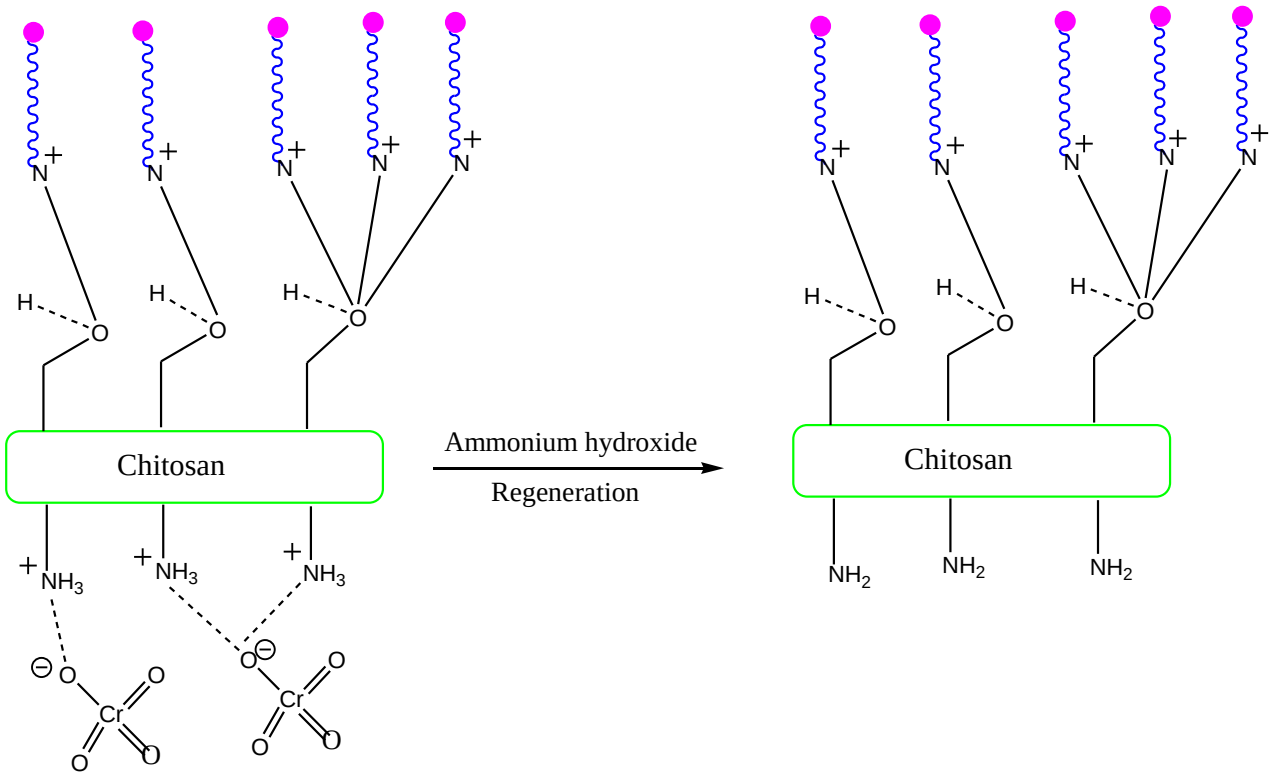

Figure 5.9. Adsorbent regeneration with ammonium hydroxide

Table 5.1 Isotherm parameters obtained from various models

Sl. No	Isotherm model	Parameters	Values
1	Langmuir	q_o (mg g^{-1})	63.69
		b (L mg^{-1})	0.0158
		R_L	0.7598
		r^2	0.95
2	Freundlich	K_F (mg $^{1-1/n}$ g^{-1} $L^{1/n}$)	2.8727
		N	1.9685
		r^2	0.94
3	Redlich Peterson	G	0.744
		B (L mg^{-1})	0.062
		A (L g^{-1})	1.0063
		r^2	0.94
4	Dubinin Radushkevich	q_m (mg g^{-1})	22.74
		β (mol^2 kJ^{-2})	7.6762
		E (kJ mol^{-1})	0.2552
		r^2	0.47
5	Elovich	q_m (mg g^{-1})	22.72
		K_E (L mg^{-1})	0.077
		r^2	0.65
6	Temkin	B	8.275
		A (L mg^{-1})	0.699
		b (kJ $mole^{-1}$)	0.299
		r^2	0.78

Table 5.2 Kinetic and intraparticle rate constant data for the adsorption of chromium(VI)

Second order rate constant k_2/(g mg^{-1} min^{-1})	Regression coefficient	First order rate constant k_1/ (min^{-1})	Regression coefficient	Intraparticle rate constant k_{int}/(mg g^{-1} $min^{-½}$)
2.6301	0.99	0.0211	0.39	0.0059

Table 5.3 Thermodynamic data for the adsorption of chromium(VI)

Temperature / (Kelvin)	ΔG^0/ (kJ mol^{-1})	ΔS^0/ (J mol^{-1} K^{-1})	ΔH^0/ (kJ mol^{-1})
303	-13.89	-257	-90
313	-6.79		
323	-6.87		
333	-5.32		

(xi) Effect of Diverse ions and Application to Real Sample

Prior to venturing towards the application of the method to a real sample, it is customary to know the effect of certain familiar cations and anions (Figure 5.10) on the adsorption of chromium(VI). We observed that cations such as Zn^{2+}, Co^{2+}, Ni^{2+}, Cd^{2+}, Fe^{2+}, Pb^{2+} and Mn^{2+} interfere by reducing the adsorption efficiency for chromium. Anions such as nitrite, sulphite, chloride, phosphate and oxalate also affect the adsorption of chromium(VI). The cationic species interfere by competing for the active binding sites in the adsorbent and moreover ferrous and manganese also are known to reduce chromium(VI) to the trivalent state [18,42] thereby reducing the adsorption efficiency. It is probable that chloride, oxalate and phosphate could interfere by competing with the

hydrogenchromate anion for electrostatic affinity with the protonated amine groups in chitosan. Sulfite and nitrite are known to reduce chromium in +6 to +3 state and hence affect the quantitative retention of chromium(VI). The method was then applied to the study the adsorption efficiency of chromium in a soil sample collected from the vicinity of an electroplating unit. The soil sample was dried and then digested with nitric acid-sulfuric acid mixture[43] and then filtered. The solution was then treated with alkaline peroxide [18,40] to oxidise any chromium (III) to the hexavalent state and diluted to a particular volume. The chromium in the sample was subjected to the adsorption method and the amount of chromium adsorbed was found to be 95.4% as determined by the standard diphenylcarbazide method. The presence of chromium in the adsorbent was verified from the Energy dispersive X ray analysis (EDS) wherein the appearance of chromium peak (Figure 5.11) indicates that the ionic liquid impregnated chitosan adsorbent shows very good prospect in its application to a real sample.

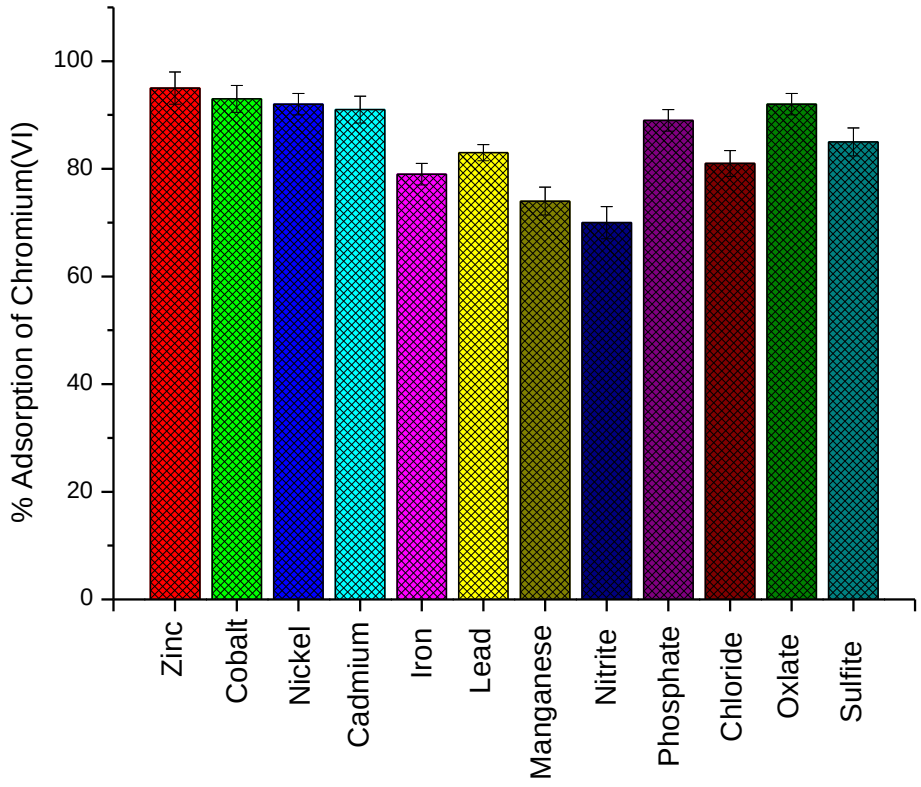

Figure 5.10. Diverse ion effect

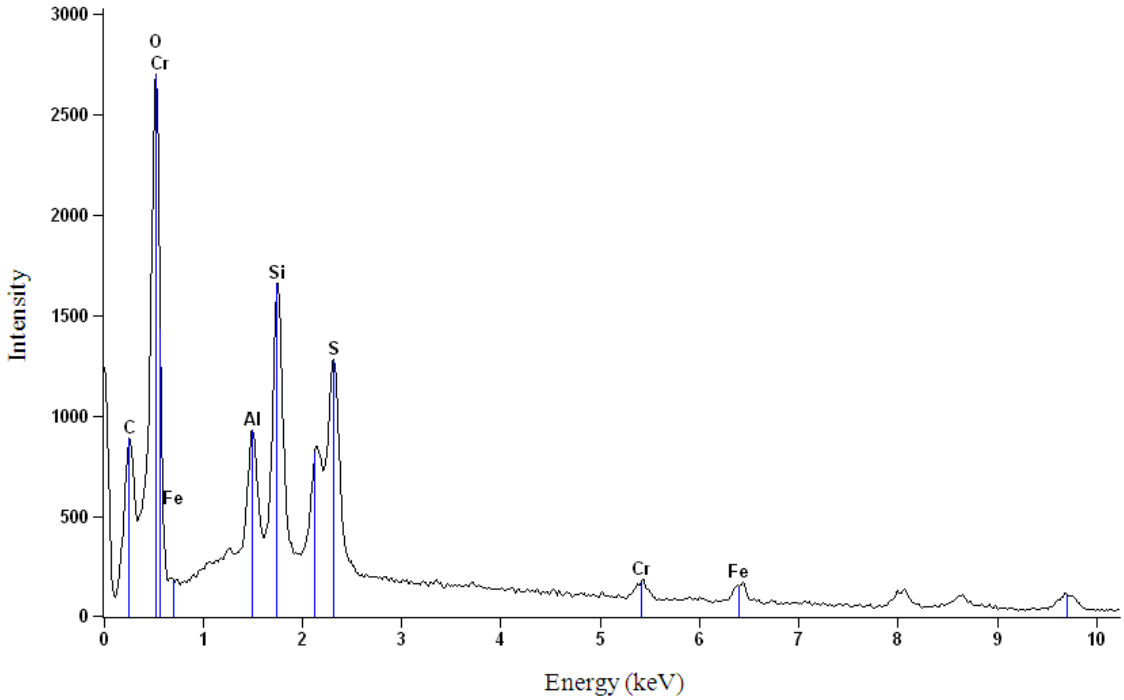

Figure 5.11. EDS spectrum of the adsorbed Cr(VI)

5.2.5 Conclusions

To sum up, this work has demonstrated the excellent three centre interaction between an ionic liquid, chitosan and chromium(VI). The hydrogen bonding and electrostatic interactions play an important role in the adsorption process. The exothermic adsorption process is ably supported by the positive co-operative effect between tetraoctylammonium ion, chitosan and hydrogenchromate anion. Langmuir adsorption isotherm gave a good fit to the adsorption data with an adsorption capacity of 63.69 mg g^{-1}. The adsorbent could be effectively regenerated using ammonium hydroxide and column studies proved the efficacy of the adsorbent in tolerating a larger sample volume. Overall, the method has brought out the worth of ionic liquid-biopolymer interaction and its usefulness in heavy metal adsorption.

A study of the interesting interaction between graphene oxide, Aliquat-336 and hexavalent chromium

5.3.1 Introduction

This chapter discusses an interesting interaction between exfoliated graphene oxide (EGO), ionic liquid (IL) Aliquat336 and hexavalent chromium. Graphene oxide was impregnated with the ionic liquid and the interaction primarily involves electrostatic affinity between the quaternary ammonium cation and surface hydroxyl groups in EGO. The IL-EGO combination functions as an effective adsorbent for hexavalent chromium. The IL-EGO adsorbent acts as a good host in welcoming the incoming guest, hydrochromate anion and several interesting interactions such as cation-π, electrostatic as well as anion-π could be conceptualized in this process. There is a growing need for an affirmative action to tackle the environmental pollution due to heavy metal discharge from various industrial effluents. Chromium pollution is an important concern that requires effective strategies in devising an appropriate remediation technology. Graphene as a two dimensional carbon nanomaterial has evoked considerable interest due to its multifarious applications.[44,45] Graphene oxide, the derivative of graphene could be obtained from graphite followed by the oxidation of graphene and its interesting chemistry finds its application as a useful entity in a broad range of chemical transformations.[46] Graphene oxide is endowed with multiple functional groups such as hydroxyl, carboxylic, carbonyl and epoxy for effective complexation with metal ions. Graphene oxide has been utilized for the removal of heavy metal ions such as copper,[47] cadmium and cobalt,[48] mercury,[49] and arsenic[50] from aqueous solution. Photocatalytic reduction of Cr(VI) has been reported using TiO_2 reduced graphene oxide composites.[51] The utility of graphene oxide has also been illustrated in the removal of humic acid [52] and organic dyes[53,54] from aqueous medium. The chemical reduction of Cr(VI) using EDTA reduced graphene oxide has been reported.[55] The effect of imidazolium based ionic liquids on exfoliated graphene oxide offers interesting insight into the various mechanistic aspects such as electrostatic, cation π and hydrogen bonding interactions.[56]

Literature reports on the utility of graphene oxide ionic liquid combination for chromium detoxification are scarce.

5.3.2 Experimental Section

(i) Preparation of Exfoliated Graphene Oxide (EGO) from Graphite

The exfoliated graphite (EG) was first prepared by the well known procedure reported earlier.[57] 6 g of graphite powder was treated mixture of conc. H_2SO_4/HNO_3 (3:1) for 24 h at ambient environment. The material was washed with Milli Q water, dried and the exfoliation was performed at 800 ^oC. 1 gram of EG was sonicated with acetone for 1 h. The powdered EG was dried and further oxidation to EGO was carried out based on the Hummers method.[53,57,58] The method involves the treatment of EG with approximately 50 mL of conc. H_2SO_4 and 6 g of $KMnO_4$ as the oxidizing agent maintaining a temperature between 0-5^oC. The temperature of mixture was raised to 95^0C followed by treatment with 25 mL of 30% H_2O_2. The resulting solid was filtered, washed with 5% HCl and the filtrate was checked for the presence of sulfate. The EGO was further washed thoroughly with Milli Q water and dried in a hot air oven at 60 ^oC for 24 hours.

(ii) Preparation of Adsorbent

2 g of EGO was taken in a round bottom flask followed by the addition of 13.8 mL of 0.03 mole aliquat-336 (IL) in acetone medium and stirred for 8 hours. The resulting mixture was washed thoroughly with water, filtered and the supernatant was checked for the presence of chloride with silver nitrate. The solid was washed with water and the IL-EGO adsorbent was dried in a hot air oven overnight and used for further adsorption studies. Comprehensive characterization of the adsorbent was done using various physico-chemical techniques to confirm the presence of IL and EGO in the adsorbent.

(iii) Adsorption Procedure

The preliminary adsorption studies were carried out by the batch method. An appropriate quantity of the polymeric sorbent was shaken with 50 mg $L^{-1}$of Cr (VI), maintaining a pH 2.5 at 25^oC. The solution was separated from the adsorbent and the metal ion uptake at different time intervals and the concentration of chromium was measured as its chelate with diphenylcarbazide [59] at a wavelength maximium of 540 nm.

5.3 3. Results and Discussion

(i) Characterization of the Polymeric Sorbent

The FT-IR spectrum obtained for graphite and EGO were in accordance with the reported literature.[47,53,60] The FT-IR spectrum (Figure 5.12) showed characteristic peaks for pure graphite corresponding to aromatic C-H stretching at 3152 cm^{-1}, C=C stretching at 1672 and 1536 cm^{-1} and C-H bending at 1401 cm^{-1}.[50] After oxidation with nitric acid/sulfuric acid and $KMnO_4$ functional groups such as hydroxyl, carboxylic acid and epoxy group are introduced characteristic of graphene oxide. In the case of EGO, the OH group stretching vibrations were obtained at 3387 cm^{-1}. The carbonyl group (C=O) stretching vibrations were seen at 1715 cm^{-1}. [47,53,60] The aromatic C=C stretching 1647 cm^{-1} and C-OH stretching peaks were obtained at 1402 cm^{-1}. The C-O-C in epoxide stretching was observed at 1128 cm^{-1}. After impregnation with ionic liquid two new peaks appeared at 2908 cm^{-1} and 2821 cm^{-1} resulting from the CH_2 stretching of aliphatic chain in Aliquat 336. Furthermore, the hydroxyl group frequency is shifted to 3214 cm^{-1}. The carbonyl group frequency and the C=C peaks are also shifted to 1724 cm^{-1} and 1671 cm^{-1} respectively. These spectral shifts could be ascribed to electrostatic interaction of the quaternary ammonium cation with the OH group and the interaction of the π electrons in the polarizable aromatic ring manifested as cation-π interaction. In the pH range 2.5-3.0, the hydroxyl groups in the adsorbent (IL–EGO) could be protonated and these positively charged surface hydroxy groups could also interact with the hydrochromate anion ($HCrO_4^-$). After adsorption of chromium two peaks appeared at 874 cm^{-1} and 770 cm^{-1} characteristic of Cr=O and Cr-O stretching frequencies in the hydrochromate anion.[61,62]

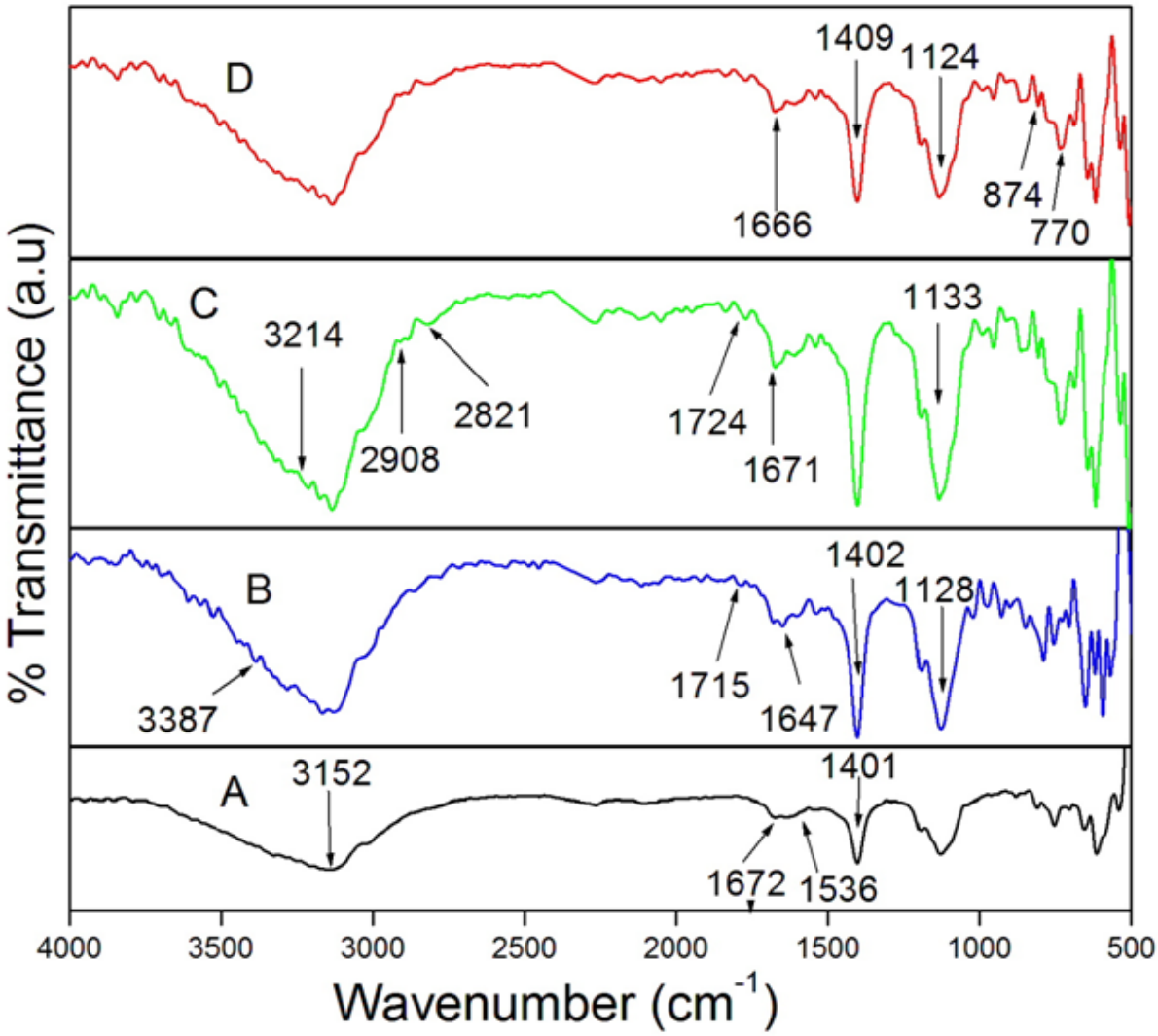

Figure 5.12. FT-IR Spectrum of (A) Graphite (B) Exfoliated graphene oxide (C) Ionic liquid impregnated EGO (D) after adsorption of chromium(VI) on IL-EGO

(ii) XRD and SEM-EDS Studies

XRD pattern (Figure 5.13) of graphite shows a diffraction peak at $2\theta = 26.49^{o}$ which corresponds to the (002) plane. The oxidation of graphite to exfoliated graphene oxide results in the appearance peaks corresponding to $2\theta = 37.3^{o}$ and 49.7^{o} which is due to the creation of the abundant oxygen-containing functional groups on the surfaces of graphene oxide. These values are in accordance with the earlier reported literature.[48,57] A slight shift in the 2θ value to 26.39^{o} with little broadening is also seen in the XRD pattern of EGO. After impregnation of ionic liquid in the EGO matrix peak sharpening occurs corresponding to $2\theta = 26.76^{o}$, 42.7^{o}, 44.8^{o} and 54.8^{o} respectively. The sharpness in the

peak intensity could be ascribed to a certain degree of crystallinity in the amorphous IL-EGO adsorbent matrix. The average crystallite size was obtained using the Debye-Scherer's equation ($0.9\lambda/ \beta \cos\theta$) where 'λ' is the wavelength of x-ray, β is the full width half maximum (FWHM) of the diffraction peak. The average crystallite size was found to be 12.76 nm. After adsorption of chromium, we could see an upward spectral shift corresponding to 26.53^{o} and 45.0^{o}.[63] There is a slight peak broadening as compared to the IL-EGO adsorbent and this shows that after the adsorption of chromium the adsorbent matrix is relatively more amorphous. We could also authenticate the adsorption of chromium from the EDS spectrum (Figure 5.14) along with other elements such as Mn, C, O and S respectively. The appearance of the peak in the range 5-6 keV is also in agreement with the earlier reported literature characteristic of chromium.[41]

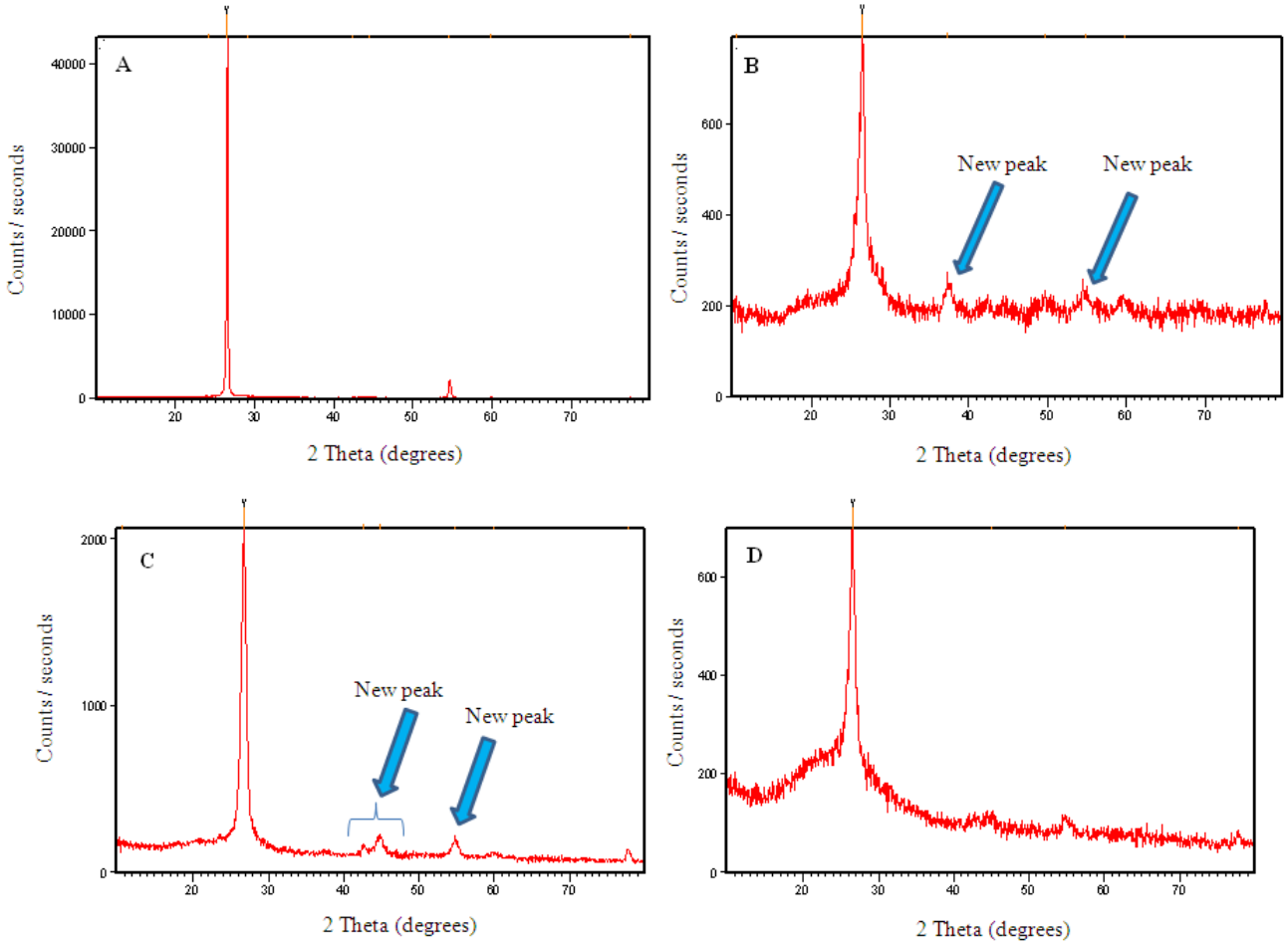

Figure 5.13. XRD pattern (A) Graphite (B) Exfoliated graphene oxide (C) Ionic liquid impregnated EGO (D) after adsorption of chromium(VI) on IL-EGO

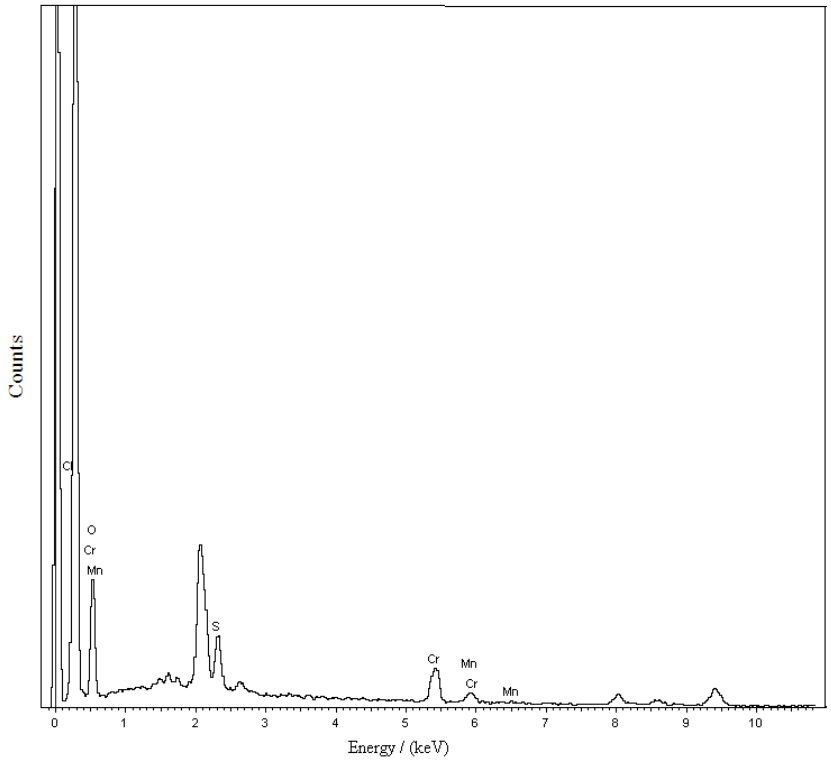

Figure 5.14. EDS spectrum of the adsorbed Cr(VI) on EGO

(iii) Interaction of EGO with Aliquat 336, Optimum pH and Mechanism of Adsorption

The presence of functional groups in EGO such as COOH, OH and C=C is a boon with regard to interaction of the ionic liquid. The ionic liquid, Aliquat -336 is essentially a long chain quaternary ammonium halide with a long hydrophobic tail and the head group contains the positively charged nitrogen atom. The trioctylammonium cation would involve in an electrostatic interaction with the surface hydroxyl and carboxyl groups and furthermore, the affinity could also be strengthened via the cation- π interaction[56,64,65] involving the conjugated aromatic ring. In an aqueous solution containing Cr(VI) ions, the interaction certainly would depend on the pH of the medium. Hence, aqueous phase pH plays an important role in the interaction of hexavalent chromium with the ionic liquid and graphene oxide. A well known fact in several adsorption systems involving chromium is its existence as various oxo anions depending on the pH of the sample solution. In the pH range 2-5, the dominant form of Cr(VI) is $HCrO_4^-$ [41,66] and increasing the pH would shift the equilibrium to CrO_4^{2-} oxy anion. At pH less than 2 the dichromate ion, $Cr_2O_7^{2-}$ is the key species that exists in solution. In the present system, the optimum pH for adsorption of hexavalent chromium on IL-EGO adsorbent was in the range 2.5-

3.5. This is a characteristic feature associated with the existence of hydrochromate anion as reported by several groups working on the removal of chromium.[41] The effect of pH on the adsorption of chromium is depicted in Figure 5.15. The trioctylammonium cation is involved in an ion-pair electrostatic interaction with the $HCrO_4^-$ anion[63] as well as protonated hydroxyl groups on the surface. The overall mechanism that could be conceptualized in this adsorption process is given in Figure 5.16. With increase in pH, the repulsion between the negatively charged EGO surface (Owing to the deprotonation of the surface hydroxyl groups) and the hydrochromate anion results in decrease in the percentage adsorption of chromium. Furthermore, the competition from hydroxyl anion for the active sites of the IL-EGO also would influence the adsorption at higher pH. The pH_{zpc} of the IL-EGO adsorbent was measured using the pH drift method.[67] The experiment was carried out at 30 °C. by taking 0.10g of the IL-EGO adsorbent in 50 ml of the 1 mol L^{-1} sodium chloride. The initial pH was adjusted using dilute sulfuric acid and sodium hydroxide. The final pH was recorded after 24 h so as to ensure the stability and the plot of initial versus final pH was used to determine the (pH_{zpc}) of the sorbent. The pH_{zpc} of the IL-EGO adsorbent (Figure 5.17) was found to be 3.5. At pH < 3.5, the surface charge of exfoliated graphene oxide is positive, and this promotes the adsorption of hexavalent chromium(VI) due to electrostatic attraction. Above pH 3.5 the surface charge of exfoliated graphene oxide becomes negative with the slow deprotonation of the surface hydroxy groups leading to electrostatic repulsion between the hexavalent chromium oxo anion and the adsorbent surface.

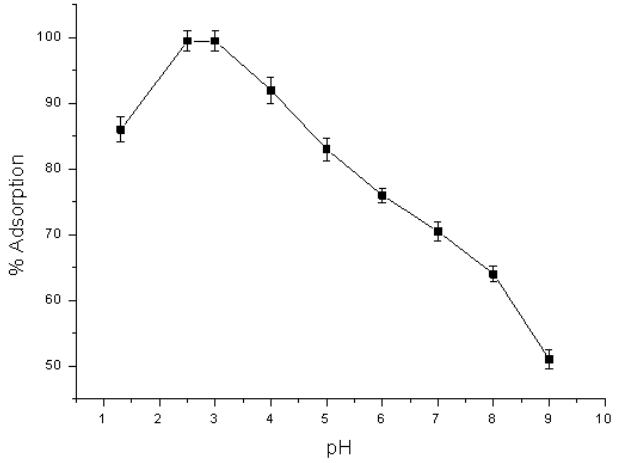

Figure 5.15. Effect of pH

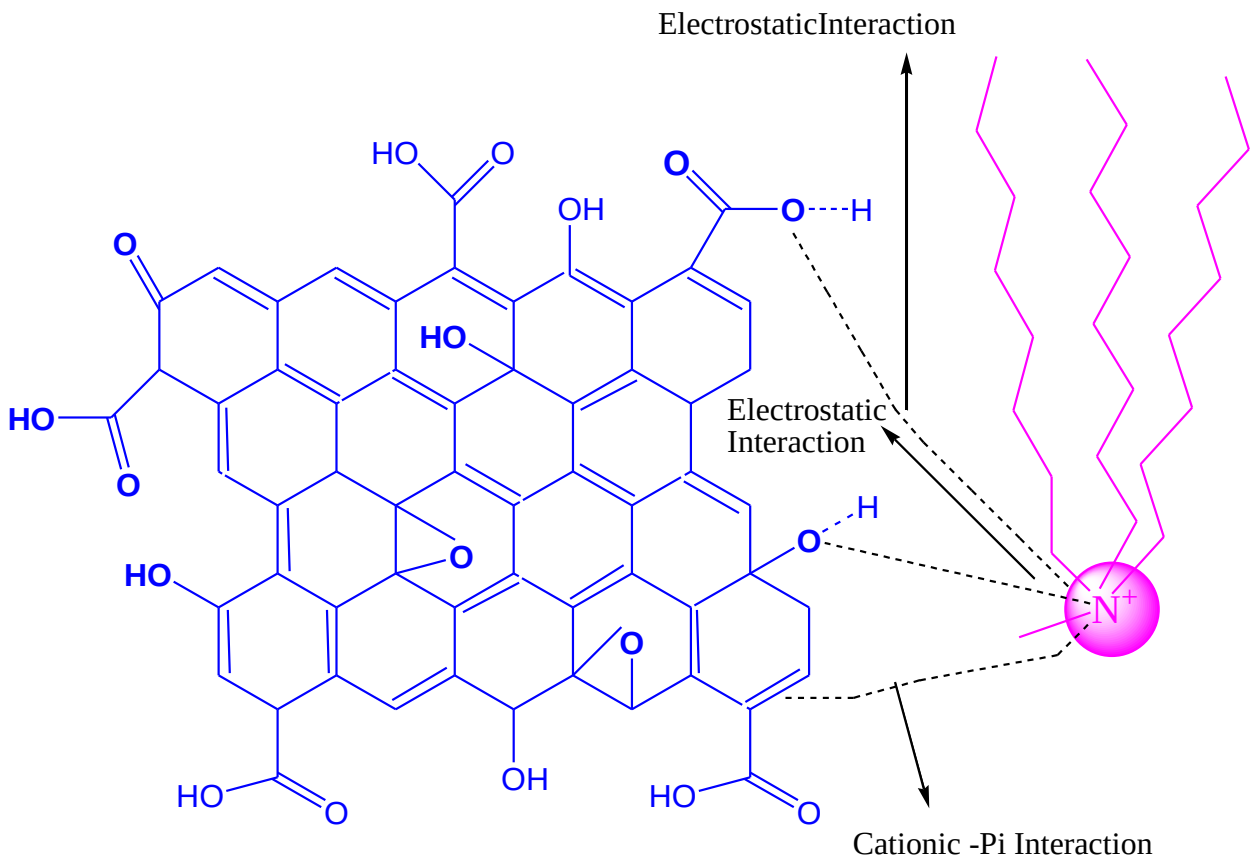

Figure 5.16. Illustration of Interaction between EGO and ionic liquid (A)

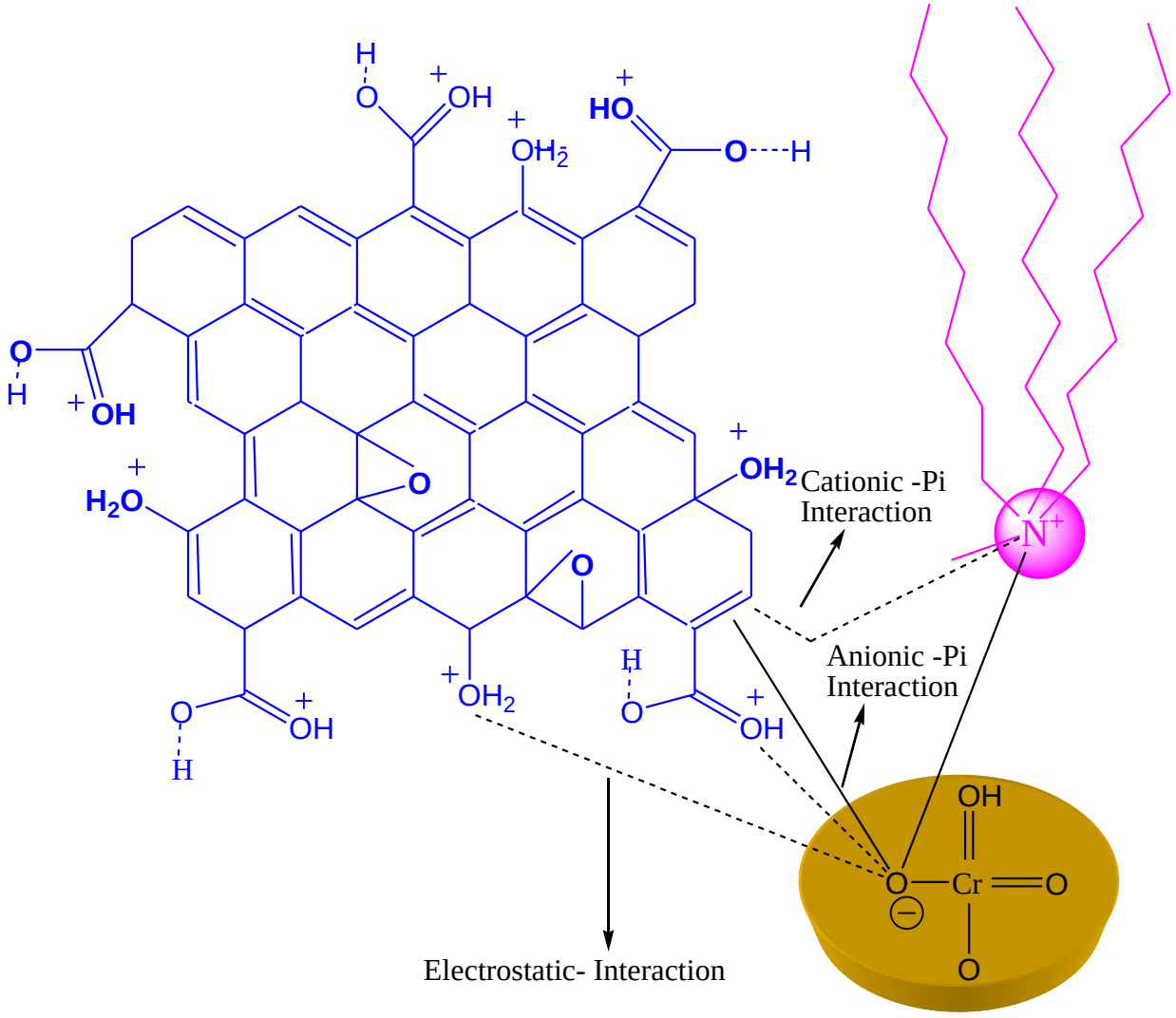

Figure 5.16. Illustration of Interaction between EGO-IL and chromium(VI) (B)

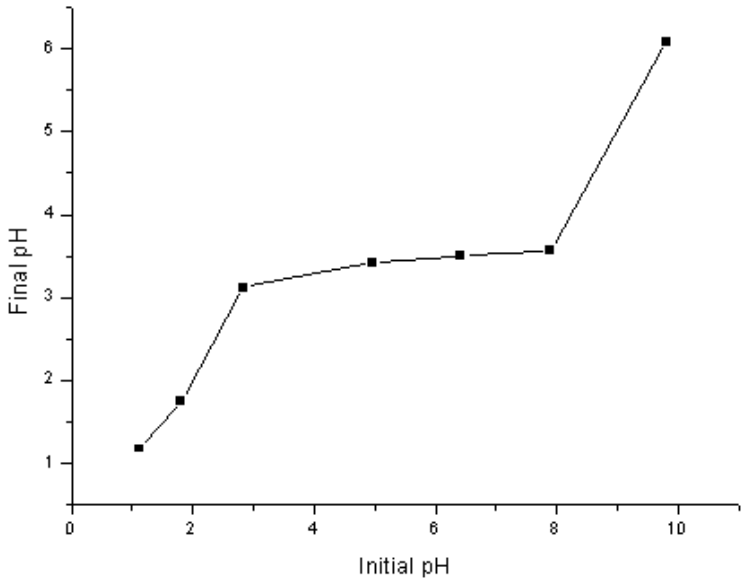

Figure 5.17. Zero point charge (pH_{zpc}) of the IL-EGO adsorbent

(iv) Adsorption Isotherms

The various isotherm (Figure 5.18A to 5.18F) models essentially correlate the amount of the hexavalent chromium adsorbed at equilibrium and the concentration in solution. Eventhough, Langmuir and Freundlich isotherms are widely used in adsorption studies, various other empirical models also offer vital insight into the nature of adsorption.[26-32] The isotherm parameters obtained through these models are given in Table 5.4. The Langmuir plot of C_e/q_e against C_e gives the corresponding isotherm parameters such as the maximum adsorption capacity (q_o) and the adsorption energy b. A high adsorption capacity of 285.71 mg g^{-1} reflects the excellent sorption potential of the IL-EGO adsorbent for Cromium(VI). Furthermore, in this model the separation factor (R_L $=1/1+bC_o$) was found to be less than unity which shows the effectiveness of interaction of the IL-EGO adsorbent with chromium(VI) oxy anion.[27] The intensity of adsorption n and the adsorption capacity K_F are two other vital parameters which are obtained from the Freundlich isotherm plot of log q_e against log C_e. When $1/n < 1$, it corresponds to a normal L-type Langmuir isotherm,[68] while $1/n > 1$ reflects a co-operative sorption.[69] As shown in Table 5.4, the values of 1/n and K_F along with a high regression coefficient of 0.99 indicate the effective uptake of chromium by the IL-EGO adsorbent in this adsorption process. The adsorption energy (β), Polanyi potential (ε) and the mean free

energy E_{DR} of adsorption are also given by yet another interesting D-R isotherm model. The E_{DR} value obtained in this study is characteristic of physical adsorption involving hexavalent chromium and the IL-EGO adsorbent. In case of the R-P isotherm, the exponent g in the equation is significant and values close to unity are an indication of the good fit to Langmuir model. In the adsorption of chromium(VI) on IL-EGO surface, the value signifies that the experimental data could be correlated based on Langmuir model as well. The low binding energy *b* obtained in the present study involving the Tempkin isotherm illustrates the electrostatic interaction[70] between the hydrochromate anion and the IL-EGO adsorbent. The adherence to Frendlich model was also established further from the individual isotherm data plots of q_e against C_e. The L shaped adsorption isotherms are in agreement with the Gile's categorization[71] and the q_e values obtained experimentally show a good correspondence to the Freundlich type isotherm as shown in Figure 5.18g. The effective electrostatic interaction between the hydrochromate anion and the IL-EGO adsorbent is evident from the ascending portion of the curve and the relatively flat terrains at higher C_e values denote the saturation of the adsorption sites.

(v) Adsorption Kinetics

The kinetic mechanism that controls the adsorption of Cr(VI) on the IL-EGO adsorbent were evaluated using the pseudo first-order, second-order and the intraparticle diffusion models. These models relate the amount of the Cr(VI) adsorbed at equilibrium and the respective rate constants at varying equilibration time. The Lageregen first order[33] and Ho [34] second order expressions are extensively used in all adsorption processes to correlate the experimental data**.** The kinetic parameters (Table 5.5) could be acquired from the relevant plots (Figure 5.19A&B**)** and the higher regression coefficient attained using the second order kinetics illustrates the applicability of this model to fit the experimental adsorption data. In addition, equilibrium adsorption capacity (q_e) values of 37.08 mg g^{-1} and 38.50 mg g^{-1} (experimental and calculated) concur well with the second order kinetic model. The transfer of $HCrO_4^-$ oxy anion from the aqueous phase to the IL-EGO adsorbent matrix could be governed by pore, surface or film diffusion processes. The kinetics of uptake of Cr(VI) could also be influenced by intraparticle diffusion and the classic Weber-Morris[35] model ($q_t = k_{int}\sqrt{t} + C$) relates the amount of hexavalent chromium adsorbed at time t to the intraparticle rate constant (k_{int}). The Weber-Morris

plot (Figure 5.19C) gives a linear fit without passing through the origin and this is an indication that the adsorption of hexavalent chromium could involve boundary layer mechanism too.

(vi) Thermodynamics of Adsorption

The adsorption process is spontaneous and exothermic with negative entropy change (Table 5.6). The Van't Hoff plot[37] (Figure 5.19D) gives the entropy and enthalpy changes accompanying the adsorption process. The decreased randomness at the IL-EGO adsorbent-hydrochromate solution interface is reflected in the ΔS^o value. The average energy of activation[72] was found to be -61.36 kJ mol^{-1} which also authenticates the exothermicity of the adsorption process. The negative free energy (ΔG^0) values corroborate the effectiveness of the electrostatic interaction between $HCrO_4^-$ and the IL-EGO adsorbent surface. Indeed, the free energy of adsorption could arise from the interaction between IL-EGO, $HCrO_4^-$-IL and $HCrO_4^-$-EGO. The overall free energy of adsorption (ΔG_{ads}) is a result of this electrostatic force of attraction as well as the cation-π interaction between the positively charged quaternary ammonium cation and the polarisable aromatic pi electron cloud[64,65]

$$\Delta G_{adsorption} = \Delta G_{IL\text{-}EGO} + \Delta G_{HCrO4^-\text{-}IL} + \Delta G_{HCrO4^-\text{-}EGO} \quad (11)$$

The feasibility of the adsorption process at low temperatures is also evident from the trend in the free energy values. Typically, the exfoliated graphene oxide would act as a primary host to the trioctylammonium cation, which in turn functions as a secondary host to the chromium(VI) solution from the bulk. Hence, the enthalpy and entropy of adsorption should also take cognizance of the interaction between the ionic liquid impregnated graphene oxide and the hydrochromate oxy anion.

$$\Delta H_{adsorption} = \Delta H_{(IL\text{-}EGO)} + \Delta H_{Cr(VI)} \quad (12)$$

$$\Delta S_{adsorption} = \Delta S_{(IL\text{-}EGO)} + \Delta S_{Cr(VI)} \quad (13)$$

$$\Delta G_{adsorption} = \Delta H_{adsorption} - T\,(\Delta S_{IL\text{-}EGO} + \Delta H_{Cr(VI)}) \quad (14)$$

Indeed, in ion-pair mechanism involving electrostatic interactions, the enthalpy and entropy factors play a significant role.[73,74] The ability of the $HCrO_4^-$ anion to interact with the head (positively charged ammonium cation) results in a compact and ordered transition state as shown below thereby leading to a decrease in the entropy.

As reported earlier[74,75] in ion-pair interactions involving metals like mercury, ions that are multiply charged ions with high charge density could be categorized as kosmotropic while singly charged large size ions are chaotropic in nature. Based on this classification, the hydrochromate anion would be regarded as chaotropic anion and is poorly solvated.

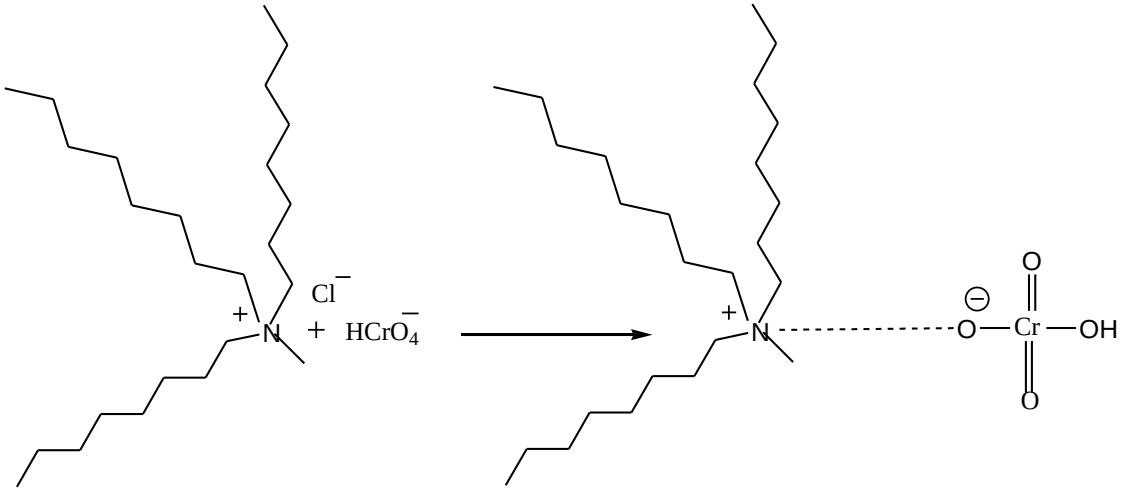

Large size quaternary ammonium cation is kosmotropic due to its hydrophobic hydration[75] accompanied by an effective and ordered interaction with the $HCrO_4^-$ anion leading to negative entropy change in the adsorption process. The counter ionic atmosphere can also influence the degree of kosmo/chaotropicity. The bulky and large trioctylammonium cation induces a certain amount of kosmotropicity in the hydrochromate anion. Hence, we can envisage a sort of symbiotic effect in this interaction leading to the entrapment of $HCrO_4^-$ anion (guest) as an ion pair with the quaternary ammonium cation on the EGO surface. A combination of solvation and electrostatic interactions[75,76] govern the overall entropy change in the adsorption process.

$$\Delta S_{ads} = \Delta S_{electrostatic} + \Delta S_{solvation} \qquad (15)$$

Since, the quaternary ammonium cation as well as the hydrochomate anion could also be solvated, this non-bonding ion-solvent interaction ushered by the electrostatic affinity reflects the negative entropy in the adsorption of chromium. Solvation is more favored at lower temperature range and we fathom the electrostatic interaction to be the predominant feature involving the negatively charged hydrochromate anion, quaternary ammonium cation and the exfoliated graphene oxide.

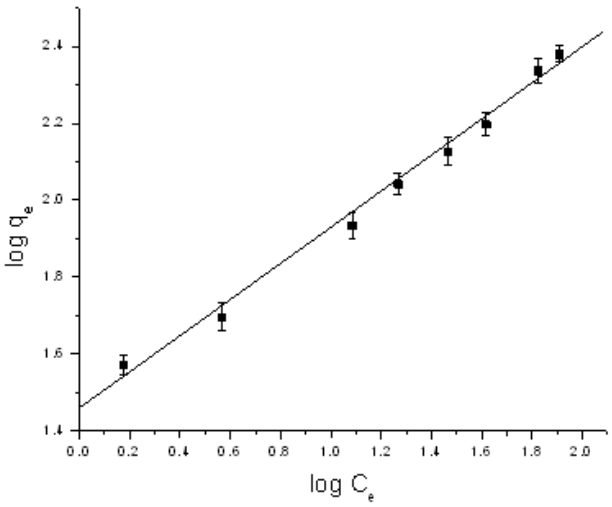

Figure 5.18A. Freundlich isotherm

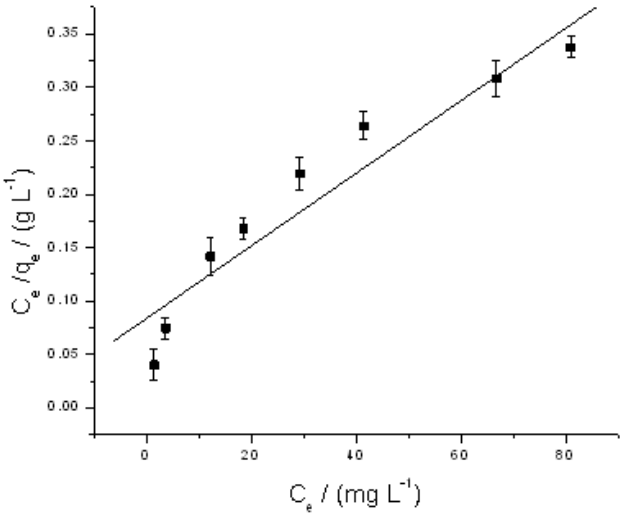

Figure 5.18B Langmuir isotherm

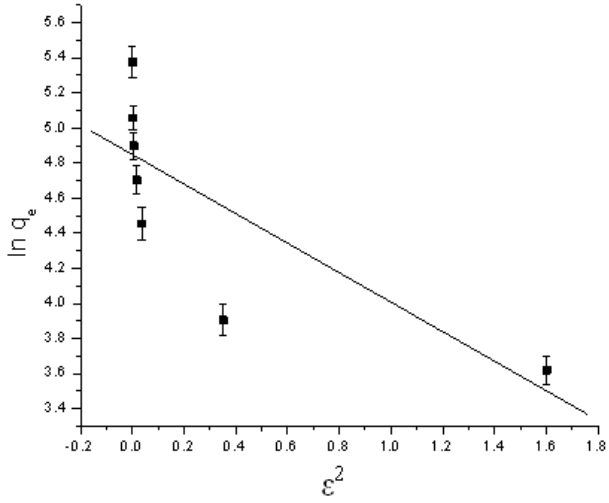

Figure 5.18C D-R isotherm

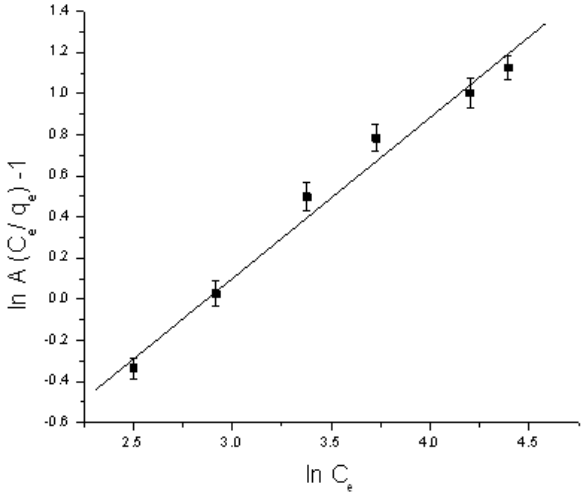

Figure 5.18D R-P isotherm

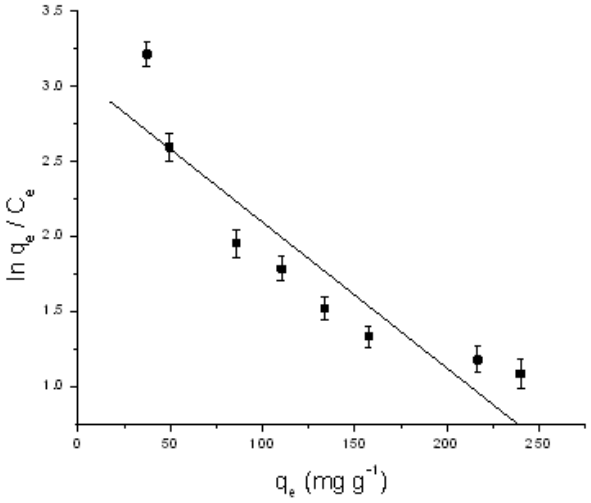

Figure 5.18E Elovich isotherm

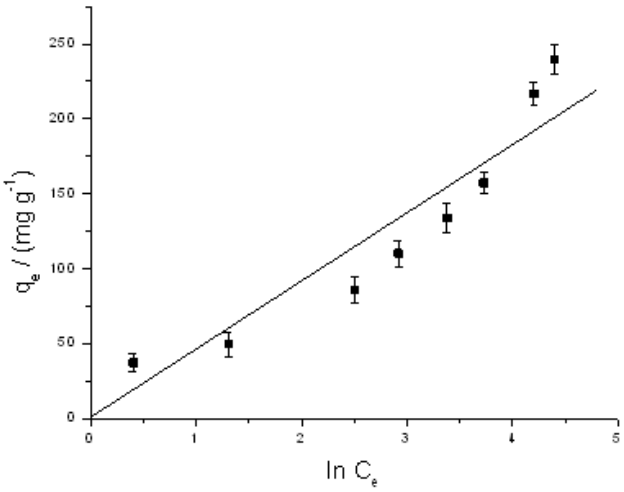

Figure 5.18F Temkin isotherm

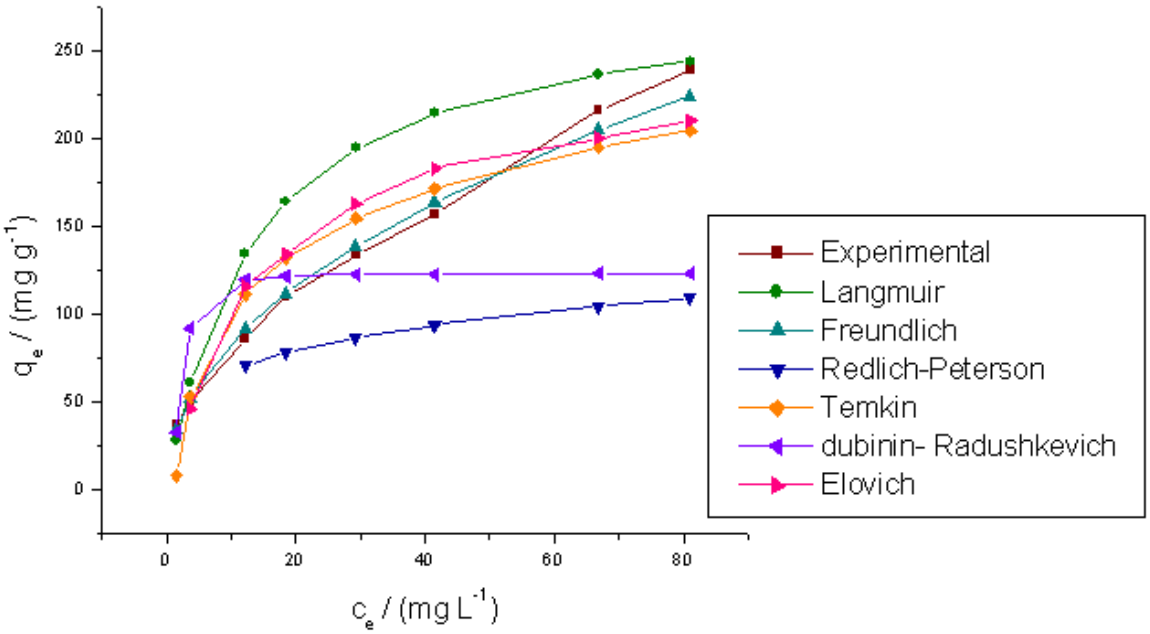

Figure 5.18g Plot of q_e against C_e

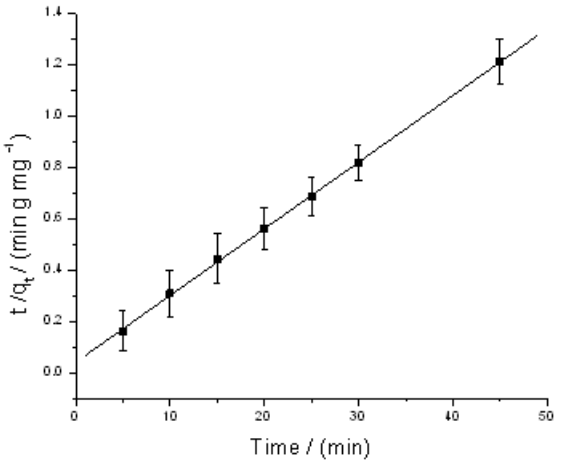

Figure 5.19A Pseudo second order kinetics

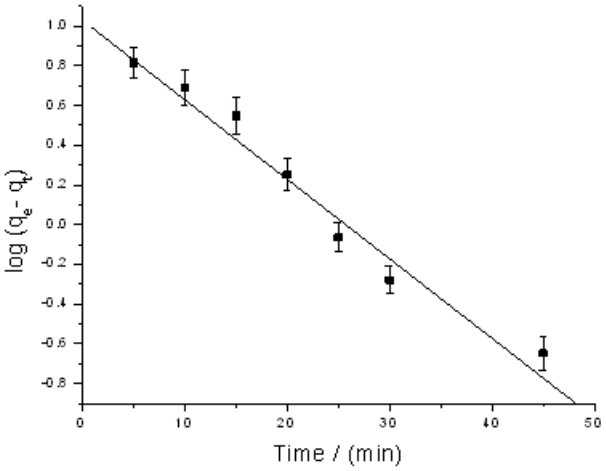

Figure 5.19B Pseudo first order kinetics

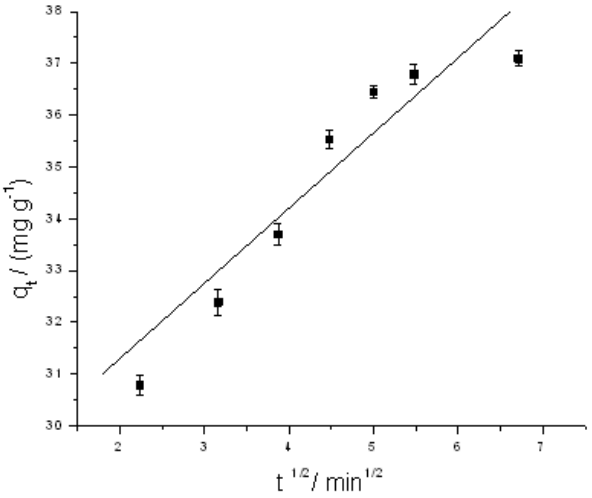

Figure 5.19C Intraparticle diffusion

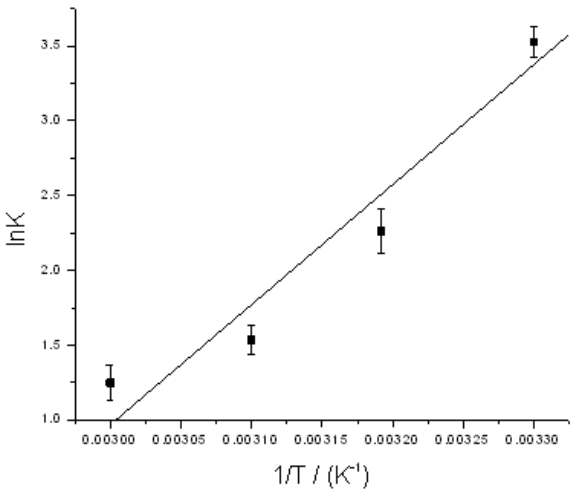

Figure 5.19D Van't Hoff Plot

(vii) Column Adsorption Study

After getting an insight towards the adsorption by batch process, we decided to test the method for a larger sample volume. Column studies were carried out by packing a glass column (3 cm diameter, 30 cm length) with 3.0 g of the IL-EGO adsorbent. With 20 mg L^{-1} Cr(VI) and a flow rate of 8 mL min^{-1} the adsorption of chromium(VI) was quantitative up to a sample volume of 1200 mL (Figure 5.20). We confirmed the adsorption by analyzing chromium in the solution phase by complexing chromium(VI) with diphenylcarbazide. Beyond, 1200 mL, the saturation of the adsorbent bed results in lowering the percentage of chromium retained in the column. In any adsorption process, the economics of the entire operation is quite important and in this perspective, regeneration of the adsorbent is a vital parameter. Hence, certain prospective reagents were chosen for desorption of chromium(VI). Ideally, the reagent so chosen should be cost effective and not damage the adsorbent bed. Some of these reagents have proved their worth in earlier adsorption studies involving chromium.[62] These include reducing agents such as sodium sulfite, ascorbic acid, sodium metabisulfite, sodium nitrite and ascorbic acid as well as reagents such as sodium hydroxide and ammonium hydroxide which could elute chromium(VI) by reducing to the less toxic Cr(III) and also to the corresponding chromate salts. The desorption ratio is calculated as follows

$$\text{Desorption ratio (\%)} = \frac{\text{Concentration of Cr(VI) desorbed into the eluate}}{\text{Concentration of Cr(VI) adsorbed onto the IL-EGO adsorbent}} \times 100$$

The percentage of chromium eluted given in Figure 5.21 illustrates that 15 mL of 2 mol L^{-1} ammonium hydroxide was very effective in the desorption of chromium as ammonium chromate in the eluate. After 12 repetitive cycles, we observed a decrease in the percentage elution of chromium. A 15 mL elution volume from a large initial sample volume of 1200 mL ensures a preconcentration factor of 80 which indicates the efficacy in detoxifying chromium from an industrial effluent.

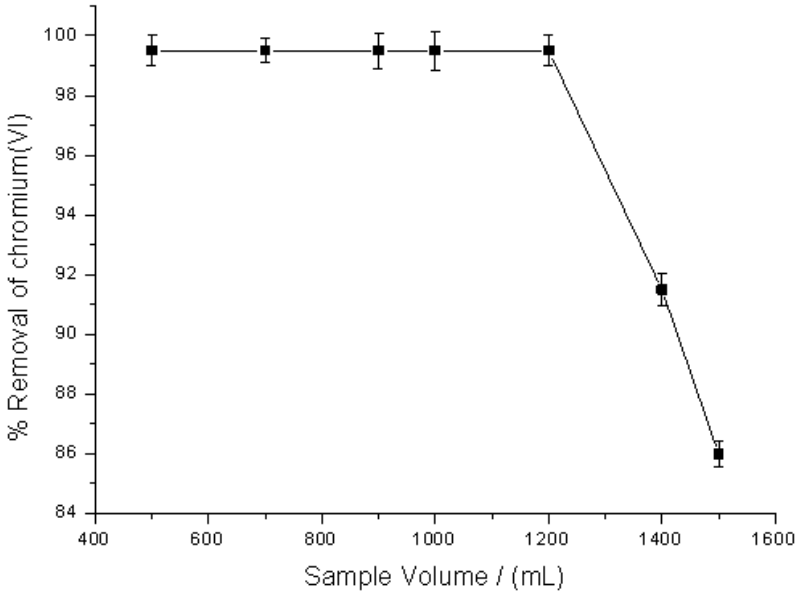

Figure 5.20 Effect of sample volume variation

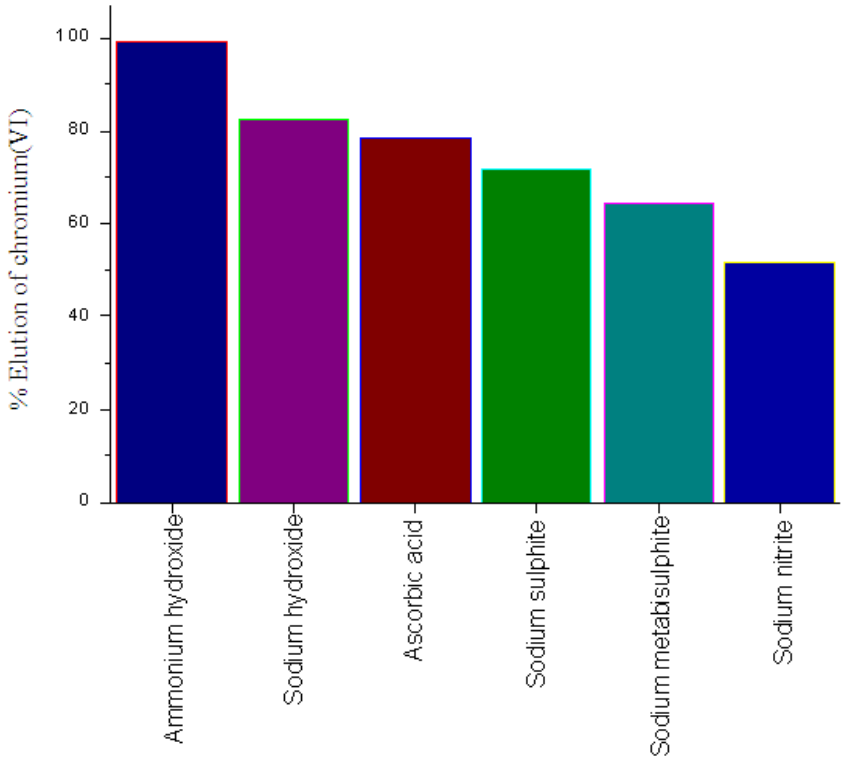

Figure 5.21 Desorption of chromium with various reagents

(viii) Effect of Different Ions

In any analytical solid phase extraction method, the effects of different ions that affect the performance efficiency are to be examined. The ions so chosen should also be representative of the real effluent sample. In this perspective, the interfering effect of ions such as Cd^{2+} (500 mg L^{-1}), Co^{2+} (500 mg L^{-1}), Zn^{2+} (500 mg L^{-1}), Ni^{2+} (500 mg L^{-1}) Fe^{2+} (100 mg L^{-1}), Pb^{2+} (500 mg L^{-1}), Hg^{2+} (250 mg L^{-1}) and Mn^{2+} (150 mg L^{-1}) were examined individually in a 250 mL sample volume containing 20 mg L^{-1} hexavalent chromium. The adsorption efficiency of Cr(VI) was not influenced by Cd^{2+}, Co^{2+}, Zn^{2+}, Ni^{2+}, Pb^{2+} while Fe^{2+} and Mn^{2+} interfere by reducing the hexavalent chromium to trivalent state.[1] In case of anionic species, at 250 mg L^{-1} level chloride, sulfate and phosphate caused considerable reduction in the adsorption of chromium(VI) by competing with $HCrO_4^-$ ion for the active sites in the IL-EGO adsorbent. Lower oxidation state ions like sulfite and nitrite would also reduce Cr(VI) thereby decreasing the percentage retention of chromium(VI) in the adsorbent column.

(ix) Testing the Adsorbent in a Real Sample and Comparison With other Carbon based Sorbents

The vibrant features of the IL-EGO adsorbent material prompted us to test the applicability of the method in a tannery waste water sample. In the tannery effluent, chromium (III) is the major species along with some amount of Cr(VI) and the associated organic components. Hence, it is imperative to digest the sample with strong acids such as nitric acid-sulfuric acid mixture to destroy the organic matter. The total chromium was then determined by oxidation with alkaline peroxide[18] by passing a known volume of the diluted effluent on the IL-EGO adsorbent column. Dilution takes care of the interference due to excess chloride and sulphate present in the effluent. The analysis of chromium in the solution phase revealed the quantitative retention of chromium (97.2 ± 0.6%) with three replicate determinations. The adsorbed chromium(VI) on the IL-EGO adsorbent could also be desorbed with ammonium hydroxide as the eluent. In order to adsorb Cr(III), the sample (after removal of organic matter by acid treatment) was passed through the column at an alkaline pH (8.0) The cationic Cr(III) is associated with the deprotonated hydroxy and carboxylic groups through electrostatic interaction (Figure 5.22) as $Cr(OH)_2^+$ and $Cr(OH)^{2+}$ species [18] respectively. The retention of Cr(III) was also

very good with an adsorption efficiency of 97.4 ± 1.1%. The adsorbed Cr(III) could be eluted from the column using dilute sulphuric acid as chromium (III) sulfate. Keeping in mind the environmental impact of chromium, the eluates were not directly discarded in the sink. These solutions were preserved and utilized in the supplementary methods which we are developing currently in our lab for chromium detoxification.

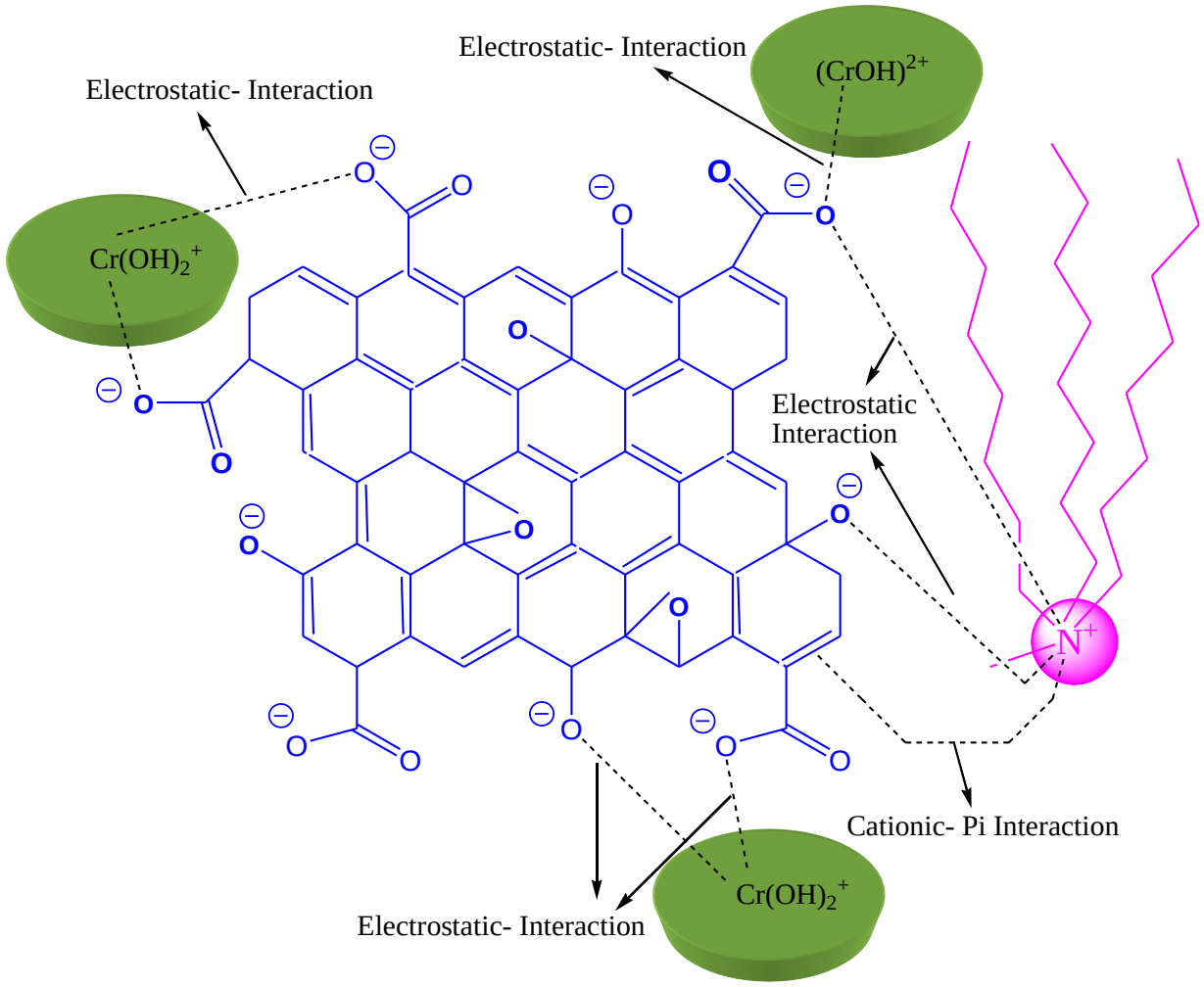

Figure 5.22 Scheme illustrating the interaction between chromium(III), exfoliated graphene oxide, and ionic liquid.

Table 5.4. Study of various isotherm models

Sl. No	Model	Isotherm parameters	
1	Freundlich	K_F (mg $^{1-1/n}$ g^{-1} $L^{1/n}$)	28.11
		N	2.11
		r^2	0.99
2	Langmuir	q_o (mg g^{-1})	285.71
		b (L mg^{-1})	0.0423
		R_L	0.073
		r^2	0.91
3	Redlich Peterson	G	0.773
		B (L mg^{-1})	0.11
		A (L g^{-1})	12.08
		r^2	0.98
4	Temkin	B	49.31
		A (L mg^{-1})	0.785
		b (kJ $mole^{-1}$)	0.05
		r^2	0.88

5	Elovich	q_m (mg g^{-1})	108.69
		K_E (L mg^{-1})	0.1883
		r^2	0.83
6	Dubinin Radushkevich	q_m (mg g^{-1})	123.21
		β (mol^2 kJ^{-2})	0.835
		E (kJ mol^{-1})	0.78
		r^2	0.61

Table 5.5. Kinetic data associated with the adsorption process

Rate constant k_2/(g mg^{-1} min^{-1})	Regression coefficient	Rate constant k_1/ (min^{-1})	Regression coefficient	Intraparticle rate constant k_{int}/(mg g^{-1} $min^{-½}$)
0.0159	0.99	0.0913	0.97	1.552

Table 5.6. Thermodynamics of adsorption

Temperature / (Kelvin)	ΔG^0/ (kJ mol^{-1})	ΔS^0/ (J mol^{-1} K^{-1})	ΔH^0/ (kJ mol^{-1})
303	-8.88	-183.71	-64.01
313	-5.89		
323	-4.1		
333	-3.4		

5.3.4 Conclusions

In conclusion, the IL-EGO adsorbent has shown admirable ability towards the adsorption of Cr(VI). There are no bottlenecks that impede the adsorption process and the facile adsorption is favored by a high adsorption capacity of 285.71 mg g^{-1} and fast sorption kinetics. The thermodynamically favorable adsorption process has paved way for detoxifying chromium from a tannery industry effluent. A notable feature is that Cr(VI) as well as Cr(III) interact with graphene oxide depending on the pH of the medium. This is of considerable significance in the remediation of chromium. Regeneration and stability of adsorbent for 12 repetitive cycles is yet another fitting tribute to this interesting adsorbent material. The ionic liquid- EGO combination has carved a niche among the various other carbon based adsorbents. Certainly, the interaction between Aliquat 336 and exfoliated graphene oxide has laid the basis for the removal of diverse metal ions as well as other pollutants.

A study on the adsorption of Hg^{2+} through its appealing interaction with biopolymer cellulose and mercaptobenzathiazole

5.4.1 Introduction

This chapter deals with the adsorption of mercury involving its interaction with cellulose and mercaptobenzathiazole (MBT). A triangular interaction is envisaged with cellulose acting as a host and MBT as guest in the first instance followed by the subsequent complexation of mercury with MBT. Thanks to the soft-soft interaction between Hg^{2+} and sulfur that augments the effective complexation with MBT. Complexation, electrostatic and hydrogen bonding are the probable mechanistic interactions. The primordial concern for heavy metal pollution has triggered the development of effective adsorbent materials for their remediation.[77] Among the various heavy metals, focus towards alleviating mercury pollution is important in view of its high toxicity.[78] The contamination of mercury from coal combustion[79] is an important issue, since particulate mercury that emanates from fly ash can cause considerable contamination to the atmosphere. The excellent ability of mercury to behave as a typical soft acid[80] makes it very well suited to interact with ligands containing sulphur as the hetero atom. Thiol functionalized silica[81] and ultra stable thiol containing ethane bridged mesoporous organo silica adsorbents[82] are known for their ability to bind Hg^{2+}. Mercaptobenzothiazole is an excellent sulphur ligand known to adsorb and form strong complexes with transition metal ions.[83-85] Chelating 2-mercaptobenzothiazole loaded resin,[86] aminopropylbenzoylazo-2-mercaptobenzothiazole bonded to silica gel,[87] 2-mercaptobenzimidazole-clay,[88] o-benzenedithiol modified cellulose resin[89] are some of the sulphur containing ligands used in conjunction with good solid supports for the adsorption of mercury. The excellent properties attributed to cellulose[90] such as biodegradability, good stability, intramolecular hydrogen bonding etc prompted us to explore its potential for the effective interaction with mercaptobenzathiazole. This would pave way for the subsequent secondary interaction with mercury as the guest. Indeed, this triangular interaction between cellulose, MBT and Hg^{2+} leads to the effective adsorption

of mercury and the efforts directed towards the development of this methodology is given in the following pages.

5.4.2 Experimental Section

(i) Chemicals

Analytical grade reagents were used as such without further purification. Milli Q water (Elix 3) as used to prepare aqueous solutions of Hg^{2+} of varying concentrations. The biopolymer, cellulose was obtained from Himedia, India. Mercury(II) chloride was procured from Merck, India and 2- mercaptobenzothiazole was obtained from Sigma Aldrich. A working solution of 100 mg L^{-1} Hg^{2+} was prepared by appropriate dilution from 1 mg mL^{-1} stock Hg^{2+}. The other necessary reagents required for adsorption studies were procured from Merck, India.

(ii) Adsorbent preparation, Pilot batch and Fixed Bed Column Study

2- mercaptobenzothiazole (0.01 mole) was dissolved in 15 mL of acetone. 5 g of cellulose was taken in a round bottom flask and 15 mL of 2- mercaptobenzothiazole solution was added gradually and reaction mixture was stirred at room temperature for 6 hours. The reaction mixture was filtered, washed with acetone and the adsorbent material was dried at room temperature and used for adsorption studies. Batch adsorption tests were carried out by equilibrating (30 mL of 100 mg L^{-1} Hg(II) solution) adjusted to pH 4 with 0.2 g of the cellulose-MBT adsorbent material. The equilibration was carried out at 150 rpm for different time intervals using an orbital incubator shaker. The adsorption of mercury was ascertained by measuring the concentration left in the aqueous phase using Cold Vapour-Atomic Absorption Spectrophotometric (CV-AAS) method.[91] Fixed bed column study was also performed using a glass column (4 cm diameter, 25 cm length) loaded with 2.5 g of the prepared cellulose-MBT adsorbent at a packing height of 3.5 cm. Maintaining a flow rate of 5 mL min^{-1} and a bed height of 3.5 cm, a 100 mL volume of 30 mg L^{-1} Hg^{2+} was delivered onto the column and the concentration of Hg^{2+} that emerges after adsorption was measured using the CV-AAS technique. The adsorption of mercury was quantitative (99.0%) and confirmed statistically through three replicate measurements with an average error of ± 0.5%. An optimized flow rate of 5 mL min^{-1} at 30 mg L^{-1} Hg^{2+} ensures effective interaction of the cellulose-MBT adsorbent with

mercury. The adsorption was also quantitative till 500 mL sample volume (Figure 5.23). At higher volumes, the effectiveness of adsorbent-adsorbate interaction decreases, thereby signifying the saturation of the adsorption bed.

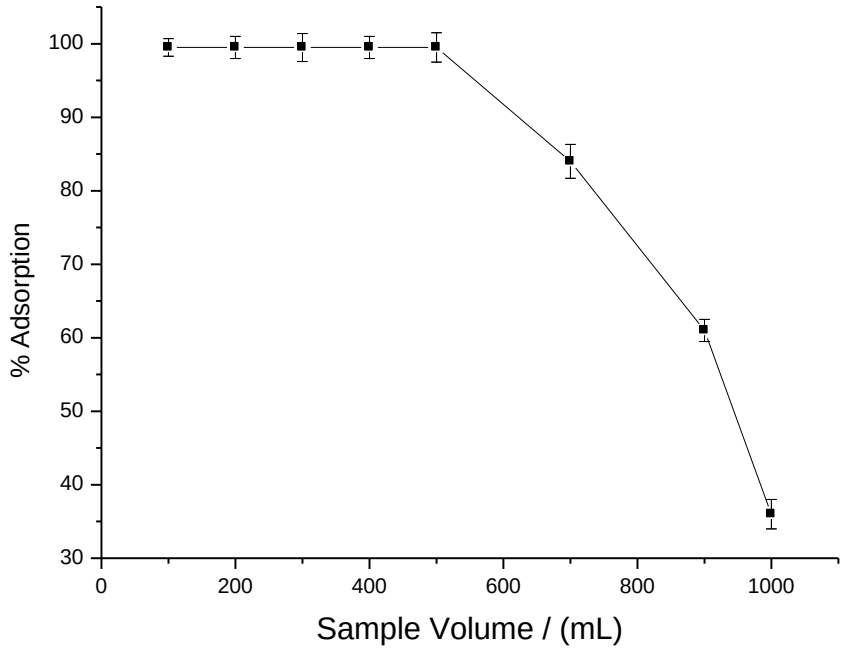

Figure 5.23. Variation of sample volume

5.4.3 Results and Discussion

(i) Surface Morphological Changes and XRD Pattern of the Adsorbent

The SEM images taken prior and after the adsorption of mercury does show (Figure 5.24) some observable changes in the surface morphology of the cellulose-MBT adsorbent with regard to the porosity and surface homogeneity. The adsorption of mercury on the surface of 2- mercaptobenzothiazole impregnated the cellulose adsorbent was also confirmed through the energy dispersive X ray (EDS) spectral analysis (Figure 5.25). The adsorption of mercury is evident from the characteristic peak in the range 1-3 keV along with C, O, N, and S typical of the adsorbent.[92] The X-ray diffraction pattern of the

adsorbent gives valuable insight into the crystalline or amorphous nature of the adsorbent. The initial amorphous feature of the adsorbent assumes a slight crystalline nature as evident from the sharpening of the peaks after the adsorption of mercury. The XRD pattern of the cellulose shows peaks (Figure 5.26) corresponding to 2θ values 14.77^0, 16.44^0, 22.71^0 and 34.62^0 respectively.[93] The interaction of 2-mercaptobenzothiazole with cellulose yields new peaks at 13.41^0, 15^0, 15.56^0, 25.19^0, 29^0 and 34.86^0 respectively. The secondary interaction of mercury with the cellulose-MBT adsorbent gives characteristic peaks at 29.50^0, 39.44^0, 47.67^0 and 48.85^0. These results indicate that the metal ion can penetrate easily onto the adsorbent surface and interact effectively with the functional groups present in cellulose and the hetero atoms present in 2 -mercaptobenzathiazole.

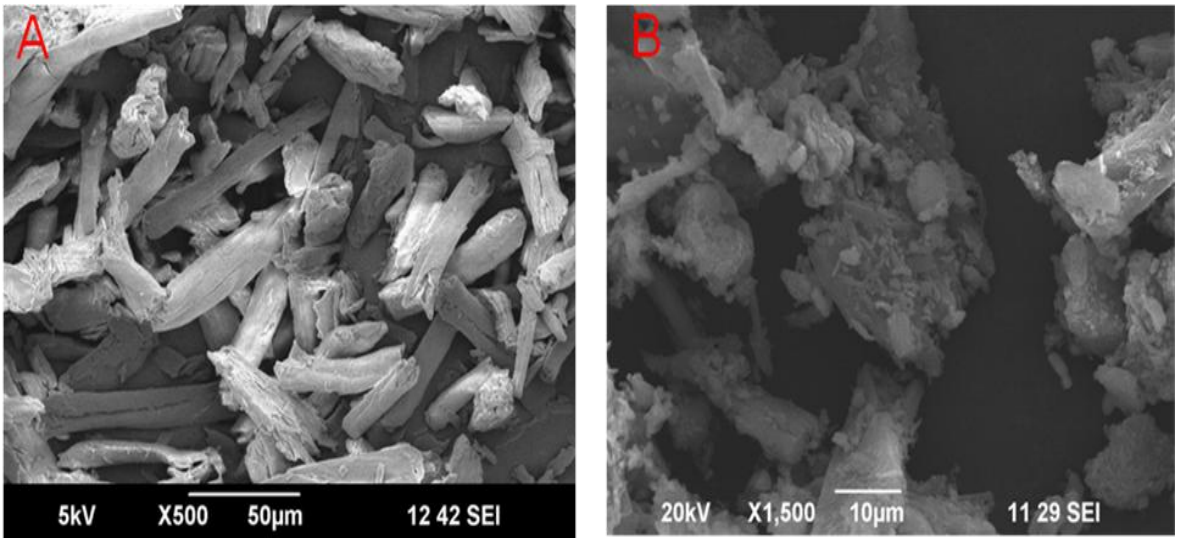

Figure 5.24. SEM images (a) Mercaptobenzothiazole impregnated cellulose adsorbent (b) After the adsorption of Hg^{2+}

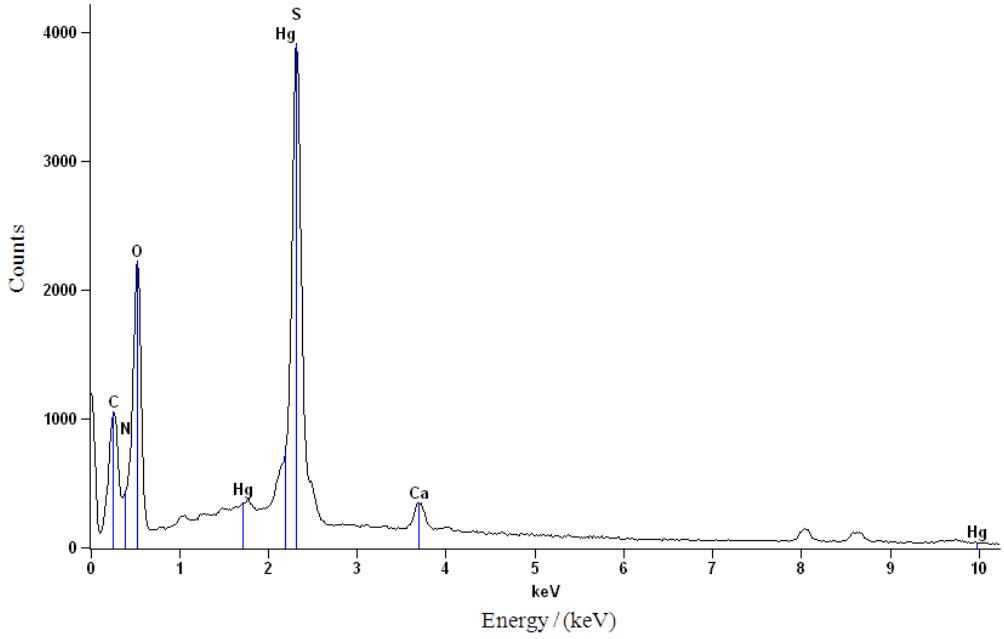

Figure 5.25. EDS spectral analysis showing the presence of adsorbed mercury

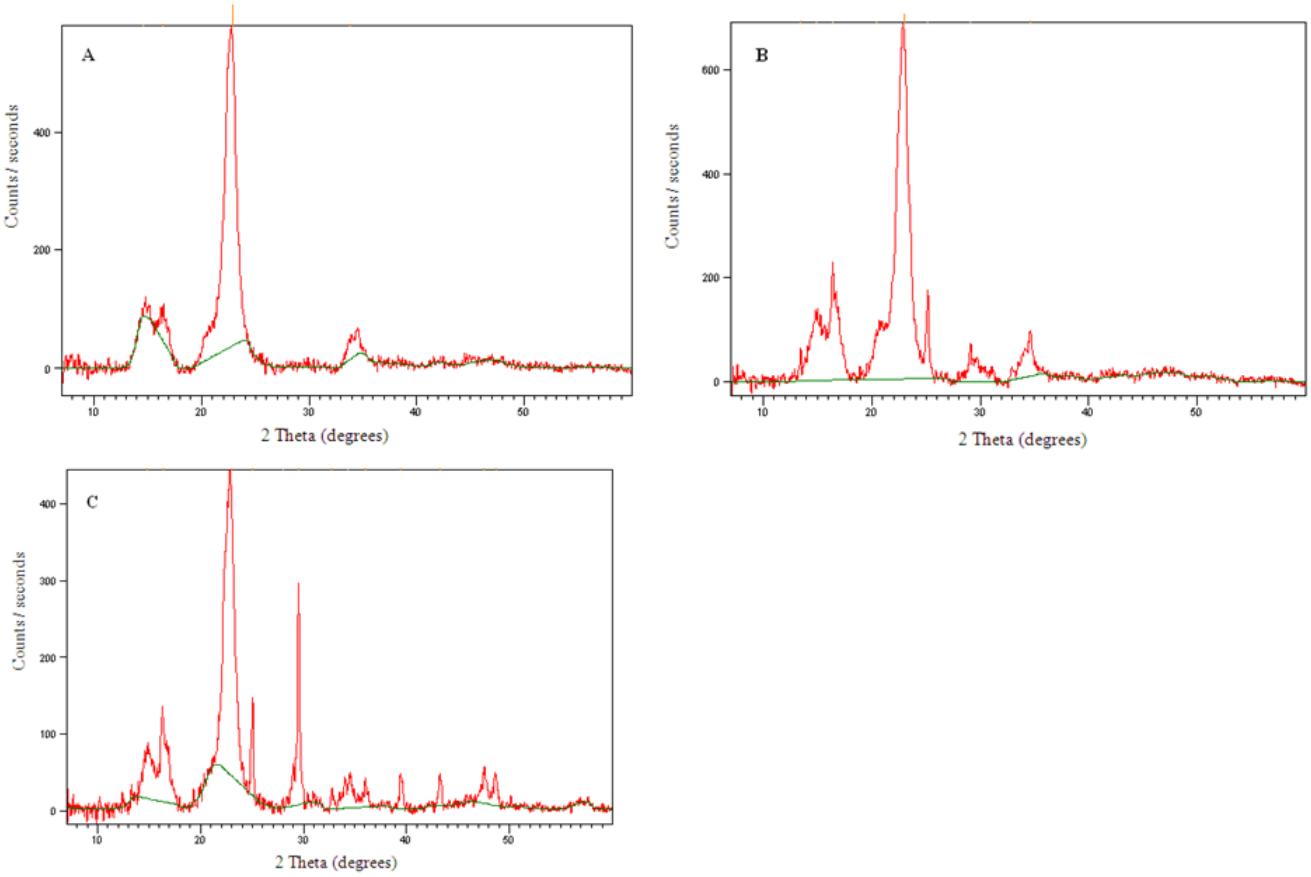

Figure 5.26. XRD pattern (a) Cellulose (b) Mercaptobenzothiazole impregnated cellulose adsorbent (c) After the adsorption of Hg^{2+}

(ii) Mechanism, FT-IR Analysis and Thermodynamics of the Adsorption Process

The interaction of Hg^{2+} with MBT on the cellulose matrix is dependent on pH of the aqueous medium. The optimum pH for the complexation was found to be in the range (3- 4.0). Beyond pH 4.0, there is a decrease in the percentage adsorption of mercury. This could be ascribed to the formation of hydroxy species of mercury $(Hg(OH)_2$, $Hg(OH)^+$ at higher pH range.[74] The sorption of heavy metals involves the interaction of the functional groups on the sorbent and several mechanisms such as ion exchange, complexation and electrostatic attraction. The interaction of cellulose-MBT- Hg^{2+} could be conceived involving the affinity between the three species (Figure 5.27). The primary interaction would involve the hydrogen bonding between the hydroxy groups in cellulose and the S

as well as N atoms present in the ligand. The lone pair directionality is quite important in the hydrogen bonding [14,94] involving the N…H-O and S-H…O interactions. Herein, cellulose acts as an effective host and the guest MBT can enter the voids present in the cellulose polymeric chain and could also anchor onto the surface of the biopolymer. The subsequent interaction would involve the affinity of Hg^{2+} with the biopolymer as well as the ligand. The mechanism of Hg^{2+} adsorption onto mercaptobenzothiazole-impregnated cellulose is proposed to occur via intermolecular hydrogen bonding, chelation (co-ordination) and electrostatic interaction.[93] Hg^{2+} being a typical soft acid has the ability to co-ordinate with sulfur and nitrogen in MBT to form a stable metal chelate-complex. The lone pair of electrons in the cellulose hydroxy groups could also interact with the metal ion through ion-dipole interactions. FT-IR spectra of the pure cellulose, mercaptobenzothiazole impregnated cellulose and Hg(II)-treated adsorbent were examined to elucidate the mechanism of interaction of Hg(II) with the adsorbent (Fig. 5). The FT-IR spectrum of the polysaccharide cellulose which fundamentally comprises of several D-glucose units shows prominent peaks characteristic of O-H, C–O and glycosidic linkages.[95] The peaks at 2962 cm^{-1} and 3372 cm^{-1} could be attributed to the C-H and O-H stretching respectively. An O-H deformation peak is observed at 1430 cm^{-1} and 1364 cm^{-1}. The peak at 889 cm^{-1} is assigned to the C-O-C stretching in the glycosidic linkages of the polysaccharide. The ring stretching of glucose is observed at 1112 cm^{-1}. The peak due to C–O stretching vibrations in cellulose is observed at 1035 cm^{-1} cellulose. The cellulose-MBT adsorbent shows characteristic peaks in the range 2500-2600 cm^{-1} attributed to the polarizable S-H stretching [96] and the peak at 1642 cm^{-1} could be ascribed to the C=N stretching vibration. The C-N (phenyl carbon-nitrogen bond) stretching frequency is observed at 1314 cm^{-1} [97]. It has been reported through density functional theory calculations that the C-S stretching frequency in IR spectrum of MBT could have a range between 572-876 cm^{-1} and notably the significant peak which we observed at 875 cm^{-1} could be attributed to the C-S region. The partial oxidation of cellulose could lead to the introduction of the carbonyl functional group observed [98] at 1796 cm^{-1}. After the adsorption of mercury, the changes are reflected by the appearance of new peaks at 1639 cm^{-1} and 3346 cm^{-1}. These changes points to the fact that the

chelation of mercury with MBT could occur through the sulfur and nitrogen atoms. The change in the O-H stretching frequency also indicates the plausible electrostatic interaction of Hg^{2+} with the lone pair of electrons present in the oxygen atom of cellulose hydroxy groups.[99] The ligand, MBT could be conformationally oriented in the cis or trans form depending on whether the S-H bond is eclipsing the C=N or the C=S bond.[100] It is more probable that in the cis form the interaction of mercury would be more facile with the hetero atoms sulphur and nitrogen. Furthermore, when 2- mercaptobenzothiazole approaches the host biopolymer in the reaction medium, there is a disorder accompanied by translational entropy gain[40] and results in the positive entropy in this primary interaction. Essentially, the biopolymer also needs to be conveniently oriented in order to house the ligand in the layer between the polymeric chains and to promote good interaction with the hetero atoms present in the ligand. This could be further corroborated by taking into account the respective Gibb's free energy changes associated with biopolymer cellulose, 2- mercaptobenzothiazole and mercury.

$$\Delta G_{biopolymer} = \Delta H_{biopolymer} - T\Delta S_{biopolymer} \quad (16)$$

$$\Delta G_{(MBT)} = \Delta H_{(MBT)} - T\Delta S_{(MBT)} \quad (17)$$

$$\Delta G_{mercury} = \Delta H_{mercury} - T\Delta S_{mercury} \quad (18)$$

$$\Delta G_{adsorption} = \Delta H_{adsorption} - T(\Delta S_{biopolymer} + \Delta S_{(MBT)} + \Delta S_{mercury}) \quad (19)$$

The entropy factor on the whole depends on the contribution that stems from the corresponding entropy changes associated with cellulose, 2- mercaptobenzothiazole and the metal ion. Hence, the $T(\Delta S_{cellulose} + \Delta S_{MBT} + \Delta S_{mercury})$ is more positive and this implies that the physico-chemical adsorption process is spontaneous. The study of the adsorption of mercury onto the cellulose-MBT adsorbent at different temperatures gives the valuable thermodynamic parameters and also aids in further corroborating the adsorption mechanism. The Van't Hoff equations relate the equilibrium constant to the Gibb's free energy, entropy and enthalpy of adsorption as follows

$$\Delta G^0 = -RT\ln K \qquad (20)$$

$$\ln K = \frac{-\Delta H^0}{RT} + \frac{\Delta S^0}{R} \qquad (21)$$

The equilibrium constant K is acquired from the ratio of concentration of Hg(II) adsorbed on the 2- mercaptobenzothiazole impregnated cellulose adsorbent to that in the aqueous phase. The positive and negative values of ΔH^0 would give an insight into the exo or endothermic nature of adsorption. The Van't Hoff plot (Figure 5.28) would yield the ensuing enthalpy and entropy changes associated with the adsorption process. We observed the ΔG^0 values to be negative with varying temperatures thereby leading to the rational conclusion that the adsorption is indeed spontaneous and endothermic (Table 5.7). Since, Hg^{2+} is a typical soft acid, it interacts effectively with sulfur and nitrogen atoms of the ligand. The negative free energy (ΔG^0) values confirm the effectiveness of the affinity between cellulose, 2- mercaptobenzothiazole and Hg^{2+} .The magnitude of ΔH^0 is generally less than 80 kJ mol^{-1} for physisorption, while for chemical adsorption it is in the range 80- 400 kJ mol^{-1}.[101] The positive entropy and enthalpy changes associated with the adsorption also reflect the randomness at the adsorbent-solution interface, endothermic adsorbent-adsorbate interaction and the decrease in the hydration of the ions.

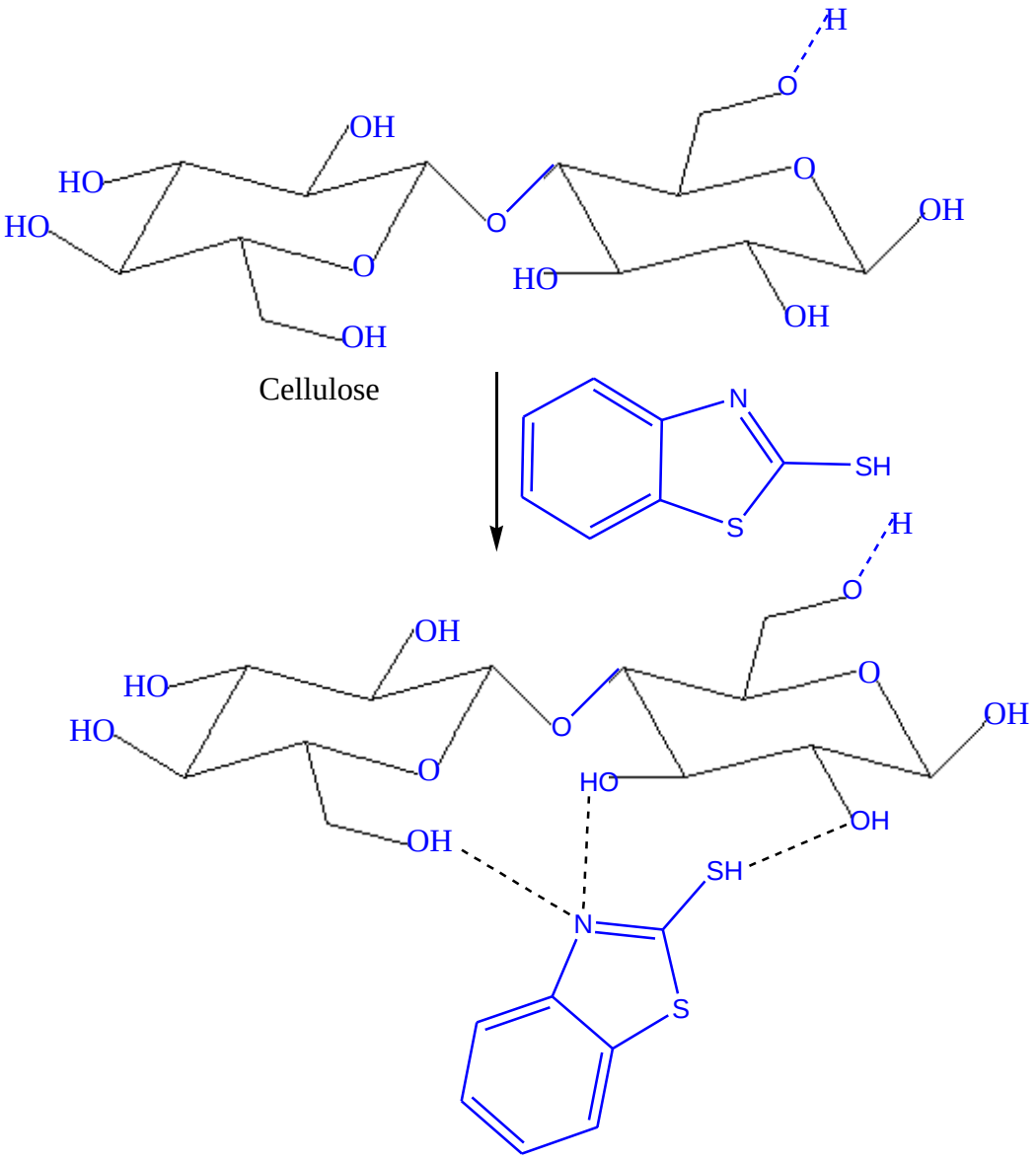
H
O
OH
HO
HO
O
O
OH
HO
OH
OH
Cellulose
N
SH
S
H
O
OH
HO
HO
O
O
O
OH
HO
OH
OH
SH
N
S

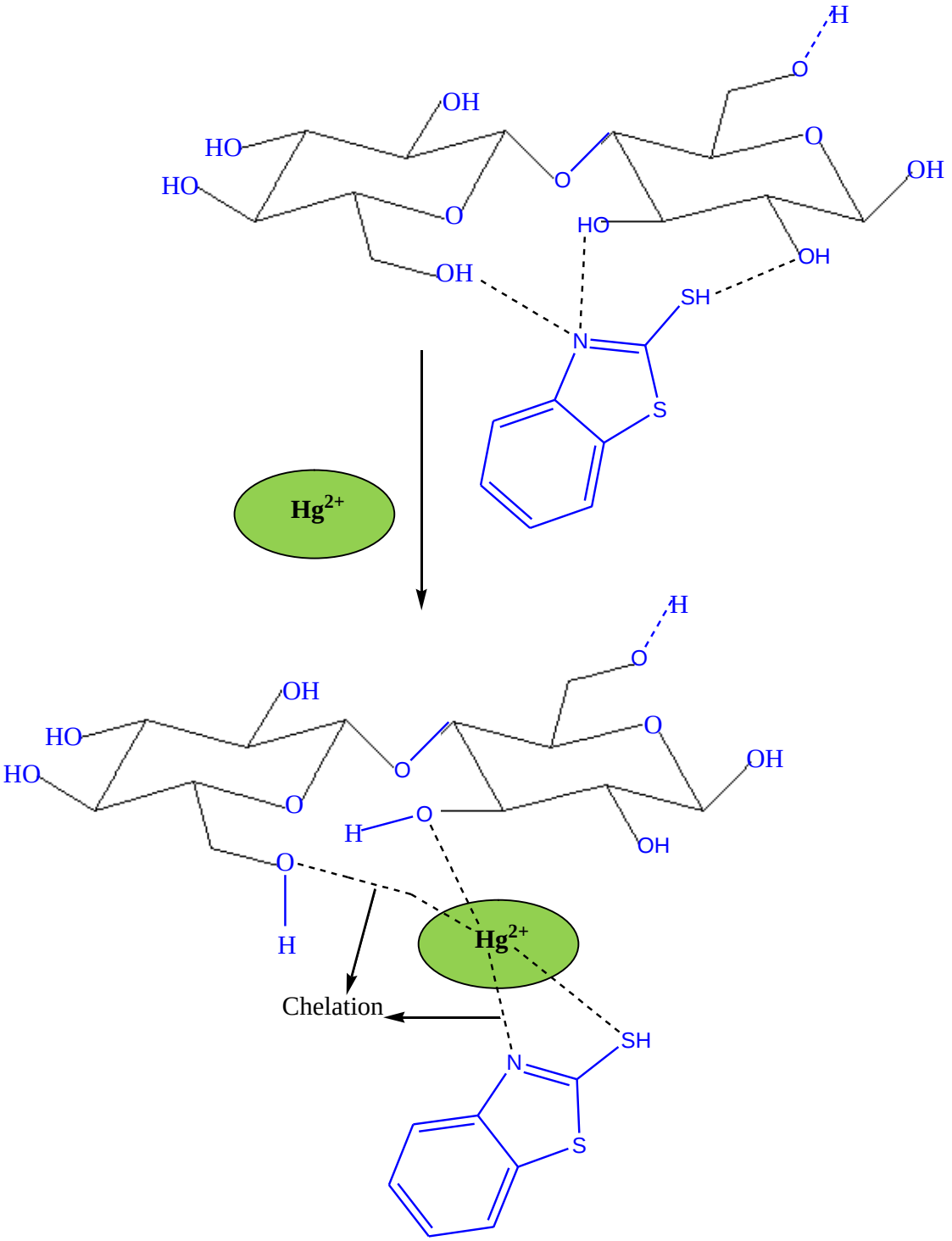

Figure 5.27 Conceptual illustrations depicting the interaction of cellulose, MBT and Hg^{2+}

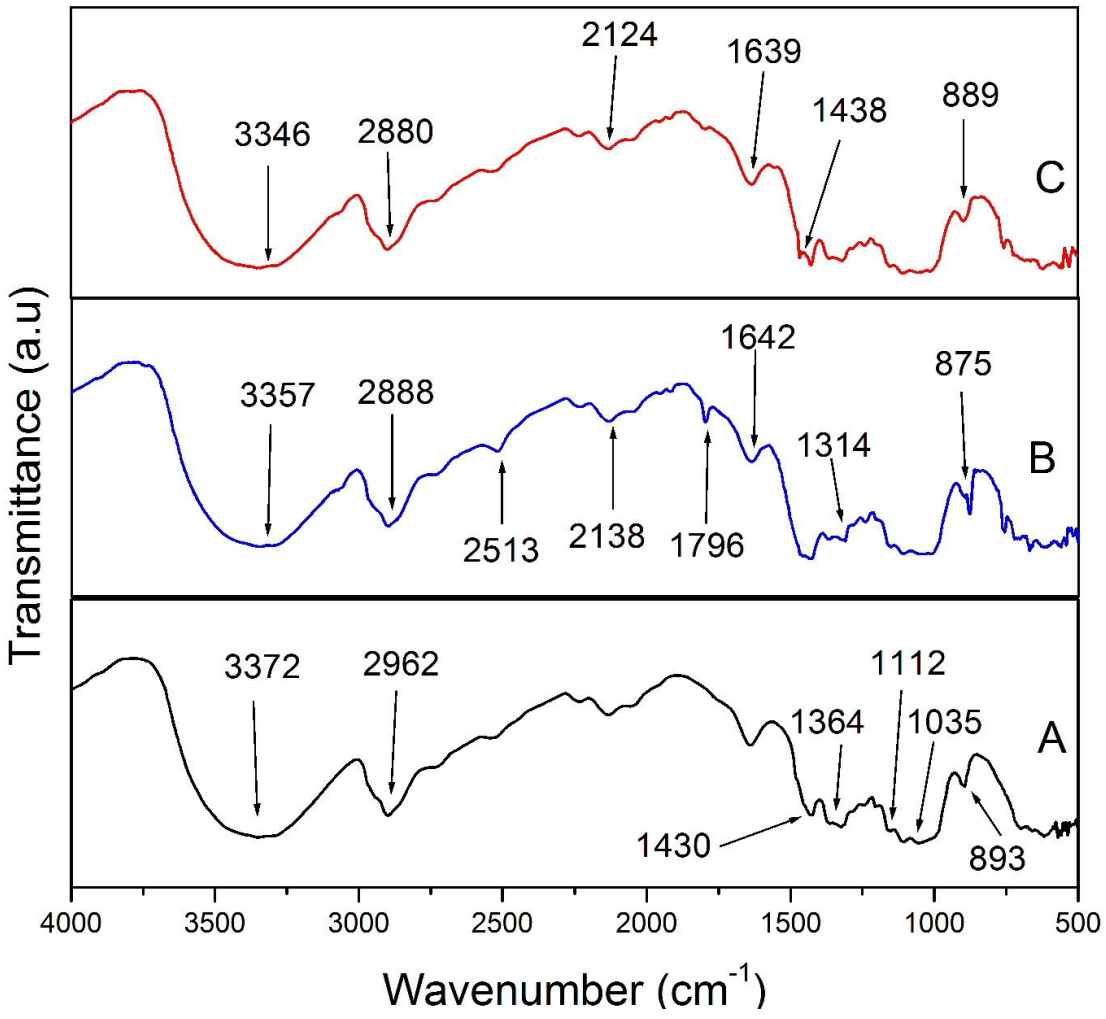

Figure 5.28 FT-IR spectrum of (A) Cellulose (B) adsorbent (C) After adsorption of Hg^{2+}

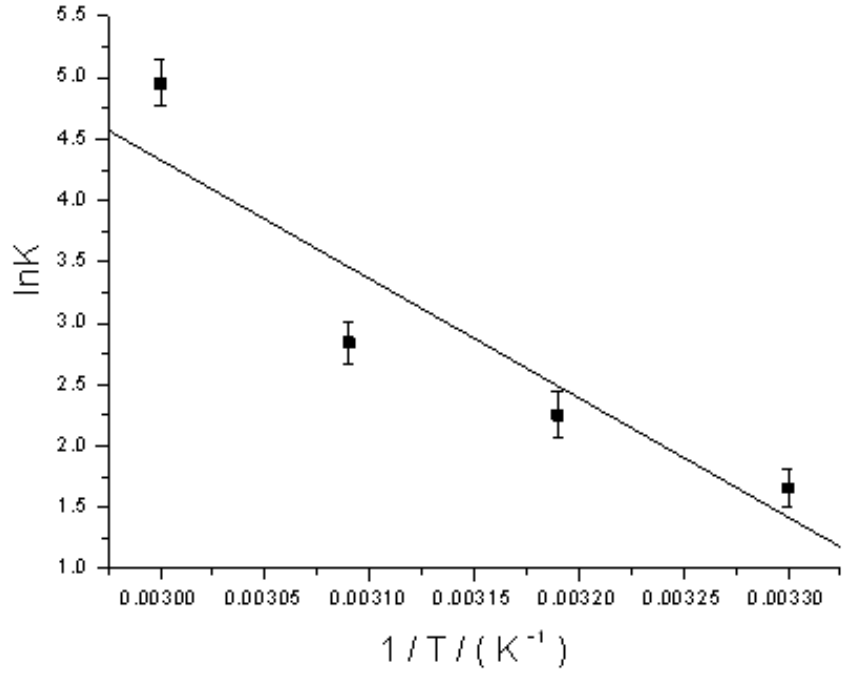

Figure 5.29. Variation of equilibrium constant with temperature

Table 5.7. Thermodynamic parameters for the adsorption of mercury

Temperature/ (Kelvin)	ΔG^0 / (kJ mol^{-1})	ΔS^0 / (J mol^{-1} K^{-1})	ΔH^0 / (kJ mol^{-1})
303	-4.17	279	81
313	-5.86		
323	-7.63		
333	-13.71		

(iii) Adsorption Kinetics and Isotherm Models

The experimental data obtained from the adsorption of mercury onto the MBT-cellulose adsorbent were assessed using the familiar Lagergen[33] and Ho[34] first and second order kinetics. The plot of log (q_e-q_t) against t (Figure 5.30a) and t/q_t against t (Figure 5.30b) would yield the required kinetic parameters. The pseudo second order model gave a good fit to the experimental data and this is also corroborated from the higher regression coefficient value. Another characteristic fact to augment this feature is obtained from the equilibrium adsorption capacity values (q_e (exp) and q_e calculated). The $q_{e\ calculated}$ and $q_{e\ exp}$ values were found to be 15.11 mg g^{-1} and 14.91 mg g^{-1} which stands testimony to the pseudo second order kinetics (Table 5.8) in fitting the experimental data. Pore, surface and intraparticle diffusion could be the possible modes of adsorption of mercury onto the MBT-cellulose adsorbent surface. The likelihood of intraparticle diffusion also is fairly inherent in understanding the adsorption process. The Weber-Morris[35] diffusion model describes this reasonably well and correlates the amount of Hg^{2+} adsorbed to the diffusion rate constant (k_{int}). A fit of the experimental data to this model yields the k_{int} from the slope of the q_t versus $\sqrt{t}$ linear plot. (Figure 5.30c). If this plot passes through origin, we could postulate that intraparticle diffusion is the only process that affects the adsorption. However, the experimental data in the present system yields a plot with a non-zero intercept and this indicates that the boundary layer effect could also influence the adsorption kinetics of mercury onto the MBT-cellulose adsorbent. Furthermore, the fact that q_t increases with the time of adsorption t, shows that at the outset the external surface diffusion could influence the adsorption kinetics followed by intraparticle diffusion as the step that defines the rate of adsorption of mercury. The well established Langmuir, Freundlich and other typical isotherm models were utilized to fit the experimental adsorption data.[26,28-30] Each of these models gives certain distinctive isotherm constants (Table 5.9) and various empirical equations are employed in calculating these parameters. The maximum adsorption capacity (q_o) and the adsorption energy b could be calculated from the Langmuir isotherm plot of C_e/q_e against C_e (Figure 5.30d). A high Langmuir adsorption capacity of 204.08 mg g^{-1} signifies the ability of 2-mercaptobenzothiazole impregnated cellulose as an excellent adsorbent for mercury. The

separation factor obtained (R_L =1/1+bC_o) obtained from this model was found to be <1 which further justifies the effectiveness of triangular interaction.[27] The fact that the experimental data could also be elucidated based on Langmuir model is evident from the value of the exponent g which is near unity as obtained from the Redlich-Peterson isotherm model ((Figure 5.30e) The Freundlich isotherm plot of log q_e versus log C_e (Figure 5.30f) is used to calculate the adsorption intensity n and the adsorption capacity K_F. The adsorption intensity n and the high regression coefficient of 0.97 indicate the effective uptake of mercury by the cellulose-MBT adsorbent. Since, 1/n is less than unity, it also indicates an ordinary L type Langmuir isotherm.[102] The various isotherm data plots of q_e against C_e (Figure 5.30g) also show that the experimental data connects well with the Freundlich isotherm model. The efficacy of the triangular interaction between cellulose, MBT and Hg^{2+} is evident from the rising portion of this plot and the saturation obtained at higher values of C_e. The mean free energy of adsorption, E_{DR} value obtained from the Dubinin-Raduksveich model (Figure 5.30h) is indicative of the physical adsorption between mercury and the 2- mercaptobenzothiazole impregnated cellulose adsorbent.

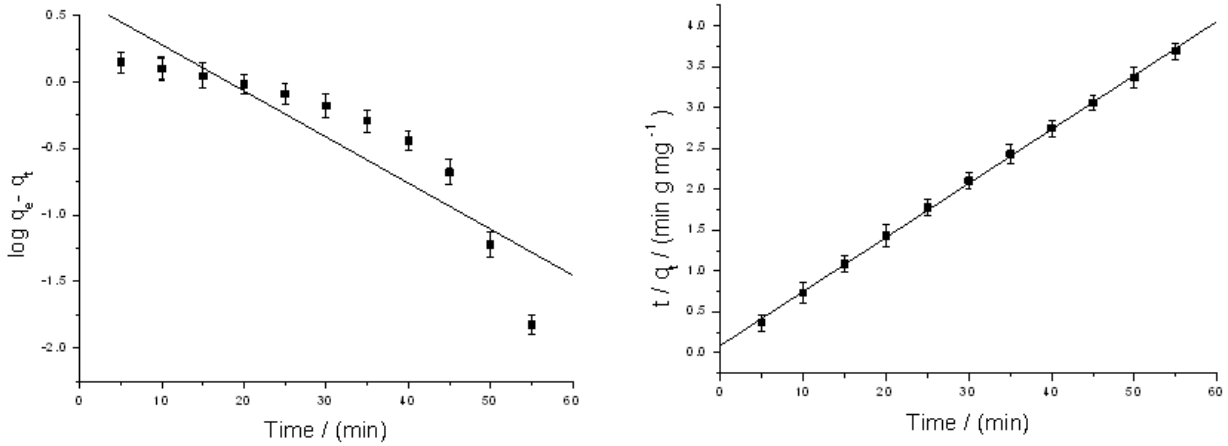

Figure 5.30. (A) Pseudo first order kinetic plot (B) Pseudo second order kinetic plot

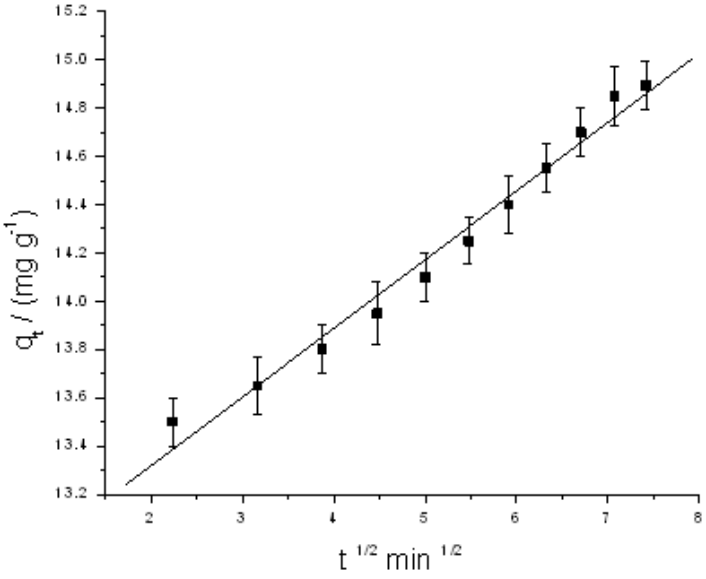

Figure 5.30 (C) Weber-Morris plot

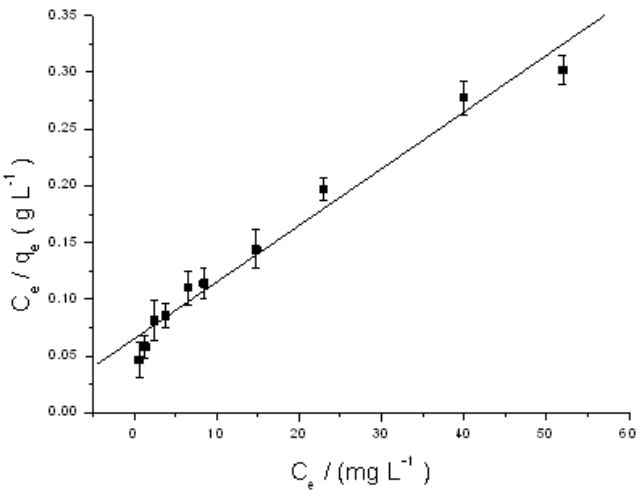

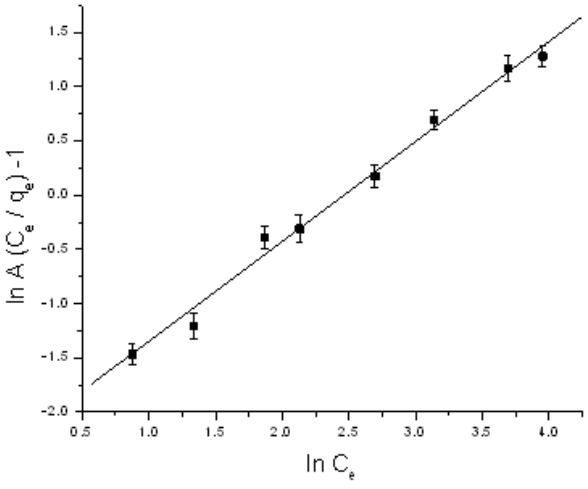

Figure 5.30 (D) Langmuir isotherm (E) Redlich–Peterson isotherm

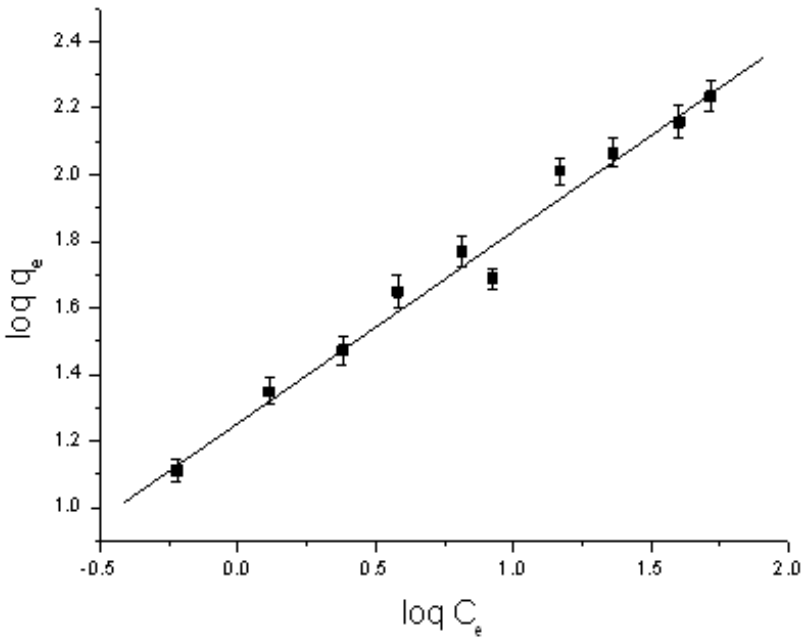

Figure 5.30(F) Freundlich isotherm

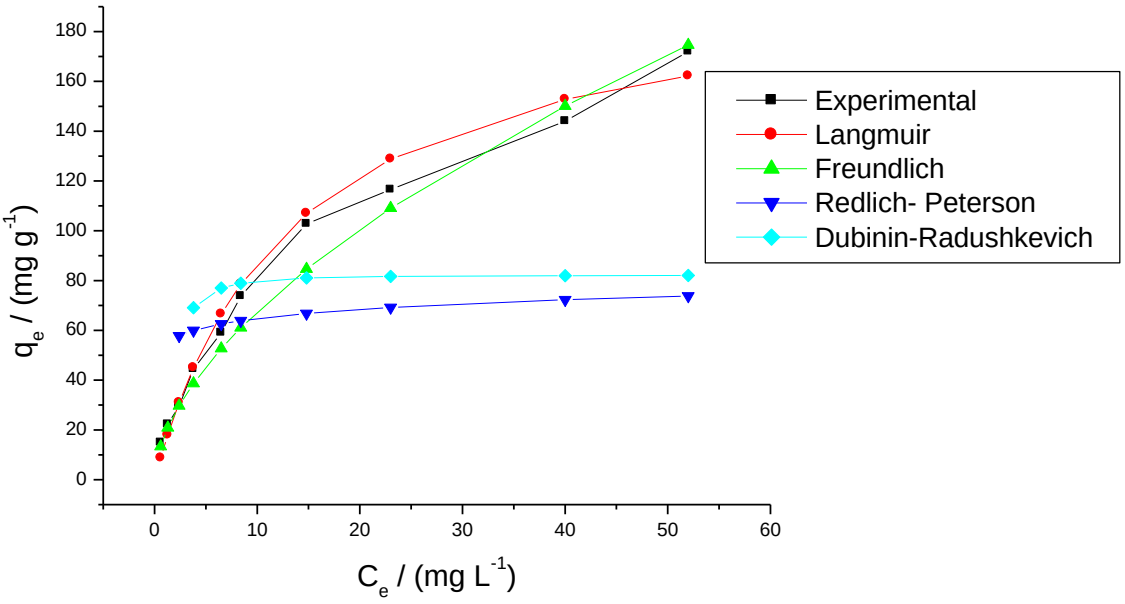

Figure 5.30 (G) Plot of q_e against C_e

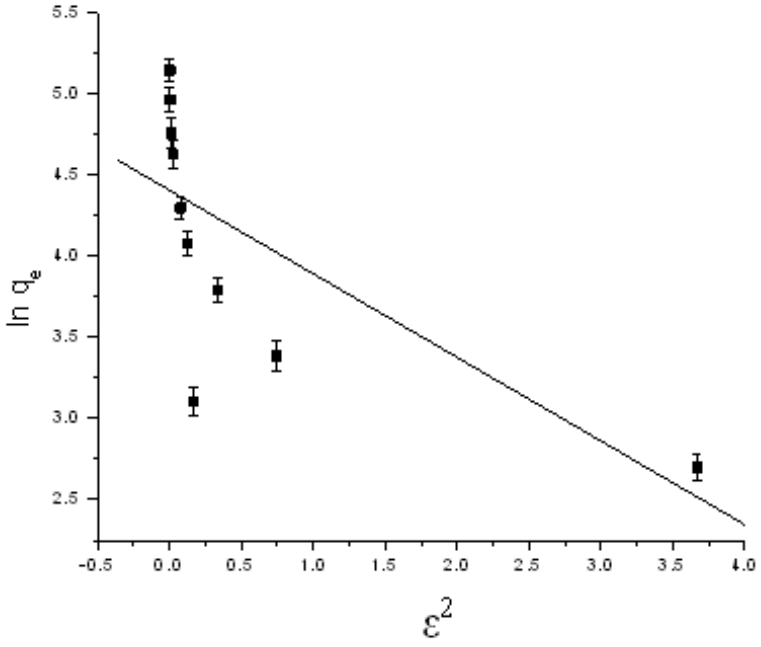

Figure 5.30 (H) Dubinin-Radushkevich Isotherm

Table 5.8. Kinetic parameters associated with the adsorption of mercury

k_2/(g mg^{-1} min^{-1})	Regression coefficient	k_1 / (min^{-1})	Regression coefficient	k_{int}/(mg g^{-1} $min^{-½}$)
0.0496	0.99	0.079	0.80	0.284

Table 5.9. Isotherm parameters

Isotherm model	Parameters	Values
Langmuir	q_o (mg g^{-1})	204.08
	b (L mg^{-1})	0.0745
	R_L	0.11
	r^2	0.97
Freundlich	K_F (mg $^{1-1/n}$ g^{-1} $L^{1/n}$)	17.93
	n	1.73
	r^2	0.97
Redlich Peterson	g	0.92
	B (L mg^{-1})	0.103
	A (L g^{-1})	15.20
	r^2	0.99
Dubinin Radushkevich	q_m (mg g^{-1})	82.12
	β (mol^2 kJ^{-2})	0.515
	E (kJ mol^{-1})	0.985
	r^2	0.50

(iv) Regeneration and Recycle of the Adsorbent

Regeneration and recycling of the adsorbent are two parameters that are imperative in any adsorption. This would reflect the stability of the adsorbent in the presence of other constituents present in real samples. We scrutinized reagents such as potassium thiocyanate (KSCN) (2 mol L^{-1}), EDTA (3 mol L^{-1}), thiourea (4 mol L^{-1}), potassium iodide (1 mol L^{-1}) and potassium chloride (2 mol L^{-1}) for the potential desorption of Hg^{2+} from the adsorbent column. Thiocyanate, EDTA and thiourea[74] are known for their ability to complex Hg^{2+} through the heteroatoms sulfur, nitrogen and oxygen. Potassium iodide and chloride could assist in desorbing Hg^{2+} as their respective tetrahalo complexes. The ability of the above mentioned reagents in the desorption of mercury were found to be KSCN (98.5%) > EDTA (89.0%) > thiourea (83%) > potassium iodide (71%) > potassium chloride (63%) respectively. In the proposed method involving the adsorption of mercury onto the cellulose-MBT adsorbent, we found that 20 mL of 2.0 mol L^{-1} (KSCN) was most effective in quantitative desorption (98.5 ±0.35 %) of Hg^{2+}. Apparently, thiocyanate has the ability to link Hg^{2+} through the soft sulfur atom more effectively in transporting the Hg^{2+} from the adsorbent surface to the aqueous phase (Figure 5.31). The high stability constant could favor the elution of mercury as its tetrathiocyanato mercury (II) complex effectively. The biopolymer-MBT adsorbent was stable for 5 adsorption-desorption cycles without any obvious decrease in the efficacy of the adsorbent column.

(v) Diverse ion Effect

The presence of N and S atoms in the MBT ligand could prove to quite conducive for a variety of transition metal ions to chelate and interfere with the adsorption process. In order to investigate the adsorption selectivity of the cellulose-MBT adsorbent, studies were conducted in the presence of metal ions such as Mn^{2+} (250 mgL^{-1}) Al^{3+} (250 mgL^{-1}) Cd^{2+} (100 mgL^{-1}), Ni^{2+} (300 mgL^{-1}) Co^{2+} (200 mgL^{-1}), Fe^{2+} (200 mgL^{-1}), Pb^{2+} (100 mg L^{-1}), Zn^{2+} (250 mgL^{-1}) and Cu^{2+} (200 mgL^{-1}) independently in a 200 mL sample volume containing 30 mg L^{-1} Hg^{2+}. Pb^{2+}, Cd^{2+}, Zn^{2+} interfered by reducing the adsorption of mercury by 20-25% at the levels mentioned above and this is ascribed to their competition with mercury for the ligand and the active adsorption sites. Anions such as SO_4^{2-} (200 mgL^{-1}), NO_3^-(250 mgL^{-1}), PO_4^{3-}(200 mgL^{-1}), Cl^- (100 mgL^{-1}) did not decrease the adsorption capacity of mercury.

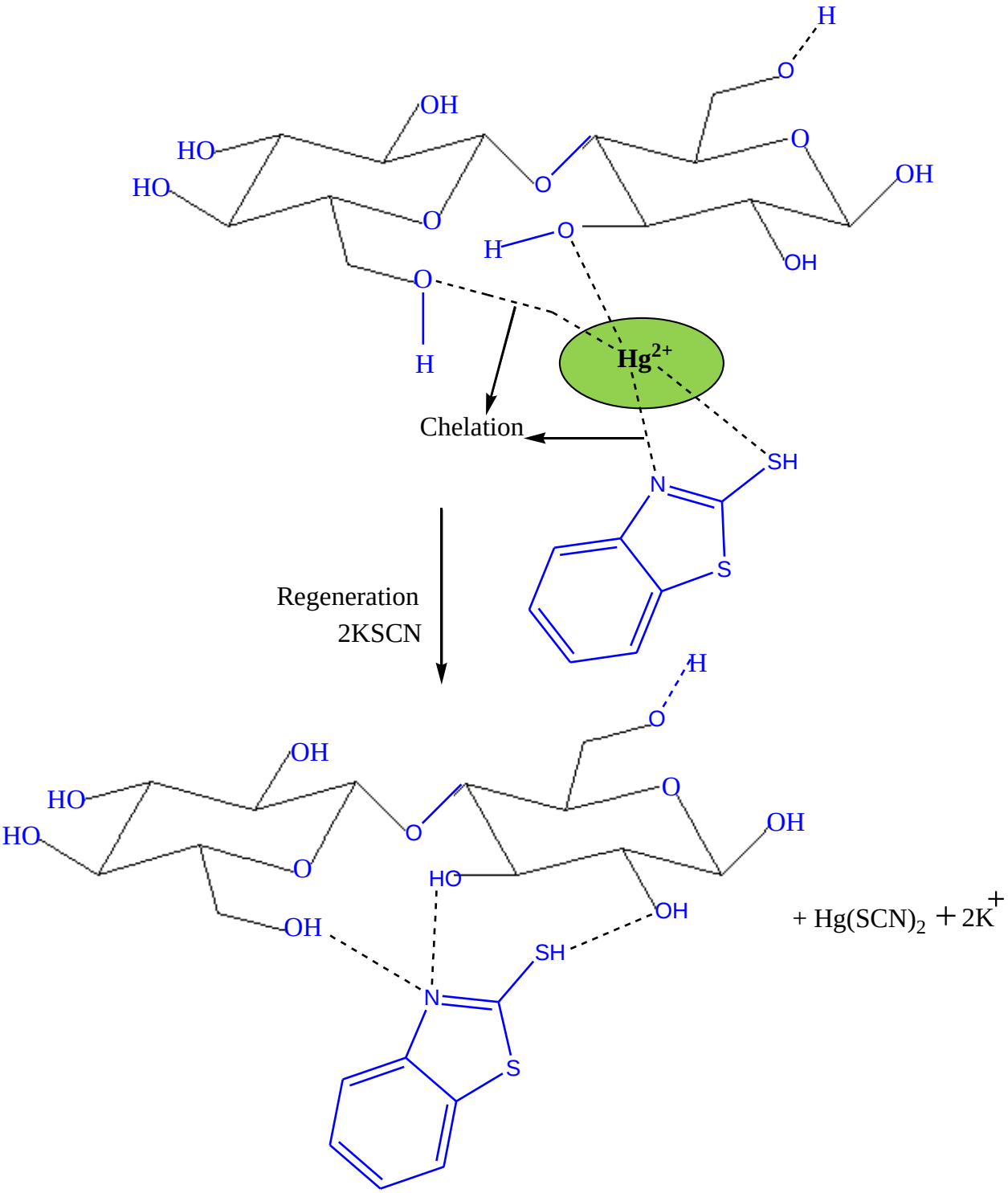

Figure 5.31 Scheme representing the regeneration of the cellulose-MBT adsorbent

(vi) Application to Study the Adsorption of Mercury from a used CFL

The effectiveness of the cellulose-MBT sorbent was tested to adsorb mercury vapor emanating from a used compact fluorescent lamp. Indeed, sulfur impregnated adsorbents[103] are quite effective in the insitu capture of mercury from compact fluorescent lamps. Preliminary studies were conducted to explore the prospective application of the biopolymer-thiol ligand for the insitu adsorption of mercury. The CFL was broken carefully and the fractured pieces were transferred to a short sealed polypropylene tube containing the adsorbent. The adsorbent powder was left in contact with the fractured lamp overnight (approx 24 hours) and the broken pieces were removed cautiously and separated from the powdered adsorbent material. The mercury vapor was adsorbed onto the surface of the adsorbent and this was ascertained from the EDS peak (Figure 5.32) obtained for mercury after the adsorption.

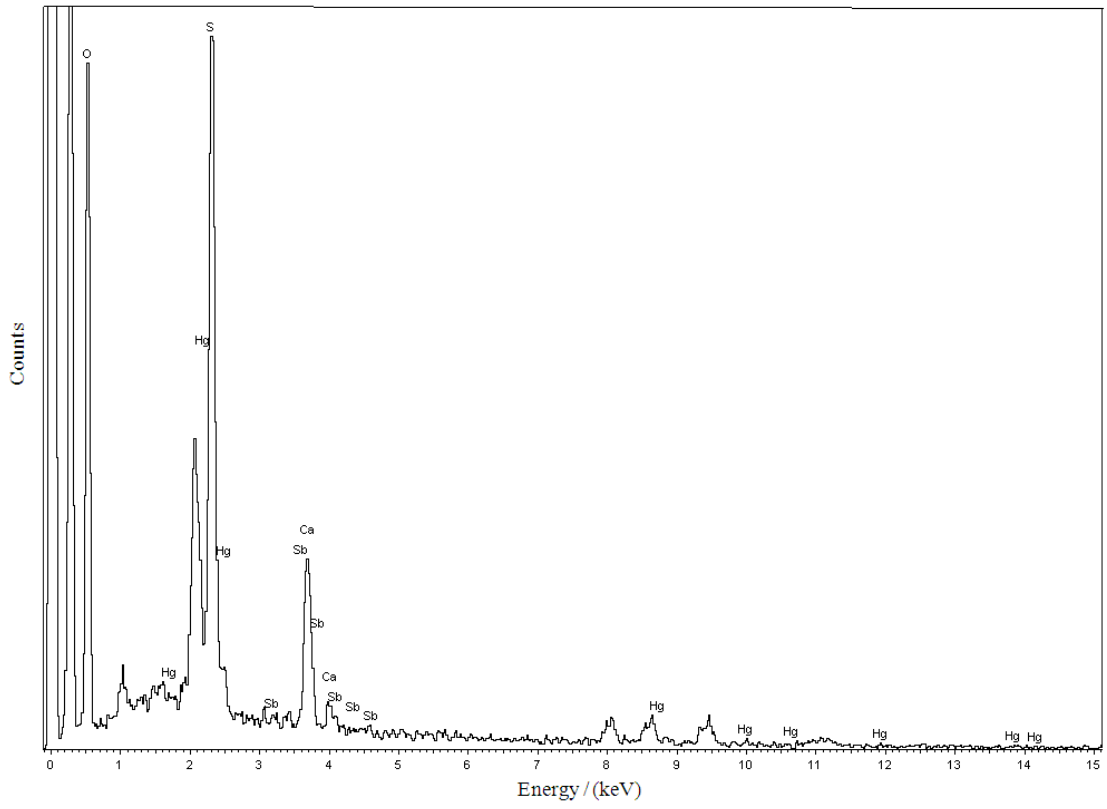

Figure 5.32. EDS spectrum of the adsorbent after insitu entrapment of mercury vapor from CFL

5.4.4 Conclusions

The legacy of biopolymer cellulose finely woven as an effective adsorbent by interaction with MBT has enhanced the adsorption of mercury. The pivotal role played by the ligand and the biopolymer has fostered the effective soft-soft interaction of the heteroatom sulfur and the lone pair-ion dipole interactions of the surface hydroxyl groups of cellulose with mercury. The pseudo second order kinetics and the thermodynamics of the entropically favorable spontaneous adsorption support the mechanism of interaction. The excellent sorption capacity (204.8 mg g^{-1}) that could be realized using this adsorbent is another high point of this method. Effective regeneration of the adsorbent using potassium thiocyanate and the enrichment to a sample volume of 500 mL is an added advantage associated with the method. Above all, the adsorbent shows considerable promise in adsorbing mercury vapour from a used CFL which could certainly lead to fascinating and diverse applications of this sulfur ligand impregnated biopolymer adsorbent.

References

1. Ravi Kumar, M. N. V. *React. Funct. Polym.* **2000**, *46,* 1.
2. Bhatnagar, A.; Sillanpaa, M. *Adv. Colloid Interface Sci.* **2009**, *152,* 26.
3. Wan Ngah, W. S.; Isa, I. M. *J. Appl. Polym. Sci.* **1998**, *67,* 1067.
4. Wan Ngah, W. S.; Liang, K. H. *Ind. Eng. Chem. Res.* **1999**, *38,* 1411.
5. Cervera, M. L.; Arnal, M. C.; De la Guardia, M. *Anal. Bioanal. Chem.* **2003**, *375,* 820.
6. Jin, L.; Bai, R. B.; *Langmuir*. **2002**, *18,* 9765.
7. Guibal, E. *Sep. Purif. Technol.* **2004**, *38,* 43.
8. Hu, X. J.; Wang, J. S.; Liu, Y. G.; Li, X.; Zeng, G. M.; Bao, Z. L.; Zeng, X. X.; Chen, A.W.; Long, F. *J. Hazard.Mater.* **2011**, *185,* 306.
9. Liu, T.; Wang, Z. L.; Zhao, L.; Yang, X. *Chem. Eng. J.* **2012,** *189,* 196.
10. Wan Ngah, W. S.; Teong, L.C.; Hanafiah, M.A.K.M. *Carbohydr. Polym.* **2011**, *83,* 1446.
11. Mendham, V. J.; Denny, R. C.; Barnes, J. D.; Thomas, M. J. K. Pearson Education, Singapore: **2002.** *1*, 668.
12. Huacai, G.; Wan, P.; Dengke, L. *Carbohydr. Polym.* **2006**, *66*, 372.
13. Depan, D.; Kumar, A. P.; Singh, R. P. *J. Biomed. Mater. Res.* **2006**, *78*, 372.
14. Sarma, M.; Chatterjee, T.; Das, S. K. *RSC Adv.* **2012**, *2*, 3920.
15. Zheng, H.; Che, S. *RSC Adv.* **2012**, *2*, 4421.
16. Levankumar, L.; Muthukumaran, V.; Gobinath, M. B. *J. Hazard. Mater.* **2009**, *161*, 709.
17. Kyzas, G. Z.; Kostoglou, M.; Lazaridis, N. K. *Chem. Eng. J.* **2009**, *152*, 440.
18. Rajesh, N.; Krishna Kumar, A. S.; Kalidhasan, S.; Rajesh, V. *J. Chem. Eng. Data.* **2011**, *56*, 2295.
19. Srinivasa Rao, P.; Sridhar, S.; Wey, M.Y.; Krishnaiah, A. *Ind. Eng. Chem. Res.* **2007**, *46*, 2155.
20. Yu, L.; He, Y.; Bin, L.; Yuee, F. *J. Appl. Polym. Sci.* **2003**, *90*, 2855.

21. Kalidhasan, S.; Santhana Krishna Kumar, A.; Rajesh, V.; Rajesh, N. *J. Colloid Interface Sci.* **2012**, *367*, 398.
22. Omotoso, O. E.; Ivey, D. G.; Mikula, R. *J. Hazard. Mater.* **1995**, *42*, 87.
23. Shen, B.; Zhai, W.; Lu, D.; Wang, J.; Zheng, W. *RSC Adv.* **2012**, *2*, 4713.
24. Neagu, V. *J. Hazard. Mater.* **2009**, *171*, 410.
25. Suksabye, P.; Thiravetyan, P.; Nakbanpote, W. *J. Hazard. Mater.* **2008**, *160*, 56.
26. Langmuir, I. *J. Am. Chem. Soc.* **1918**, *40*, 1361.
27. Hall, K. R.; Eagleton, L. C.; Acrivos, A.; Ver Meulen, T. *Ind. Eng. Chem. Fundam.* **1966,** *5*, 212.
28. Freundlich, H. M. F. *Z. Phys. Chem.* **1906**, *57*, 385.
29. Redlich, O.; Peterson, D. L. *J. Phys. Chem.* **1959**, *63*, 1024.
30. Dubinin, M. M.; Radushkevich, L.V. *Proc. Acad. Sci. USSR Phys. Chem. Sect.* **1947,** *55* 331.
31. Elovich, S. Y.; Larinov, O. G. *Izv. Akad. Nauk. SSSR, Otd. Khim. Nauk.* **1962,** *2*,209.
32. Temkin, M. I. *Zh. Fiz. Chim.* **1941**, *15*, 296.
33. Lagergren, S. *K. Sven.Vetenskapsakad. Handl.* **1898,** *24*, 1.
34. Ho, Y. S. *J. Hazard. Mater.* **2006**, *136*, 681.
35. Weber, W. J.; Morris, J. C. *J. Sanit. Eng. Div. Am. Soc. Civil Eng.* **1963**, *89*, 3.
36. Sengil, I. A.; Ozacar, M.; Turkmenler, H. *J. Hazard. Mater.* **2009**, *162*, 1046.
37. Donia, A. M.; Atia, A. A.; El-Boraey, H. A.; Mabrouk, D. *Sep. Purif. Technol.***2006** *49*, 64.
38. Houk, K. N.; Leach, A. G.; Kim, S. P.; Zhang, X. *Angew. Chem. Int. Ed.* **2003,** 4872.
39. Hughes, A.; Anslyn, E. *Proc. Natl. Acad. Sci. U. S. A.* **2007**, *104*, 6538.
40. Santhana Krishna Kumar, A.; Kalidhasan, S.; Rajesh, V.; Rajesh, N. *Ind. Eng. Chem. Res.* **2012**, *51*, 58.
41. A. S. Krishna Kumar, S. Kalidhasan, Vidya Rajesh, N. Rajesh, *J. Environmental Science & Health: Part A.* **2011,** 46, 1598.

42. Kalidhasan, S.; Sricharan, S.; Ganesh, M.; Rajesh, N. *J. Chem. Eng. Data*. **2010,** *55* 5627.
43. Rama Krishna, K.; Philip, L. *J.Hazard. Mater.* **2005**, *121*, 109.
44. Rao, C.N.R.; Sood, A. K.; Subrahmanyam K. S.; Govindaraj, A. *Angew. Chem. Int. Ed.,* **2009, *48,*** 7752.
45. Li, D.; Muller, M. B.; Gilje, S.; Kaner R. B.; Wallace, G. G. *Nature Nanotechnol,* **2008**, *3*, 101.
46. Dreyer, D. R.; Park, S.; Bielawski C. W.; Ruoff, R. S. *Chem. Soc. Rev.* **2010**, *39,* 228.
47. Yang, S. T.; Chang, Y.; Wang, H.; Liu, G.; Chen, S.; Wang, Y.; Liu Y.; Cao. A. *J. Colloid Interface Sci.* **2010**, *351,* 122.
48. Zhao, G.; Li, J.; Ren, X.; Chen, C.; Wang, X. *Environ. Sci. Technol.* **2011**, *45,* 10454.
49. Gao, W.; Majumder, M.; Alemany, L. B.; Narayanan, T. N.; Ibarra, M. A.; Pradhan, B.K.; Ajayan, P. M. *ACS Appl. Mater. Interfaces.* **2011**, ***3,*** 1821.
50. Mishra, A. K.; Ramaprabhu, S. *J. Hazard. Mater.* **2011**,*185*, 322.
51. Liu, X.; Pan, L.; Lv, T.; Zhu, G.; Lu, T.; Sun, Z.; Sun, C. *RSC Adv.*, **2011,** *1,* 1245.
52. Hartono, T.; Wang, S.; Ma, Q.; Zhu, Z. *J. Colloid Interface Sci.,* **2009,** *333,* 114.
53. Ramesha, G. K.; Kumara, A. V.; Muralidhara, H. B.; Sampath, S. *J. Colloid Interface Sci.* **2011,** *361,* 270.
54. Bradder, P.; Ling, S. K.; Wang, S. B.; Liu, S. M. *J. Chem. Eng. Data,* **2011,** 56, 138.
55. Ma, H. L.; Zhang, Y.; Hu, Q. H.; Yan, D.; Yu, Z. Z.; Zhai, M. *J. Mater. Chem.* **2012,** *22,* 5914.
56. Acik, M.; Dreyer, D. R.; Bielawski, C. W.; Chabal, Y. J. *J. Phys. Chem. C,* **2012,** *116,* 7867.
57. Ramesh, P.; Bhagyalakshmi, S.; Sampath, S. *J. Colloid Interface Sci.,* **2004,** *274,* 95.
58. Hummers, W. S.; Offeman, R. E. *J. Am. Chem. Soc.* **1958,** *80,* 1339.
59. Clesceri, L. S.; Greenberg, A. E.; Eaton, A. D. American Public Health Association, Washington. **1998.**

60. Li, W.; Tang, X. Z.; Zhang, H. B.; Jiang, Z. G.; Yu, Z. Z.; Du, X. S.; Mai, Y. W. *Carbon,* **2011,** *49,* 4724.

61. Singh, V.; Sharma, A. K.; Kumari, P.; Tiwari, S. *Ind. Eng. Chem. Res.* **2008,** *47,* 5267.

62. Santhana Krishna Kumar, A.; Gupta, T.; Kakan, S. S.; Kalidhasan, S.; Manasi, Rajesh,V.; Rajesh, N. *J. Hazard. Mater.* **2012,** *239-240,* 213.

63. Kalidhasan, S.; Santhana Krishna Kumar, A.; Rajesh, V.; Rajesh, N. *J. Colloid Interface Sci.* **2012,** *367,* 398.

64. Ma, J. C.; Dougherty, D. A. *Chem. Rev.* **1997,** *97,* 1303.

65. Mooibroek, T. J.; Gamez, P.; Reedijk, J. *Cryst. Eng. Comm.,* **2008,** *10,* 1501.

66. Malkoc, E.; Nuhoglu, Y. *Chem. Eng. Process,* **2007,** *46,* 1020.

67. Lopez-Ramon, M. V.; Stoeckli, F.; Moreno-Castilla, C.; Carrasco-Marin, F. *Carbon,* **1999,** *37,* 1215.

68. Selvi, K.; Pattabhi, S.; Kadirvelu, K.; *Bioresour. Technol.* **2001,** *80,* 87.

69. Garg, V. K.; Gupta, R.; Kumar, R.; Gupta, R. K. *Bioresour. Technol.,* 2004, **92,** 79.

70. Qureshi, I.; Memon, S.; Yilmaz, M. *J. Hazard. Mater*. **2009,** *164,* 675.

71. Giles, C. H.; Mckay, R. B. *J. Bacteriol.* **1965,** *89,* 390.

72. Abd. El-Latif, M. M.; Ibrahim, A. M.; El-Kady, M. F. *J. Am. Sci.* **2010,** *6,* 267.

73. Gounder, R.; Iglesia, E. *Acc. Chem. Res.* **2012,** *45,* 229.

74. Santhana Krishna Kumar, A.; Kalidhasan, S.; Rajesh,V.; Rajesh, N. *Ind. Eng. Chem. Res.* **2012,** *51,* 11312.

75. Zhao, H. *J. Chem. Technol. Biotechnol.* **2006,** *81,* 877.

76. Santhana Krishna Kumar, A.; Ramachandran, R.; Kalidhasan, S.; Rajesh, V. N. Rajesh, *Chem. Eng. J.* **2012,** *211-212,* 396.

77. Mallampati, R.; Valiyaveettil, S. *RSC Adv.* **2012,** *2,* 9914.

78. Lee, K. J.; Lee, T. G. *J. Hazard. Mater.* **2012,** *241–242,* 1.

79. Fuente-Cuesta, A.; Lopez-Anton, M. A.; Diaz-Somoano, M.; Martínez-Tarazona, M. R. *Chem Eng. J.* **2012,** *213,* 16.

80. Pearson, R. G. *J. Am. Chem. Soc.* **1963,** *85,* 3533.

81. Perez-Quintanilla, D.; Del. Hierro, I.; Fajardo, M.; Sierra, I. *J. Hazard. Mater.* **2006,** *134,* 245.
82. De. Canck, E.; Lapeire, L.; De Clercq, J.; Verpoort, F.; Van Der Voort, P. *Langmuir,* **2010,** *26,* 10076.
83. Dias Filho, N. L.; Polito, W. L.; Gushikem, Y. *Talanta,* **1995,** 42, 1031.
84. Pu, Q.; Su, Z.; Hu, Z.; Chang, X.; Yang, M. *J. Anal. At. Spectrom*, **1998,** *13,* 249.
85. Safavi, A.; Iranpoor, N.; Saghir, N. *Sep. Purif. Tecnnol.* **2004,** *40,* 303.
86. Chwastowska, J.; Rogowska, A.; Sterlinska, E.; Dudek, J. *Talanta,* **1999,** *49,* 837.
87. Ma, W. X.; Liu, F.; Li, K. A.; Chen, W.; Tong, S. Y. *Anal. Chim. Acta,* **2000,** *416,* 191.
88. Manohar, D. M.; Anoop Krishnan, K.; Anirudhan, T. S. *Water Res.* **2002,** *36,* 1609.
89. Takagai, Y.; Shibata, A.; Kiyokawa, S.; Takase, T. *J. Colloid Interface Sci.* **2011,** *353,* 593.
90. Gonçalves, G.; Marques, P. A. A. P.; Trindade, T.; Neto, C. P.; Gandini, A. *J. Colloid Interface Sci.* **2008,** *324,* 42.
91. Karunasagar, D.; Balarama Krishna, M. V.; Anjaneyulu, Y.; Arunachalam, J. *Environ. Pollut.,* **2006,** *143,* 153.
92. Ghoshal, S.; Bhattacharya, P.; Chowdhury, R. *J. Hazard. Mater.* **2011,** *194,* 355.
93. Tang, H.; Chang, C.; Zhang, L. *Chem. Eng. J,* **2011,** *173,* 689.
94. Cotton, F. A. *Advanced Inorganic Chemistry*, 6th Ed. John Wiley & Sons, ISBN: 8126513381, Singapore, **2007.**
95. Wang, S. L.; Lee, J. F. *Chem. Eng. J.* **2011,** *174,* 289.
96. Coates, J. Interpretation of Infrared spectra: A Practical Approach, John Wiley & Sons Ltd, Chichester, **2000.**
97. Hong, L. X.; Xin, T. Z.; Zhou, Z. X. *Spectrochim. Acta A* **2009,** *74,* 168.
98. Lojewska, J.; Miskowiec.P.;Lojewski, T.; Proniewicz, L. M. *Polym. Degrad. Stab.* **2005,** *88,* 512.
99. Mahanta, N.; Valiyaveettil, S. *RSC Adv.* **2012,** *2,* 11389.

100. Mohamed, T. A.; Mustafa, A. M.; Zoghaib, W. M.; Afifi, M. S.; Farag, R. S.; Badr, Y. *J. Mol. Struct.* (*THEOCHEM*) **2008,** *868*, 27.
101. Shen, X. E.; Shan, X. Q.; Dong, D. M.; Hua, X. Y.; Owens, G. *J. Colloid Interface Sci.* **2009,** *330*, 1.
102. Santhana Krishna Kumar, A.; Rajesh, N. *RSC Adv.* **2013,** *3*, 2697.
103. Johnson, N. C.; Manchester, S.; Sarin, L.; Gao, Y.; Kulaots, I.; Hurt, R. H. *Environ. Sci. Technol.* **2008,** *42*, 5772.

SUMMARY AND CONCLUSIONS

6.1 Summary and Conclusions

The first chapter gives a comprehensive overview, the chemistry of chromium and mercury, and the various techniques for their detoxification. The toxic nature of chromium and mercury vividly describes the importance of the removal of these heavy metals from electroplating and tannery effluents and coal fly ash sample, which constitutes the major source of chromium and mercury pollution. Hence, efforts were directed towards the development of effective methods for the detoxification of chromium and mercury.

The second chapter explains the materials and methods adopted for this work.

The third chapter of the thesis deals with the high potential of polystyrene-divinyl benzene based sorbent impregnated with a long chain amine for the removal of chromium. The polymeric sorbent is efficient and could endure the treatment in both acidic and alkaline media. The adsorption kinetics is fast, and follows a pseudo second order model and is also in accordance with the Langmuir adsorption isotherm model with an adsorption capacity of 171.82 mg g^{-1}. The study of the thermodynamic parameters showed that the adsorption process decreases with an increase in temperature. Column studies proved that the system could tolerate a large sample volume (1 Litre) with effective separation from a synthetic mixture of various ions. Cr(VI) could be effectively removed at acidic pH based on the electrostatic attraction of hydrochromate with the protonated amine, whereas Cr(III) was retained in the column at alkaline pH due to the interaction of the amine with $Cr(OH)_2^+$ and $Cr(OH)^{2+}$ species. The adsorbed chromium in the respective oxidation states could be recovered from the column using sulfuric acid and sodium hydroxide respectively, without any appreciable loss in the performance efficiency for 15 cycles. The validity of the proposed method is very well illustrated for the separation of chromium in real effluent samples with average removal efficiency greater than 98 %.

The second method illustrates the ability of an aliphatic primary amine impregnated polymeric sorbent for the effective detoxification of chromium(VI). Amberlite XAD-4 proved to be an effective host for the impregnation of the n-octylamine as the guest. The removal efficiency depends on the nature of the amine impregnated in the resin matrix. The adsorption process was in accordance with the pseudo second order kinetic model and the thoroughly characterized adsorbent had a maximum adsorption capacity of 75.93 mg g^{-1}. The column study illustrated the potential of the adsorbent to remove chromium from a sample volume of 600 mL. The study of adsorption thermodynamics indicated the adsorption process to be spontaneous at room temperature. The adsorbent could be effectively regenerated and reused for 9 adsorption-desorption cycles without affecting the performance efficiency of the column. The method proved to be very effective in the removal of chromium from tannery wastewater.

The fourth chapter of the thesis deals with the effectiveness of interaction between tetrachloromercurate(II) anion and trioctylamine in acidic medium. The sorption kinetics favors the pseudo second order kinetic model and a maximium adsorption capacity of 140.84 mg g^{-1} in concurrence with the Langmuir isotherm. The adsorption process is consistent with the mechanism involving the electrostatic interaction between the tetrachloromercurate(II) anion and the protonated amine in the clay. The thermodynamically favorable adsorption process is driven by negative enthalpy and entropy changes respectively. The adsorbent material could be effectively regenerated using thiourea and the method could be scaled to a sample volume of 800 mL. As low as 10 ppb of mercury could be effectively adsorbed in the column. Finally, the method has proved to be successful in the adsorption of mercury from coal fly ash, which is a vital source of mercury pollution.

In the second method, dodecylamine modified sodium montmorillonite adsorbent has proved to be very effective in the solid phase extraction of hexavalent chromium. The electrostatic interaction of hydrogentetraoxochromate(VI) anion with the protonated primary amine is supported by a Langmuir adsorption capacity of 23.69 mg g^{-1}. The second order kinetic model and the thermodynamically favorable exothermic adsorption process further

strengthen the efficacy of this adsorbent. A sample volume of 300 mL could be tolerated on a laboratory scale with 10 mg L^{-1} concentration of Cr(VI). Furthermore, the regeneration of the adsorbent is possible using sodium hydroxide as the eluent. The practical application in detoxifying chromium from a tannery wastewater sample highlights the potential of this dodecylamine modified clay adsorbent material for environmental remediation.

In the third method, the interaction between the cellulose and NaMMT has demonstrated the potential application of a biopolymer composite material for the effective adsorption of chromium. The biopolymer composite exhibits an adsorption capacity of 22.2 mg g^{-1} and the experimental data showed a good fit to the Langmuir adsorption isotherm model. The spontaneity of adsorption was ascertained from the thermodynamic properties and the experimental data showed excellent adherence to second order kinetics. The mesoporous nature of the material was established from the nitrogen adsorption isotherm study and there is no significant change in the crystalline nature of the composite adsorbent after the adsorption of chromium. A sample volume of 400 mL could be quantitatively treated by column method at 100 mg L^{-1} concentration of Cr(VI) with a preconcentration factor of 50. The efficiency of the method is well illustrated in terms of regeneration of the composite material in a facile manner. The adsorbent could be reused with quantitative recovery for 10 cycles and its applicability to detoxify chromium from wastewater has shown good prospects in addressing the global environmental concern for heavy metal pollution.

In the final method, chitosan-NaMMT clay composite prepared under microwave conditions has proved to very effective in the adsorption and removal of chromium from a large sample volume. The biopolymer composite exhibits an adsorption capacity of 133 mg g^{-1} and interestingly the crystallinity of the composite material was retained after adsorption of chromium. The mesoporous nature and the nano pore size prove to be a value addition for the retention of chromium. The study of the sorption thermodynamics indicates spontaneity and the endothermic nature of adsorption. The material could also be regenerated by using simple reducing agents, thereby making the process eco-friendly and benign.

The first method in the fifth chapter highlights the preparation, characterization and application towards the removal of toxic Cr(VI) using the excellent three centre interaction between an ionic liquid, chitosan and chromium(VI). The hydrogen bonding and electrostatic interactions play an important role in the adsorption process. The exothermic adsorption process is ably supported by the positive co-operative effect between tetraoctylammonium ion, chitosan and hydrogenchromate anion. Langmuir adsorption isotherm gave a good fit to the adsorption data with an adsorption capacity of 63.69 mg g^{-1}. The adsorbent could be effectively regenerated using ammonium hydroxide and column studies proved the efficacy of the adsorbent in tolerating a larger sample volume. Overall, the method has brought out the worth of ionic liquid-biopolymer interaction and its usefulness in heavy metal adsorption. Similarly, the ionic liquid-exfoliated graphene oxide adsorbent has shown admirable ability towards the adsorption of Cr(VI). The facile adsorption is favored by a high adsorption capacity of 285.71 mg g^{-1} and fast sorption kinetics. The thermodynamically favorable adsorption process has paved way for detoxifying chromium from a tannery industry effluent. A notable feature is that Cr(VI) as well as Cr(III) interact with graphene oxide depending on the pH of the medium. This is of considerable significance in the remediation of chromium. Regeneration and stability of adsorbent for 12 repetitive cycles is yet another fitting tribute to this interesting adsorbent material. The ionic liquid- EGO combination has carved a niche among the various other carbon based adsorbents. Certainly, the interaction between Aliquat 336 and exfoliated graphene oxide has laid the basis for the removal of diverse metal ions as well as other pollutants.

The final work in this chapter describes the removal of mercury using biopolymer cellulose finely woven as an effective adsorbent by interaction with mercaptobenzathiazole. The pivotal role played by the ligand and the biopolymer has fostered the effective soft-soft interaction of the heteroatom sulfur and the lone pair-ion dipole interactions of the surface hydroxyl groups of cellulose with mercury. The pseudo second order kinetics and the thermodynamics of the spontaneous adsorption process support the mechanism of interaction. The excellent sorption capacity (204.8 mg g^{-1}) that could be realized using this adsorbent is another high point of this method. Effective regeneration of the adsorbent using

potassium thiocyanate and the enrichment to a sample volume of 500 mL is an added advantage associated with the method. Above all, the adsorbent shows considerable promise in adsorbing mercury vapour from a used Compact Flourescent Lamp (CFL) which could certainly lead to fascinating and diverse applications of this sulfur ligand impregnated biopolymer adsorbent. Indeed, the cellulose-MBT adsorbent opens the doors towards the decontamination of mercury from other anthropogenic sources of pollution as well.

6.2 Scope for Future Work

The results obtained in this study offered many new and interesting possibilities for future research. Some of them are listed below-

1. Suitably grafted biopolymers using microwave and ultrasound assisted preparation would open up the scope for the better selectivity and enhancement in adsorption capacity for chromium and mercury.

2. The interaction of biopolymers (chitosan, cellulose) with exfoliated graphene oxide opens up further exciting possibilities towards the removal of diverse metal ions.

Table 6.1. Summary of the Methods

Sl No	Adsorbent	Modifier	Metal	Efficiency (%)	pH	Isotherm	Eluent	Characterization techniques
1	Amberlite XAD-4	n-Octylamine	Cr	98.0	2.5	Langmuir	NaOH	FT-IR, SEM, EDX, XRD, ^{13}CNMR
2	AmberliteXAD-1180	Trioctylamine	Cr	99.5	2-3	Langmuir	NaOH	FT-IR, EDX, XRD,
3	Na Montmorillonite	Dodecylamine	Cr	97.5	2.5	Freundlich	NaOH	FT-IR, SEM, EDX, BET, XRD,
4	Na Montmorillonite	Trioctylamine	Hg	99.5	2.5-3.5	Langmuir	Thiourea	FT-IR, BET, EDX, XRD
5	Na Montmorillonite	Cellulose	Cr	97.0	3.8-5.5	Langmuir	NaOH	FT-IR, BET, EDX, XRD,
6	Na Montmorillonite	Chitosan	Cr	99.5	5.0	Langmuir	NaOH	FT-IR, SEM, EDX, BET, XRD,
7	Chitosan	TOABr	Cr	99.0	3-4	Langmuir	NH_4OH	FT-IR, SEM, EDX,
8	Exfoliated Graphene Oxide	Aliquat-336	Cr	99.5	2.5-3.5	Langmuir	NH_4OH	FT-IR, EDX, XRD,
9	Cellulose	2-Mercapto Benzothiazole	Hg	98.0	4.0	Freundlich	KSCN	FT-IR, SEM, EDX, XRD

List of Publications

1. **A. Santhana Krishna Kumar,** N. Rajesh, Exploring the interesting interaction between graphene oxide, Aliquat-336(a room temperature ionic liquid) and chromium (VI) for wastewater treatment, **RSC Advances, 2013, 3, 2697-2709.**
2. S. Kalidhasan, **A. Santhana Krishna Kumar,** V. Rajesh, N. Rajesh, Enhanced adsorption of hexavalent chromium arising out of an admirable interaction between a synthetic polymer and an ionic liquid, **Chem. Eng. J. 222, 2013, 454–463.**
3. **A. Santhana Krishna Kumar,** S. Kalidhasan, V. Rajesh, N. Rajesh, A meticulous study on the adsorption of mercury as a tetrachloromercurate(II) anion with trioctylamine modified sodium montmorillonite and its application to a coal fly ash sample, **Ind. Eng. Chem. Res. 51, 2012, 11312−11327.**
4. **A. Santhana Krishna Kumar,** S. Kalidhasan, V. Rajesh, N. Rajesh, Application of cellulose-clay composite biosorbent toward the effective adsorption and removal of chromium from industrial wastewater, **Ind. Eng. Chem. Res. 51, 2012, 58-69.**
5. **A. Santhana Krishna Kumar,** Timsi Gupta, Shruti Singh Kakan, S. Kalidhasan, Manasi, Vidya Rajesh, N. Rajesh, Effective adsorption of hexavalent chromium through a three centre (3c) co-operative interaction with an ionic liquid and biopolymer. **J. Hazard. Mater. 239-240, 2012, 213-224.**
6. **A. Santhana Krishna Kumar,** Revathi Ramachandran, S. Kalidhasan, V. Rajesh, N. Rajesh, Potential application of dodecylamine modified sodium montmorillonite as an effective adsorbent for hexavalent chromium, **Chem. Eng. J. 211-212, 2012, 396-405.**
7. S. Kalidhasan, Vinusha Reddy Chollety, Priyanka Amba Gupta, **A. Santhana Krishna Kumar,** Vidya Rajesh, N. Rajesh, Microwave assisted solvent free green preparationand physicochemical characterization of surfactant-anchored cellulose and its relevance toward the effective adsorption of chromium, **J. Colloid Interface Sci. 372, 2012. 88-98.**

8. S. Kalidhasan, **A. Santhana Krishna Kumar,** Vidya Rajesh, N. Rajesh, An efficient ultrasound assisted approach for the impregnation of room temperature ionic liquid onto Dowex 1 × 8 resin matrix and its application toward the enhanced adsorption of chromium (VI). **J. Hazard. Mater. 213–214, 2012, 249–257.**
9. S. Kalidhasan, **A. Santhana Krishna Kumar,** V. Rajesh, N. Rajesh, Ultrasound-assisted preparation and characterization of crystalline cellulose–ionic liquid blend polymeric material: A prelude to the study of its application toward the effective adsorption of chromium, **J. Colloid Interface Sci. 367, 2012, 398-408.**
10. N. Rajesh, **A.S. Krishna Kumar,** S. Kalidhasan, Vidya Rajesh, Trialkylamine impregnated macroporous polymeric sorbent for the effective removal of chromium from industrial wastewater. **J. Chem. Eng. Data, 56, 2011, 2295-2304.**
11. **A. S. Krishna Kumar,** S. Kalidhasan, Vidya Rajesh, N. Rajesh, An enhanced adsorption methodology for the detoxification of chromium using n-octylamine impregnated Amberlite XAD-4 polymeric sorbent, **J. Environ. Sci. Health: Part A. 46, 2011, 1598-1610.**
12. **A. Santhana Krishna Kumar,** S. Kalidhasan, V. Rajesh, N. Rajesh, Microwave assisted preparation and characterization of biopolymer-clay composite material and its application for chromium detoxification from industrial effluent, **Adv. Mat. Lett. 2, 2011, 383-391.**
13. S. Kalidhasan, **A.S. Krishna Kumar,** Vidya Rajesh, N. Rajesh, A preliminary spectroscopic investigation on the molecular interaction of metal-diphenylthiocarbazone complex with cellulose biopolymer and its application. **Spectrochimica. Acta A. 79, 2011, 1681-1687.**
14. **A. Santhana Krishna Kumar,** S. Kalidhasan, Vidya Rajesh, N. Rajesh, Adsorptive demercuration by virtue of an appealing interaction involving mercaptobenzothiazole and cellulose, **Ind. Eng. Chem. Res (communicated)**

Abstracts in National Conferences

1. **A. Santhana Krishna Kumar,** Chinta Uday Kumar, Vidya Rajesh and N. Rajesh. Graft polymerization of n-butylacrylate onto chitosan for the remediation of hexavalent chromium, **National Conference on "Chemistry for Sustainable Development" (SusCon-2012),** GITAM University, Visakhapatnam Oct- 2012.
2. **A. Santhana Krishna Kumar,** S. Kalidhasan, Vidya Rajesh and N. Rajesh. Cellulose impregnated with mercaptobenzothiazole for the effective adsorption of mercury from aqueous solution, **CRSI National Symposium in Chemistry (NSC-14)** NIIST, Trivandrum, Feb 2012.
3. **A. Santhana Krishna Kumar,** Vidya Rajesh and N. Rajesh. An efficient approach for the adsorption of chromium using dodecylamine modified sodium montromorillonite clay **at International Conference on Vistas in Chemistry** held at IGCAR, Kalpakkam, Oct 2011.
4. **A. Santhana Krishna Kumar,** Vidya Rajesh and N. Rajesh. Green composite for the effective adsorption of heavy metal chromium, **National Seminar on Nanostructured Materials and Applications at** Madurai Kamaraj University (MKU), Mar. 2011.
5. **A. Santhana Krishna Kumar,** S. Kalidhasan and N. Rajesh, Amine impregnated in polymeric resin matrix for the removal of toxic chromium from industrial waste water, **CRSI-National Symposium in Chemistry (NSC-12)** at Indian Institute of Chemical Technology(IICT), Hyderabad, Feb 2010.
6. S. Kalidhasan, **A. Santhana Krishna Kumar** and N. Rajesh, Microwave assist synthesis of water soluble surfactant coated cellulose sorbent for the removal of toxic chromium from industrial waste water, **Mid-CRSI symposium** at National Institute for Interdisciplinary Science and Technology (NIIST), Trivandrum, June 2010.
7. S. Kalidhasan, **A. Santhana Krishna Kumar** and N. Rajesh, 2010. Self-assembled bilayer of cellulose/quartenary ammonium salt as adsorbent for the removal of toxic chromium from industrial effluents, **National Conference in Green and Sustainable Chemistry (NCGSC)** at Birla Institute of Technology and Science (BITS), Pilani, Feb 2010.

Abstracts in International Conferences

1. **A. Santhana Krishna Kumar,** N. Rajesh. Long chain amine impregnated exfoliated graphene oxide for the effective removal of chromium from tannery wastewater. 7thSingapore international chemical conference & 12th Asia- pacific international symposium on capillary electrophoresis and microscale separation and analysis (SICC-7) **National University of Singapore, Singapore,** December, 2012.
2. **A. Santhana Krishna Kumar,** Timsi Gupta, Shruti Singh, S. Kalidhasan, Vidya Rajesh, N. Rajesh Chitosan-Ionic liquid blend polymeric sorbent material for the effective adsorption of chromium. **International Conference on Nanomaterials and Nanotechnology(ICNANO-2011)** Delhi University, India, December 2011.
3. **A. Santhana Krishna Kumar,** S. Kalidhasan and N. Rajesh. Removal of chromium from industrial effluents using Amberlite XAD-1180 resin impregnated with n-octylamine, **2nd International Conference on Natural Polymers (ICNP-2010)** at Mahatma Gandhi University (MGU), 2010, India.

Participation in Conferences/Workshop

1. **INDO-UK Workshop on Current Development of Wastewater Treatment,** National Institute of Technology (NIT)-Tiruchirapalli, India, August 2011

BIOGRAPHY OF Prof. N. RAJESH

Prof. N. Rajesh Department of Chemistry, Birla Institute of Technology and Science, Pilani, Hyderabad Campus, India obtained his Master's degree and Ph. D from Indian Institute of Technology (IIT), Madras, India. He has been involved in teaching and research for the past 18 years. He is a fellow member of the Royal Society of Chemistry (FRSC) London. His research interests include development of greener sorbents for the effective detoxification of heavy metals and dyes from industrial effluents. He has several research publications in peer reviewed journals and is also an expert reviewer for various international journals. Currently, his group is engaged in the development of novel biopolymer, graphene and clay based sorbents for heavy metal remediation. He has collaborative interaction with various institutes such as National Center for Compositional Characterization of Materials (NCCCM), Hyderabad, India and Central Leather Research Institute (CLRI), Chennai, India. He is a member of American Chemical Society (ACS) and a life member of Chemical research society of India (CRSI) and Indian Science Congress (ISC). He has several ongoing funded projects and also successfully completed projects sponsored by UGC and DST, India.

BIOGRAPHY OF Mr. A. SANTHANA KRISHNA KUMAR

Mr. A. Santhana Krishna Kumar obtained his Masters degree in Chemistry from Thiagarajar College, Madurai, India in 2008 and started his work as junior research fellow in the Department of Chemistry at BITS Pilani, Hyderabad campus, India. He is well versed in various separation methods, has good number of publications to his credit and presented his work in several national and international conferences. Currently, his research interests focus on the development of suitably customized polymeric composites for heavy metal removal from industrial effluents.